

Selectivity in Propene Polymerization with Metallocene Catalysts

Luigi Resconi,^{*,†} Luigi Cavallo,[‡] Anna Fait,[†] and Fabrizio Piemontesi[†]

Montell Polyolefins, Centro Ricerche G. Natta, P.le G. Donegani 12, 44100 Ferrara, Italy, and Dipartimento di Chimica, Università di Napoli "Federico II", Via Mezzocannone 4, 80134 Napoli, Italy

Received September 16, 1999

Contents

I. Introduction	1253	C. Use of Matrix Multiplication Methods in Statistical Models	1315
II. Basic Concepts	1256	VII. Regiocontrol	1316
A. Structure of Group 4 Metallocenes	1256	A. Stereochemistry of Regioirregular Insertion	1316
B. Activation	1256	1. ¹³ C NMR Analysis	1316
C. Elements of Chirality	1258	2. Molecular Modeling	1317
D. Polymerization Mechanism	1260	B. Reactivity of a Secondary Growing Chain	1319
E. Mechanisms of Stereocontrol in Primary Insertion (Site vs Chain-End Control)	1262	1. Copolymerization with Ethene	1319
F. Regiochemistry of Propene Insertion	1264	2. Chain Release	1320
G. ¹³ C NMR Analysis of Polypropenes	1264	C. Regioselectivity: Influence of the Catalyst Structure	1320
III. Elementary Steps	1264	1. Influence of the Metal	1320
A. Alkene-Free Species	1265	2. Influence of the Cocatalyst	1320
B. Agostic Interactions	1266	3. Influence of the π -Ligands: Experimental Data	1321
C. Olefin Coordination	1268	4. Influence of the π -Ligands: Molecular Modeling Analysis	1322
D. Insertion	1270	5. Relationship between Regioselectivity and Type of Stereoselectivity	1323
E. Insertion Barrier	1273	D. Influence of Monomer Concentration	1325
F. Chain Release	1274	E. Influence of Polymerization Temperature	1326
G. Formation and Reactivation of Mt-Allyl Species	1277	F. 2,1 \rightarrow 3,1 Isomerization Mechanism	1326
H. Mechanism of Enantiomorphic Site Control in Primary Insertion	1278	VIII. Kinetics	1326
I. Mechanism of Chain-End Control in Primary Insertion	1281	A. Activity versus Metal	1328
IV. Stereocontrol: Influence of the Catalyst	1282	B. Activity versus Catalyst/Cocatalyst Ratio	1328
A. Isotactic Polypropene: C_2 -Symmetric Metallocenes	1282	C. Activity versus Time	1329
1. Chiral <i>ansa</i> - C_2 -Symmetric Metallocenes	1284	D. Kinetic Models: Activity versus Monomer Concentration	1331
2. Unbridged Isospecific	1294	E. Activity versus Temperature	1333
3. Combining Two Symmetries: C_2 - <i>meso</i> - C_5	1295	F. Activity versus Solvent	1334
B. Syndiotactic Polypropene: C_5 -Symmetric Metallocenes	1300	G. Molecular Weight	1334
C. C_1 -Symmetric Metallocenes: from Hemiisotactic to Isotactic Polypropene	1303	IX. Influence of Hydrogen	1336
V. Stereocontrol: Influence of Polymerization Conditions	1309	X. Outlook	1338
A. Influence of Monomer Concentration	1309	XI. Acknowledgments	1339
1. C_2 -Symmetric Catalysts	1309	XII. References	1339
2. C_1 -Symmetric Catalysts	1310		
B. Influence of Polymerization Temperature	1310		
C. Epimerization of the Primary Growing Chain	1311		
VI. Statistics of Polymerization	1312		
A. General Remarks	1312		
B. Mechanisms of Stereocontrol and Statistical Models	1312		
1. Chain-End Control (Bernoullian Model)	1313		
2. Enantiomorphic-Site Control	1313		

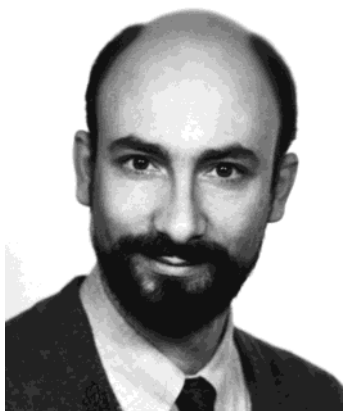
I. Introduction

The outstandingly rapid scientific and technological development of metallocene-based catalysts for olefin polymerization is a perfect example of the successful application of organometallic chemistry to homogeneous catalysis¹ and of the teaching that understanding reactions at the molecular level can provide to the more matter-of-fact fields of heterogeneous ca-

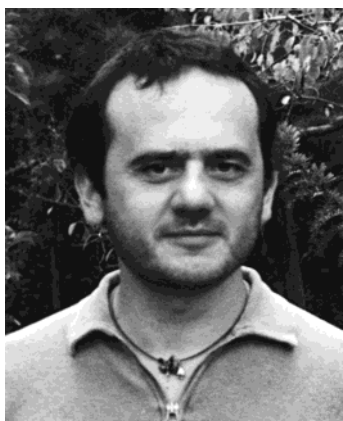
* To whom all correspondence should be addressed. E-mail: luigi.resconi@eu.montell.com.

[†] Centro Ricerche G. Natta.

[‡] Università di Napoli "Federico II".



Luigi Resconi was born in 1958 in Brescia, Italy, and obtained his Doctor in Chemistry degree from the University of Milano in 1984 with a thesis on Ni and Fe anionic carbonyl clusters under the direction of Giuliano Longoni. After a scholarship at the ETH-Zürich with Piero Pino, where he began to study C_2 -symmetric group 4 metallocenes, in May 1985 he joined the Ziegler–Natta research group at the Istituto G. Donegani (then the Corporate Research Center of Montedison) in Novara, Italy. Throughout 1989 he has been a visiting scientist at Stanford University in the group of Robert Waymouth, where he started the investigation on the cyclopolymerization of 1,5-hexadiene catalyzed by zirconocene/alumoxane systems. Since 1990 he has been project leader of the Homogeneous Catalysis research project, first with Himont, and then with Montell Polyolefins since its formation in 1995. He is currently senior scientist and program manager at the Centro Ricerche G. Natta of Montell in Ferrara, Italy, where he contributed to the development of several new metallocene catalysts for the synthesis of polyolefins, work that led to over 40 patent applications and several scientific publications. Current research activities of his group include the design and development of new homogeneous catalysts for olefin polymerization, the investigation of chain transfer and isomerization reactions in the stereospecific polymerization of 1-olefins, and the improvement of synthetic strategies aimed at more efficient preparations of metallocenes and other organo-metallic catalysts.



Luigi Cavallo was born in Pozzuoli, near Naples, in 1962. He obtained his Ph.D. in Chemistry in 1990 under the direction of Paolo Corradini and Gaetano Guerra, with a thesis on the mechanisms of stereospecific polymerizations. He has been a visiting scientist at the University of Calgary in the group of Tom Ziegler, where he contributed to the development of combined quantum mechanics/molecular mechanics techniques. His research interests focus on studies on the mechanisms of 1-olefins polymerization—with both homogeneous and heterogeneous catalysts—and of conjugated dienes and styrene, and on the mechanisms of organo-metallic reactions, especially the enantioselective ones, as the (salen)–Mn catalyzed epoxidation of olefins. He is interested in the development of computational methodologies also.

talysis² and material sciences.³ Indeed, titanocene dichloride⁴ was used in combination with aluminum alkyl chlorides as early as 1957 to provide soluble and chemically more defined and hence better un-



Anna Fait was born near Brescia, Italy, in 1961, and obtained her Doctor in Chemistry degree from the University of Milano in 1985 with a thesis on Ni polycarbido carbonyl clusters under the direction of Giuliano Longoni. After a brief experience in the organic chemistry department of Società Italiana Resine, she joined the Reactor Engineering Department of Montedipe in 1986, where she dealt with process optimization, later becoming leader of the same group. In 1993 she joined Himont (now Montell). She is now responsible for the Engineering and Research Development group of the Centro Ricerche G. Natta of Montell in Ferrara, Italy. Her group's activities cover unit operations study, kinetic investigation, determination of chemical and physical parameters, and catalysis and process development.



Fabrizio Piemontesi was born in Borgosesia, Italy, in 1960. He obtained his Doctor in Chemistry degree from the University of Milano in 1987 with a thesis on alkylation and transamination reactions of amino acid residues coordinated on metal ions, under the direction of L. Casella. After a postdoc at the University of Milano with L. Garlaschelli, where he studied the synthesis of Ni and Pd phosphorane complexes, in March 1989 he joined the Ziegler–Natta research group of Himont at the Istituto G. Donegani in Novara, Italy, where he began his activity on group 4 metallocene research. After the relocation of the group to the Centro Ricerche G. Natta of Montell in Ferrara, he shifted his research interests to the NMR analysis of polymers and polymerization statistics.

derstandable models of the $TiCl_3$ -based heterogeneous polymerization catalysts.^{5–10} However, the early catalysts based on $Cp_2MtX_2/AlRCl_2$ or AlR_3 (Cp = cyclopentadienyl, Mt = metal, R = alkyl group) had a quite low activity in ethene polymerization and failed to homopolymerize 1-olefins altogether. Analogous research with zirconocene dichloride in combination with AlR_3 was started by Breslow¹¹ but met with limited success, until the serendipitous discovery of the activating effect of small amounts of water¹² on the system $Cp_2MtX_2/AlMe_3$ (X = Cl or alkyl group)¹³ and the subsequent controlled synthesis of methylalumoxane (MAO) by the group of Sinn and Kaminsky¹⁴ provided organometallic and poly-

mer chemists with a potent cocatalyst¹⁵ able to activate group 4 metallocenes (and a large number of other transition metal complexes, too) toward the polymerization of virtually any 1-olefins as well as several cyclic olefins.¹⁶ However, the activity of Cp₂-MtX₂/MAO catalysts, although impressive toward the homo- and copolymerization of ethene, was moderate with propene and, more important, did not produce stereoregular polymers. Very low molecular weight, atactic oils were obtained in all cases.

Besides the availability of suitable organometallic cocatalysts, the development of stereoselective, practical metallocene-based catalysts required the development of chiral, stereorigid metallocenes^{17–19} and of many new organic and organometallic reactions. Between 1984 and 1986, two key discoveries were made: the effect that different alkyl-substituted cyclopentadienyl ligands can induce on metallocene performances in olefin polymerization (the ligand effect)^{20,21} and the discovery that stereorigid, chiral metallocene catalysts can induce enantioselectivity in 1-olefin insertion.^{22,23} Since then, thanks to the combined efforts of industrial and academic research groups worldwide, an impressive leap forward toward the knowledge of, and control over, the mechanistic details of olefin insertion, chain growth, and chain release processes at the molecular level has been made.

The success of group 4 metallocenes in olefin polymerization arises not only from their intrinsic understandability in terms of “simple” steric effects but also from the challenge they posed in terms of organic and organometallic syntheses: while the heterogeneous catalysts are much more difficult to study in terms of elementary steps than the homogeneous ones, the latter in turn are in general more difficult to synthesize. The synthesis of the ligands and the corresponding metallocenes have been reviewed.^{24–27}

There is no unambiguous chemical definition for what a “metallocene catalyst” is. Obviously, not all biscyclopentadienyl transition metal complexes (metallocenes) are, or can be turned into, olefin polymerization catalysts. For the purpose of the present review, we limit the definition of metallocene catalysts to the biscyclopentadienyl complexes of transition metals of group 4 (titanium, zirconium, or hafnium) as well as a few examples of group 3 metals (Sc, Y, La). Therefore, the monocyclopentadienyl (e.g. CpTiCl₃) and monocyclopentadienylamido complexes (e.g. the so-called “constrained geometry catalyst” Me₂Si(Me₄Cp)(N-*t*-Bu)TiCl₂ and the like) are not discussed here: for recent reviews of homogeneous polymerization catalysts based on soluble, well-defined, nonmetallocene complexes of transition metals, see refs 28–30.

Among all catalysts for the linear polymerization of hydrocarbyl olefins, the class of group 4 metallocene-based systems is the only one enabling control over the whole range of molecular weights (from olefin dimers and oligomers, to ultrahigh molecular weight polymers) and microstructures (stereoregularity, regioregularity, comonomer distribution) of polyolefins in a very wide range, making possible the

synthesis of improved and new polyolefin materials. The most important progresses in the field, which have largely outpaced those made in heterogeneous Ti-based and Cr-based catalysts, are the understanding of the catalyst structure/polymerization mechanism/polymer structure relationships and, in part as a consequence of it, the synthesis of a large number of novel polyolefin structures, such as random, stereoblock, and syndiotactic polyolefins. Because of the large capital investment required, a large part of research has been done in industrial laboratories, and some results have only been reported in the patent literature. Metallocenes are now successfully employed in the industrial or preindustrial production of several different ethene-based polymers, in different processes, from solution to slurry to gas-phase. The feasibility of adapting metallocene catalysts to the production of propene-based materials, such as isotactic and syndiotactic polypropenes, in existing processes has been demonstrated either in pilot or industrial plant scale.

The polymerization of propene and higher 1-olefins introduces the problems of stereoselectivity (enantioface selectivity or enantioselectivity) and regioselectivity.^{31–33}

Since enantioface selectivity requires stereorigidity in addition to proper ligand symmetry and metallocene catalysts display a quite rich insertion chemistry as well as C–H and C–C activation chemistry, flocks of organic and organometallic chemists have been lured into this field. Theoretical chemists also got involved and contributed much to shed light on the mechanistic behavior of these catalysts at the molecular level. In fact, the well-defined chemical structure of metallocenes offered the exceptional opportunity for the application of emerging computational methods in an effective manner. The elementary steps and the mechanism of stereocontrol of olefin polymerization by group 3 and 4 metallocenes probably represent the most thoroughly studied organometallic reactions. The outcome of almost 20 years of highly competitive and enthusiastic research has been multifold: the performance of metallocene and related catalysts has been enormously improved; an impressive number of new molecules and new reactions to make them have been produced; new polyolefin materials have been invented; and the understanding of the elementary steps involved in the reaction between olefins and transition-metal carbon bonds has been expanded considerably.

The most successful and best studied metallocene catalysts are the chiral, C₂-symmetric *ansa*-zirconocenes, for which a large number of insertion, isomerization, and chain release reactions have been documented in the polymerization of propene. Chiral, C₂-symmetric *ansa*-zirconocenes are isospecific by virtue of their symmetry, producing isotactic polypropenes that, in comparison to Ti-based heterogeneous catalysts, have narrower molecular weight distributions, isotacticities spanning from almost atactic to perfectly isotactic, an often incomplete regioregularity (indicated by the detection of isolated secondary propene units), a random distribution of stereo- and regioerrors in the polymer chain, and lower molecular

weights, due to several facile β -hydride transfer reactions. Like any other active species involved in fast catalytic processes, metallocenes too obey Heisenberg's uncertainty principle: we cannot watch them at work without modifying them, although remarkable progress has been made in determining what an active site actually looks like. In fact, a quite detailed and predictive understanding can be reached by peering at the active sites through the X-ray structure of the metallocene catalysts precursors, the molecular modeling of the hypothetical active species, and the microstructure and end group structure of the polymers made with them. Indeed, the polymer microstructure is largely the fingerprint of the catalyst that made it.

The choice of metallocene-made polypropene as a subject worth a review stems from two considerations: the first is that, although quite a few reviews and monographies have appeared on the subject of metallocene-catalyzed polymerization of olefins,^{3,16,34–46} only two focused on polypropene;^{36,46} in addition, the catalytic polymerization of propene, although 45 years old, is still evolving at such a frantic pace that it needs to be reviewed quite often. Isotactic polypropene (*i*-PP) is produced in some 25 million tons per year with Ti/MgCl₂-based heterogeneous catalysts and is one of the fastest growing polyolefins, both in terms of sheer production volume and in the number of applications.^{47–49} The fact that metallocene catalysts can give access to PP structures not previously attainable with conventional catalysis is giving even more impetus to this market.

This review covers the homopolymerization of propene with group 4 metallocene catalysts, and special emphasis is dedicated to isotactic polypropene. Reference to other poly(1-olefins) and copolymerization between propene and minor amounts of ethene will be done only when relevant to the discussion.

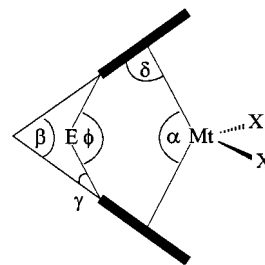
As sources of information we use here only the available scientific publications, and patent literature is cited only occasionally. This choice is due mainly to the fact that patent examples produce only very limited polymer characterization data. Views expressed on this review are those of the authors, which are not necessarily those of our employers.

II. Basic Concepts

A. Structure of Group 4 Metallocenes

As defined in the Introduction, group 4 metallocenes are d⁰, pseudotetrahedral organometallic compounds in which the transition metal atom bears two η^5 cyclopentadienyl ligands and two σ -ligands (Chart 1). The two cyclopentadienyl ligands remain attached to the metal during polymerization (for this reason they are also referred to as "ancillary" or "spectator" ligands) and actually define the catalyst stereoselectivity and activity as we will describe in detail. One or both of the two σ -ligands are removed when the active catalyst is formed. Due to their aromaticity, cyclopentadienyl anions are six-electron donors and very robust ligands. The most commonly encountered cyclopentadienyl-type ligands are cyclo-

Chart 1. General Structure of a Group 4 Bent Metallocene with the Most Relevant Angles^a



^aMt = Ti, Zr, Hf; E = R₂C, R₂Si, CH₂CH₂, etc.; X = 2 e⁻ σ -ligand.

pentadienyl itself (C₅H₅⁻, or Cp), alkylated cyclopentadienyls such as pentamethylcyclopentadienyl (Me₅Cp⁻, or Cp*), indenyl (C₉H₇⁻, or Ind), and fluorenyl (C₁₃H₉⁻, or Flu). Two good reference books on the synthesis, characterization, and reactivity of cyclopentadienyl ligands and group 4 metallocenes are available.^{25,27}

The carbon atoms of the Cp ligands can bear hydrogen or other substituents such as alkyl, aryl, or silyl groups: up to 10 different substituents are possible on a metallocene, and this high structural diversity is the reason for the high steric and electronic versatility of the Cp ligands. Different substituents change not only the size and shape of the Cp ligands, but also the Cp–Mt–Cp distances and angles. This is shown in Table 1 for a series of different zirconocenes.

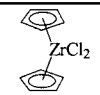

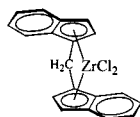
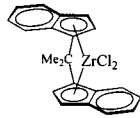
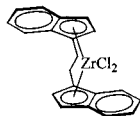
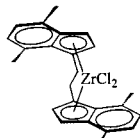
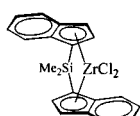
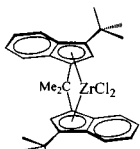
All chemical transformations relevant to metal/olefin reactions occur at the three orbitals in the plane between the two Cp rings (the "wedge" or belt). Although the electronic structure of bent bis(cyclopentadienyl) transition metal complexes has been investigated by several authors,^{52–55} the first detailed analysis of the electronic structure of group 4 metallocenes, and the implications on their chemistry, has been performed by Lauher and Hoffmann.⁵⁶ Their analysis was based on the generic metallocene reported in Scheme 1, with eclipsed Cp rings and hence of C_{2v} symmetry, and with the angle α equal to 136°. The metallocene equatorial belt is in the *yz* plane, and the C₂ axis is along the *z* axis.

As already pointed out by Brintzinger and Bartell,⁵² of the five frontier orbitals, the most important to the following discussion are the three low-lying 1a₁, b₂, and 2a₁ orbitals reported in Figure 1. All three orbitals have significant extent in the *yz* plane, which corresponds to the plane defining the equatorial belt of the metallocene. The b₂ orbital is chiefly d_{*yz*} in character, while the two a₁ orbitals in addition to contribution from the d_{*x²-y²*} and d_{*z²*} orbitals, contain s and p_{*z*} contributions. The 1a₁ orbital resembles a d_{*z²*} orbital and is directed along the *y* axis, while the 2a₁ orbital is the highest in energy among the three orbitals and points along the *z* axis. Other authors previously reached similar conclusions.

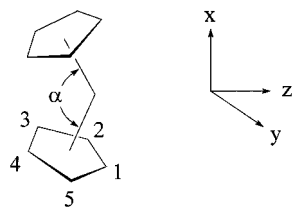
B. Activation

It is now well-established that the active polymerization species is a metallocene alkyl cation.⁵⁷ By reaction of a metallocene dichloride or dialkyl (the

Table 1. Relevant Angles (deg) of Selected Cp'ZrX₂ Complexes^a

Zirconocene	ϕ	α	γ	β	δ	ref
		129.0		53.5	88.8	50
	99.8	116.6	14.2	71.4	86.0	50
	101.4	117.4	14.5	72.4	84.8	51
	99.7	118.1	14.4	70.9	85.0	51
		126.9		62.1	84.6	51
		125.3		59.9	85.8	51
	94.6	127.8	16.3	61.8	84.8	51
	100.1	118.3	12.5	75.1	83.0	50

^a See Chart 1 for definition of the listed angles.

Scheme 1^a

^a Modified from ref 56.

stable, inactive precatalyst) and a suitable Lewis or Brønsted acid (whose conjugated base is a poorly coordinating anion), a very reactive, highly Lewis acidic cationic metal center is generated. Of the three metals, Zr is the most active, followed by Hf and Ti. The latter also suffers from deactivation at the higher temperatures, possibly because of reduction to Ti^{III}.

MAO is the most widely used cocatalyst, able to activate the largest number of metallocenes and other soluble complexes. It is obtained by the controlled hydrolysis of AlMe₃, but its composition is far from

being known. Cryoscopic, GPC, and NMR studies have shown that MAO is a mixture of several different compounds, including residual (coordinated) AlMe₃ and possibly AlO₃ units, in dynamic equilibrium.^{58–62} The generally accepted mechanism of metallocene activation by MAO is shown schematically in Scheme 2.

The true nature of the activating species in MAO has not been elucidated yet. An interesting and very detailed study carried out by Barron and co-workers^{63,64} on the hydrolysis products of Al(*t*-Bu)₃ might give some important insight on the structure(s) of oligomeric methylalumoxane. In light of Lasserre's and Barron's results, dynamic cage structures are more likely than linear or cyclic structures.

Recent DFT calculations of Zakharov and co-workers on models of MAO with structures (MeAlO)_{*n*}, with *n* = 4, 6, 8 and 12, also found that cage structures with *n* > 4 are more stable than cyclic structures.⁶⁵ According to their calculations, the cage structures with *n* = 6, 8, and 12 are more stable than

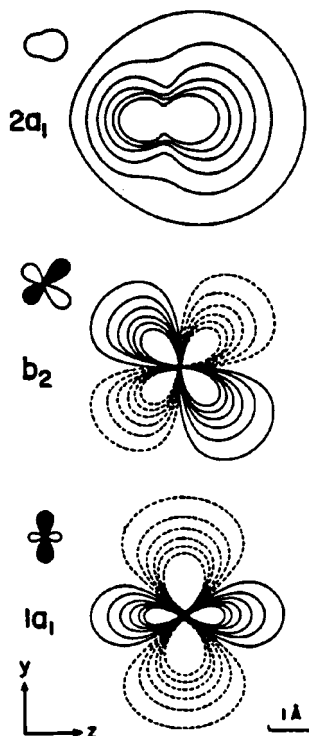
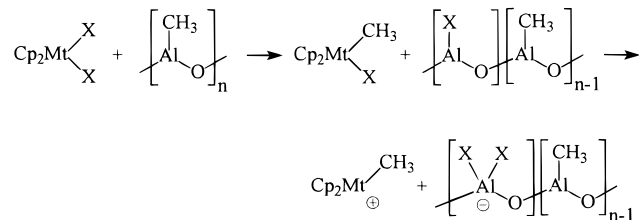


Figure 1. Contour diagram in the yz plane of the three most important extended Hückel molecular orbitals of the generic bent metallocene Cp_2Mt . Solid and dashed lines correspond to positive and negative contour of the wave function.⁵⁶

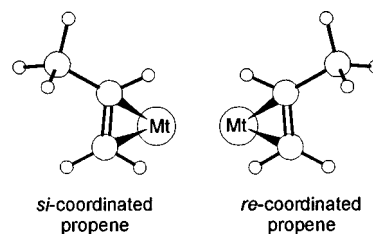
Scheme 2



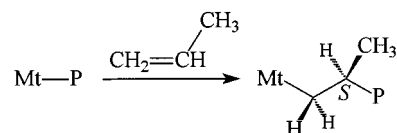
cyclic structures by roughly 15 kcal/mol of MeAlO unit.

Main drawbacks of MAO as cocatalyst are its relatively high cost, due to the high cost of the AlMe_3 parent compound; the large amount needed (typically $\text{Al/Zr} = 10^3\text{--}10^4$ M are used, although in supported systems Al/Zr ratios as low as 100 M has proven sufficient); the high residual content of catalyst residues (alumina) in the final product, especially for systems of not very high activity, as it is often the case in propene polymerization; and the intrinsic danger connected to the use of extremely pyrophoric AlMe_3 . To solve the above problems, MAO surrogates have been investigated. Reports in the patent literature include the use of MAO/ $\text{Al}(i\text{-Bu})_3$ mixtures⁶⁶ or the hydrolysis products of $\text{Al}(i\text{-Bu})_3$ and other branched aluminum alkyls.^{67–69} A different strategy toward simpler and cheaper metallocene-based systems has been the use of boron compounds such as $\text{B}(\text{C}_6\text{F}_5)_3$, $\text{NR}_3\text{H}^+\text{B}(\text{C}_6\text{F}_5)_4^-$ and $\text{Ph}_3\text{C}^+\text{B}(\text{C}_6\text{F}_5)_4^-$ in combination with metallocene dialkyls.^{46,70–76} As catalyst activation is discussed in detail in another review of this issue, we will not further discuss this point. We only add that, in most practical cases and

Scheme 3



Scheme 4. A New Stereogenic Center Is Formed at Every Insertion of a Prochiral Olefin Such as Propene, into the Metal-Growing Chain Bond (Mt-P)^a



^a For example, a methine of S chirality is formed upon insertion of a re -coordinated propene.

in order to have more reproducible results and save on the amount of cocatalyst, adding small amounts of AlR_3 (such as $\text{Al}(i\text{-Bu})_3$ and AlEt_3) to the reaction system is a common procedure to scavenge impurities and, in some cases, to alkylate the metallocene dichlorides.^{77,78}

C. Elements of Chirality

In this section we present the elements of chirality relevant to the stereospecific polymerization of propene with group 4 metallocenes. First of all, coordination of a prochiral olefin, such as propene, gives rise to nonsuperimposable coordinations.⁷⁹ To distinguish between the two propene coordinations, we prefer the nomenclature re , si —defined for specifying heterotopic half-spaces⁷⁹—instead of the nomenclature R , S —defined for double or triple bonds π -bonded to a metal atom^{80,81}—in order to avoid confusion with the symbols R and S used for other chiralities at the same catalytic site, or the nomenclature Re , Si —defined for reflection-variant units⁸²—and used by Pino and co-workers in refs 83–86. The use of the si , re nomenclature can be confusing when different monomers are considered, because the name of a fixed enantioface of an 1-olefin depends on the bulkiness of the substituent in position 1. However, since propene is the only monomer considered in this review, this problem does not exist here. We only remark that the re and si coordinations sketched in Scheme 3 correspond to the R and S coordinations, respectively.

A second element of chirality is the configuration of the tertiary carbon atom of the growing polymer chain nearest to the metal atom. In fact, a new stereogenic center is formed in the growing chain at every propene insertion (Scheme 4). The standard Cahn–Ingold–Prelog R , S nomenclature^{81,82} can be used here.

A third element of chirality is the chirality of the catalytic site, which, in particular, can be of two different kinds: (i) the chirality arising from coordinated ligands, other than the alkene monomer and the growing chain. For the case of metallocenes with

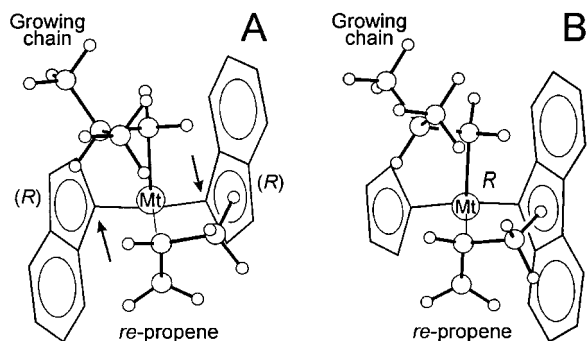


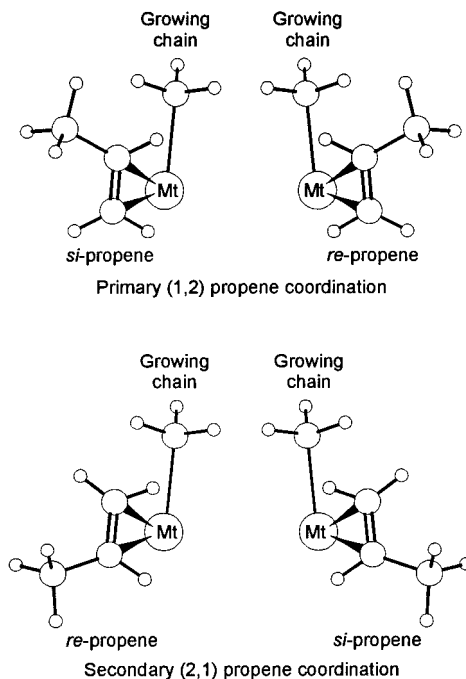
Figure 2. On the left, a model catalytic complex comprising a $\text{Me}_2\text{C}(\text{1-Ind})_2$ ligand, a propene molecule *re*-coordinated and an isobutyl group (simulating a growing primary polypropene chain). The chirality of coordination of the bridged π -ligand is (R,R) , labeled according to the absolute configurations of the bridgehead carbon atoms which are marked by arrows. On the right, a model catalytic complex comprising a $\text{Me}_2\text{C}(\text{Cp})(9\text{-Flu})$ ligand, a propene molecule *re*-coordinated and an isobutyl group. No chirality of coordination of the bridged π -ligand exists, while R is the chirality at the metal atom.

prochiral ligands, it is possible to use the notation (R) or (S) , in parentheses, according to the Cahn–Ingold–Prelog rules^{81,82} extended by Schlögl.⁸⁷ For instance, the (R,R) chirality of coordination of the $\text{Me}_2\text{C}(\text{1-Ind})_2$ ligand, labeled according to the absolute configurations of the bridgehead carbon atoms (marked by arrows), is shown in Figure 2. (ii) An intrinsic chirality at the central metal atom, which for tetrahedral or assimilable to tetrahedral situations can be labeled with the notation R or S , by the extension of the Cahn–Ingold–Prelog rules, as proposed by Stanley and Baird.⁸⁸ This nomenclature has been used to distinguish configurationally different olefin-bonded intermediates which may arise by exchanging the relative positions of the growing chain and of the incoming monomer.^{89–91} For instance, the model with intrinsic R chirality at the central metal atom is shown in Figure 2, for the case of a metallocene with a $\text{Me}_2\text{C}(\text{Cp})(9\text{-Flu})$ ligand. For the case of models with C_1 symmetric metallocenes, we will mainly use the more mnemonic notation, according to which the relative disposition of the ligands that presents the coordinated monomer in the more (less) crowded region is referred to as “inward (outward) propene coordination”,⁹² although the extended nomenclature R, S could have been used as well.

As it will be shown in detail in the following, one or both of these kinds of chirality at the catalytic site can be present in the models. For the case of model complexes in which two carbon polyhapto ligands are tightly connected through chemical bonds (the so-called bridge), which are then stereorigid (we shall call them *ansa* using the nomenclature introduced by Brintzinger), only the chirality of kind ii can change during the polymerization reaction.

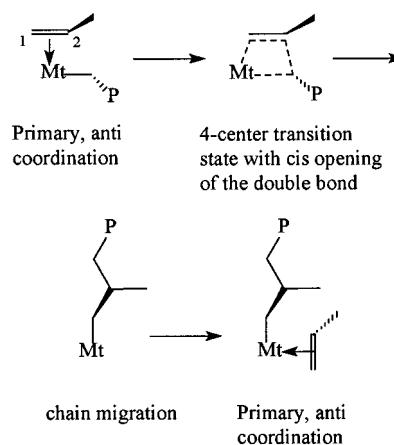
Since 1-olefins are prochiral, in principle they can coordinate and insert into a transition metal–carbon bond in four different ways (Scheme 5). Whether the olefin insertion is primary or secondary defines the *regiochemistry* of insertion (thus the catalyst *regioselectivity* and the *regioregularity* of the polymer),

Scheme 5. Four Possible Insertion Modes of a Prochiral Olefin Such as Propene, into the Mt-Growing Chain (here simulated by a methyl group) Bond^a



^a Primary propene insertion occurs when the CH_2 group of the olefin binds to the metal. Top views: the two coordination intermediates that will give rise to primary propene insertion. Secondary propene insertion occurs when the CH_2 group of the olefin binds to the growing chain. Bottom views: the two coordination intermediates that will give rise to secondary propene insertion.

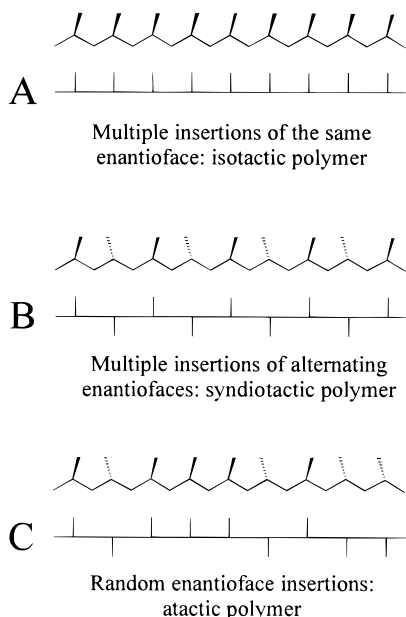
Scheme 6



while the choice of the olefin enantioface (or enantioface selectivity) defines the *stereochemistry* of each insertion (the catalyst *stereoselectivity*). The insertion of an 1-olefin into a metal–carbon bond is mostly primary (1,2), with a few exceptions that will be discussed in detail, for the case of metallocenes, in sections VII and IX.

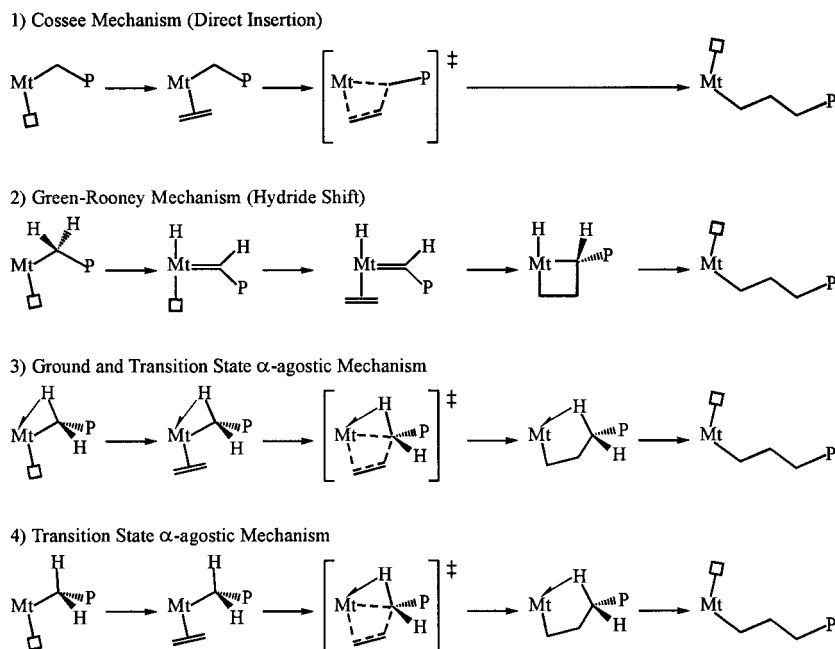
Since every propene insertion, whatever its orientation, creates a new stereogenic center, the catalyst *stereoselectivity* (and the *stereoregularity* or *tacticity* of the polymer) is determined by the stereochemical relationship(s) between the stereogenic carbon atoms in the polymer chain.

Scheme 7. Chain Segments Are Shown in Their trans-Planar and Modified Fisher Projections



In Ziegler–Natta catalysis, and in general in coordination polymerization, a polyolefin is produced by multiple insertion of olefins into a metal–carbon bond. Olefin insertion occurs by cis opening of the double bond (both new bonds are formed on the same side of the inserting olefin) and with *chain migratory insertion* (it is the alkyl group on the metal—the growing chain—that migrates to the olefin, with a net exchange of the two available coordination positions on the metal center). When insertion is primary, the 1-olefin enantioface which is inserted preferentially is the one which, in the transition state, places its substituent anti to the first C–C bond of the growing chain, since this arrangement minimizes nonbonded interactions (Scheme 6).

Scheme 8^a



^a Adapted from ref 102.

Multiple insertions of the same enantioface produce a polymer chain with chiral centers of the same configuration, i.e., an isotactic polymer (A in Scheme 7). Multiple insertions of alternating enantiofaces produce a polymer chain with chiral centers of alternating configuration, i.e., a syndiotactic polymer (B in Scheme 7). Random enantioface insertions produce a polymer chain with no configurational regularity, i.e., an atactic polymer (C in Scheme 7).

While both isotactic and syndiotactic polypropenes are partially crystalline materials with relatively high melting points (up to 160–170 °C for *i*-PP, and ~150 °C for *s*-PP), atactic polypropene (*a*-PP) is a fully amorphous polymer, since it lacks long-range stereochemical regularity.

D. Polymerization Mechanism

The key features of the insertion mechanism are that the active metal center bearing the growing alkyl chain must have an available coordination site for the incoming monomer, and that insertion occurs via chain migration to the closest carbon of the olefin double bond, which undergoes cis opening with formation of the new metal–carbon and carbon–carbon bonds: the new C–C bond is then on the site previously occupied by the coordinated monomer molecule.

So far, two main mechanistic schemes (1 and 2 in Scheme 8) have been proposed for olefin polymerization catalyzed by group 3 and 4 transition metals. The first of these mechanisms is named after Cossee^{7,93–97} and substantially occurs in two steps: (i) olefin coordination to a vacant site and (ii) alkyl migration of the σ -coordinated growing chain to the π -coordinated olefin. At the end of the reaction, a net migration of the Mt–chain σ -bond to the coordination position previously occupied by the olefin occurs. The second mechanism is due to Green and Rooney^{55,98}

and involves an oxidative 1,2-hydrogen shift from the first C atom of the growing chain to the metal, giving rise to an alkylidene hydride species bonded to the metal. A four-center metallacycle is then generated by reaction of the alkylidene moiety with a coordinated monomer molecule. The final step is a reductive elimination reaction between the hydride species bonded to the metal and the metallacycle. The Green–Rooney mechanism is ruled out because $14-e^-$, cationic d^0 metallocenes are effective polymerization catalysts, and these complexes lack the required d electrons for formal oxidative addition. The last two mechanisms of Scheme 8 are improved versions of the Cossee mechanism. The third one (also referred to as “Modified Green–Rooney mechanism”) is due to Green, Rooney, and Brookhart^{99–101} and requires the presence of a stabilizing α -agostic interaction both in the ground-state olefin complex and in the four-center transition state. Finally, the fourth mechanism (very similar to the modified Cossee mechanism 3) requires the presence of an α -agostic interaction in the transition state only.

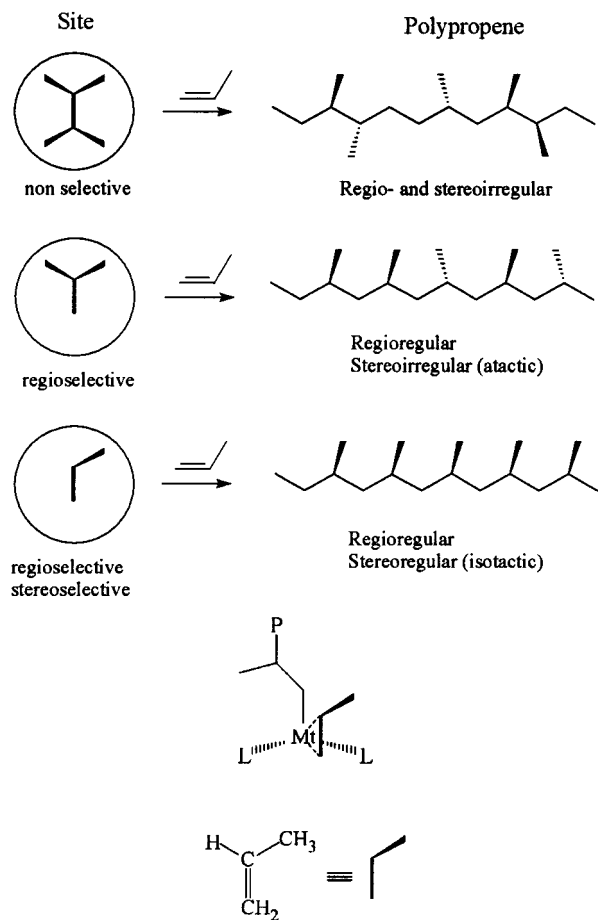
Although differences do exist between the original and α -agostic assisted Cossee mechanisms, they all agree that monomer insertion is a two-step process, that is, coordination followed by insertion. Moreover, they concord that the active metal center bearing the growing alkyl chain must have an available coordination site for the incoming monomer and that the olefin insertion occurs by (i) cis opening of the double bond and (ii) with *chain migratory insertion*. These mechanisms also indicate that in order to undergo insertion, an olefin has to coordinate face-on to the metal, with its double bond parallel to the metal–carbon bond. Whether the metal–olefin complex is a real chemical species or the olefin undergoes direct insertion into the metal–carbon bond has been a matter of debate for many years. However, several experimental and theoretical studies of the last years have established that such species do exist,^{103–111} although as transient species, and are required to explain some kinetic evidence (see section VIII).

A distinction must be made here between active center and active site: a metallocene-type active center (or active species) has a minimum of two sites (the two tetrahedral positions previously occupied by the two σ -ligands of the metallocene precatalyst) on which chain growth can take place. The nature of the active site is determined by the metal, the Cp ligands geometry, and the structure of the metal-bonded chain end. Thus, the different types of last inserted monomer unit (primary or secondary, *re* or *si* face) increase the number of possible active sites. The different sites can be different in reactivity, regioselectivity, and enantioface selectivity, and as a result, the active center itself changes during a single chain growth but statistically behaves in the same way from one polymer chain to the next. Therefore, such a species is a single-center catalyst.

If only one site can coordinate the olefin, then there is a limited number of polymer microstructures that can be obtained (Scheme 9).

Metallocene catalysts allow formation of virtually any polyolefin structure because of the two-site, chain

Scheme 9. The Key-in-the-Lock Model: One Lock, One Key^a

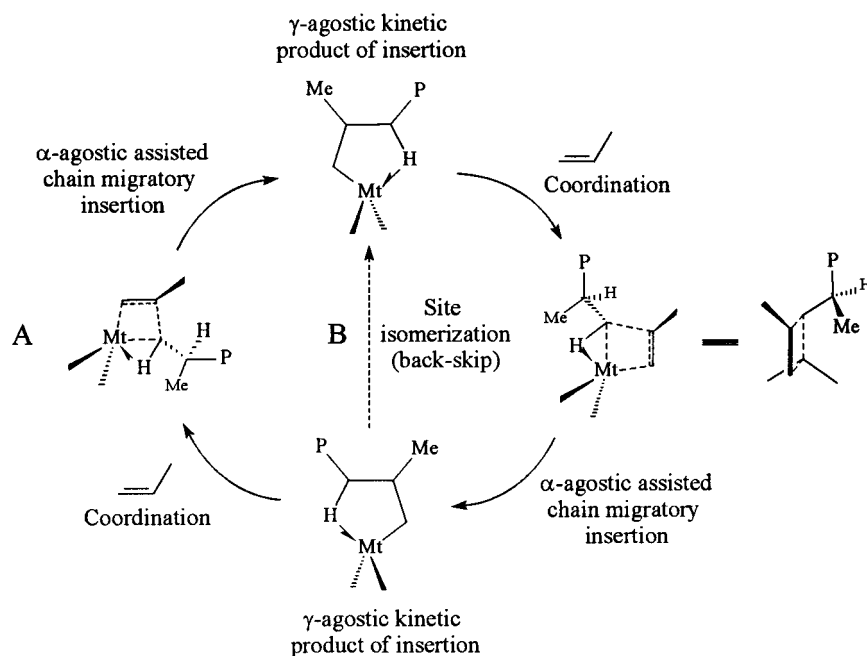


^a If the site is nonselective at all (top), propene can insert in four different ways, giving rise to a regio- and stereoirregular polypropene. If the site is regioselective but not stereoselective (middle), propene can insert in two different ways only, corresponding to nonselective primary insertion, giving rise to a regioregular but atactic polypropene. If the site is both regioselective and stereoselective (bottom), propene can insert one way only, giving rise to a regioregular and isotactic polypropene.

migratory insertion with site-switching mechanism, shown in Scheme 10. The relationship between metallocene site symmetry and polymer stereochemistry has been fully understood. We can visualize the general mechanism for enantioface selectivity, in the chain migratory insertion with site switching operating with metallocene catalysts (enantiomorphic site control), using the key-in-the-lock formalism with *two locks*. Every active metal atom has two available coordination sites (the two locks) that can both insert the olefin and that can be different in either shape or chirality. Because of site switching, the monomer has to be inserted alternately on each site.

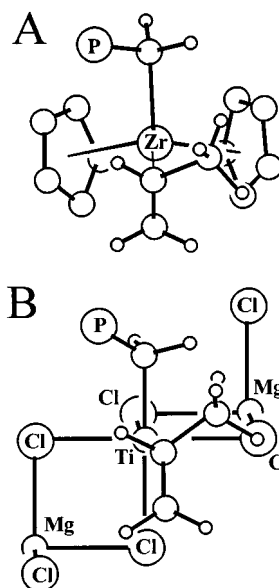
For metallocenes, pathway A is the rule, while pathway B is an occasionally skipped insertion, or it can be a competing pathway only for some highly asymmetric ligands such as, for example, in the aspecific *meso*- $C_2H_4(1-Ind)_2ZrCl_2$.⁹²

It is important to note that there are some differences between metallocenes and the available models for heterogeneous, Ti-based, catalysts: according to Arlman and Cossee,^{93–96} an octahedral, stereoselective Ti on the surface of a crystalline lattice has only

Scheme 10. The Key-in-the-Lock Model: Two Locks, One Key^a

^a Every active metal atom has two available coordination sites (the two locks), which can both insert the olefin, and that can be different in either shape or chirality. In the framework of the chain migratory insertion mechanism, the monomer has to be inserted alternately on each site, and the structure of the resulting polypropene depends on the combination of the regio- and enantioselectivity of the two active sites.

one site able to coordinate and insert the olefin. The growing chain, which has to migrate to the site previously occupied by the olefin in order to allow for insertion, then goes back to its former position, that is, strictly following pathway B (chain back-skip at every insertion). As a result, and because the ligands around the Ti atom cannot be modified at will, these catalysts are, in practice, able to produce either isotactic or atactic polypropene only (Scheme 9). On the other hand, the presence of two active polymerization sites on the same metal center of metallocene catalysts, sites that can be different in shape or symmetry, allow for a much larger set of possible polymer microstructures than with any other catalyst. In addition, as metallocenes are discrete molecules whose molecular structures can be studied in detail, the shape of the active sites can be tuned in order to obtain the desired type and degree of stereoregularity. Finally, this fine-tuning can also be done on the chain release reactions (see section III.F), thus allowing a high degree of molecular weight control. In summary, the most important differences between metallocene and heterogeneous, Ti-based polymerization catalysts are (i) metallocenes are soluble, well-characterized, and homogeneous (in the sense of chemical composition), while heterogeneous Ti catalysts contain a wide variety of active centers. (ii) Because of the above chemical homogeneity, a large fraction of the metal atoms is active in metallocene-based systems, compared to only a small fraction (usually less than 1%) of surface Ti atoms in TiCl_3 or supported TiCl_4 catalysts. (iii) Metallocene cations are pseudotetrahedral, while surface Ti is octahedral (Scheme 11). The mechanism of chain growth is different for the two classes of catalysts, with two sites available for coordination–insertion on metallocene centers, and only one on surface Ti

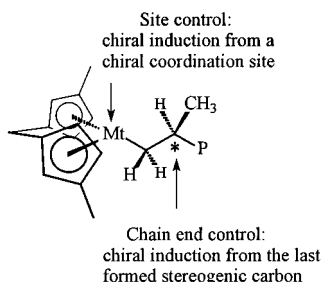
Scheme 11

atoms. (iv) According to the most recent models, stereoselective surface Ti atoms have local C_2 ⁹⁷ or isospecific C_1 symmetry (hence can produce isotactic polymers only), while metallocenes can be of C_1 , C_2 , and C_s symmetry; in addition, the ligand environment (in terms of both sterics and electronics) in metallocenes can be changed to a very large extent.

E. Mechanisms of Stereocontrol in Primary Insertion (Site vs Chain-End Control)

There are two possible sources of enantioface selectivity in olefin insertion. The most effective one is the stereogenicity of the metal active site; in this case, the mechanism of stereoselection is referred to

Scheme 12



as *enantiomorphic site control*, that is, the chiral induction comes from the asymmetry of the reaction site. It is the chirality relationship of the two coordination sites of the catalytic complex that determines the stereochemistry of the polymer. We have also seen that every monomer insertion generates a new stereogenic center. As a consequence, chiral induction (that is, enantioface preference) can come from the last unit, and this mechanism is referred to as *chain-end control* (Scheme 12).

Hence, there can be four stereospecific polymerization mechanisms in primary polyinsertion, all of which have been documented with metallocene catalysts (Scheme 13): the two originated by the chiralities of the catalyst active sites, referred to as *enantiomorphic site control* (isospecific²² and syndiospecific^{112,113} site control), can be relatively strong, with differences in activation energy ($\Delta\Delta E^\ddagger$) for the insertion of the two enantiofaces up to 5 kcal/mol. A value of 4.8 kcal/mol has been found by Zambelli and Bovey for a Ti-based heterogeneous catalyst.¹¹⁴

Because of the mechanism of enantioface selectivity and the two-site, chain migratory insertion mechanism, the microstructure of a poly(1-olefin) made with a given metallocene is, to a large extent, predictable. In a series of landmark papers, Ewen and co-workers^{22,46,112,113,116-118} and Kaminsky and co-workers²³ described a series of stereoselective metallocene catalysts which define what are now referred to as "Ewen's symmetry rules". These are summarized in Chart 2. When the metallocene molecule is C_{2v} , *meso* C_s -symmetric, or highly fluxional, an aspecific polymerization has to be expected.

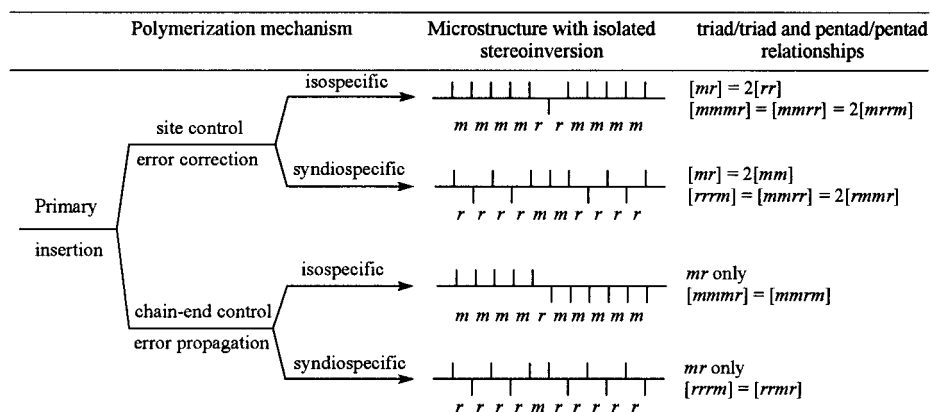
Chart 2. Steric Control as a Function of Metallocene Symmetry (Ewen's Symmetry Rules)^a

Symmetry	Sites	Polymer
C_{2v} Achiral	A, A Homotopic	Atactic
C_2 Chiral	E, E Homotopic	Isotactic
C_s Achiral	A, A Diastereotopic	Atactic
C_s Prochiral	E, -E Enantiotopic	Syndiotactic
C_1 Chiral	E, A Diastereotopic	Hemi-isotactic

^a E = enantioselective site; A = nonselective site.

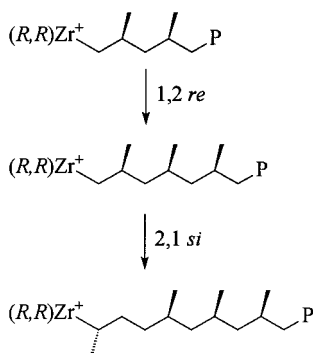
The most important cases of symmetry-related polymerizations (that is based on the mechanism of site control) of propene are discussed in sections III and IV. When the two sources of chiral induction are either absent or too weak to be effective, atactic or nearly atactic polyolefins are produced.

Truly atactic polypropene is produced by two types of metallocenes: Achiral, C_{2v} -symmetric unbridged (e.g. Cp_2ZrCl_2) and by extension any alkyl-substituted metallocene lacking stereorrigidity (e.g. $(MeCp)_2ZrCl_2$,

Scheme 13. Mechanisms of Stereocontrol in Primary 1-Olefin Polyinsertion^a

^a If the enantiomorphic site control is operative (top-half view), stereoerrors do not propagate, and the corresponding iso- and syndiotactic polymers are characterized by the presence of *rr* and *mm* triads, respectively. If chain-end control is operative (bottom-half view), stereoerrors propagate, and the corresponding iso- and syndiotactic polymers are characterized by the presence of isolated *r* and *m* diads, respectively. Reprinted from ref 115. Copyright 1992 American Chemical Society.

Scheme 14



$\text{Ind}_2\text{ZrCl}_2$) as well as bridged, stereorigid, C_{2v} -symmetric metallocenes (e.g. $\text{Me}_2\text{Si}(\text{Cp})_2\text{ZrCl}_2$ or $\text{Me}_2\text{Si}(\text{Me}_4\text{Cp})_2\text{ZrCl}_2$)^{115,119} and the achiral, *meso* isomers of *ansa*-metallocenes, such as *meso*- $\text{C}_2\text{H}_4(1\text{-Ind})_2\text{ZrCl}_2$, and *meso*- $\text{C}_2\text{H}_4(4,5,6,7\text{-H}_4\text{-1-Ind})_2\text{ZrCl}_2$.^{120,121} High molecular weight atactic polypropene has been produced with $\text{C}_2\text{H}_4(9\text{-Flu})_2\text{ZrCl}_2$ ¹²² and $\text{Me}_2\text{Si}(9\text{-Flu})_2\text{ZrCl}_2$.^{123,124} Since the synthesis of atactic polypropene with metallocene catalysts has been reviewed elsewhere,¹²⁵ it will not be further discussed here.

F. Regiochemistry of Propene Insertion

Olefin insertion into metallocene $\text{Mt}-\text{C}$ bonds is largely predominantly primary. However, one of the features of most isospecific metallocene catalysts is their generally lower regioselectivity compared to heterogeneous Ziegler–Natta catalysts: indeed, despite the fact that primary propene insertion is clearly favored by electronic factors (see section III.E), isolated secondary propene units are often detectable in *i*-PP samples and their presence is the signature of a metallocene catalyst. Tail-to-head propene insertions, currently referred to as *secondary* or *2,1* insertions, occur in *i*-PP from isospecific metallocene catalysts with high but opposite (with respect to primary insertions) enantioface selectivity (Scheme 14).

These regiodefects have a strong effect in lowering crystallinity and melting point of *i*-PP. At the same time, there is also a close correlation between catalyst regioselectivity on one side and catalyst activity and polymer molecular weight on the other, due to the lower monomer insertion rate at a secondary growing chain end, and the competing β -H transfer to the monomer after a secondary insertion. Because of these two aspects, understanding the factors controlling the regioselectivity of a metallocene catalyst is important for catalyst design. The characterization of the different regioerrors by ^{13}C NMR and the molecular modeling studies performed on the subject are discussed in section VII.A. The relative amounts of the different regiodefects are highly dependent on the metallocene ligand structure and the polymerization conditions employed (polymerization temperature and monomer concentration). Unfortunately, possibly due to the often low concentration of regioerrors and the requirement of a high-field NMR instrument and long acquisition times, few detailed studies have been carried out on the regioselectivity of metallocene catalysts and the dependence of the

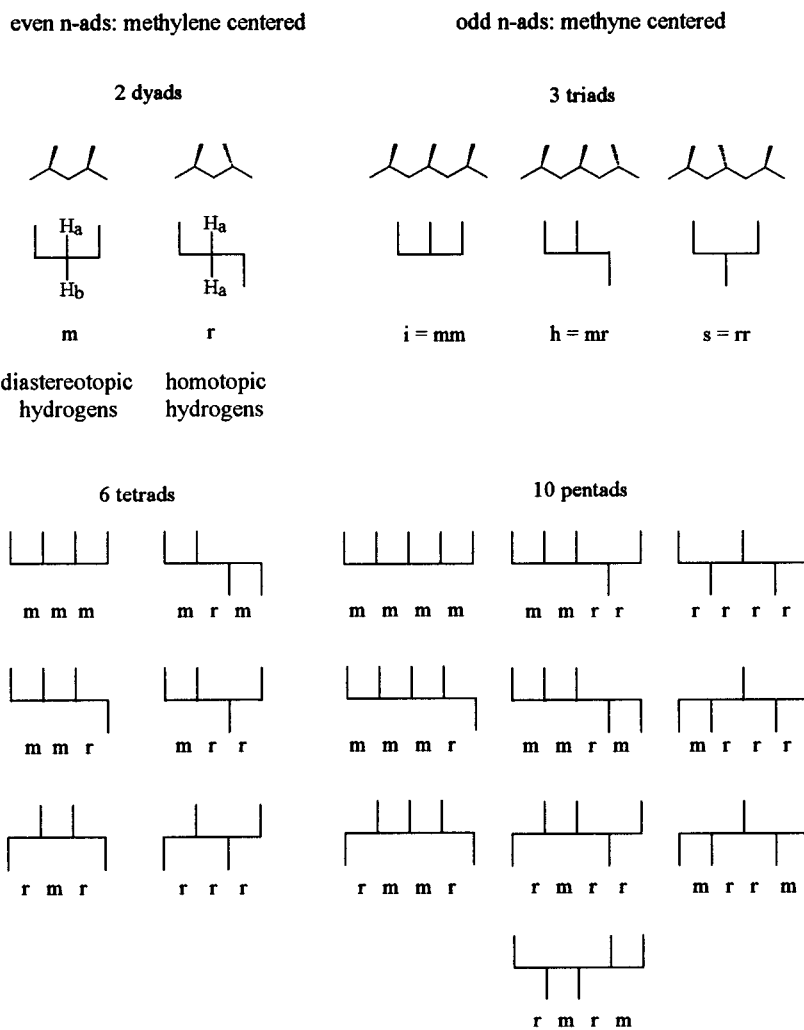
type and amounts of regioerrors on the ligand structure and the polymerization conditions. The available data are discussed in sections VII.C–E. The lower reactivity of a secondary growing chain with respect to a primary growing chain has been confirmed in three ways: by studying the activating effect of hydrogen (see section IX), by copolymerization with ethene,^{126–129} and by end group analysis.^{130,131} The latter two aspects are discussed in section VII.B. In section VII.F we discuss the proposed mechanisms of isomerization of a secondary growing chain into a 3,1 unit.

G. ^{13}C NMR Analysis of Polypropenes

The most powerful (if not the only) tool for the determination of the microstructure of polyolefins and the polymerization mechanism is solution ^{13}C NMR.^{132–135} In the case of polypropene, the chemical shift of the methyl groups is highly sensitive to the relative stereochemistry of neighboring monomer units, that is, each methyl C has a different chemical shift depending on the configuration of the adjacent methylenes, up to five on each side (a sequence length of 11 consecutive monomer units). Usually, statistical analysis is done at the pentad (sequence length of five consecutive monomer units) level. The degree of isotacticity can be given as the pentad, triad, or diad content (% *mmmm*, % *mm*, % *m*, respectively, Chart 3). For polyolefins of low stereoregularity, the degree of iso (syndio) tacticity is better given as the diad excess, % *m* – *r* (% *r* – *m*).¹¹⁵ Isolated insertion errors (as both secondary units or opposite enantiofaces) are easily and quantitatively detected by ^{13}C NMR analysis, and triad/pentad analysis gives unambiguous identification of the polymerization mechanism. Some useful relationships for the four stereospecific polymerization mechanisms discussed above (see Scheme 13) are (a) isospecific site control: main peak, *mmmm*; misinsertions, $[mr] = 2[rr]$; $[mmmr] = [mmrr] = 2[mrrm]$; (b) syndiospecific site control: main peak, *rrrr*; misinsertions, $[mr] = 2[mm]$; $[rrrm] = [mmrr] = 2[rmmr]$; (c) isospecific chain-end control: main peak, *mmmm*; misinsertions, *mr* only; $[mmmr] = [mrrm]$; (d) syndiospecific chain-end control: main peak, *rrrr*; misinsertions, *mr* only; $[rrrm] = [rmmr]$. Site control is identified by the relationships $2[rr]/[mr] = 1$ (isospecific) and $2[mm]/[mr] = 1$ (syndiospecific). Chain-end control is identified by the relationship $4[mm][rr]/[mr]^2 = 1$. The average block length is obtained as $2[m]/[r] + 1$ (isospecific triad test) and $2[r]/[m] + 1$ (syndiospecific triad test). The proton spectra (400 MHz, $\text{C}_2\text{D}_2\text{Cl}_4$, 120 °C) of *i*-PP and *s*-PP are compared in Figure 3. The methyl pentad region of the 100 MHz ^{13}C NMR spectra of atactic, isotactic, and syndiotactic polypropene is shown in Figure 4a. By comparison with the methine (Figure 4b) and methylene (Figure 4c) regions of the ^{13}C NMR spectra, it is evident how much more stereochemical information can be extracted from the methyl resonances.

III. Elementary Steps

Many quantum mechanics studies have been devoted to clarifying the elementary steps of olefin

Chart 3. Nomenclature and Symmetry of Stereosequences in Polypropene^a

^a *m* = "meso" diad, *r* = "racemic" diad, *i* = isotactic triad *mm*, *h* = heterotactic triad *mr*, *s* = syndiotactic triad *rr*.

coordination and insertion in systems based on the simplest Cp₂Mt metallocenes, bridged or not. Since propene increases considerably the number of situations to be studied (propene can coordinate in four different ways, while ethene just in one), and the insights gained into the elementary coordination and insertion steps would not be much deeper, the largest amount of these investigations used ethene as monomer, and only a few of them considered propene. For this reason, the following sections regarding the coordination and insertion steps will mainly focus on ethene. As the topic becomes the mechanism of stereocontrol, obviously propene and chiral ligands (hence more complex than Cp₂) have to be considered. So far, all studies regarding the enantioselectivity in primary or secondary insertion, as well as the effect of ligand substitution on both enantioselectivity and regioselectivity, have been accomplished by using the molecular mechanics approach. However, the recent development of combined quantum mechanics/molecular mechanics, QM/MM, techniques certainly represents one more weapon in the armory of computational chemists.^{137–145} This technique merges the accuracy of the QM methods in describing the reactive part of the system—breaking/forming of bonds—with the computational advantages of the MM meth-

ods in describing the steric effect due to the catalyst ligands.

A. Alkene-Free Species

The position of a single σ -bonding ligand is extremely relevant to homogeneous polymerizations. In fact, the destiny of the growing chain at the end of each insertion step—i.e., whether it remains in the position previously occupied by the monomer, or it is free to switch between the two coordination positions, or it is preferentially oriented along the local symmetry axis relating the two Cp rings—is *fundamental* in determining the stereoselective behavior of *C*₁ and *C*_s-symmetric catalysts. This will be discussed in more detail in section IV.

To understand the geometries assumed by the growing chain in the absence of a further ligand (e.g. counterion, solvent, monomer) we have to understand the interactions between a simple σ -bonding ligand with the bare Cp₂Mt skeleton. With the usual extended Hückel molecular orbitals analysis, Hoffmann elegantly showed that a simple σ -bonding ligand, as H⁻, which approaches the d⁰ metallocene skeleton along the *z* axis (corresponding to the local symmetry axis in Scheme 15) will interact very well with the high-energy 2a₁ orbital (see Figures 5 and 1), some-

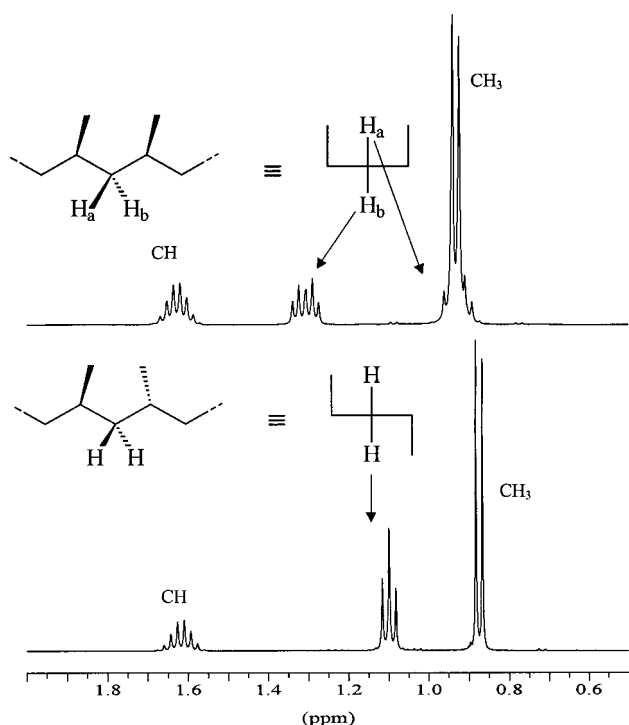


Figure 3. ^1H NMR (400 MHz, $\text{C}_2\text{D}_2\text{Cl}_4$, 120°C) of *i*-PP (top) and *s*-PP (bottom). Assignments of the diastereotopic methylene protons in *i*-PP are according to ref 136.

what with the $1a_1$ orbital, and not at all with the b_2 orbital.⁵⁶ If a different geometry is adopted, one with the H^- ligand forming an angle $\alpha \neq 0^\circ$ with the z axis, stabilizing interactions of the σ -orbital of the H^- ligand with the low-lying $1a_1$ and b_2 orbitals of the metallocene can be obtained. For the hypothetical Cp_2TiH^+ system, the energy minimum is calculated to come at about $\alpha = 65^\circ$.

Other authors subsequently revisited these conclusions at higher levels of theory, which should provide more reliable energetics. However, the results are not clear-cut. As for the simple model systems of the type $\text{Cl}_2\text{TiCH}_3^+$ and $\text{H}_2\text{TiCH}_3^+$, calculations based on classical *ab initio*,^{146–150} GVB,¹⁵¹ DFT,^{148,150} and top-level CCSD(T) methods¹⁵⁰ are in agreement with the conclusions of Hoffmann. As the models include the more representative Cp rings, the results obtained with different methods are contradictory. If the σ -ligand is H^- , all the reported calculations are in agreement with results of Hoffmann.^{151–154} On the contrary, when the σ -ligand is CH_3^- , the HF and MP2 calculations of Morokuma on $\text{H}_2\text{Si}(\text{Cp})_2\text{Mt}(\text{CH}_3)^+$ (Mt = Ti, Zr, Hf),^{153,155} the Car–Parrinello molecular dynamics simulations of Meier on the same Ti system,¹⁵⁶ and the HF calculations of Ahlrichs on the $\text{Cp}_2\text{Ti}(\text{CH}_3)^+$ system¹⁴⁹ suggested that the CH_3 group is oriented along the symmetry axis, although in the crystalline structure of $[\text{1,2-(CH}_3)_2\text{C}_5\text{H}_3]_2\text{Zr}(\text{CH}_3)^+\cdot\text{CH}_3\text{B}(\text{C}_6\text{F}_5)_3^-$ the methyl group is clearly off-axis.⁷⁵ Morokuma and co-workers suggested that the off-axis orientation of the methyl group (see Scheme 15) in the crystalline structure could be due to the presence of the negative counterion. With the methyl group off-axis, a better electrostatic interaction between the two charged ions could be obtained. On the contrary, the MP2 and DFT calculations of Ahlrichs on the Cp_2 -

$\text{Ti}(\text{CH}_3)^+$ system¹⁴⁹ and the DFT calculations of Ziegler on the $\text{Cp}_2\text{Ti}(\text{CH}_3)^+$ and $\text{H}_2\text{Si}(\text{Cp})_2\text{Zr}(\text{CH}_3)^+$ systems¹⁵² suggested that the CH_3 group is off-axis oriented.

The GVB calculations of Goddard and co-workers, moreover, showed that the value of the Cp-Mt-Cp bending angle α influences the relative stability of the on- and off-axis geometries.¹⁵¹ The on-axis geometry is favored by larger α values, due to an increased steric pressure of the Cp rings on the R group, which clearly favors the on-axis geometry.

A systematic study by Ziegler and co-workers on various d^0 systems of the type $\text{L}_2\text{MtCH}_3^{n+}$ ($n = 0, 1$), where Mt is a group 3 or 4 metal atom and L is CH_3 , NH_2 , or OH ,¹⁵⁷ suggested an increased preference for the off-axis conformation as one moves down within a triad. This result was explained by a reduced steric pressure of the L ligands (which favors the on-axis geometry) of the L ligands bonded to a big metal at the bottom of the triad. Moreover, the energy of the $2a_1$ orbital, which is responsible for on-axis bonding, increases along the triad and therefore the preference for the off-axis geometry is enhanced.¹⁵⁷

As for d^0 group 3 metallocenes, Goddard¹⁵¹ and Ziegler^{157,158} and their co-workers found on-axis geometries for the Cp_2ScH ,¹⁵¹ Cp_2ScCH_3 ,¹⁵⁸ and $\text{L}_2\text{-MtCH}_3$ ¹⁵⁷ (L = CH_3 , NH_2 , OH) species. The preferential on-axis geometry for all the neutral Sc species was ascribed to the higher s orbital contribution to bonding for group 3 metals with respect to group 4 metals.^{151,157}

Finally, it is worth noting that all the above studies have shown that the potential energy surface corresponding to the swing motion of the σ bonding ligand in the equatorial belt of the metallocene is very shallow. In all cases, the favored geometry, either on- or off-axis, is favored by no more than 5 kcal/mol when Cp rings are present.

As an alkyl group longer than a simple methyl group is σ -bonded to the metal atom, the situation is different, due to the possible formation of β - and γ -agostic bonds. With group 4 metallocenes, all authors substantially found an off-axis geometry when a β - or γ -agostic bond is present. However, the systematic study of systems of the type $\text{L}_2\text{MtC}_2\text{H}_5^{n+}$ ($n = 0, 1$), where Mt is a group 3 or 4 metal atom and L is CH_3 , NH_2 , or OH , performed by Ziegler and co-workers, showed that the β -agostic bond only weakly perturbs the potential energy surface, which substantially remains similar to those present in the systems $\text{L}_2\text{MtCH}_3^{n+}$.¹⁵⁷ Finally, it is clear that the presence of a γ -agostic bond favors off-axis geometries, since the on-axis geometry would push the C atom which participates in the γ -agostic interaction toward the Cp rings.

B. Agostic Interactions

As we will see, agostic interactions^{102,159–161} are almost ubiquitous in Ziegler–Natta catalysis. The X-ray structures of $(\text{MeCp})_2\text{Zr}[(\text{Z})\text{-C}(\text{Me})=\text{C}(\text{Me})(n\text{-Pr})](\text{THF})^+$ and of $(\text{MeCp})_2\text{Zr}(\text{C}_2\text{H}_5)(\text{PMe}_3)^+$, obtained by Jordan and co-workers,^{162,163} represent typical examples of such interactions. In both cases, see Figures 6 and 7 short Zr-C_β and Zr-H_β distances

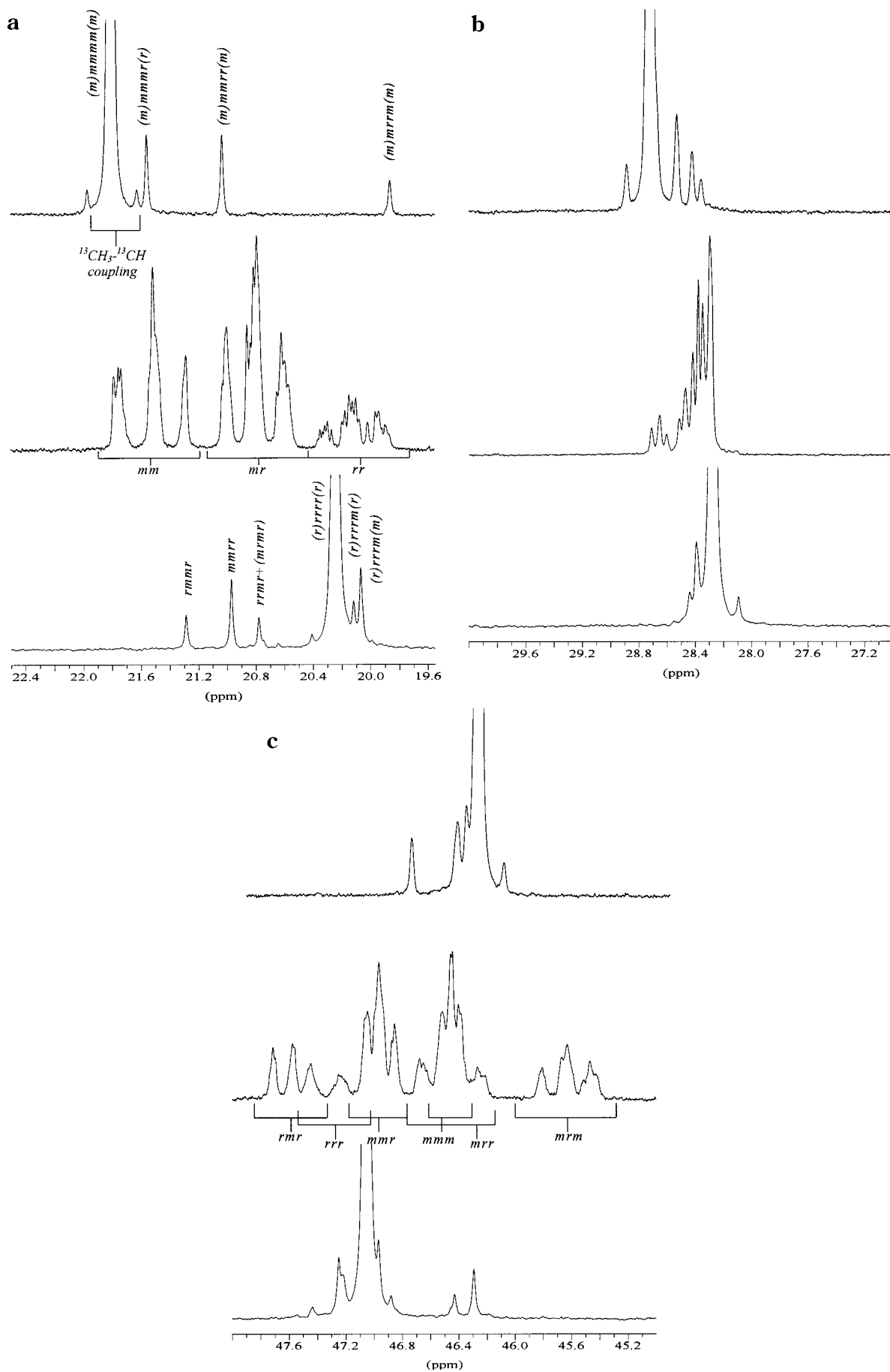


Figure 4. The 100 MHz ^{13}C NMR spectra of isotactic (top), atactic (middle), and syndiotactic (bottom) polypropenes: (a) methyl pentad region, (b) methine pentad region, and (c) methylene pentad region.

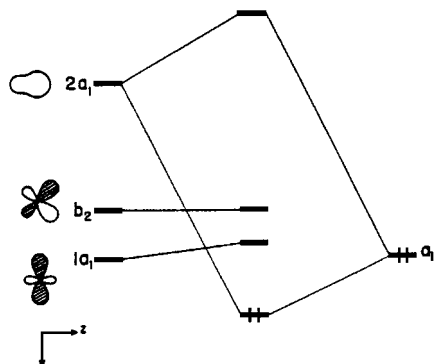
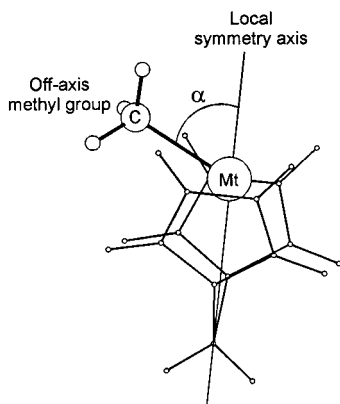


Figure 5. Interaction diagram for the generic d^0 bent metallocene Cp_2Mt , on the left, and H^- , on the right. The orbitals are sketched in the yz plane.⁵⁶

Scheme 15



(about 2.7 and 2.2 Å, respectively) are observed, together with a small $Zr-C_\alpha-C_\beta$ angle (about 90°). Similar agostic interactions were also reported by other authors.^{164–166}

The nature of the agostic interaction was studied by Morokuma, with *ab initio* calculations on the $Ti-(C_2H_5)(PH_3)_2Cl_2H$ complex.^{167,168} An agostic interaction mainly consists of a delocalization of electron density from the $C-H$ σ -bonding orbital to empty d orbitals of the metal. The agostic interactions most important to Ziegler–Natta polymerization by group 4 metals are the α -, β -, and γ -interactions from the corresponding $C_\alpha-H$, $C_\beta-H$, and $C_\gamma-H$ σ -bonding orbitals. The geometry of *n*-butyl groups showing α -, β -, and γ -agostic interactions are shown in Figure 8.

Usually, the most stable geometry corresponds to the β -agostic, followed by the γ and then the α ones. As examples, for the $H_2Si(Cp)_2Zr(n\text{-propyl})^+$ system Morokuma and co-workers calculated the γ -agostic geometry to lay 2.0 kcal/mol above the β -agostic one,¹⁵³ while for the $Cp_2Zr(n\text{-propyl})^+$ system, Ziegler and co-workers calculated that the γ - and the α -agostic geometries lay 6.4 and 11.2 kcal/mol above the β -agostic one.¹⁶⁹

Although the agostic interactions are mainly due to donative interaction from the $C-H$ bond, Morokuma¹⁴⁶ and Ziegler¹⁶⁹ noticed that some donation can occur from the $C-C$ σ -bonding orbitals as well. The two molecular orbitals sketched in Figure 9 indicate such donation from both the $C_\alpha-C_\beta$ and $C_\beta-C_\gamma$ bonds.¹⁴⁶

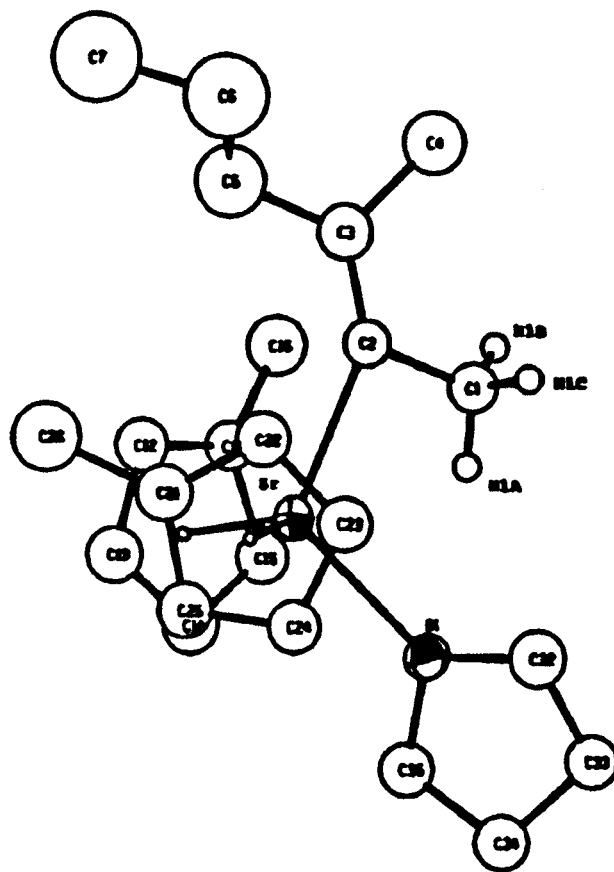


Figure 6. X-ray structure of $(MeCp)_2Zr[(Z)-C(Me)=C(Me)-(n\text{-Pr})](THF)^+$. Reprinted from ref 162. Copyright 1989 American Chemical Society.

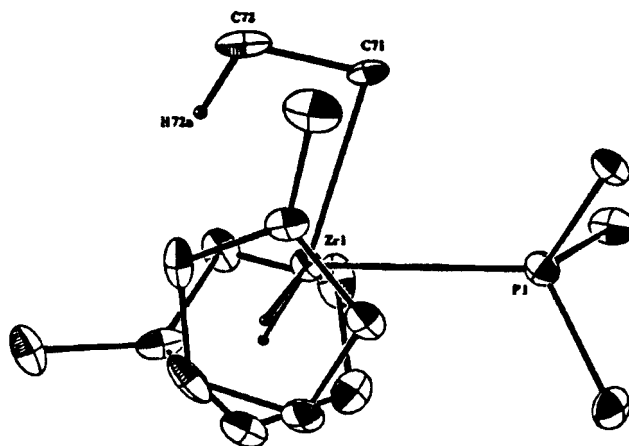


Figure 7. X-ray structure of $(MeCp)_2Zr(C_2H_5)(PMe_3)^+$. Reprinted from ref 163. Copyright 1990 American Chemical Society.

C. Olefin Coordination

The electronics behind olefin coordination to group 4 cationic L_2MtR^+ species has been studied in details by Marynick, Morokuma, and co-workers.^{146,170} Their analysis indicates that while the $Mt-R$ bond in the C_s -symmetric $Cl_2TiCH_3^+$ species chiefly involves a metal orbital which corresponds to the $1a_1$ orbital of Figure 1, the olefin coordination is due to in-phase interactions between the olefin π -orbital with metal orbitals corresponding to the $2a_1$, mainly, and to one lobe of the $1b_2$ orbitals of Figure 1. A good overlap between the olefin π -orbital and these metal orbitals

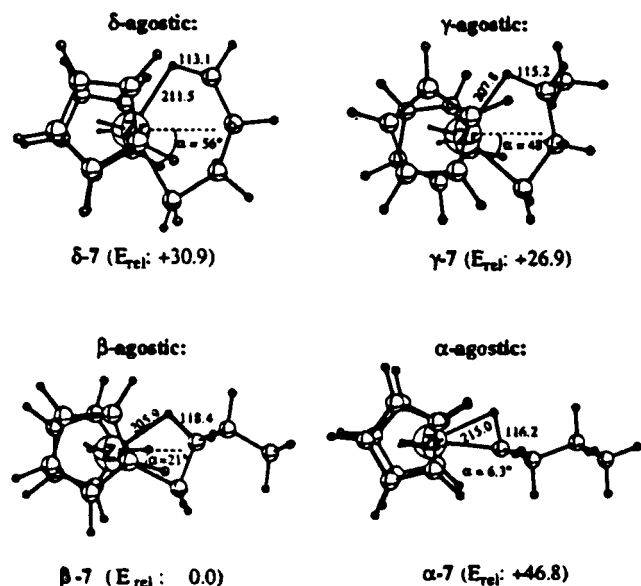


Figure 8. Orientations of the *n*-butyl alkyl group in Cp₂-Zr(*n*-butyl)⁺. Relative energies in kJ/mol, distances in pm, angles in deg.¹⁶⁹

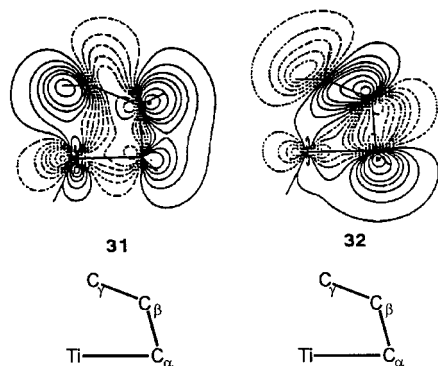


Figure 9. Contour maps of occupied molecular orbitals (MO) showing donative interaction from the C_β-C_γ and C_γ-H bonds (MO 31) and from the C_α-C_β and C_β-C_γ bonds (MO 32).¹⁴⁶

is obtained also when the olefin is rotated by 90°, to assume a geometry in which the C-C double bond is perpendicular to the equatorial belt of the metallocene. This implies a small electronic barrier to olefin rotation. Finally, since group 4 cations contain d⁰ metals, no back-bonding from the metal to the olefin π*-orbital is present. The orbital interaction diagram depicted in Figure 10 shows the most important orbitals involved in the coordination of ethene to the Cl₂TiCH₃⁺ system. The main interaction occurs between the lowest vacant orbitals of the TiCH₃⁺ fragment, MOs 21a' and 22a', which resemble the MOs 2a₁ and b₂ of Figure 1, with the doubly occupied π-orbital of the ethene fragment, 6a'.

The olefin uptake energy to alkene-free group 4 metallocenes of the type Cp₂Mt(alkyl)⁺ has been calculated by several authors. When the alkyl group is the simple methyl group, olefin coordination usually occurs in a barrierless fashion, and uptake energies in the range 15–30 kcal/mol (depending on the particular computational approach/metallocene considered) have been calculated.^{149,152,153,171} There are a few exceptions to this general behavior. For example, in the coordination of ethene to the Cp₂-

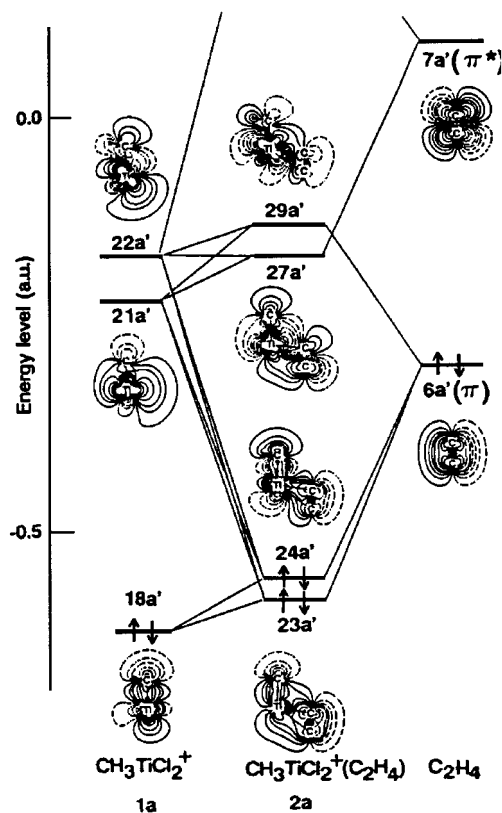


Figure 10. Orbital interaction diagram for coordination of the ethene fragment (on the right) to the Cl₂TiCH₃⁺ fragment (on the left). The MOs of the full TiCH₃(ethene)⁺ complex are depicted in the middle. Only the most important MOs are included.¹⁴⁶

TiCH₃⁺ system, computed at correlated MP2 level by Ahlrichs and co-workers, the olefin complex is not a stable species and directly inserts into the Ti-methyl σ-bond.¹⁴⁹ Also, the coordination of ethene to systems of the type Cp₂Mt(alkyl)⁺(CH₃ClAl[O(Al(CH₃)₃AlHCH₃)₂]⁻—the last fragment simulating MAO—has been calculated by Fusco and co-workers: according to their analysis, the formation of an ethene complex with the olefin sandwiched between the Cp₂Mt-(alkyl)⁺ and (CH₃ClAl[O(Al(CH₃)₃AlHCH₃)₂]⁻ fragments is unfavored by roughly 5–10 kcal/mol.^{172,173} Finally, according to Rytter, Ystenes, and co-workers,¹⁷¹ ethene coordination to the bulky (Me₅-Cp)₂ZrCH₃⁺ system requires the overcoming of a small energy barrier, essentially due to repulsive interactions between the olefin and methyl groups of the Me₅Cp ligands, and the olefin uptake energy is only 2–3 kcal/mol. For neutral d⁰ scandocenes, the interaction between the olefin and the metallocene is reduced due to the absence of the favorable electrostatic cation-olefin interaction.^{152,174} As a consequence, ethene uptake energies have been calculated to be roughly 20 kcal/mol lower than the corresponding uptake energies for the analogous cationic group 4 metallocene.

For group 4 metallocenes, ethene uptake energies in the range 5–10 kcal/mol have been calculated when alkyl groups longer than methyl are bonded to the metal atom and β- or γ-agostic interactions are present.^{152,169,171} The olefin uptake still is a barrierless process, unless bulky ligands as Me₅Cp rings are considered.¹⁷¹ The substantially lower uptake energy

values calculated in the presence of alkyl groups longer than methyl are ascribed to the presence of a β - or γ -agostic interaction that stabilizes the alkene free metallocene. Propene has been found to interact better than ethene with the metallocene, since slightly higher uptake energies, roughly 2–3 kcal/mol, have been calculated for coordination of a propene molecule.¹⁷⁵ However, steric hindrance can be particularly relevant. As an example, the propene uptake energy to the unencumbered $\text{H}_2\text{C}(\text{1-Ind})_2\text{Zr}(\text{isobutyl})^+$ β -agostic system amounts to 12.7 kcal/mol, whereas the presence of the bulky *tert*-butyl group in the $\text{H}_2\text{C}(\text{3-}t\text{-Bu-1-Ind})_2\text{Zr}(\text{isobutyl})^+$ β -agostic system reduces the propene uptake energy to 6.6 kcal/mol only.¹⁷⁵

Although olefin uptake energies close to 10 kcal/mol were calculated, the coordinated olefin has a quite high mobility. As previously discussed in terms of molecular orbitals, rotation of the coordinated olefin around the axis connecting the metal atom to the center of the C–C double bond is easy. This is suggested also by the static *ab initio* calculations of Morokuma and co-workers, which calculated the barrier for olefin rotation in the system $\text{Cl}_2\text{TiCH}_3\text{-(ethene)}^+$ to be lower than 1 kcal/mol,¹⁴⁶ and by the first principles molecular dynamics simulation of the $\text{Cp}_2\text{ZrC}_2\text{H}_5\text{-(ethene)}^+$ system by Ziegler and co-workers.¹⁷⁶ The latter simulation also indicated that the olefin is quite capable of dissociating from the metal atom at room temperature.

Before concluding this section, it has to be remembered that all the above calculations have been obtained by neglecting solvent effects. For cationic group 4 metallocenes, the solvent/metallocene interaction is mainly electrostatic (as the olefin/metallocene interaction). Therefore, it is reasonable to expect similar solvent/metallocene and olefin/metallocene coordination energies and a small barrier due to solvent displacement.¹⁷⁷ Moreover, the uptake energy values only represent a contribution to the total free energy of coordination. In fact, an always unfavorable uptake entropy has to be accounted for. Although few experimental data are available, it is reasonable to assume that the $-T\Delta S$ contribution to the free energy of olefin coordination to group 4 metallocenes at room temperature is close to the 10 kcal/mol value observed at 300 K for Ni and Pd compounds.¹⁷⁸ The few computational data also suggest a $-T\Delta S$ contribution close to 10 kcal/mol.^{157,179} As a consequence, olefin uptake energies higher than 10 kcal/mol are required to form stable olefin complexes in the gas phase. Again, the picture is quite different in solution, since olefin coordination probably requires the displacement of a coordinated solvent molecule. The entropy loss due to the olefin coordination could be counterbalanced by the entropy gain due to the dissociation of a coordinated solvent molecule. In conclusion, it is reasonable to expect that coordination/dissociation of the olefin from the metallocene is a process with a low energy barrier and with low energy gain/loss.

Experimentally, examples of olefin adducts of d^0 metallocenes are scarce. Moderately stable olefin adducts have been obtained when the olefin is

tethered to the metal^{105–108,180} or to the Cp ligands.¹¹¹ The experimental ΔG^\ddagger values for metal olefin dissociation are close to 10 kcal/mol.^{105,107,111} Probably, the presence of the tether reduces strongly the entropy gain that favors the olefin dissociation, inducing the so-called “chelation effect”. Upper bounds to the olefin uptake energy can be obtained by measurements of the π - σ - π processes in fluxional allyl derivatives of group 3¹⁸¹ and group 4¹⁸² metallocenes. Again, ΔG^\ddagger values close to 10 kcal/mol were observed. Systematic studies on olefin coordination to transition metals (not being part of a metallocene, though) have been reported by Siegbahn,¹⁸³ Bauschlicher,¹⁸⁴ and Ziegler¹⁵⁷ and their co-workers.

D. Insertion

The insertion reaction of a coordinated olefin into the Mt-C σ -bond, where Mt is a group 4 metallocene, or a model of it, has been the subject of several theoretical studies.^{56,146–150,152,153,156,169–171,174,176,177,185–190}

All authors agree that the insertion reaction occurs through a slipping of the olefin toward the first C atom of the growing chain and that the four-center transition state assumes an almost planar geometry. In Figures 11 and 12, the geometry of the transition states for ethene insertion into the Zr-CH_3 bond of the $\text{H}_2\text{SiCp}_2\text{ZrCH}_3^+$ and $\text{Cp}_2\text{ZrCH}_3^+$ systems, calculated by Morokuma¹⁵³ and Ziegler,¹⁵² respectively, are presented.

Although obtained with substantially different computational approaches—Hartree–Fock for $\text{H}_2\text{SiCp}_2\text{ZrCH}_3^+$ and DFT for $\text{Cp}_2\text{ZrCH}_3^+$ —the similarities between the two structures are quite strong. The main features of the geometries reported in Figures

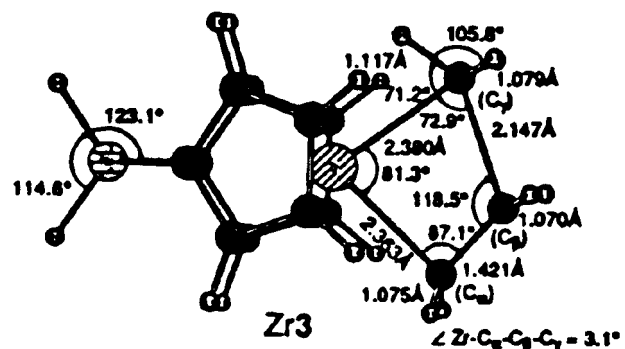


Figure 11. Hartree–Fock optimized structure of the transition state for insertion of ethene into the Zr-CH_3 bond of the system $\text{H}_2\text{Si}(\text{Cp})_2\text{ZrCH}_3^+$.¹⁵³

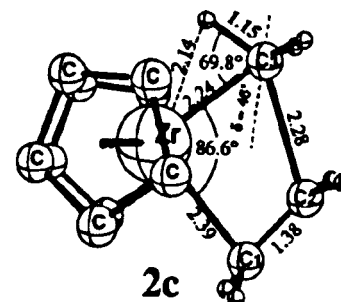


Figure 12. DFT optimized structure of the transition state for insertion of ethene into the Zr-CH_3 bond of the system $\text{Cp}_2\text{ZrCH}_3^+$.¹⁵²

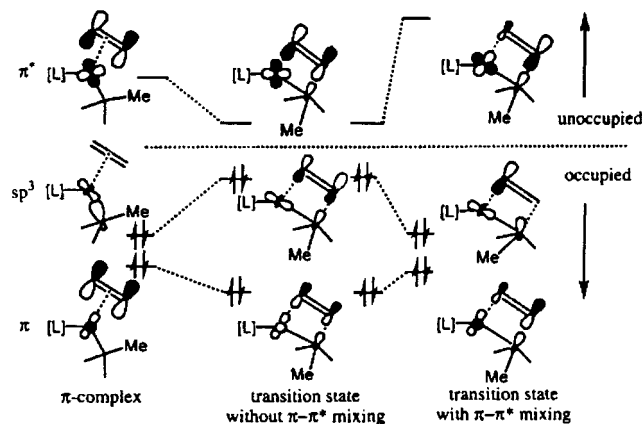


Figure 13. Molecular orbital diagram of the mixing process involved in the insertion of olefin into a metal-carbon bond. Orbital occupations are shown for the formal d^0 configuration on the metal.¹⁹¹

11 and 12 indicate a very asynchronous transition state. In fact, in both structures the Zr-C bond that is going to be formed is only 5–10% longer than in the products, while the other bond being formed, the new C-C bond, is roughly 40% longer than in the products. Finally, the Zr-C bond that is going to be broken is only 5% longer than in the reactants, while the ethene C-C bond distance is quite closer to the value it has in the reactants than in the products. All these observations indicate an early transition state of very tight geometry. For a model based on the analogous group 3 Cp_2ScCH_3 system, the transition state is only slightly more advanced relative to the one for the cationic zirconocene.^{152,174}

The electronics behind the insertion reaction is generally explained in terms of a simple three-orbital four-electron scheme. Hoffmann and Lauher early recognized that this reaction is an easy reaction, indeed, for d^0 complexes, and they also recognized the relevant role played by the olefin π^* -orbital in determining the insertion barrier.⁵⁶ According to them, the empty π^* -orbital of the olefin can stabilize high-energy occupied d orbitals of the metal in the olefin complex, but this stabilization is lost as the insertion reaction approaches the transition state. The net effect is an energy increase of the metal d orbitals involved in the back-donation to the olefin π^* -orbital.⁵⁶ Since for d^0 systems this back-donation does not occur, d^0 systems were predicted to be barrierless, whereas a substantial barrier was predicted for d^2 systems.⁵⁶

A similar picture has been suggested by the DFT calculations of Ziegler and co-workers through a systematic study of the chain propagation reaction by complexes with d^0 and d^0f^n transition metals.¹⁹¹ Their discussion is based on the MO diagram shown in Figure 13. In agreement with Hoffmann and Lauher, for d^0 systems the lowest unoccupied molecular orbital (LUMO) of the olefin complex chiefly corresponds to a bonding olefin π^* -d metal interaction. In the transition state, the occupied sp^3 orbital of the first C atom of the growing chain (the one bonded to the metal) and the occupied π -orbital of the olefin form an energetically unfavorable bonding/antibonding combination. Now, if the empty π^* -

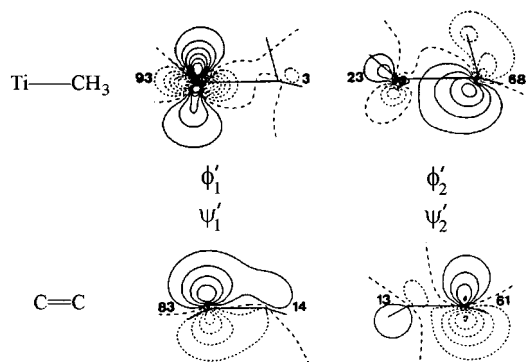


Figure 14. Dominant pairs of interacting orbitals in the transition state for ethene insertion into the Ti-methyl bond of the $Cl_2TiCH_3^+$ system. Adapted from ref 185.

orbital of the olefin mixes in, the antibonding character of the highest occupied molecular orbital (HOMO) is transformed in a substantially more stable, nonbonding HOMO, while the energy of the LUMO rises due to the π - π^* mixing. Again, for d^0 systems, the insertion reaction is substantially barrierless, since the LUMO energy does not contribute to the total energy, whereas for d^2 systems it is not, since for these systems the HOMO corresponds to the high-energy LUMO of d^0 systems. To quantify this point, Ziegler and co-workers compared the insertion barrier for ethene insertion into the cationic d^0 $Cp_2TiC_2H_5^+$ and neutral d^1 $Cp_2TiC_2H_5$ systems. The insertion barrier for the neutral d^1 system is roughly 20 times higher than the insertion barrier for the cationic d^0 system.¹⁹¹ Finally, it is worth noting that Hoffmann and Ziegler predicted that d^1 and d^2 complexes can be suitable polymerization catalysts if other ligands can accept the d electrons in orbitals orthogonal to the π^* olefin orbital, which corresponds to a reduction of the relevance of the d - π^* interaction,^{56,191} while Ziegler also noted that if the occupied metal d orbitals are lower in energy, e.g. for late transition metals, the destabilization due to the disruption of the metal to olefin π^* orbital back-donation is smaller, and hence low insertion barriers are again possible.¹⁹¹

Fujimoto and co-workers analyzed the main orbital interaction at the transition state for ethene insertion into the Ti-C bond of the complex $Cl_2TiCH_3^+$,¹⁸⁵ with the paired interacting orbital method.¹⁹² The most important fragments are reported in Figure 14. The ϕ_1' , Ψ_1' and ϕ_2' , Ψ_2' pairs are responsible for the formation of the new Ti-C and C-C bonds, respectively. The contribution of the olefin π^* -orbital to the Ψ_1' and Ψ_2' fragment orbitals is striking. A similar analysis was performed by Shiga and co-workers,¹⁸⁶ which in agreement with the analysis of Hoffmann⁵⁶ also predicted that ethene insertion is facile for d^0 complexes whereas it is not with d^2 complexes, and by Morokuma and co-workers.¹⁴⁶ Similar mixing of the olefin π^* was also observed by Jolly and Marynick.¹⁷⁰

The presence of a favorable α -agostic interaction which stabilizes the transition state is another point of convergence between various authors.^{146,148-150,152,153,156,169,171,174,176,177,187-190} Before continuing, it is worth noting that a short Zr-H(α) distance (indicative of an α -agostic interaction) is

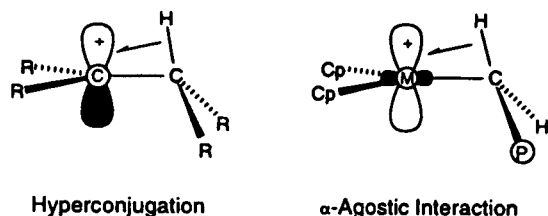


Figure 15. A comparison between hyperconjugation and α -agostic interactions.¹⁰²

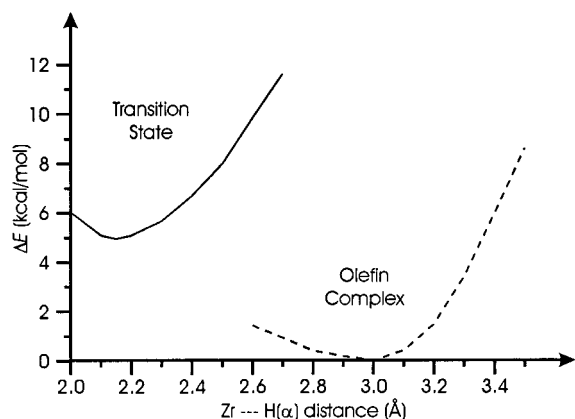


Figure 16. Relative energies of the transition state (continuous line) and of the olefin complex (dashed line) for propene insertion into the Zr–methyl bond of the $\text{H}_2\text{Si}(\text{Cp})_2\text{ZrCH}_3^+$ system, as a function of the Zr–H(α) distance.¹⁷⁵

almost inevitable as the sp^3 orbital of the chain C atom bonded to Zr tilts away from the Zr–C axis to be oriented toward the closest C atom of the olefin, giving rise to the bonding interactions with the olefin itself.

The energy changes along the reaction path for insertion of ethene into the Zr–methyl bond of the $\text{Cp}_2\text{ZrCH}_3^+$ system, with normal and deleted Zr–H(α) overlap integrals—that is, considering or not the agostic interaction—were calculated by Brintzinger and co-workers using the extended Hückel method, which offers a qualitative but valuable chemical picture of the problem. Their analysis indicate that the Zr–H(α) interaction is rather absent in the olefin complex, due to an unfavorable antibonding overlap between the bonding Zr–CH₃ and C–H(α) orbitals. As the reaction proceeds along the reaction path, a net stabilization due to the Zr–H(α) interaction arises close to the transition state.¹⁸⁷ According to Janiak, the α -agostic stabilization becomes important through an increase in electron deficiency of the metal that switches from a formally $16e^-$ Zr in the $\text{Cp}_2\text{ZrCH}_3(\text{C}_2\text{H}_4)^+$ reactant to the formally $14e^-$ Zr in the $\text{Cp}_2\text{ZrC}_3\text{H}_7^+$ product.¹⁸⁸ Similar ideas were developed by Grubbs and Coates, who also made a nice relationship between the hyperconjugative stabilization by β -hydrogen atoms of substrate undergoing nucleophilic substitution reactions in organic chemistry and the agostic stabilization by α -hydrogen atoms in Ziegler–Natta catalysis (Figure 15).¹⁰²

Another estimate of the transition state stabilization due to the α -agostic interaction can be obtained by looking at the plot reported in Figure 16. The continuous line represents the DFT energy of the transition state for propene insertion into the Zr–

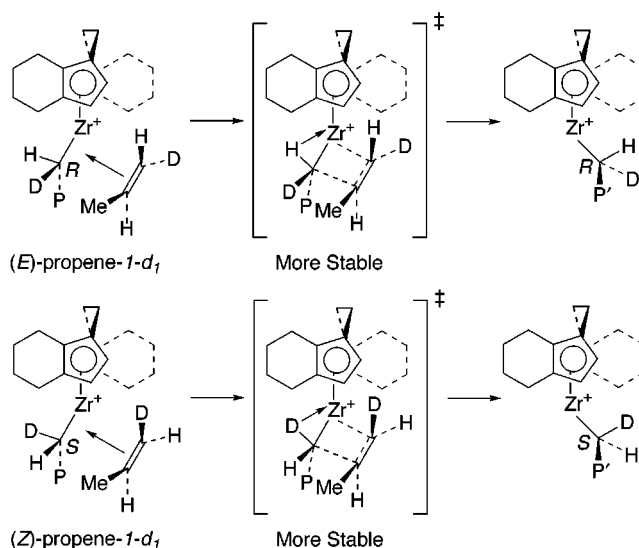


Figure 17. Stereokinetic isotope effects in the polymerization of *E*- and *Z*-propene-1- d_1 using a C_2 -symmetric metallocene. The transition state with an α -hydrogen agostic interaction is considered to be more stable than the transition state with an α -deuterium agostic interaction. Reprinted from ref 102. Copyright 1996 American Chemical Society.

methyl bond of the $\text{H}_2\text{Si}(\text{Cp})_2\text{ZrCH}_3^+$ system, as a function of the Zr–H(α) distance. The fully optimized metallocene–propene complex is assumed as the reference state at 0 kcal/mol. It is clear that the transition state energy is sensibly dependent on the Zr–H(α) distance and that the substantially low energy barrier—corresponding to the energy difference between the minimum of the two curves, 5.0 kcal/mol—would be quite higher if the Zr–H(α) distance in the transition state would be fixed at 3.0 Å, which is the value that the Zr–H(α) distance assumes in the olefin complex. However, it has to be noted that at too high values of the Zr–H(α) distance, the methyl group cannot tilt away from the Zr–C axis and point the sp^3 orbital in an optimal way to enhance the incipient bonding interactions with the olefin. This represents a further contribution to the transition state destabilization at high Zr–H(α) distances. For ethene insertion with the neutral d^0 scandocene Cp_2ScCH_3 ,^{152,174} the α -agostic interaction is less pronounced. The weaker α -agostic interaction was ascribed to the less electron deficiency of Sc with respect to Zr and was argued to be at the origin of the slightly higher insertion barrier, about 3 kcal/mol.^{152,174}

The relevance of α -agostic interactions has been experimentally investigated by using isotopically labeled substrates to probe for their role during olefin insertion.^{193,194} Following a reasoning developed by Grubbs et al.,^{102,195} Kraudelat and Brintzinger investigated the hydrodimerization of deuterated 1-hexene with $\text{Cp}_2\text{ZrCl}_2/\text{MAO}$.¹⁹³ They measured *erythro/threo* ratios in accordance with a value of $k_{\text{H}}/k_{\text{D}} \approx 1.3$,¹⁸⁷ which is consistent with an α -agostic assisted insertion reaction.^{102,195} Moreover, Leclerc and Brintzinger performed polymerization of *E*- and *Z*-propene-1- d_1 using a C_2 -symmetric metallocene.^{194,196} As shown in Figure 17, polypropenes made from the *E*-isomer should have molecular weights greater than polymers

made from the *Z*-isomer, if the insertion reaction is α -agostic assisted, since the *E*-isomer should correspond a faster insertion rate. This holds in the assumption that chain release reactions rates are equal for both isomers. These elegant mechanistic studies gave as a result that polymers made from the *E*-isomer had molecular weights about 1.3 times greater than polymers made from the *Z*-isomer, indeed, again in accordance to a value of $k_H/k_D \approx 1.3$.¹⁸⁷ Finally, similar results were obtained with neutral scandocene catalysts by Piers and Bercaw.¹⁹⁷ They observed similar kinetic isotope effects in the hydrocyclizations and hydrodimerizations of deuterated species.

Before concluding this section, it has to be noted that the presence of an α -agostic interaction facilitates the insertion reaction, but it is not necessary. As pointed out by Brintzinger and co-workers, whenever the electron deficiency of the transition state is diminished, by electron-donating ligands, coordination of a solvent molecule or of a second olefin, or some contact with the counterion, the agostic stabilization would undoubtedly lose most of its advantage.¹⁸⁷ Moreover, the substantial enantioselectivity of propene insertion into a secondary polypropylenic growing chain on C_2 -symmetric metallocenes,^{198,199} as after a regioirregular insertion, indicates that in this case the insertion reaction occurs with a methyl group occupying the position usually taken from the α -agostic hydrogen atom. This idea finds support in the molecular mechanics study of Corradini and co-workers.²⁰⁰ However, Brintzinger also noticed that the presence of an α -agostic interaction at the transition state is entirely compatible with the steric requirements of substituted chiral *ansa*-metallocenes.¹⁸⁷ That is, the preferred transition state geometry based on electronic considerations is remarkably similar to the transition state geometry based on steric requirements (the so-called "chiral orientation of the growing chain" mechanism; see section III.H).

E. Insertion Barrier

Regarding the height of the insertion barrier, the situation is much more controversial. Since simplified ligands as Cl or H—often used to model Cp rings—substantially increase the height of the insertion barrier, we limit this discussion to calculations including full Cp rings. The first prediction of the barrier for the insertion reaction $Cp_2TiCH_3^+ +$ ethene by Jolly and Marinick gave a barrier of 9.8 kcal/mol at the MP2 level.¹⁷⁰ However, it has to be considered that their geometries were determined by using a simpler semiempirical method, and only energetics were evaluated at the MP2 level. The same insertion reaction was studied by Ahlrichs and co-workers, which found a considerable energy barrier and a transition state only without inclusion of electron correlation.¹⁴⁹ On a correlated level, they found that the insertion reaction occurs on a very flat, downhill potential energy surface. Similar conclusions were also reached by Meier and co-workers, who investigated the ethene + $H_2Si(Cp)_2TiCH_3^+$ reaction by using the Car–Parrinello method.¹⁵⁶ For the ethene

insertion reaction on the Cp_2ZrR^+ ($R = CH_3, C_2H_5$) and $H_2Si(Cp)_2ZrCH_3^+$ zirconocenes and on the Cp_2-ScCH_3 scandocene, the static DFT calculations of Ziegler and co-workers predicted almost negligible insertion barriers, <3 kcal/mol.^{152,169,174}

For insertion on the $Cp_2ZrC_2H_5^+$ system, they also performed first principles molecular dynamics calculations,²⁰¹ and a 5 kcal/mol free energy barrier was predicted. However, they also warned that quite longer simulation times were needed for quantitative predictions.¹⁷⁶ For the insertion reactions ethene + $H_2Si(Cp)_2MtCH_3^+$ ($Mt = Ti, Zr, Hf$), Morokuma and co-workers performed calculations at different levels of ab initio theory.¹⁵³ They showed that the predicted barrier sensibly depends on the particular level of theory and that MP2 barriers seems to be somewhat underestimated with respect to calculations at the higher RQCISD level of theory. They also noted that larger basis sets were needed for accurate RQCISD predictions. Nonetheless, their calculations suggested that activation energies, about 5 kcal/mol, have to be expected within the metal triad. Moreover, considering the energy of the free reactants as the reference state, the transition state with the Zr atom is more stable than those with the Hf or Ti atoms.¹⁵³ This is in agreement with the higher reactivity of Zr-based systems.

Cruz and co-workers investigated ethene insertion with the $Cp_2ZrCH_3^+$ and $H_2Si(Cp)_2ZrCH_3^+$ systems. According to them, exactly the same barrier of 6.6 kcal/mol is obtained by MP2 and DFT methods for the $Cp_2ZrCH_3^+$ system, while for the unbridged systems both methodologies suggested the absence of an insertion barrier.¹⁹⁰ Recently, for the insertion reactions ethene + $Cp_2ZrCH_3^+$ and ethene + $(Me_5Cp)_2ZrCH_3^+$, the DFT calculations of Rytter, Ystenes, and co-workers predicted insertion barriers of 6.2 and 4 kcal/mol, respectively.¹⁷¹ The smaller insertion barriers with the bulkier Me_5Cp rings were explained in terms of augmented steric pressure on the olefin complex.

In conclusion, all the above calculations indicate that the propagation step is a facile reaction and that barriers in the range 0–5 kcal/mol are predicted. As noted by Ahlrichs and co-workers, barriers of this magnitude would hardly be distinguishable from strict downhill potentials as far as kinetics are concerned.¹⁴⁹

As for the final state after the insertion step, all authors do agree that the α -agostic interaction occurring in the transition state evolves into a γ -agostic one. Moreover, the γ -agostic is usually predicted to correspond to the kinetic product that, through a conformational rearrangement of low energy, could be converted into the thermodynamic β -agostic product.^{146,148–150,152,153,156,169,171,174,176,177,187–190}

Quite a few calculations of activation barriers for propene insertion have been performed. Morokuma and co-workers predicted that primary propene insertion on the $Cl_2TiCH_3^+$ system has an insertion barrier about 6 kcal/mol higher than the corresponding ethene insertion reaction.¹⁴⁶ More recent DFT calculation for propene insertion on the $H_2SiCp_2-ZrCH_3^+$ systems predicted a barrier for primary

propene insertion about 3 kcal/mol higher than the corresponding ethene insertion reaction.¹⁷⁵

Regarding the origin for the intrinsic preference for primary versus secondary propene insertion, the ab initio calculations of Morokuma and co-workers on approximated transition state geometries for primary and secondary propene insertion into the Ti–methyl σ -bond of the system $\text{Cl}_2\text{TiCH}_3(\text{propene})^+$ indicated that secondary propene insertion was disfavored by 4.6 kcal/mol relative to primary propene insertion.¹⁴⁶ The latter is essentially stabilized by favorable electrostatic interaction and less serious exchange repulsion,¹⁴⁶ in agreement with the experimental results and the Markovnikov rule of organic chemistry. Their Mulliken analysis on the transition state for ethene insertion into the Ti–methyl σ -bond indicated that the ethene C atom that is going to be bonded to the metal atom is more negatively charged relative to the ethene C atom that is going to be bonded to the methyl group. Thus, they argued that the additional methyl group of the propene would give a more favorable electrostatic interaction with the C atom of the olefin closer to the methyl group than to the metal atom. That is, primary insertion is favored over secondary insertion. Moreover, in the transition state for the secondary insertion, the propene methyl group is closer to the additional metal ligands than for primary insertion, causing a larger exchange repulsion.¹⁴⁶ More recent DFT calculations on the primary and secondary propene insertion into the Zr–methyl σ -bond of the system $\text{H}_2\text{Si}(\text{Cp})_2\text{ZrCH}_3(\text{propene})^+$ substantially confirmed the analysis of Morokuma. The fully optimized transition state for the secondary propene insertion is 3.5 kcal/mol above the optimized transition state for the primary propene insertion.¹⁷⁵

When the insertion reaction takes place on models of growing chain longer than simple methyl groups, reaction paths due to different orientations/rearrangements of the growing chain have to be considered. Ziegler and co-workers performed static and dynamics DFT calculations for ethene insertion on $\text{Cp}_2\text{ZrC}_2\text{H}_5^+$ systems, while Rytter, Ystenes, and co-workers performed DFT calculations for ethene insertion on the $\text{Cp}_2\text{ZrC}_3\text{H}_7^+$ and $(\text{Me}_5\text{Cp})_2\text{ZrC}_3\text{H}_7^+$ systems considering both frontside and backside ethene approach to the catalyst (corresponding to ethene approach from the C–H agostic bond side, or from the from Zr–C σ -bond side, respectively).^{152,171} The frontside insertion requires a rearrangement of the growing chain from a β -agostic to an α -agostic orientation. This barrier was predicted to be about 3–5 kcal/mol and, according to the authors, represents the highest energetic barrier along the whole catalytic cycle.^{169,171} Similar conclusions were reached by Cavallo and Moscardi, who performed combined QM/MM calculations for propene insertion with the $\text{Me}_2\text{C}(3-t\text{-Bu-1-Ind})_2\text{Zr}(\text{isobutyl})^+$ system.²⁰² As for the backside approach, the insertion can occur without any particular rearrangement. The activation barrier is about 7 kcal/mol high and is slightly assisted by a β -agostic interaction.¹⁶⁹ Støvneng and Rytter, and more recently Rytter, Ystenes, and co-workers studied the propagation step on a γ -agostic growing chain

for ethene polymerization on the $\text{Cp}_2\text{ZrC}_3\text{H}_7^+$ system.^{171,189} The last authors investigated the same reaction path with the analogous $(\text{Me}_5\text{Cp})_2\text{ZrC}_3\text{H}_7^+$ system also.¹⁷¹ They found that the insertion can occur easily also in the presence of the γ -agostic interaction, with activation barriers lower than 3 kcal/mol. As for the presence of further ligands as counterion, solvent, or other monomer molecules, it has to be recalled that Ystenes has proposed the so-called “trigger mechanism”.²⁰³ This mechanism involves a two-monomer transition state, where the entering of a new monomer unit triggers the insertion of the already complexed monomer. Specific calculations to support this model are not available.

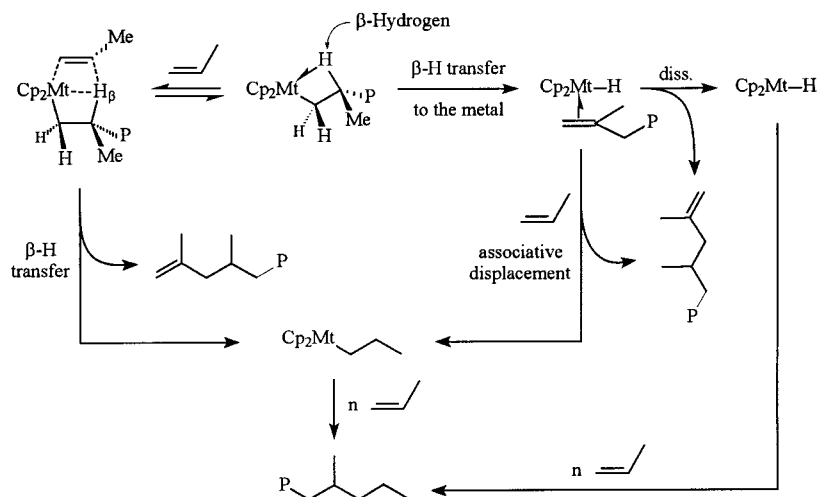
Finally, systematic studies on olefins insertion with transition metal based systems (not being part of a metallocene, though) have been reported by Siegbahn^{204,205} and Ziegler¹⁹¹ and their co-workers.

A clear experimental estimate of the intrinsic reaction barrier to propene insertion is still missing. The elegant NMR analysis of Erker and co-workers estimated the intrinsic activation barrier for 1-alkene insertion into the Zr–C bond of the $(\text{MeCp})_2\text{Zr}(\mu\text{-C}_4\text{H}_6\text{-borate betaine})$ to be about 10–11 kcal/mol. However, this activation barrier can probably be considered an upper value, since it corresponds to 1-alkene insertion into the Zr-allyl-like bond.¹⁸²

F. Chain Release

Ziegler–Natta catalysts participate in a double catalytic cycle: one is the multiple insertion of olefins at a given metal center, and the second is the production of multiple chains on the same catalytic center. The two cycles are connected by the set of reactions that terminate the growth of a polymer chain by producing a free polymer chain and an active metal–hydride or metal–alkyl species on which a new polymer chain will grow. We term all these reactions “chain release” reactions, contrary to the common use of the terms “chain transfer” or “chain termination”, to avoid confusion with β -transfer reactions, which usually but not always—cause chain release, and with termination reactions that, for example in anionic or radical polymerizations, terminate chain growth by also terminating the catalyst. The chain release reactions have been already reviewed¹³¹ and are summarized below. The kinetic implications for the control of molecular weight are discussed in section VIII.

(1) β -Hydride transfer after a primary insertion (Scheme 16) produces vinylidene-terminated, *n*-propyl-initiated PP and follows the rate law $R_t = k_{(\beta\text{-H})_0}[C]$, when it is unimolecular (β -hydride transfer to the metal), and $R_t = k_{(\beta\text{-H})_1}[C][M]$, when it is bimolecular (either by concerted β -hydride transfer to the coordinated monomer or by associative displacement). Both neutral group 3 and cationic group 4 metallocene alkyl complexes readily undergo spontaneous β -hydride transfer to the corresponding metal hydrides and alkenes, as shown by Bercaw^{206,207} and Jordan.^{208,209} Primary bimolecular hydrogen transfer (β -hydride transfer to the monomer), already identified as the preferred chain release pathway in the polymerization of propene with

Scheme 16. Hydride Transfer Reactions^a

^a Cp = cyclopentadienyl, Mt = metal, P = polymer chain.

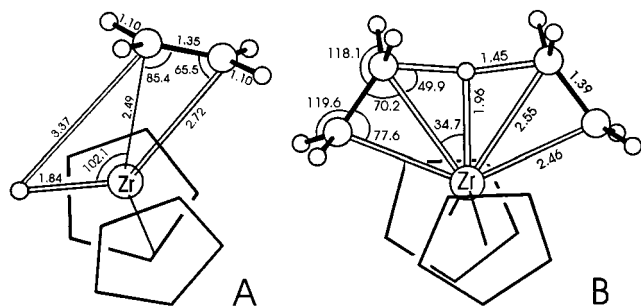


Figure 18. DFT optimized structure of the transition states for unimolecular β -hydrogen transfer to the metal, on the left, and bimolecular β -hydrogen transfer to the monomer, on the right.¹⁵⁴

heterogeneous catalysts,^{210–213} has been identified by Tsutsui and co-workers in the copolymerization of propene with ethene, with the system $\text{Cp}_2\text{ZrCl}_2/\text{MAO}$.²¹⁴

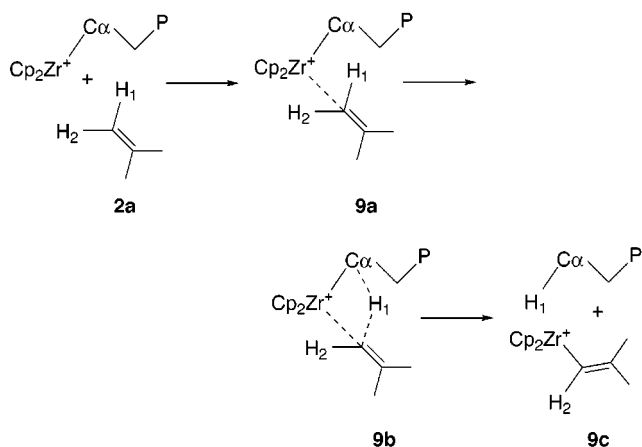
Both unimolecular β -hydrogen transfer to the metal and bimolecular β -hydrogen transfer to a coordinated monomer molecule have been theoretically investigated (Figure 18).

Unimolecular β -hydrogen transfer to the metal from an ethyl group σ -bonded to the metal has been predicted to be a process of considerably high energy.^{152,154,171,215} Activation barriers close to 20 kcal/mol were calculated, and the final complex, corresponding to ethene coordinated to the hydride metallocene complex, was predicted to be very unstable. In fact, the reinsertion barrier of ethene into the Mt-H bond was calculated to be lower than 3 kcal/mol.^{153,154,171,215} When alkyl groups longer than ethyl, like *n*-propyl, *n*-butyl, or *iso*-butyl groups, are used to simulate the growing chain, considerably lower barriers, about 10–15 kcal/mol, were calculated.^{153,171,215} Proscenc and Brintzinger ascribed the lower energy for β -hydrogen transfer from the longer alkyl chain to the stabilization of positive charge at the $\text{C}(\beta)$ atom in the transition state by hyperconjugative effects,²¹⁵ while Rytter, Ystenes, and co-workers suggested that this difference is essentially due to the difference in reaction enthalpy during saturation of an olefinic double bond, which is about 3 kcal/

mol more exothermic for ethene than for longer α -olefins.²¹⁶ Finally, Rytter and co-workers investigated the effect of steric pressure on the chain release reaction, by comparing the $\text{Cp}_2\text{Zr}(n\text{-propyl})^+$ and $(\text{Me}_5\text{Cp})_2\text{Zr}(n\text{-propyl})^+$ systems.¹⁷¹ The barrier for β -hydrogen transfer in the model with the substituted Me_5Cp ligands was calculated to be only 2 kcal/mol higher than that from the model with the unsubstituted Cp ligands.

However, all authors found the intermediate with the olefin-like chain end coordinated to the metallocene hydride to be a very unstable species, independently of the length of the alkyl group used to simulate the growing chain, and that a complete dissociation of the olefin-like chain end is energetically very unfavorable, about 20 kcal/mol.^{152,154,171} On these bases, the metallocene(hydride)(olefin) complex is predicted to be very stable toward olefin dissociation, even considering an unfavorable entropic contribution to the olefin coordination of about 10 kcal/mol at room temperature. This implies that the barrier of the simple β -hydrogen transfer to the metal step could be not representative of the real energy barrier needed for this chain release process, unless associative displacement of the olefin-like chain end by a monomer or a solvent molecule takes place. The associative displacement of the coordinated olefin-like chain end by approaching an ethene molecule to the metallocene hydride complex attempted by Rytter and co-workers inevitably led to reinsertion of the olefin-like chain end into the Zr-H bond.¹⁷¹

Bimolecular β -hydrogen transfer to the monomer in the $\text{Cp}_2\text{ZrC}_2\text{H}_5(\text{ethene})^+$ system was investigated by Ziegler and co-workers¹⁶⁹ and by Cavallo and Guerra,¹⁵⁴ while transfer in the $\text{Cp}_2\text{ZrC}_3\text{H}_7(\text{ethene})^+$ system was investigated by Rytter and co-workers.¹⁷¹ The energy barrier for this transfer reaction, independently of the length of the alkyl group, was calculated to be about 9 kcal/mol. Moreover, Rytter and co-workers also predicted that transfer to a coordinated monomer in the $(\text{Me}_5\text{Cp})_2\text{ZrC}_3\text{H}_7(\text{ethene})^+$ system should have a substantially high barrier, about 16 kcal/mol. Finally, combined QM/MM calculations by Cavallo and Moscardi calculated an activa-

Scheme 17¹⁵²

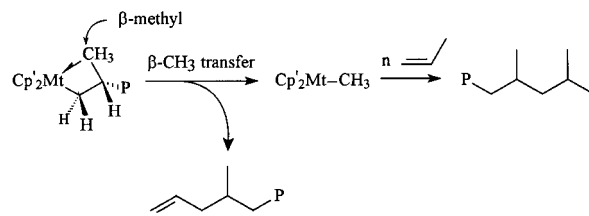
tion barrier of 9.5 kcal/mol for the β -hydrogen transfer to the monomer with the system $\text{Me}_2\text{Si}(1\text{-Ind})_2\text{Zr}(\text{isobutyl})(\text{propene})^+$, showing that steric hindrance is not relevant for relatively unencumbered isospecific C_2 -symmetric metallocenes.¹⁷⁵

Ziegler and co-workers also investigated the C–H activation, using the $\text{Cp}_2\text{ZrCH}_3(\text{ethene})^+$ system as a model.¹⁵² The transition state for C–H activation was predicted to be about 8 kcal/mol above an edge-on ethene adduct coordinated to the metal through the two C–H bonds of one of the CH_2 moieties of the olefin (structure **9a** in Scheme 17). The barrier to this chain release process is surprisingly low and would be the preferred termination path, contrary to the experimental facts. However, the ethene adduct they considered as reactant is about 9 kcal/mol above the olefin π -complex usually considered in Ziegler–Natta catalysis. Hence, we think that the real barrier to C–H activation has to be considered as the energy difference between the calculated transition state and the *most* stable ethene complex. This would give an energy barrier of about 17 kcal/mol, quite higher than the activation barriers predicted for β -hydrogen transfer either to the metal or to the monomer.

Finally, the interested reader can find a systematic study on β -hydrogen transfer, either to the metal or to the monomer, with transition metal based systems (not being part of a metallocene, though) in ref 217.

(2) β -Methyl transfer, a notable example of C–C bond activation at early transition metal centers,^{218–222} produces PP chains initiated by isobutyl and terminated by the allyl group $\text{CH}_2=\text{CH}-\text{CH}_2-\text{CH}(\text{CH}_3)-\text{P}$. This chain release reaction, first documented by Watson in the oligomerization of propene with $(\text{Me}_5\text{-Cp})_2\text{LuMe}$,²²³ and later observed by Teuben^{224,225} and Resconi¹¹⁹ with $(\text{Me}_5\text{Cp})_2\text{Zr}$ - and Hf catalysts, was recently found to be quite common, whenever the metal has highly substituted cyclopentadienyl ligands.^{50,76,123,130,131,207,209,226,227} Jordan²⁰⁹ and Bercaw²⁰⁷ have shown that β -methyl transfer is unimolecular ($\beta\text{-CH}_3$ transfer to the metal), $R_t = k_t(\beta\text{-CH}_3)[\text{C}]$ (Scheme 18).

From a molecular modeling standpoint, Eisenstein, Teuben, and co-workers investigated β -hydrogen and β -methyl transfer reactions to the metal using the $\text{Cl}_2\text{Zr}(n\text{-propyl})^+$ system as starting point for both chain release reactions.²²⁸ They observed that a

Scheme 18. Methyl Transfer ($\beta\text{-CH}_3$ transfer to the metal): $R_t = k_t(\beta\text{-CH}_3)[\text{C}]^a$ 

^a Cp' = highly substituted cyclopentadienyl.

considerable energy difference is predicted between the two π -complexes obtained at the end of the elimination step. In particular, the π complex deriving from the β -methyl transfer, $\text{Cl}_2\text{ZrCH}_3(\text{ethene})^+$, is about 12 kcal/mol more stable than the π complex deriving from the β -hydrogen transfer, $\text{Cl}_2\text{ZrH}(\text{propene})^+$. Furthermore, after dissociation of the respective olefin, $\text{Cl}_2\text{ZrCH}_3^+ + \text{ethene}$, is even more favored (about 18 kcal/mol) relative to $\text{Cl}_2\text{ZrH}^+ + \text{propene}$. They argued that the higher stability of the products of the β -methyl transfer should be related to the capability of the CH_3 group to form an α -agostic interaction.

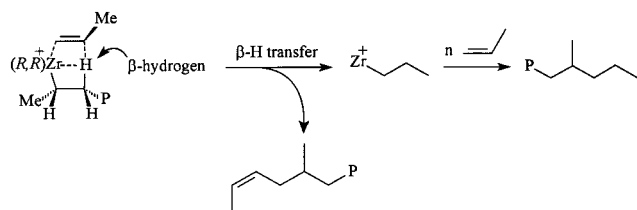
The modeling of the bimolecular β -methyl transfer to a coordinated propene molecule was attempted by Cavallo and others. DFT calculations on the $\text{Cl}_2\text{Zr}(\text{isobutyl})^+$ system¹⁷⁵ and combined QM/MM calculations on the $\text{Me}_2\text{C}(3\text{-}t\text{-Bu-1-Ind})_2\text{Zr}(\text{isobutyl})^+$ system²²⁹ gave extremely high activation barriers, which ruled it out as a viable chain release mechanism. However, experimental evidence is building up that it can also occur via associative displacement with the monomer.^{131,229–231}

(3) β -H transfer after a *secondary* propene insertion is an important chain release reaction, since it is the cause for the drop in molecular weights observed in those metallocenes for which a secondary insertion generates a slower propagating species (see section VII). This reaction has been shown to occur from the methylene. In principle, also this transfer can be unimolecular or bimolecular, producing a metal–hydride (or metal–propyl) initiating species and a PP chain terminated with either a 3-butenyl (hydride transfer from the terminal CH_3) or a 2-butenyl end group (hydride transfer from the CH_2). In practice, only the internal vinylene has been observed^{130,232–234} and analysis of the change of end groups concentration and structure with the catalyst *rac-C}_2\text{H}_4(4,7\text{-Me}_2\text{-1-Ind})_2\text{ZrCl}_2/\text{MAO} with propene concentration has shown that this chain release reaction occurs by transfer to the coordinated monomer, following the rate law $^sR_t = ^s k_t(\beta\text{-H})[^s\text{C}][\text{M}]$ (Scheme 19).^{130,131}*

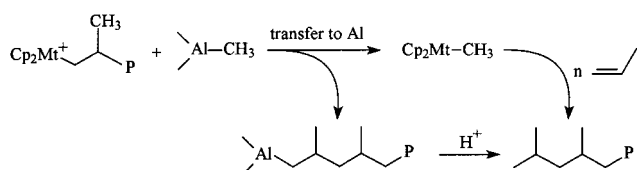
(4) Transalkylation to the aluminum cocatalyst produces, after hydrolysis, PP with saturated end groups on both ends (Scheme 20); in the case of MAO-cocatalyzed propene polymerization, transalkylation likely occurs with the AlMe_3 present in MAO, generating isobutyl end groups on both polymer ends.

This release reaction has proven quite useful, especially when used with ^{13}C -labeled AlR_3 compounds, to establish the enantioface selectivity of the first monomer insertion.^{235–238} While common with heterogeneous catalysts,²³⁹ it is not so relevant with

Scheme 19. β -H Transfer to the Monomer after a Secondary Insertion: $R_t = s k_{(\beta-H)} [^sC][M]$ (sC = active center bearing a secondary growing chain)



Scheme 20. Chain Transfer to Aluminum: $R_t = k_{t,Al}[C][Al]$



metallocenes, since it only occurs at high Al/Zr ratios, or under conditions of low productivity.^{240–244}

(5) Chain release by chain transfer to an added transfer agent, different from an AlR₃ compound, is the most simple way to control the molecular weight of polyolefins, and molecular hydrogen is the most useful chain transfer agent in both heterogeneous^{245–247} and homogeneous^{83,248–252} Ziegler–Natta catalysis. Hydrogen has the added advantage to increase the catalyst productivity and has been used in combination with metallocene catalysts for mechanistic purposes, especially to shed light on the influence of secondary propene insertions; see section IX.

The ¹³C NMR chemical shift of the more commonly recurring PP chain end groups are collected in Table 2.

G. Formation and Reactivation of Mt–Allyl Species

Allylic activation represents a possible evolution path for the intermediate which is obtained after unimolecular β -hydrogen transfer to the metal, that is, the olefinic chain end coordinated to the metallocene hydride complex. The DFT calculations of Ziegler and co-workers on the geometrically constrained H₂Si(Cp)(NH)Ti–R⁺ system²⁵³ and of Brintzinger and Proscenc on the Cp₂Zr(methallyl)⁺ system²⁵⁴

and the combined QM/MM calculations of Ziegler and co-workers on the Ph₂C(Cp)(9-Flu)Zr–R⁺ system¹⁴⁴ and of Cavallo and Moscardi on the Me₂C(3-*t*-Bu-1-Ind)₂Zr(isobutyl)⁺ system²⁰² showed that the allylic-like chain end can be easily formed from the olefin Mt–H intermediate, with activation barriers lower than 5 kcal/mol. According to Ziegler and co-workers, the product of the allylic activation, that is, the metallocene complex with an allylic-like chain end and a hydrogen molecule coordinated to the metal, is not a stable species when entropic contributions are accounted for, and the H₂ molecule is thus ejected (Scheme 21).¹⁴⁴

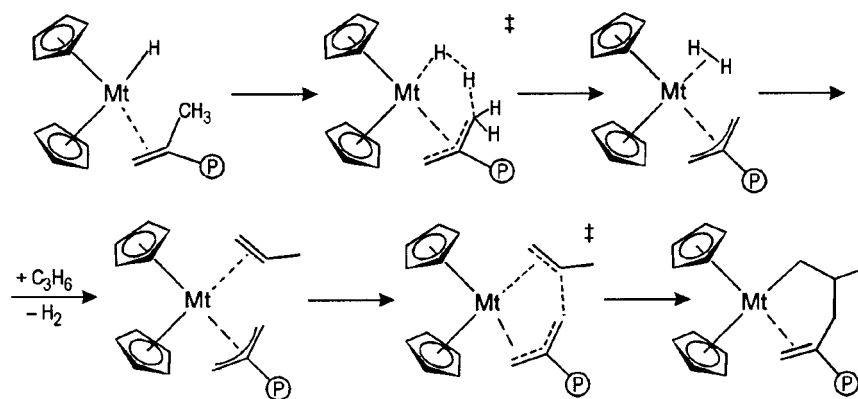
The reactivation of this allyl complex requires coordination of a new monomer molecule and its insertion into the Mt–allyl bond. The uptake of a new monomer molecule is not an easy step at all. Ziegler and co-workers showed that ethene uptake energy to the Ph₂C(Cp)(9-Flu)Zr(C₃H₅)⁺ system, about 10 kcal/mol, is substantially lower than the ethene uptake energy to the unencumbered Cp₂Zr(C₃H₅)⁺ system, while Brintzinger, Lieber, and Proscenc, as well as ourselves, found that propene coordination to the metal–(2-alkylallyl)⁺ species leads to weakly propene coordinated adducts.^{144,202,254} Moreover, the bulkier the metallocene ligand, the worse propene coordination is. The activation barrier for insertion of a new monomer is strongly dependent on the bulkiness of the system. For propene insertion into the unencumbered Cp₂Zr(methallyl)⁺ system, Proscenc and Brintzinger predicted a ΔE^\ddagger of about 15 kcal/mol,²⁵⁴ and for ethene insertion into the Ph₂C(Cp)(9-Flu)Zr(allyl)⁺ system, Ziegler and co-workers predicted a ΔE^\ddagger of about 6 kcal/mol,¹⁴⁴ while for propene insertion on the encumbered Me₂C(3-*t*-Bu-1-Ind)₂Zr–(2-ethyl-allyl)⁺ system, Cavallo and Moscardi predicted a ΔE^\ddagger of about 7 kcal/mol.²⁰²

While all the insertion reactions above-discussed considered alkene insertion into the Zr–allyl bond in which the allyl group is η^3 -bonded to the metal, Brintzinger and Proscenc also investigated propene insertion into a Zr–methallyl bond in which the allyl group is σ -bonded to the metal. They found a substantially higher ΔE^\ddagger , thus suggesting that insertion on a η^3 -bonded allyl group is probably the most viable mechanism.²⁵⁴ When considering the insertions of both propene enantiofaces on the chiral Me₂C(3-*t*-Bu-

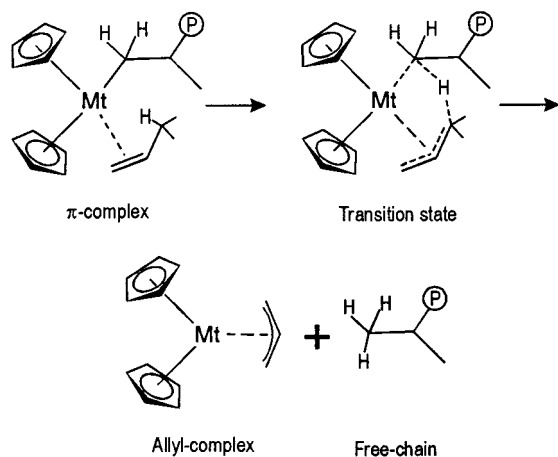
Table 2. ¹³C NMR Chemical Shifts and Carbon Numbering of Common Polypropene Chain End Groups

C	<i>n</i> -propyl	isobutyl	2,3-dimethyl-butyl	allyl	vinylidene	isobutenyl	<i>cis</i> -2-butenyl
1	14.47	22.61	17.76	115.57	111.38	18.01	12.91
2	20.12	25.79	31.93	137.67	144.87	129.23	124.48
3	39.68	23.83	20.56	41.38	22.6	25.7	129.66
4	30.50	47.50	36.47	30.80		132.30	34.37
5	20.81	?	16.30	20.64		30.61	31.37
6	45.98	21.13	43.05	45.33			?
7				?			45.54
8				21.43			

Scheme 21



Scheme 22



1-Ind)₂Zr(2-ethyl-allyl)⁺ system, we found only a small energy difference between the two transition states, about 2 kcal/mol, which suggests a relatively scarce enantioface selectivity for propene insertion on the L₂Zr(allylic chain)⁺ complex (Figure 19). This is related to the absence of a chirally oriented alkyl growing chain and is in good agreement with the experimentally observed low enantioselectivity for this particular insertion reaction.²²⁹

All authors found that the product of alkene insertion into the metal–allyl bond corresponds to a C=C double bond back-bitten to the metal atom. Ziegler and co-workers showed that the back-biting of this double bond should not hinder the subsequent propagation steps.¹⁴⁴

Finally, it is worth noting that formation of allylic species does not necessarily require the sequence of steps above-described. In fact, allylic hydrogen trans-

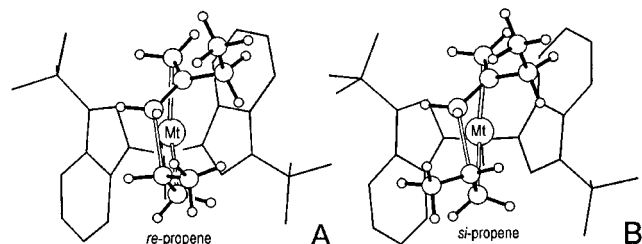


Figure 19. Transition state geometries for propene insertion into the Zr-(η^3 -2-ethylallyl) bond. The small energy difference between the two transition states is related to the absence of a chirally oriented growing chain.²⁰²

fer from a coordinated alkene to the growing chain σ -bonded to the metal, thus generating an allyl group and liberating an alkane molecule (see Scheme 22) is conceivable. This mechanism of allyl formation has been proposed by Schumann, Marks, and co-workers²⁵⁵ to rationalize the formation of lanthanocene allyl complexes and by Horton²⁵⁶ and by van der Heijden and Hessen²⁵⁷ to rationalize the formation of zirconocene allyl complexes from isobutene in zirconocene–alkyl systems.

H. Mechanism of Enantiomorphic Site Control in Primary Insertion

The two stereospecific processes, originated by the chiralities of the catalyst active sites and referred to as *enantiomorphic site control* (isospecific²² and syndiospecific^{112,113} site control), can be relatively strong, with differences in activation energy ($\Delta\Delta E^\ddagger$) for the insertion of the two enantiofaces up to 5 kcal/mol. A value of 4.8 kcal/mol has been found by Zambelli and Bovey¹¹⁴ for a Ti-based heterogeneous catalyst. The driving force for enantioface selectivity with group 4 metallocene catalysts has been rationalized using the same conceptual scheme developed by Corradini and Guerra to rationalize the stereoselectivity of the classical heterogeneous Ziegler–Natta catalysts.^{258–262}

The models used by Corradini, Guerra, and co-workers,^{90–92,200,263–273} as well as by other authors,^{89,147,155,274–277} comprise a monometallic, cationic active center of the type L₂MtR⁺. The molecular modeling of group 4 metallocenes fully accounts for the highly variable stereoselectivities in both primary and secondary propene insertion and for the regioselectivity obtained with different ligands. To understand in detail the proposed mechanism of stereocontrol, we start with a description of the role played by the ligand in the direct selection of the propene enantioface. Already the first studies on propene polymerization with heterogeneous catalytic systems indicated poor enantioselectivity for propene insertion into the Ti–CH₃ bond.²⁶⁰ This feature has been confirmed also for the metallocene-based homogeneous catalytic systems by different research groups.^{89,90,147,155,264,275} In fact, energy differences usually smaller than 1 kcal/mol have been calculated between the minimum energy geometries for *si* and *re* coordinations of propene to the C₂H₄(1-Ind)₂TiCH₃⁺ and C₂H₄(H₄-1-Ind)₂TiCH₃⁺ systems^{147,264} and be-

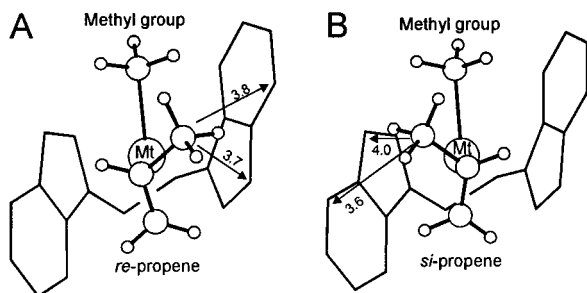


Figure 20. Molecular mechanics minimum energy geometry for *re* and *si* propene coordination on the (*R,R*)-C₂H₄(1-Ind)₂Zr(methyl) model. Distances in Å.

tween approximated transition states for propene insertion into the Zr–CH₃ bond of several C₂-symmetric Zr-based complexes containing the H₂Si(Cp)₂ and the H₂Si(1-Ind)₂ ligands with different alkyl substitution patterns.^{155,275} Similar calculations on some C_s and C₁ symmetric catalysts indicated a similar behavior.^{89,90,147,155} As an example, the structures A and B of Figure 20 clearly show that the propene methyl group is sufficiently far from the metallocene skeleton for both propene enantiofaces coordination. Therefore, the chirality of the ligand is unable to efficiently select between the two propene enantiofaces in the absence of a growing chain larger than CH₃.

The above results are in agreement with the experimental studies of Zambelli^{235,278} and Erker²⁷⁹ and their co-workers about the stereoselectivity in the first polymerization step. In fact, ¹³C NMR studies of the polymer end groups have shown that in the first step of polymerization, when the alkyl group bonded to the metal is a methyl group, the propene insertion is essentially nonenantioselective, whereas, when the alkyl group is an isobutyl group, the first insertion is enantioselective as the successive insertions. This holds both for heterogeneous²³⁵ and homogeneous Ziegler–Natta catalysts.^{278,279} The results of molecular mechanics calculations on the proposed metallocene models relative to possible initiation steps are in perfect agreement with these experimental findings and also rationalize²⁶⁴ the partial enantioselectivity of a catalytic system based on the C₂H₄(1-Ind)₂ ligand for 1-butene insertion into the Mt–CH₃ bond.²⁷⁸

Before concluding, it has to be remarked that some enantioselectivity for primary propene insertion into the Zr–methyl σ-bond cannot be excluded in principle. However, all the experimental evidence up to date strongly exclude that this kind of “direct enantioselectivity” is responsible for the enantioselectivity in primary propene insertion into the Zr–C(growing chain) σ-bond (i.e. the propagation step) with these catalysts.

Next, we turn our attention to the role played by the growing chain in determining the enantioselective behavior. In Figure 21, the two minimum energy situations of the system (*R,R*)-C₂H₄(1-Ind)₂Zr(isobutyl)(ethene)⁺ are reported. According to the calculations of Corradini and co-workers, structure A of Figure 21 is more stable than structure B by roughly 4–5 kcal/mol.²⁶⁷ Structure A presents the growing chain in an open sector, and steric repulsions with the

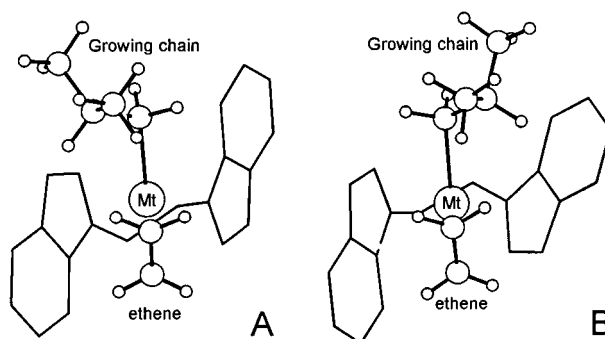


Figure 21. Molecular mechanics minimum energy geometry for ethene coordination on the (*R,R*)-C₂H₄(1-Ind)₂Zr(isobutyl) model.

ligand framework are null. Structure B, instead, presents the growing chain repulsively interacting with the ligand. As a consequence, already in the presence of the achiral ethene monomer, the growing chain has a *preferential chiral orientation* which is determined by the chirality of the metallocene.

We have discussed above how the ligand chiral framework is unable to operate a direct chiral recognition of the enantioface of the incoming propene monomer and how the ligand's chiral framework is able to chirally orient the growing chain. Now, we will discuss how this chiral orientation of the growing chain is able to discriminate between the two enantiofaces of the incoming propene monomer, since all authors do agree on this fact.

The molecular mechanics minimum energy situations determined by Corradini, Guerra, and co-workers for the system (*R,R*)-C₂H₄(1-Ind)₂Zr(isobutyl)(propene)⁺, with the propene monomer *re* and *si* coordinated, are reported in Figure 22A–C.^{200,263,273} Structure A, with a *re*-coordinated propene, is more stable than structures B and C, with a *si* coordinate propene. The higher stability of structure A is due to the absence of repulsive interactions among the ligand framework, the growing chain, and the propene molecule. The minimum energy situation found by Castonguay and Rappé for propene insertion on the *rac*-C₂H₄(1-Ind)₂Zr(polymer)⁺ system and its tetrahydro derivative¹⁴⁷ and the most favored approximate transition state found by Morokuma and co-workers for propene insertion on the *rac*-H₂Si(1-Ind)₂Zr(polymer)⁺ system^{155,275} are extremely similar to structure A of Figure 22. It is relevant to note that in the favored structure the growing chain develops freely in an open sector, and the methyl group of the propene is anti to (i.e. away from) the β-C atom (and followings) of the growing chain, to avoid steric interaction with the chain itself. These features are retained in all the models and for all the ligands modeled so far. Finally, Rappé and co-workers also found that the same propene enantioface which is favored when a long growing chain is σ-bonded to the Zr atom is also (slightly) favored for propene insertion into the Zr–methyl bond, that is, in the initiation step.¹⁴⁷ This aspect has been indeed experimentally proven by Longo: propene insertion into the *rac*-C₂H₄(1-Ind)₂Zr–¹³CH₃ bond is slightly enantioselective (ΔΔE[‡] ≈ 0.5 kcal/mol) with the same enantioface preference as that of propagation, while in the case

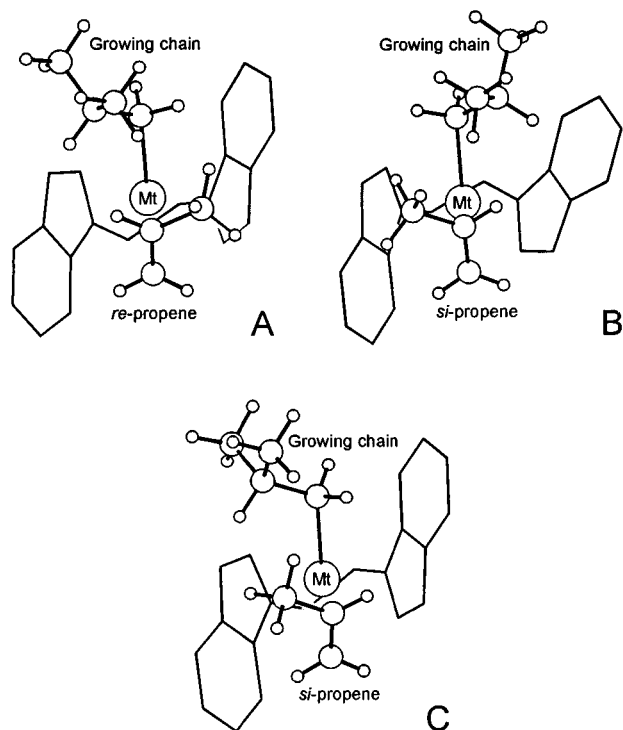


Figure 22. Molecular mechanics minimum energy geometry for *re* and *si* propene coordination on the (*R,R*)- $C_2H_4(1-Ind)_2Zr(isobutyl)$ model.

of the $Me_2C(Cp)(9-Flu)Zr-^{13}CH_3$ bond it is only marginally enantioselective ($\Delta\Delta E^\ddagger \approx 0.2$ kcal/mol) with the opposite enantioface preference as that of propagation.²⁸⁰ This means that enantioselectivity could at least partially be due to a double stereodifferentiation,²⁸¹ but in any case the direct π -ligand–monomer interaction is negligible with respect to the π -ligand–polymer chain and polymer chain–monomer interactions. An important exception is represented by π -ligands carrying substituents in the 4-position of indene: in this case, the direct π -ligand–monomer interaction is appreciable and with the opposite enantioface preference as that of propagation and in the end results in a higher number of 2,1 insertions (see section VII).

As for insertion of the unfavored propene enantioface, the one that originates a stereoerror, different pathways have been considered by Corradini and co-workers on one side and by Rappé, Morokuma, and co-workers on the other. According to Corradini, Guerra, and co-workers, the insertion reaction of the unfavored propene enantioface occurs with a geometry similar to structure B of Figure 22.^{91,92,200,263,266,267,271,272} This structure corresponds to the less stable geometry among the three structures of Figure 22. In fact, the growing chain is not oriented in an open sector anymore and repulsively interacts with the ligand framework. However, these repulsive interactions will be weakened as the insertion reaction takes place, since the $Mt-C(chain)$ bond is going to be broken and the remaining of the growing chain will be pushed away from the active center. Besides, the relative anti orientation of the methyl group of the propene and the β -C atom of the growing chain will not add any steric hindrance to the insertion reaction.

According to Rappé, Morokuma, and co-workers, instead, the insertion reaction of the unfavored propene enantioface occurs with a geometry similar to that of structure C of Figure 22.^{147,155,274,275} At the level of the olefin complex, structure C is slightly higher in energy than structure A, due to repulsive interactions between the propene monomer and the growing chain. However, in this structure the methyl group of the propene is syn (i.e. close) to the β -C atom (and followings) of the growing chain. Although these repulsive interactions are small at the coordination stage, their intensity will grow up when the insertion reaction takes place, and the tight four-center transition state will be reached.

In this respect, MM calculations on approximate transition state geometries by Morokuma and co-workers on the propene insertion into the $Zr-C(isobutyl)$ σ -bond of the achiral $H_2Si(Cp)_2Zr(isobutyl)^+$ system showed that the syn orientation of the methyl group of propene and of the growing chain is disfavored by more than 5 kcal/mol relative to the anti orientation.¹⁵⁵ Furthermore, MM calculations on approximate transition state geometries of several C_2 -symmetric metallocenes^{272,273} indicated that, at the transition state level, structure C—with a syn orientation of the methyl group of propene and of the growing chain—is disfavored by roughly 3 kcal/mol relative to structure B—with an anti orientation of the methyl group of the propene and of the growing chain.

In short, the above analysis indicates that the enantioselectivity of these catalysts is not due to direct interactions of the π -ligands of the metallocene with the monomer, but to interactions of the π -ligands of the metallocene with the growing chain, determining its chiral orientation which, in turn, discriminates between the two prochiral faces of the propene monomer. The mechanism of the *chiral orientation of the growing chain* is grounded on the seminal works of Corradini and co-workers on the enantioselectivity of the classical heterogeneous Ziegler–Natta catalysts.^{258–262} Moreover, it is worthy to note that the conformation consistent with a chiral orientation of the growing chain places one of the α -hydrogen atoms of the growing chain in a position which is extremely favorable for the formation of an α -agostic interaction that has been shown to facilitate the insertion reaction.¹⁹⁴

The catalytic complexes based on the *rac*- $C_2H_4(1-Ind)_2$ ligand and its tetrahydroindenyl homologue were also investigated by Chien and co-workers.²⁷⁶ In particular, they investigated propene insertion on growing chains presenting different agostic interactions with the metal atom. Using geometrical constraints, they simulated insertion of propene on growing chains showing no and α -, β -, and γ -agostic interactions. Since no sketches of the models are presented, is difficult to clearly understand which geometries were computed. However, according to their calculations, the presence of the α -agostic interaction increases the enantioselectivity of 0.7 kcal/mol, while the β - and γ -agostic interactions sensibly reduce the enantioselectivity, and insertion

on the γ -agostic chain is substantially nonenantioselective.²⁷⁶

The enantioselective mechanism above depicted is in accordance with the elegant analysis and optical activity measurements by Pino et al. on the saturated propene oligomers obtained with this kind of catalyst (under suitable conditions), proving that *re* insertion of the monomer is favored in case of (*R,R*) chirality of coordination of the $C_2H_4(1-Ind)_2$ ligand.⁸³ Moreover, similar studies on simultaneous deuteration and deuteriooligomerization of 1-alkenes using catalysts based on (*R,R*) $C_2H_4(H_4-1-Ind)_2$ zirconium derivatives have shown that in the dimerizations and oligomerizations of 1-alkenes (propene, 1-pentene, 4-methylpentene) the *R* enantioface of the olefin is predominantly involved, whereas in the deuteration of 1-alkenes (1-pentene, styrene) the *S* enantioface is favored.⁸⁶ These results confirm that the growing chain plays a primary role in enantioface discrimination in stereospecific polymerization catalysis. The presence of opposite enantioselectivities in deuteration and oligomerization has been rationalized by Corradini, Guerra, and co-workers²⁶⁸ by means of molecular mechanics calculations analogous to those previously described. This constitutes further valuable support to the proposed catalytic models and enantioselective mechanism. More recent results by Bercaw relative to deuteration and deuteriodimerization experiments on isotopically chiral 1-pentene are also in agreement with a mechanism involving a chiral orientation of the growing chain.²⁸²

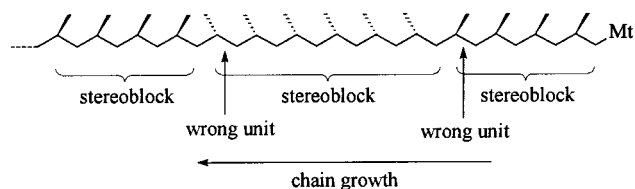
I. Mechanism of Chain-End Control in Primary Insertion

Chain-end control is less effective than site control, the $\Delta\Delta E^\ddagger$ between the insertion of the two enantiofaces being around 2 kcal/mol. Relevant examples of chain-end control are the isospecific polymerization of propene with Cp_2TiR_2/MAO (Scheme 23)^{22,283–285} and with Cp_2ZrR_2/MAO ²⁸⁶ and the syndiospecific polymerization of 1-butene with $(Me_5Cp)_2MtCl_2/MAO$ ($Mt = Zr, Hf$).¹¹⁵

Note that isospecific chain-end control is effective only at low temperature, producing PP with low stereoregularity and low molecular weight. For the simplest system described by Ewen, the lower the polymerization temperature, the higher both the activity and isotacticity become, with the highest value being reached at $-45\text{ }^\circ\text{C}$ ($m = 0.85$). Further decrease in polymerization temperatures has no effect on isotacticity. Molecular weights have a bell-shaped dependence on T_p with a maximum at around $-45\text{ }^\circ\text{C}$. The insertion mistakes are diagnostic of chain-end control: as chiral induction comes from the last formed stereogenic carbon, whenever a wrong enantioface is inserted, the error propagates itself until another error occurs^{20,22} (Scheme 23 and Figure 23).

The frequency of these misinsertions is quite high, being about 8% in the more isotactic samples. This value results in an average stereoblock length of only about 12 units and explains the low melting point ($\approx 60\text{ }^\circ\text{C}$) and low crystallinity ($<20\%$) observed for this material and its physical properties, which are

Scheme 23



typical of a thermoplastic elastomeric polypropene.^{287,288} For polymerization temperatures above $0\text{ }^\circ\text{C}$, an essentially atactic polymer is obtained. Due to the above limitations, which add to a low catalyst activity, this polypropene remains a scientific curiosity.

The possible origin of the low stereoselectivity for the chain-end-controlled catalytic systems based on metallocenes including two cyclopentadienyl rings has been discussed by Corradini, Guerra, and co-workers.²⁸⁹ The two possible diastereomeric preinsertion intermediates for *si* and *re* coordinations of the monomer for the case of a *si* chain—that is, a growing chain in which the last monomeric unit has been obtained by addition of a *si*-coordinated propene—are shown in Figure 24, parts A and B, respectively. These models would lead to a *si-si* and *re-si* propene enchainments, that is, to an isotactic and syndiotactic diad, respectively.

These models of preinsertion intermediates are geometrically similar to those found for stereorigid metallocenes (see Figure 22A). Moreover, they present the propene methyl group and the second carbon atom (and its substituents) of the growing chain in a relative anti disposition. The chain-end control of the enantioselectivity for these poorly isospecific systems could be related to easier insertion paths starting from models for isospecific propagation (Figure 24A). In fact, calculations relative to other significant points of the insertion paths—possibly closer to the transition states—indicated that for syndiotactic propa-

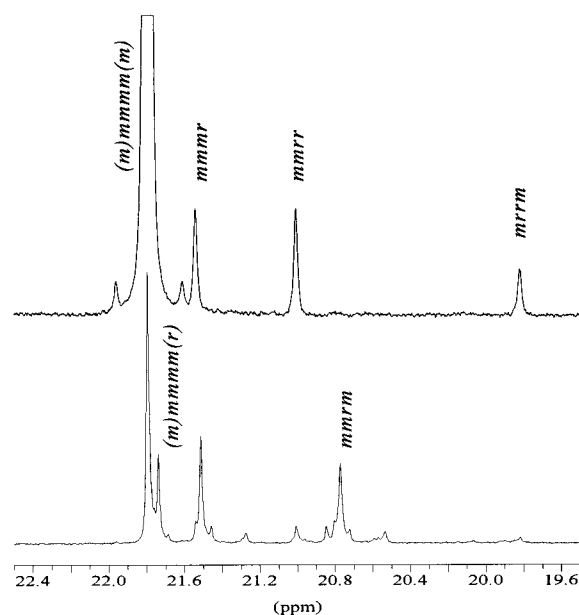


Figure 23. ^{13}C NMR (100 MHz, $C_2D_2Cl_4$, $120\text{ }^\circ\text{C}$, ref. $mmmm$ at 21.8 ppm) of two *i*-PP samples prepared under site control (top) and chain-end control (bottom) ($mmmm = 48.8\%$, $mmmr = 19.2\%$, $mmrm = 19.2\%$).

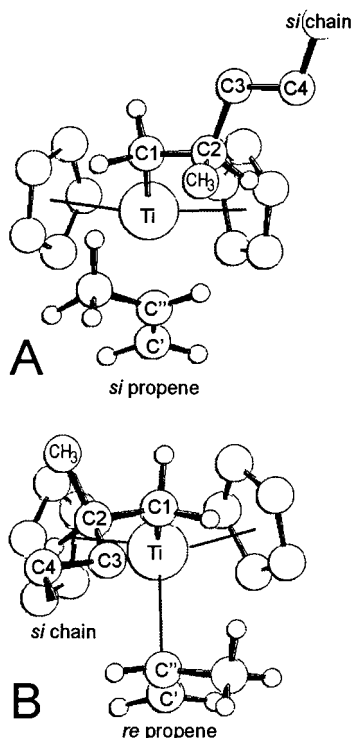


Figure 24. Molecular mechanics minimum energy geometry for *re* and *si* propene coordination on the Cp_2Ti -(growing chain) model. The growing chain is labeled as *si*-chain, since the chirality of its tertiary carbon atom closest to the metal has been obtained by a primary insertion of a *si*-coordinated propene. For the model corresponding to isospecific propagation (a) the chain (atoms C3, C4...) points away from the olefin, while for the model corresponding to syndiospecific propagation (b) it points toward the olefin.

gation the positions of a higher number of C atoms of the growing chain should be changed in the rate-determining step. According to the "least nuclear motion",^{97,290,291} the path that corresponds to the minimum displacement of atoms should be slightly favored, and hence the model should be slightly isospecific.²⁸⁹

IV. Stereocontrol: Influence of the Catalyst

Certainly one of the main reasons for the enormous scientific interest raised by metallocene catalysts has been the discovery that stereoselectivity in propene polymerization can be driven to an unprecedented extent, thanks to the flexibility of the cyclopentadienyl ligands substitution, and the consequent challenge offered to the synthetic chemist. Although the principal aim has been to make more and more isospecific catalysts, there is little chance, in our view, that metallocenes can rival the latest generations of $MgCl_2$ -supported Ti catalysts in the industrial production of highly isotactic polypropene. On the other hand, for the very reason that metallocenes are so uniquely stereotunable, their real potential lies in the unprecedented possibility of producing polypropenes of virtually any degree of stereoregularities and molecular weights, in particular, the range of polypropenes with reduced isotacticity (from the lower crystallinity and lower melting point PP to the elastomeric and amorphous PP), which will soon

challenge PS and flexible PVC in their own fields of application.^{125,292–295}

In the following, we will review the most interesting examples of stereoregular polymerizations and analyze the correlation between ligand substitution and catalyst behavior. Our view of the evolution of metallocene catalysts for polypropene is shown in Chart 4. The strong influence of the polymerization conditions will be discussed in section V. The influence of the cocatalyst type and of the catalyst/cocatalyst ratio has not been, in our opinion, exhaustively investigated; in any case, for MAO-cocatalyzed systems, our experience with chiral zirconocenes is that the aluminum concentration has a major influence on catalyst activity but neither on microstructure nor on *i*-PP molecular weight when the polymerization is carried out in liquid propene. The available data will also be discussed in section V.

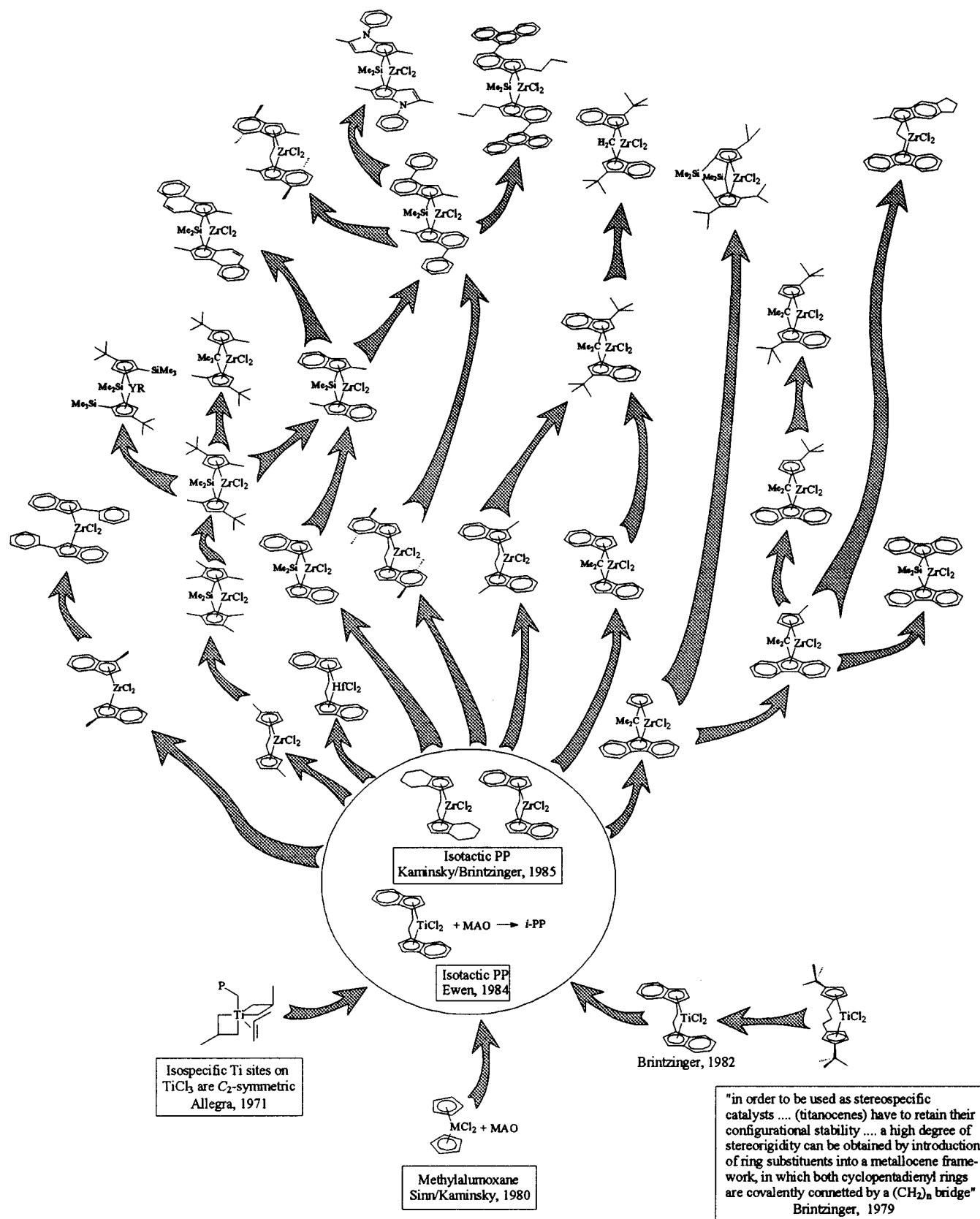
A. Isotactic Polypropene: C_2 -Symmetric Metallocenes

The most important mechanism of stereospecific polymerization is isospecific enantiomorphic site control,²⁹⁶ which allows today the production of more than 25 million tons per year of isotactic polypropene and its copolymers, in a wide range of molecular weights and crystallinities. As already mentioned in section II, the molecular architecture of polypropenes obtained from *ansa*-zirconocenes is strongly dependent on the biscyclopentadienyl ligand structure.

By using Brintzinger's *ansa*-titanocene $C_2H_4(1-Ind)_2TiCl_2$,¹⁸ Ewen first proved the correlation between metallocene chirality and isotacticity,²² a textbook example of shape selective catalysis. The C_2 -symmetric, *racemic* form yields isotactic polypropene while the achiral, *meso* form produces low molecular weight atactic polypropene. However, this titanocene is unstable at normal temperatures and has a quite low activity and a low stereoselectivity, producing *i*-PP with only 71% *mm* and a T_m of 94 °C. Shortly after Ewen's disclosure, Kaminsky and Brintzinger reported that a similar C_2 -symmetric zirconocene, racemic $C_2H_4(H_4-1-Ind)_2ZrCl_2$ (C_2 -I-1H₄),¹⁹ produced much higher yields of *i*-PP,²³ although the polymer properties were not reported at that time. In the following 15 years, several different classes of C_2 -symmetric, racemic *ansa*-metallocenes for the isospecific polymerization of 1-olefins have been devised, a huge number of different ligand structures have been synthesized, and the substituent effect on polymer properties and catalyst activity is now mastered to a high level. As far as the transition metal is concerned, Hf usually produces higher molecular weights than Zr and Ti, but Zr is by far the most active and practically the only metal used. The prototype of this class of metallocenes is Brintzinger's *rac*- $C_2H_4(1-Ind)_2ZrCl_2$ (C_2 -I-1 in Chart 5), which is also the best studied zirconocene from both the synthetic^{19,297–303} and catalytic standpoints.^{50,232,304,305}

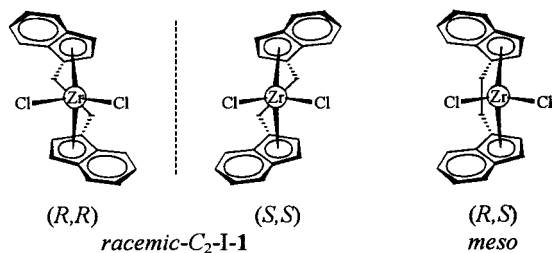
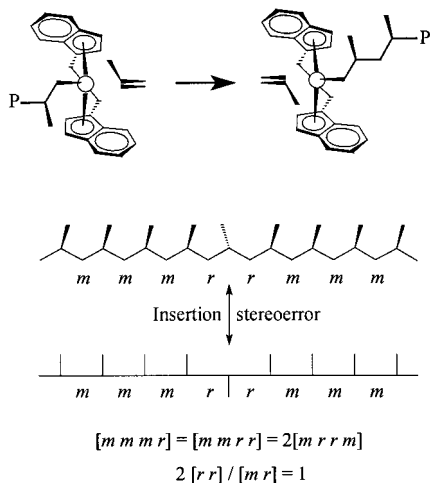
The two chiral enantiomers exert isospecific enantiomorphic site control by virtue of their C_2 symmetry, while the *meso* (achiral) isomer produces

Chart 4



atactic polypropene. Taking into account all the requirements for olefin insertion at metallocene catalysts described in sections II and III, the formation of isotactic polymers is easily accounted for (Scheme 24). For the sake of the following discussion, we will divide the isospecific catalysts operating by

site control into three main classes: the *ansa*- C_2 -symmetric (class I), the nonbridged, fluxional but chiral (class II), and the *ansa*- C_1 -symmetric (class III) (Chart 6). The most important, class I, will be discussed first, while class III will be discussed in section IV.C.

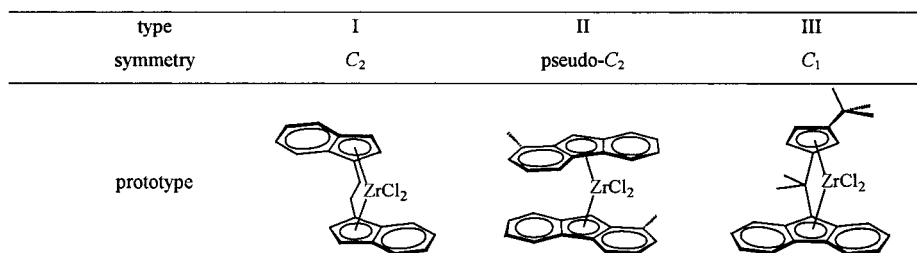
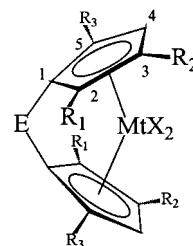
Chart 5. *racemic* and *meso*-C₂H₄(1-Ind)₂ZrCl₂**Scheme 24.** C₂-Symmetric Metallocenes: Isotactic Polypropene (site control)

1. Chiral *ansa*-C₂-Symmetric Metallocenes

The class based on chiral, stereorigid, racemic C₂-symmetric zirconocenes with bridged bis(3-alkylcyclopentadienyl) or bisindenyl ligands produce *i*-PP by enantiomeric site control with both isotacticities and molecular weights ranging from very low to very high. Chiral, C₂-symmetric *ansa*-zirconocenes produce polypropenes with microstructures ranging from almost atactic to almost perfectly isotactic and often containing isolated regioirregularities (see section VII).

The metallocene symmetry is maintained by a group (the bridge) that links the two cyclopentadienyl ligands, thus blocking their rotation; these compounds are usually referred to as chiral *ansa*-metallocenes and have the general formula shown in Chart 7.

Position 1 on the Cp is the connection to the bridge E, where E is usually CH₂CH₂, Me₂C, or Me₂Si; positions 3, 4 (the front positions) bear the β substituents, while the 2,5-positions (the rear ones) bear the α-substituents, where α and β indicate the distance from the bridge. The rear substituents are optional

Chart 6**Chart 7**

and have a secondary effect only on stereoselectivity (but a major one on chain release rate, as will be discussed in section VIII.A), while the front one is the one imparting the required symmetry to the molecule.

The basics of the mechanism which rules the enantioselectivity of monomer insertion have been described in sections III.H.I. Before entering into the maze of details on the correlations between catalyst structure and polymer microstructure, it is useful to discuss the results of the molecular modeling studies.

A systematic rationalization of the effects of different substitution patterns of the basic bridged biscyclopentadienyl and bisindenyl skeletons has been pursued by several research groups. A systematic comparison of models of different metallocenes can be obtained by inspection of Table 3 and Chart 8. The only advantage with respect to a comparison between calculations performed by different authors, or during the years by the same research group, is that all the reported numbers are calculated in exactly the same way.⁹¹ The application of standard molecular mechanics force fields to model organometallic systems in such an extensive way has no equals. During the years, more refined models and force fields have been developed³⁰⁶⁻³⁰⁹ that allowed the molecular modeling of Ziegler-Natta catalytic systems to improve from a very qualitative picture to semiquantitative results.

To better discuss the influence of the different ligand substitution patterns on the performance of C₂-symmetric isospecific metallocenes, it is convenient to subdivide them into biscyclopentadienyl (I-A), bisindenyl (I-B), and bisfluorenyl (I-C) types. The key substitution positions that have been demonstrated to be most important in determining the catalyst performance are indicated in Chart 9.

Chiral *ansa*-Metallocenes of Type I-A. There have been a few but quite important experimental studies on substituted biscyclopentadienyl ligands, the earlier one having shed considerable light on the correlation between Cp substitution and *i*-PP isotacticity and molecular weight.^{310,311} Representative

Table 3. Calculated Nonbonded Energy Contributions to Enantioselectivity for Preinsertion Intermediates ($\Delta\Delta E_{\text{enant}}$) and for Approximated Transition States ($\Delta\Delta E^{\ddagger}_{\text{enant}}$)

ligand ^a	metal atom	chirality of coordination of the π -ligand	propene coordination position	$\Delta\Delta E_{\text{enant}}^b$	$\Delta\Delta E^{\ddagger}_{\text{enant}}^b$	favored propene enantioface	$E_{\text{out}} - E_{\text{inw}}$
<i>C</i> ₂ -Symmetric Ligands							
1	Zr	(<i>R,R</i>)	—	0.1		<i>si</i>	
2	Zr	(<i>R,R</i>)	—	3.3		<i>re</i>	
3	Zr	(<i>R,R</i>)	—	7.0	5.9	<i>re</i>	
4	Zr	(<i>R,R</i>)	—	3.7		<i>re</i>	
5	Zr	(<i>R,R</i>)	—	3.8	2.3	<i>re</i>	
6	Zr	(<i>R,R</i>)	—	3.6		<i>re</i>	
7	Zr	(<i>R,R</i>)	—	0.0		—	
8	Zr	(<i>R,R</i>)	—	4.3	4.3	<i>si</i>	
9	Zr	(<i>R,R</i>)	—	0.0		—	
10	Zr	(<i>R,R</i>)	—	3.7		<i>re</i>	
11	Zr	(<i>R,R</i>)	—	6.4	5.0	<i>re</i>	
12	Zr	(<i>R,R</i>)	—	4.4		<i>re</i>	
13	Zr	(<i>R,R</i>)	—	4.9	3.0	<i>re</i>	
14	Zr	(<i>R,R</i>)	—	4.8	3.2	<i>re</i>	
15	Zr	(<i>R,R</i>)	—	0.1	0.3	<i>re</i>	
16	Zr	(<i>R,R</i>)	—	4.0	2.4	<i>si</i>	
17	Zr	(<i>R,R</i>)	—	5.3	3.1	<i>re</i>	
18	Zr	(<i>R,R</i>)	—	5.9	5.7	<i>re</i>	
19	Zr	(<i>R,R</i>)	—	5.5	3.8	<i>re</i>	
20	Zr	(<i>R,R</i>)	—	5.6		<i>re</i>	
21	Zr	(<i>R,R</i>)	—	5.3		<i>re</i>	
22	Zr	(<i>R,R</i>)	—	5.1	3.8	<i>re</i>	
23	Zr	(<i>R,R</i>)	—	4.3	3.5	<i>re</i>	
23	Ti	(<i>R,R</i>)	—	5.6	3.5	<i>re</i>	
24	Zr	(<i>R,R</i>)	—	5.7	4.7	<i>re</i>	
24	Ti	(<i>R,R</i>)	—	7.4		<i>re</i>	
25	Zr	(<i>R,R</i>)	—	1.4	1.3	<i>re</i>	
26	Zr	(<i>R,R</i>)	—	5.7	3.2	<i>re</i>	
27	Zr	(<i>R,R</i>)	—	6.1	10.1	<i>re</i>	
28	Zr	(<i>R,R</i>)	—	1.9		<i>re</i>	
29	Zr	(<i>R,R</i>)	—	4.7		<i>re</i>	
<i>C</i> _s -Symmetric Ligands							
30	Zr		<i>R</i>	3.7	2.1	<i>re</i>	
31	Zr		<i>R</i>	3.2	1.6	<i>re</i>	
32	Zr		<i>R</i>	2.3		<i>re</i>	
33	Zr		<i>R</i>	4.8		<i>re</i>	
<i>C</i> ₁ -Symmetric Ligands							
34	Zr	(<i>R</i>)	<i>R</i> \equiv inward	4.6		<i>re</i>	2.9
			<i>S</i> \equiv outward	1.1		<i>si</i>	
35	Zr	(<i>R</i>)	<i>R</i> \equiv inward	7.6		<i>re</i>	4.6
			<i>S</i> \equiv outward	2.1		<i>re</i>	
36	Zr	(<i>R</i>)	<i>R</i> \equiv inward	6.3		<i>re</i>	3.1
			<i>S</i> \equiv outward	2.2		<i>re</i>	
37	Zr	(<i>R</i>)	<i>R</i> \equiv inward	4.4		<i>re</i>	3.4
			<i>S</i> \equiv outward	1.5		<i>si</i>	
38	Zr	(<i>R</i>)	<i>S</i> \equiv inward	0.1		<i>re</i>	−0.9
			<i>R</i> \equiv outward	3.8		<i>re</i>	
39	Zr	(<i>R</i>)	<i>S</i> \equiv inward	0.3		<i>re</i>	−0.9
			<i>R</i> \equiv outward	2.6		<i>re</i>	

^a See Chart 8. ^b The calculation method is described in refs 91, 272, and 273.

examples are reported in Table 4 and Chart 10. In the series *rac*-Me₂Si(*R*_nCp)₂ZrCl₂, the influence of the alkyl substituent on C(2) on molecular weight and of the alkyl substituent on C(3) on isospecificity are introduced for the first time. The structurally related, but higher performance, 2-(*R*)-indenyl catalysts are discussed in the next session. Already the simplest ligand design, as is Me₂Si(3-MeCp)₂, affords a stereoselective catalyst, *rac*-Me₂Si(3-MeCp)₂ZrCl₂ (*C*₂-I-2). One of these zirconocenes (*C*₂-I-3) is now reportedly being considered suitable for industrial *i*-PP production.³¹²

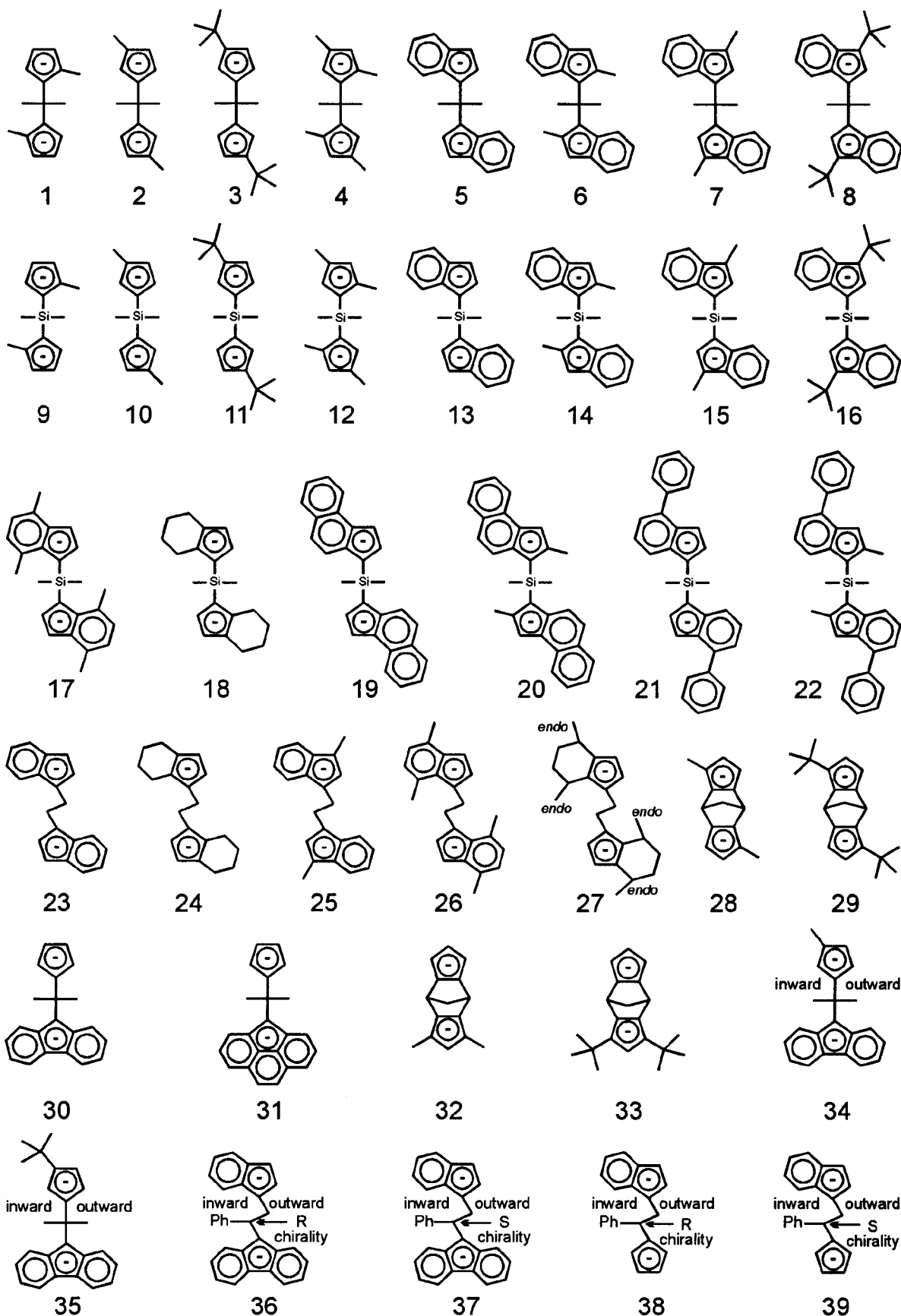
In Me₂Si-bridged systems, replacing a Me group with a *t*-Bu group β to the bridge worsens catalyst

performance, in terms of both activity and PP molecular weight, while adding a methyl group on C(2) improves the latter. These effects are more dramatic for polymerizations in liquid propene, suggesting that it is the bimolecular chain release by β -hydride transfer to the monomer, rather than the unimolecular β -hydride transfer to the metal, to be hindered by alkyl substitution on C(2). Also, the same effect is seen in Me₂C-bridged systems.³¹³

Analogues of *C*₂-I-4 with MeP= (inactive) and Me₂P+= (active) bridges have been reported.³¹⁴

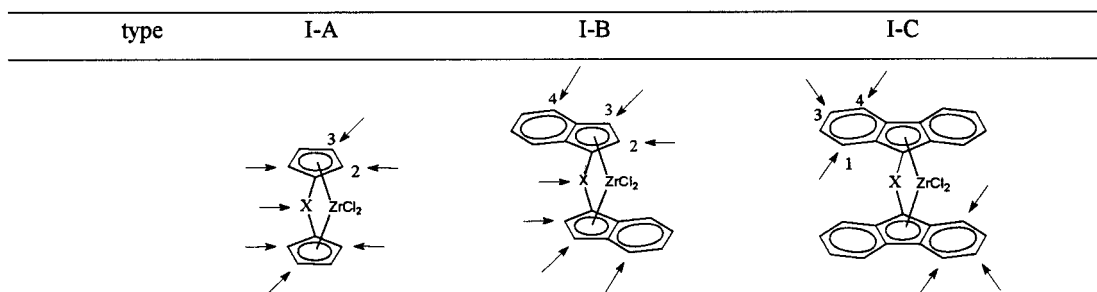
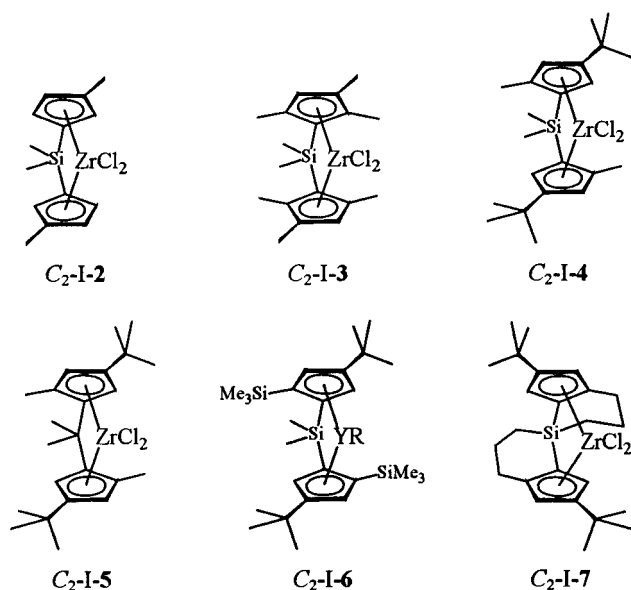
Three variations of the basic ligand design have been created by Brintzinger in order to prevent formation of the *meso* isomers: systems with a double

Chart 8



Me_2Si bridge,³¹⁵ with a spiroilane bridge,³¹⁶ and ligands with a biphenyl bridge that prevents the occurrence of meso isomers in the metalation step,

since the two 3,4-dimethylcyclopentadienyl ligands have homotopic faces.³¹⁷ However, only biscyclopentadienyl systems with a spiroilane bridge such as

Chart 9. Substitution Positions Most Relevant to Catalyst Performance in C_2 -Symmetric Biscyclopentadienyl, Bisindenyl, and Bisfluorenyl $ansa$ - C_2 -Symmetric Isospecific Zirconocenes**Chart 10. Representative Examples of C_2 -Symmetric $ansa$ -Biscyclopentadienyl Zirconocenes**

C_2 -I-7 have shown polymerization activity, although with a lower performance compared to their single bridged analogues.

The [*rac*- $Me_2Si(2-Me_3Si-4-t-BuCp)_2YH$] $_2$ (C_2 -I-6) was the first single-component isospecific catalyst to be developed, and it shows a similar stereoselectivity to the related zirconocenes, although a much lower activity. Probably both the dimeric nature of this system and the absence of a scavenger contributed to the low activity (low fraction of active centers), although the low molecular weight is in line with an intrinsically low monomer insertion rate.³¹⁸ Also divalent C_2 -symmetric samarium compounds have been shown to generate isospecific catalysts.³¹⁹

From a molecular modeling perspective, Corradini and Guerra, as well as Morokuma and their co-workers, have confirmed that a simple and small alkyl substituent such as a methyl group on the 3- and 3'-positions of the $C_2H_4(Cp)_2$ ²⁶⁷ and $H_2Si(Cp)_2$ ¹⁵⁵ ligands (see also entries **2** and **10** in Table 3) is already capable of ensuring enantioselectivity. Moreover, the bulkier the alkyl group on the 3- and 3'-positions, the higher the enantioselectivity. In fact, the enantioselectivity increases by roughly 3 kcal/mol, on going from the $Me_2Si(3-MeCp)_2$ ligand²⁷³ to the $Me_2Si(3-t-BuCp)_2$ ligand;²⁷² compare also entries **2** and **10** with entries **3** and **11** in Table 3. On the

contrary, methyl groups on the 2- and 2'-positions of the $C_2H_4(Cp)_2$ ligand²⁶⁷ (see also entries **1** and **9** in Table 3) are not able to ensure enantioselectivity. This clearly implies that the C_2 -symmetry is not a condition sufficient for enantioselectivity.^{267,273} However, a methyl group on positions 2 and 2' usually slightly enhances the enantioselectivity due to the alkyl group on the 3 and 3' positions of the cyclopentadienyl rings. In fact, Morokuma and Corradini calculated that a methyl group on positions 2 and 2' increases the enantioselectivity for primary propene insertion with the $H_2Si(3-MeCp)_2Zr$,¹⁵⁵ $Me_2Si(3-MeCp)_2Zr$,²⁷³ $Me_2C(3-MeCp)_2Zr$,²⁷³ and $Me_2Si(3-t-BuCp)_2Zr$ ²⁷² systems by roughly 1 kcal/mol. Compare also entries **2** and **4**, and **10** and **12** in Table 3. These calculations further support the broadly accepted idea that the substituents on the β -position are the ones which determine the stereocontrol, while the substituents on the α -position only have a secondary effect on stereocontrol.

Chiral $ansa$ -Metallocenes of Type I-B. The C_2 -symmetric chiral $ansa$ complexes based upon the strapped bisindenyl ligand represent the most successful class of isospecific zirconocenes, and countless variations of Brintzinger's basic design (C_2 -I-1) have been made, often requiring some quite inventive synthetic chemistry.^{26,27} As shown in Chart 9, in addition to the type of bridging unit, three indene positions are most important in determining catalyst performance: C(2) (α to the bridge), C(3) (β to the bridge), and C(4) on the condensed benzene ring. We shall in the following review first the molecular modeling studies, then the experimental data on the influence of the bridge and the different substitutions.

Models. As for alkyl substituents on the bridged bisindenyl skeleton, the most remarkable effects are obtained when substituents are present on the 3- and 3'-positions. If the substituents are methyl groups (entries **7**, **15**, and **25** in Chart 8, all calculations performed by Corradini,²⁶⁷ Morokuma,²⁷⁵ and Rappé^{147,274} indicated a substantial absence of enantioselectivity (see Table 3). In this case, the growing chain has no preferential orientation, since it repulsively interacts either with the methyl group on position 3 of the Cp ring (see Figure 25A) or with the six-membered group of the indenyl group (see Figure 25B). The absence of a chiral orientation of the growing chain implies that none of the two propene enantiofaces inserts preferentially. If the substituents on the 3- and 3'-positions are *tert*-butyl groups

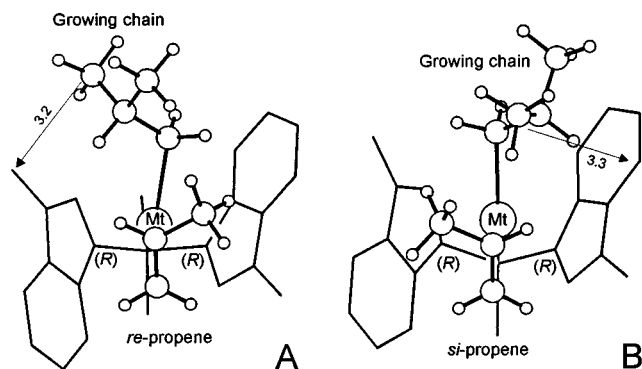


Figure 25. Molecular mechanics minimum energy geometry for *re* and *si* propene coordination on the (R,R) - $\text{Me}_2\text{-Si}(3\text{-Me-1-Ind})_2\text{Zr(isobutyl)}$ model. Short interaction distances in Å.

(entries **8** and **16** in Table 3), the model is again isospecific.²⁷² However, it is relevant to note that in this case the *tert*-butyl group is sterically more demanding than the indenyl group, and hence, the growing chain is preferentially oriented toward the indenyl group, favoring the insertion of the *si* propene enantioface for the (R,R) chirality of coordination of the *tert*-butyl-substituted bisindenyl ligand (see Figure 26), whereas for the parent unsubstituted (R,R) coordinated indenyl ligand, insertion of the *re* propene enantioface is favored.

These findings are in agreement with the experimental observation that prevalently atactic PP is obtained with the $\text{C}_2\text{H}_4(3\text{-Me-1-Ind})_2\text{ZrCl}_2/\text{MAO}$ and $\text{Me}_2\text{Si}(3\text{-Me-1-Ind})_2\text{ZrCl}_2/\text{MAO}$ catalysts,^{116,320} while moderately isotactic PP is obtained with the $\text{Me}_2\text{Si}(3\text{-}t\text{-Bu-1-Ind})_2\text{ZrCl}_2/\text{MAO}$ ^{322,323} and highly isotactic PP with the $\text{Me}_2\text{C}(3\text{-}t\text{-Bu-1-Ind})_2\text{ZrCl}_2/\text{MAO}$ ^{50,272} and $\text{H}_2\text{C}(3\text{-}t\text{-Bu-1-Ind})_2\text{ZrCl}_2/\text{MAO}$ catalysts.³²⁴

Methyl substituents on the 4- and 4'-positions of the bridged bisindenyl skeleton (entries **17**, **21**, **22**, **26** and **27** in Chart 8 and Table 3) have been shown to slightly increase the enantioselectivity of each insertion step.^{272,274,275} Rappé and Morokuma systematically increased the size of the substituent R on the 4- and 4'-positions of the $\text{C}_2\text{H}_4(1\text{-Ind})_2$ ²⁷⁴ and $\text{H}_2\text{Si}(1\text{-Ind})_2$ ²⁷⁵ ligands coordinated to a Zr atom. Within the R = hydrogen, methyl, ethyl, isopropyl, and *tert*-butyl series, the methyl and isopropyl groups are the ones which most enhance the enantioselectivity, whereas the *tert*-butyl group reduces the enantioselectivity. The last result has been ascribed to direct repulsive interactions of the *tert*-butyl group with the methyl group of the propene which, in the case of the favored propene enantioface, points toward the *tert*-butyl group.²⁷⁴ A similar increase of enantioselectivity due to the presence of methyl group on positions 4 and 4' was also found by Corradini and co-workers, which calculated an increase of roughly 1 kcal/mol in the enantioselectivity for primary propene insertion into the Zr–C(isobutyl) σ -bond of the $\text{C}_2\text{H}_4(1\text{-Ind})_2$ and $\text{C}_2\text{H}_4(\text{H}_4\text{-1-Ind})_2$ ligands, when methyl groups are present in both 4,4'- and 7,7'-positions.²⁷²

Methyl substituents on the 5,5', 6,6', and 7,7'-positions of the bisindenyl skeleton have been shown to have a negligible effect on enantioselectivity,^{267,274}

Table 4. Propene Polymerization with Representative Substituted Bis-Cp Zirconocene/MAO Catalysts

catalyst	T_p , °C	$\text{Al}_{\text{MAO}}/\text{Zr}$, molar ratio	propene (solvent)	activity, $\text{kg}_{\text{PP}}/(\text{mmol}_{\text{Zr}} \cdot \text{h})$	\bar{M}_w	\bar{M}_w/\bar{M}_n	T_m , °C	% mmmm ^a	% 2,1 ^b	ref
$\text{rac-C}_2\text{H}_4(3\text{-Me-Cp})_2\text{ZrCl}_2$	40	2 000	3 bar (toluene)	5.8	19 600	2.3	133	92.2	nr	120
$\text{rac-C}_2\text{H}_4(3\text{-}i\text{-Pr-Cp})_2\text{ZrCl}_2$	40	2 000	3 bar (toluene)	4.5	19 400	2.2	136	94.6	nr	120
$\text{rac-C}_2\text{H}_4(3\text{-}t\text{-Bu-Cp})_2\text{ZrCl}_2$	40	2 000	3 bar (toluene)	1.0	17 400	2.5	141	97.6	nr	120
$\text{rac-Me}_2\text{Si}(3\text{-Me-Cp})_2\text{ZrCl}_2$ (C₂-I-2)	30	10 000	3 bar (toluene)	16.3	13 700	2.3	148	92.5	nr	310
$\text{rac-Me}_2\text{Si}(3\text{-}t\text{-Bu-Cp})_2\text{ZrCl}_2$	30	10 000	3 bar (toluene)	0.3	9 500	2.3	149	93.4	nr	310
$\text{rac-Me}_2\text{Si}(2,4\text{-Me}_2\text{-Cp})_2\text{ZrCl}_2$	30	10 000	3 bar (toluene)	11.1	86 500	1.9	160	97.1	nr	310
$\text{rac-Me}_2\text{Si}(2,4\text{-Me}_2\text{-Cp})_2\text{ZrCl}_2$	70	15 000	liquid propene	97	31 000	1.9	149	89.2	nr	320
$\text{rac-Me}_2\text{Si}(2,3,5\text{-Me}_3\text{-Cp})_2\text{ZrCl}_2$ (C₂-I-3)	30	10 000	3 bar (toluene)	1.6	133 900	2.0	162	97.7	nr	310
$\text{rac-Me}_2\text{Si}(2,3,5\text{-Me}_3\text{-Cp})_2\text{ZrCl}_2$ (C₂-I-3)	50	15 000	liquid propene	207	184 500	1.9	161	96.4	0.3	312
$\text{rac-Me}_2\text{Si}(2\text{-Me-4-}t\text{-Bu-Cp})_2\text{ZrCl}_2$ (C₂-I-4)	50	300	liquid propene	5	4 000 (M_n)	2.7	149	97	0.2	321
$\text{rac-Me}_2\text{Si}(2\text{-Me-4-}t\text{-Bu-Cp})_2\text{ZrCl}_2$ (C₂-I-4)	70	15 000	liquid propene	10	19 000	2.0	155	94.3	nr	320
$\text{rac-Me}_2\text{Si}(2\text{-Me-4-}t\text{-Bu-Cp})_2\text{ZrCl}_2$ (C₂-I-4)	50	3 000	liquid propene	15	17 000 (M_n)	1.9	153	99.5 ^c	0.4	313
$\text{rac-Me}_2\text{C}(2\text{-Me-4-}t\text{-Bu-Cp})_2\text{ZrCl}_2$ (C₂-I-5)	50	8 000	liquid propene	73	103 000	1.9	162	99.5 ^c	0.16	318
$[\text{rac-Me}_2\text{Si}(2\text{-Me}_3\text{-Si-4-}t\text{-Bu-Cp})_2\text{YH}]_2$ (C₂-I-6)	25	none	25% v/v ($\text{Me}_6\text{C}_8\text{H}_{11}$)	very low	4 200 (M_n)	2.3	157	97.0	nr	313
C₂-I-7	50	1 200	2 bar (toluene)	2	9 800	1.8	128	97	2.5 ^d	316

^a From ¹³C NMR. The values are referred to the total methyl signals. ^b Total of regioerrors (see section VII). ^c On primary insertions only. ^d 3,1 units. nr = not reported.

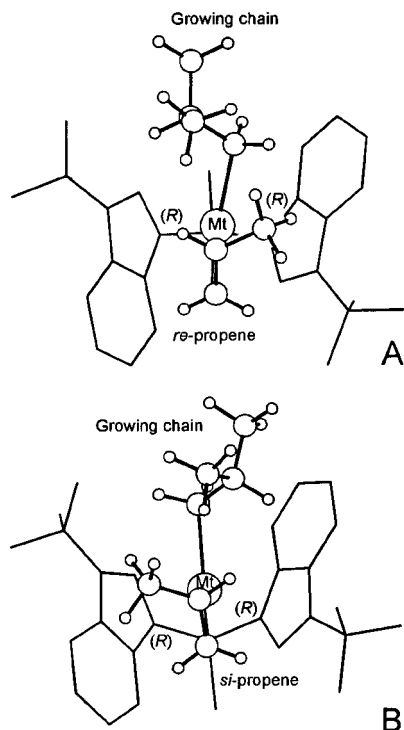
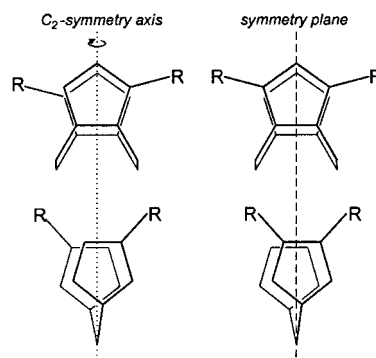


Figure 26. Molecular mechanics minimum energy geometry for *re* and *si* propene coordination on the (*R,R*)-Me₂-Si(3-*t*-Bu-1-Ind)₂Zr(isobutyl) model.

while methyl groups on the 2- and 2'-positions of the bridged bisindenyl skeleton, as for the systems based on the bridged biscyclopentadienyl skeleton, have been shown to slightly increase enantioselectivity.^{272–275} For instance, compare entries **13** and **14**, and **19** and **20** in Table 3. For entries **13** and **14**, compare the ΔE^\ddagger values. Furthermore, a six-membered ring fused on the 4,5- and 4',5'-positions of the bridged bisindenyl skeleton, as in the bridged (benz-[e]ind)₂ ligand (entries **19** and **20** in Table 3), basically behaves as a bisindenyl skeleton presenting methyl groups in the 4 and 4' positions. That is, slightly more enantioselective than the catalyst based on the parent ligand.^{273,275}

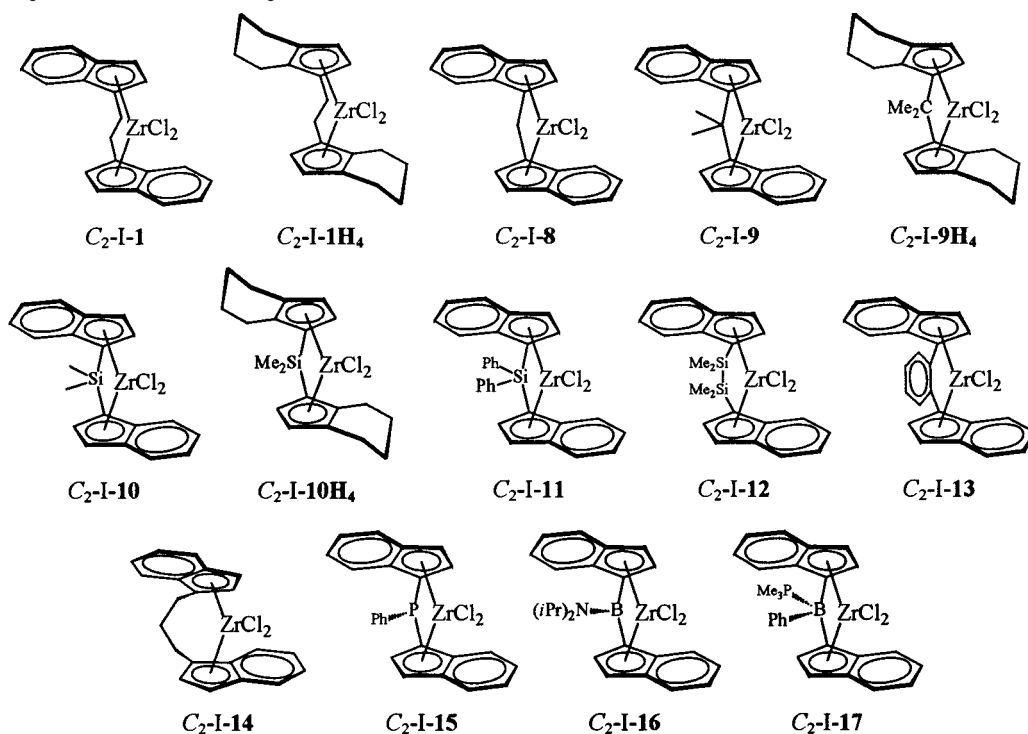
The calculation results listed in Table 3 are also able to account for the influence of the bridge on isospecificity. In fact, in agreement with the experimental results (see, e.g., ref 91), the calculated enantioselectivities for a given π -ligand are generally smaller for the Me₂C bridge than for the Me₂Si bridge (compare entries **2**, **4–6** with entries **10**, **12–14** in Table 3), while for the case of the C₂H₄ bridge, the enantioselectivities are often intermediates (compare entries **5**, **13**, and **23** in Table 3). Moreover, a double bridge usually reduces the calculated enantioselectivities with respect to the corresponding singly bridged complex (compare entries **28** and **29** with either entries **2** and **3** or entries **10** and **11** in Table 3), and it has been argued that this is due to the different orientation of the substituents which generate the enantioselectivity. For isospecific C₂-symmetric doubly bridged ligands, the substituents are more distant from the local symmetry axis (or local symmetry plane for syndiospecific C_s-symmetric ligands) relative to singly bridged ligands (Scheme 25).²⁷¹

Scheme 25



Experimental Results. Influence of the Bridge. A large series of unsubstituted bisindenyl chiral *ansa*-zirconocenes with different bridges have been prepared. Some examples are shown in Chart 11. Stereoselectivity and molecular weight increase in the order H₂C < Me₂C < C₂H₄ < Me₂Si. R₂Ge bridges have also been used, as well as a plethora of R₂Si bridges with different R groups. Several bisindenyl complexes have been made which have longer bridges, such as 1,3-propylene³²⁵ and *o*-xylilene,^{326,327} but in all cases their catalytic performance becomes poorer in terms of both stereoselectivity and activity. This effect is very likely due to increased fluxionality and a strong deviation from C₂-symmetry. The –Me₂-SiCH₂CH₂SiMe₂–³²⁸ and –Me₂SiOSiMe₂–^{329,330} bridges render the corresponding *ansa*-bisindenyl or bis-(tetrahydroindenyl) zirconocenes inactive toward propene homopolymerization. The B-bridged bisindenyls, very recently made by Ashe³³¹ and Rietz,³³² do not seem to offer any advantages with respect to the simpler C-bridged systems. The P-bridged systems, reported by Schaverien³³³ and Alt,³³⁴ show a much decreased activity with respect to the C-bridged analogues. Selected polymerization data for unsubstituted bisindenyl chiral *ansa*-zirconocenes with different bridges, together with their corresponding tetrahydro complexes, are shown in Table 5.

Influence of Indene Substitution. As it is the case of *ansa*-bis(3-alkylcyclopentadienyl) complexes,^{310,312} the introduction of an alkyl substituent in the 2 position (α to the bridge) of *ansa*-bisindenyl zirconium complexes increases both stereoregularity and molecular weight of the produced polypropene³³⁵ and reduces the amount of regioirregularities, in comparison to the unsubstituted analogue. This effect is stronger in the indenyl systems compared to the cyclopentadienyl systems. The first example, *rac*-Me₂-Si(2-Me-1-Ind)₂ZrCl₂³³⁵ (Chart 12), led to the recent important development of the first zirconocenes whose performance approaches that of industrial Ti-based catalysts.³²⁰ A 4,7-dimethyl substitution as in C₂-I-**18**²⁹⁷ slightly increases stereoselectivity, but is detrimental to both regioselectivity and (as a direct consequence of the lower regioselectivity) to molecular weight.¹³⁰ Combining substitution in the 4- and 2- positions led to some of the most successful isospecific zirconocenes. In fact, *rac*-Me₂Si(2-Me-Benz[e]ind)₂ZrCl₂ (C₂-I-**25**),³³⁶ *rac*-Me₂Si(2-Me-4-Ph-1-Ind)₂ZrCl₂ (C₂-I-**28**),³²⁰ and similar 2,4-substituted indenyl systems produce *i*-PP with increased activity, isotacticity, and molecular weight compared to the

Chart 11. C_2 -Symmetric Bisindenyl ZirconocenesTable 5. Liquid Propene Polymerization with *rac*-Bisindenyl Zirconocene/MAO Catalysts: Influence of the Bridge and Indene Hydrogenation^a

zirconocene (racemic)	Al/Zr, M	T_p , °C	A , kg/(mmol _{Zr} ·h)	% <i>mmmm</i> ^b	% 2,1 ^c	T_m , °C	\bar{M}_v	\bar{M}_n	ref
C_2 -I-8	4 000	50	62	71.4 ₀	0.5	110	5 300		50
C_2 -I-9	3 000	50	66	80.6 ₉	0.4	127	11 000	6 500	50
C_2 -I-9	8 000	70	145	76.7 ₅	0.6	124		5 600	50
C_2 -I-9H ₄	3 000	50	37	95.8 ₈	0.6	147	25 300		131
C_2 -I-1 ^d	8 000	50	140	87.4 ₇	0.6	134	33 600		50
C_2 -I-1	8 000	70	252	83.4 ₇	0.7	125	19 600		50
C_2 -I-1H ₄	20 000	50	37	91.5 ₀	1.0	137	29 300		131
C_2 -I-10	3 000	50	17	90.3 ₀	0.5	144	56 000		50
C_2 -I-10	nr	70	190	81.7	nr	137	36 000 (\bar{M}_w)		341
C_2 -I-10H ₄	8 000	50	54	94.9 ₁	0.5	148	30 300		131
C_2 -I-11	nr	70	40	80.5	nr	136	42 000 (\bar{M}_w)		341
C_2 -I-12	nr	70	3	40.2	nr	73	9 000 (\bar{M}_w)		341
C_2 -I-15	nr	67	2	63.0	1.0	117	23 000	11 000	333
C_2 -I-16	nr	70	51	71.8	nr	113	nr		331
C_2 -I-17 ^e	1 000	60	0.2	85	nr	nr	62 000 (\bar{M}_w)		332

^a Polymerization conditions: 1-L stainless steel autoclave, 0.4 L of propene, 50 °C, 1 h, zirconocene/MAO aged 10 min.

^b Determined assuming the enantiomorphic site model, on primary insertions only; see ref 232. ^c Total secondary insertions determined by ¹³C NMR as described in ref 232; end groups not included. ^d Average values. ^e In toluene, 2 bar propene. nr = not reported.

biscyclopentadienyl and the unsubstituted bisindenyl zirconocenes. On the basis of industry reports, C_2 -I-25 and C_2 -I-28 have been successfully supported on a carrier, retaining their high activity also at low Al/Zr ratios, and have met the requirements for plant scale production of *i*-PP. Along this evolutionary line, *rac*-Me₂Si[2-Me-4-(α -naphthyl)-1-Ind]₂ZrCl₂ (C_2 -I-29), *rac*-Me₂Si[2-(*n*-Pr)-4-(phenanthryl)Ind]₂ZrCl₂ (C_2 -I-30),³³⁷ and *rac*-Me₂Si[2-Et-4-(α -naphthyl)-1-Ind]₂ZrCl₂³³⁸ have been reported to yield *i*-PP with even higher T_m and molecular weight. Some relevant results are reported in Table 6, together with the direct comparison with their analogues without a 2-methyl substituent. Concerning the pentad values reported in Tables 4–6, it is worth noting that, when regioirregularities are not explicitly reported, the

mmmm value is likely measured on the total of methyl signal and not (see section VI) on the primary insertions only. As an example, C_2 -I-28 is reported to have a 95% pentad content.³²⁰ Our analysis of *i*-PP made with C_2 -I-28 under similar conditions gave a *mmmm* value, measured on the primary insertions only, of more than 99%! The difference is due to 0.5% of 2,1 units (see section VII), which are then responsible for the melting point of 157 °C. *rac*-C₂H₄(2,4,7-Me₃-1-Ind)₂ZrCl₂ (C_2 -I-19)³³⁹ has also been reported to yield highly isotactic ($T_m > 160$ °C) and regioregular PP, but with a lower molecular weight, although the results were obtained at very low polymerization temperature and the quality of the published spectra is not good enough to support the authors' claims. For liquid propene polymerization at $T_p = 70$ °C, the

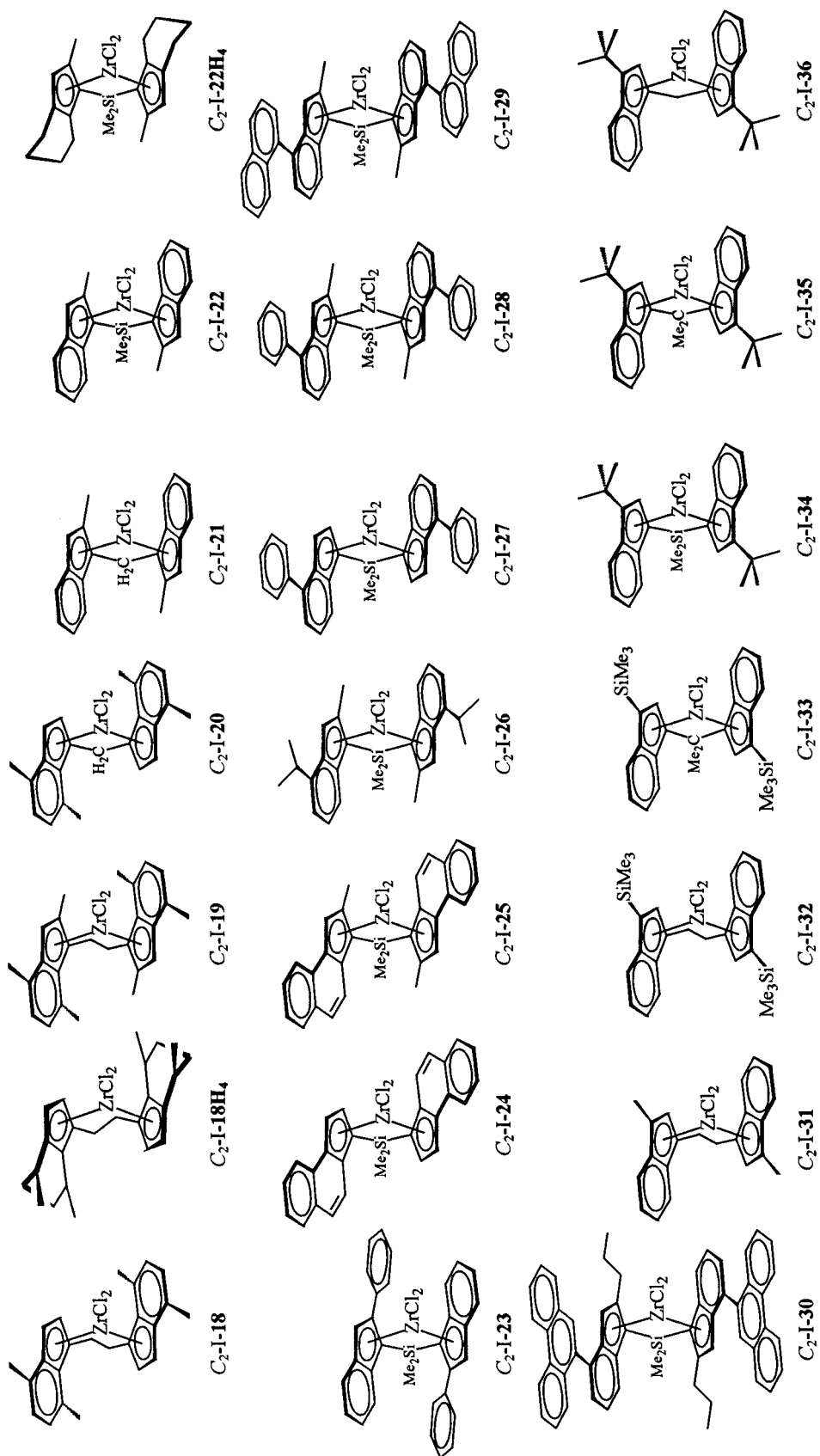
Chart 12. C_2 -Symmetric Substituted Bisindenyl Zirconocenes

Table 6. Propene Polymerization with *rac*-Bisindenyl Zirconocene/MAO Catalysts: Influence of Indene Substitution^a

zirconocene (racemic)	Al/Zr, molar ratio	T_p , °C	A , kg/(mmol _{Zr} h)	% <i>mmmm</i>	% 2,1	T_m , °C	\bar{M}_w	\bar{M}_n	ref
<i>C</i> ₂ -I-18 ^b	2 000	50		91.8 ₄	1.9	131		3 400	342
<i>C</i> ₂ -I-18	2 000	70		90.7	2.4	nd		2 800	342
<i>C</i> ₂ -I-18H ₄	2 000	50	5	nd	18				131
<i>C</i> ₂ -I-18H ₄		70		nd	23.6				341
<i>C</i> ₂ -I-19	^c	30	21	90.6	nr	158		19 000	339
<i>C</i> ₂ -I-21	2 000	50	20	85.8	0.8	122		2 500	202
<i>C</i> ₂ -I-21	2 000	70	56	63.9 ₆					202
<i>C</i> ₂ -I-22	4 000	50	33	94.2 ₅					50
<i>C</i> ₂ -I-22	15 000	70	99	88.5	nr	145	195 000		320
<i>C</i> ₂ -I-22H ₄	15 000	70	40	87.4	nr	144	55 000		320
<i>C</i> ₂ -I-23	1 000	20	2.4	87	nr	139	444 000		343
<i>C</i> ₂ -I-24	15 800	50	288 ^d	90	0.7	142	39 600		336
<i>C</i> ₂ -I-24	15 000	70	274	80.5	nr	138	270 000		320
<i>C</i> ₂ -I-25	15 800	50	145 ^e	93	0.3	152	247 700		336
<i>C</i> ₂ -I-25	15 000	70	403	88.7	nr	146	330 000		320
<i>C</i> ₂ -I-26	15 000	70	245	88.6	nr	150	213 000		320
<i>C</i> ₂ -I-27	15 000	70	48	86.5	nr	148	42 000		320
<i>C</i> ₂ -I-28	10 000	50	1300	99.5 ₅	0.5				324
<i>C</i> ₂ -I-28	15 000	70	755	95.2	nr	157	729 000		320
<i>C</i> ₂ -I-29		70	875	99.1	nr	161	920 000		320
<i>C</i> ₂ -I-29	350	50	22.5 ^f	98.6	0.3	156	380 000		337
<i>C</i> ₂ -I-30	350	50	46.8 ^f	99.2	0.2	160	400 000		337
<i>C</i> ₂ -I-31	8 000	50	28	19.9 ₆	0	amorphous	15 800 (\bar{M}_n)		50
<i>C</i> ₂ -I-32		70	0.5	10.5	nr	liquid	700		341
<i>C</i> ₂ -I-33	3 000	50	74	85.9	0	135	70 900 (\bar{M}_n)		50
<i>C</i> ₂ -I-33	3 000	70	44	80.7	0	127	44 300 (\bar{M}_n)		50
<i>C</i> ₂ -I-34	2 000	1	2.6	75.5 (<i>mm</i>)	nr		5 000		323
<i>C</i> ₂ -I-35	8 000	50	125	94.8	0	152	89 400 (\bar{M}_n)		50
<i>C</i> ₂ -I-35	8 000	70	110	91.2	0	142	25 300 (\bar{M}_n)		50
<i>C</i> ₂ -I-36	1 000	50	37	97.0	0	162	236 800		324
<i>C</i> ₂ -I-36	1 000	70	48	95.2	0	154	74 100		324

^a Liquid propene polymerizations, unless otherwise specified. See Table 4. ^b Average values. ^c Cocatalyst Ph₃CB(C₆F₅)₄/Al(*i*Bu)₃. ^d In toluene, 7 bar, 20 min. ^e In toluene, 5 bar, 12 min. ^f In toluene, 1 bar, 15 min.

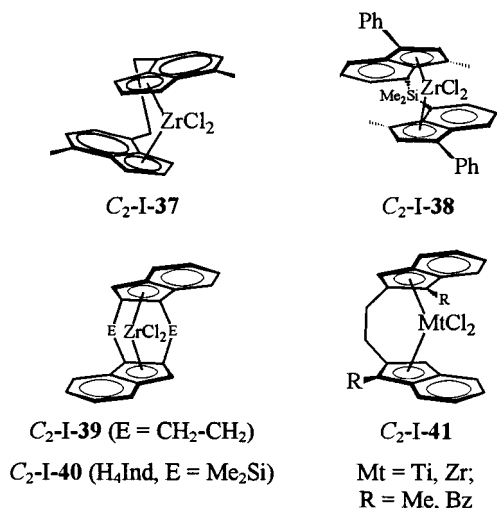
Hoechst group had previously reported that *C*₂-I-19 produces *i*-PP with a relatively low molecular weight ($M_w = 30\,600$) and a low melting point of 145 °C.³⁴⁰

The newest version of *C*₂-symmetric *ansa*-bisindenyl system has been proposed, once more, by Ewen.³²² This novel design is constituted of two strapped indenyls with a bulky substituent on C(3) of indene. The prototype of this class, *rac*-Me₂Si(3-*t*-Bu-1-Ind)₂ZrCl₂, was however reported by Miyake³²³ to have a lower stereoselectivity compared to that of the early *C*₂-symmetric zirconocenes. We recall here that both *rac*-C₂H₄(3-Me-1-Ind)₂ZrCl₂ and *rac*-Me₂Si(3-Me-1-Ind)₂ZrCl₂ were previously shown to be practically aspecific, and also to produce low molecular weight polypropenes.^{116,341} It was the observation that *C*₂-I-31 is fully regioselective, and also the availability of a new and easy synthesis of isopropylidene-bridged bisindenyl ligands,³⁰¹ that lead to the conceivment of *rac*-Me₂C(3-*t*-Bu-1-Ind)₂ZrCl₂ (*C*₂-I-35) as the best possible candidate for an improved isospecific zirconocene catalyst.⁵⁰ It was found that *C*₂-I-35/MAO is at the same time fully regioselective and produces *i*-PP with higher molecular weights than those obtained with *C*₂-I-1–*C*₂-I-18, especially at the lowest T_p . *C*₂-I-35/MAO, with *mmmm* always above 90%, is also highly stereoselective. It is worth noting that this behavior is not only a feature related to the bulky *tert*-butyl group on C(3), but is also due to the single C bridge, which imparts to the molecule a high rigidity and a large bite angle ($\beta = 75.2^\circ$, the largest of all zirconocenes shown in Table 1). If any of these

features is missing, a decrease in catalyst performance is observed. In fact, neither a silicon bridge nor an ethylene bridge produce good catalysts, as observed in the case of *rac*-Me₂Si(3-*t*-Bu-1-Ind)₂ZrCl₂ and *rac*-C₂H₄(3-Me₃Si-1-Ind)₂ZrCl₂.³⁴¹ The closely related *C*₂-I-36/MAO, with *mmmm* in the range 95–98%, is even more stereoselective and produces higher molecular weights than *C*₂-I-35/MAO and is one of the simplest chiral zirconocenes to synthesize.³²⁴

Influence of Changing the Bridging Position. Two basic variations of the classical 1,1'-bridging structure have been reported. Bosnich³⁴⁴ and Halterman³⁴⁵ synthesized a series of 2,2'-bisindenyl or tetrahydroindenyl ligands in which the two indenyls have homotopic faces and hence have the advantage of producing only one stereoisomer of the corresponding metallocenes (the same approach has been followed by Brintzinger in the case of 2,3-dimethylcyclopentadiene³¹⁷). Although elegant, this strategy is synthetically more demanding than the conventional bridging between the 1,1'-positions, and the polymerization performance of these systems should be expected to be disappointing.

Bridging the two 4,4'-positions has led to isospecific systems (Chart 13): *racemic* *C*₂-I-37 shows a quite low activity, producing PP of moderate isotacticity (*mmmm* = 63.5%, $T_m = 101^\circ\text{C}$ at $T_p = 50^\circ\text{C}$) and viscosity average molecular weight ($M_v = 15\,000$).³⁴⁶ As in the classic 1,1-bridged systems, varying Cp substitution generates a notable increase in per-

Chart 13. C_2 -Symmetric *ansa*-Bisindenyl Zirconocenes with Bridging Positions Different from 1,1'

formance: for example, *rac*- $Me_2Si(4,4'-(3-Me-1-PhInd)_2ZrCl_2$ (C_2 -I-38) produces *i*-PP with good activity, acceptable molecular weights, and good melting points (in liquid propene at $T_p = 70^\circ C$ and $Al_{(MAO)}/Zr = 5000$, $A = 224.7 \text{ kg}/(\text{mmol}_{Zr} \text{ h})$, $mmmm = 98.2\%$, 0.1% 3,1 units, $T_m = 155^\circ C$, and $M_n = 62\,000$).³⁴⁷

Doubly bridged bisindenyl zirconocenes such as C_2 -I-39^{315,348} have also been prepared, but polymerization results are not promising. For example, C_2 -I-40 does not seem to survive the reaction with the cocatalyst and gives very low polymer yields, presumably after degradation to a single bridged species.³¹⁵ Although an interesting series of C_2 -symmetric, 2,2'-bridged bisindenyl complexes of both Ti and Zr (C_2 -I-41) have been prepared by Nantz and co-workers,³⁴⁹ they have not been used in propene polymerization. Schaverien and co-workers also prepared C_2 -I-41 (Zr, R = Me), studied its polymerization performance under a variety of conditions, and found that it produces propene oligomers, but their tacticity was not described.³⁵⁰

Influence of Heteroatoms. Several attempts at introducing heteroatoms into the bisindenyl system have been made, with the clear aim of adding an electronic factor to systems whose performance is dictated by sterics (Chart 14).

Collins found that *rac*- $C_2H_4[5,6-(MeO)_2-1-Ind]_2ZrCl_2/MAO$ (C_2 -I-42) shows a much lower activity with respect to C_2 -I-1; the resulting *i*-PP is however identical to that made with C_2 -I-1 under identical conditions.²⁹⁷ Winter and co-workers prepared a series of heteroatom-substituted, racemic bridged bisindenyl zirconocenes,³⁵¹ including the 5-chloroindenyl, the 5,6-dichloro, and the 2-methoxy derivative C_2 -I-43, but all of them gave worse performance than the corresponding all-carbon zirconocenes. For example C_2 -I-43, in liquid propene at $70^\circ C$, gave with a very low activity an *i*-PP with $T_m = 127^\circ C$ and $M_w = 24\,500$.

Brintzinger has reported that *rac*- $Me_2Si(2-Me_2N-1-Ind)_2ZrCl_2/MAO$ (C_2 -I-44) polymerizes propene to *i*-PP with 85% *mmmm*, $T_m = 132^\circ C$ ($T_p = 50^\circ C$, $P = 2 \text{ bar}$) and a low M_n of 31 000.³⁵² This catalyst however suffers from a long induction period of 2–3 h, but is then active for many hours. Brintzinger observed that, in C_2 -I-44, the NMe_2 fragment is not coplanar with the indenyl part, hence the lone pair on nitrogen is not delocalized into the aromatic system. The Hoechst group and Näsman and co-workers have introduced $OSiMe_3$ ³⁵¹ and $OSiMe_2-t-Bu$ ^{353,354} groups in the 2-position of an *ansa*-bisindenyl zirconocene, e.g. C_2 -I-45. At $20^\circ C$ and 2 bar of propene, C_2 -I-45 produces a moderately isotactic, low molecular weight PP ($T_m = 148$, $M_w = 19\,100$), a performance similar to that of C_2 -I-1. C_2 -I-45H₄ is markedly less active, producing *i*-PP with a similar isospecificity and higher molecular weights. Recently, Ewen, Elder, and Jones³⁵⁵ have successfully introduced heteroatoms into the aromatic system of a series of chiral *ansa*-zirconocenes. For example, C_2 -I-46 has a very high activity in the production of *i*-PP of high molecular weight and relatively high melting point, with a performance challenging that of C_2 -I-

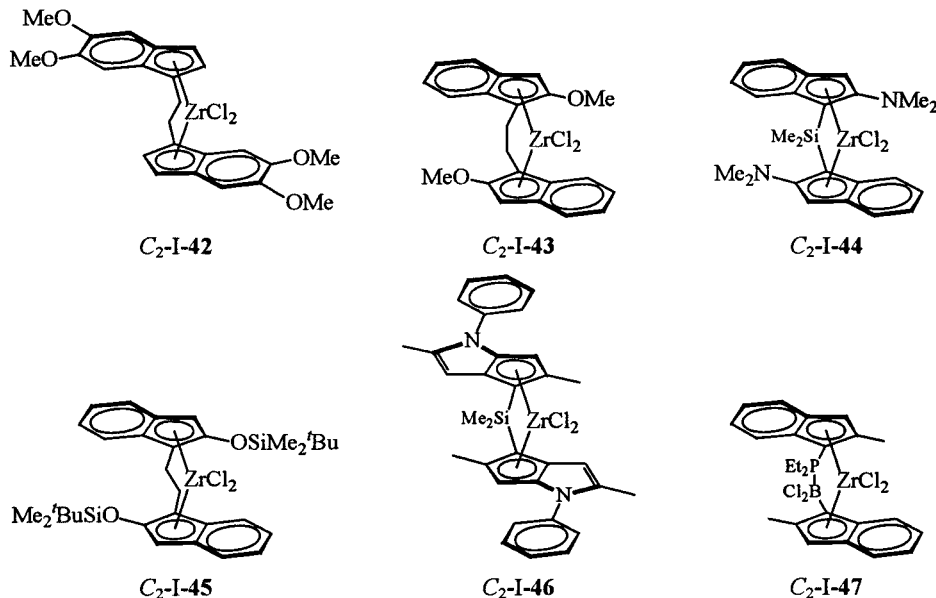
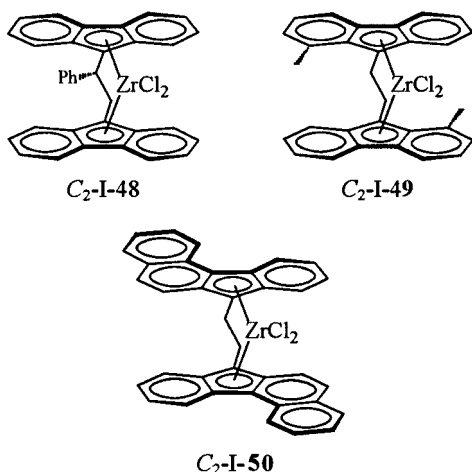
Chart 14. C_2 -Symmetric Substituted Bisindenyl Zirconocenes Containing Heteroatoms

Chart 15



28. This class of catalysts, being so much more versatile in terms of ligand variation, is likely going to improve the performance of the current best metallocene catalysts and expand the range of achievable polypropylene microstructures. A further step toward this direction has been recently taken by Ostoja Starzewsky and co-workers, who introduced the concept of donor/acceptor bridges.³⁵⁶

In these systems, the bridge is constituted by one boron and one phosphorus atoms that engage each other into a dative bond which withstands reaction of the metallocene with the cocatalyst, but is likely reversible at the higher polymerization temperatures, thus providing access to stereoblock polymers. For example, *C*₂-I-47 yields, after activation with Al(*i*-Bu)₃/Me₂PhNHB(C₆F₅)₄, at room temperature, *i*-PP with *m**m**m**m* = 94% and a very high viscosity average molecular weight \bar{M}_v of 2×10^6 ; these values decrease to \bar{M}_v = 434 000 and *m**m**m**m* = 82% for *T*_p = 50 °C, while the melting points of the polymers remain relatively unaffected by the change in polymerization temperature. In addition, since the melting points are significantly higher than the *m**m**m**m* value would imply, the authors suggest that atactic–isotactic stereoblock *i*-PP is formed.

Chiral *ansa*-Metallocenes of Type I-C. Three examples of *ansa*-bisfluorenyl zirconocenes designed to be isospecific, *C*₂-I-48,³⁵⁷ *C*₂-I-49,¹²² and *C*₂-I-50,³⁴⁸ have been reported (Chart 15). While *C*₂-I-48 (where the substituent is on the bridge rather than on the fluorenes) can be obtained as the racemate only, for both *C*₂-I-49 and *C*₂-I-50 a 1:1 *rac*:*meso* mixture was obtained. *C*₂-I-48 is isospecific by site control, although both isotacticity (*m**m**m**m* ranging from 64.1% at *T*_p = 30 °C to 31.2% at *T*_p = 70 °C) and molecular weights are quite low. It should be noted however, that these results were obtained at a low propene concentration of 0.7 mol/L. Similarly, *C*₂-I-49 produces amorphous but tendentially isotactic PP (*m**m**m**m* = 67.9% at *T*_p = 0 °C), while *C*₂-I-50 produces “almost completely atactic” PP. All these zirconocenes have low propene polymerization activities: this behavior contrasts the relatively high activities of both C₂H₄(9-Flu)₂ZrCl₂/MAO and Me₂-Si(9-Flu)₂ZrCl₂/MAO in both ethene³⁵⁹ and propene¹²³ polymerizations and also the very high activity of *C*₂-

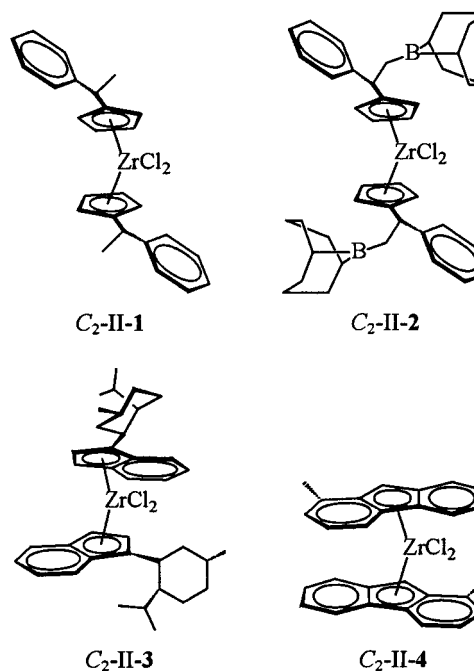
I-50 in ethene polymerization.³⁵⁸ However, strong differences in activity of a catalyst between ethene and propene are not uncommon.

2. Unbridged Isospecific

There are a few examples of unbridged metallocenes which are stereoselective by site control. Examples have been reported with substituted cyclopentadienyl, indenyl, and fluorenyl ligands, the latter being apparently the most stereoselective. The biscyclopentadienyl system *C*₂-II-1 (Chart 16) produces, at low polymerization temperature (−50 °C), a low molecular weight, low isotactic PP (*m**m**m**m* = 51%) with a double stereodifferentiating mechanism, partly site control (27%, *b* = 0.96) partly chain-end control (73%, *p* = 0.79). The related, but much bulkier, *rac*-[Cp-CH(Ph)CH₂(9-BBN)]₂ZrCl₂ (*C*₂-II-2) produced at −50 °C a more isotactic PP (*m**m**m**m* = 75%), with predominance of site control (67%, *b* = 0.95).^{281,360} A series of chiral (3-*R*-Ind)₂ZrCl₂ (e.g., *R* = neoisomenthyl, 5′ α -cholestan-3′ α -yl) was shown to be appreciably stereoselective, albeit always at low polymerization temperature.^{361,362} In these cases, the mode of enantioselectivity is predominantly site control. For example, one of the two *rac*-like diastereoisomers of (3-neoisomenthylindenyl)₂ZrCl₂ (*C*₂-II-3) produced high molecular weight *i*-PP with *m**m**m**m* = 77% at *T*_p = −30 °C, while the two diastereoisomers of the analogous bis[3-(5′ α -cholestan-3′ α -yl)]indenyl complex both produced high molecular weight *i*-PP (*m**m**m**m* = 80% at *T*_p = −30 °C). We must note here that in all cases catalyst activities are quite low, this being connected to the low *T*_p used to maximize enantioselectivity.

The only example of a bisfluorenyl system is also the most selective of this class.^{363,364} Both (1-methylfluoren-9-yl)ZrCl₂ (*C*₂-II-4) and its Hf analogue produce *i*-PP by site control, at normal polymerization temperatures. *C*₂-II-4 is obtained as the *rac*-isomer

Chart 16. Isospecific Zirconocenes of Class II



only and after activation with MAO produces ($T_p = 60^\circ$) *i*-PP with a remarkable (for a nonbridged zirconocene) 82.9% *mmmm* pentad content and a $T_m = 145^\circ\text{C}$. The polymer molecular weight is quite low ($M_w = 65\,000$), as is catalyst activity.

3. Combining Two Symmetries: C_2 -*meso*- C_s

Before discussing the combination of the catalytic performance of catalysts combining two different symmetries, we briefly discuss the behavior of the *meso* isomers of *ansa*-zirconocenes. This background is necessary to understand the performance of both Waymouth's "oscillating" catalysts discussed in this section and the C_1 -symmetric systems discussed in section IV.C.

As discussed in section II, the *meso* isomers of *ansa*-metallocenes produce atactic polypropene and are usually much less active than their racemic counterparts. Both *meso*- $C_2H_4(1\text{-Ind})_2ZrCl_2$ and *meso*- $C_2H_4(H_4\text{-}1\text{-Ind})_2ZrCl_2$ ¹²⁰ produce statistically atactic, low molecular weight PP. The *meso* isomers of C_2 -I-22, C_2 -I-25, C_2 -I-27, and related 2,4-substituted bisindenyl systems¹²¹ produce higher molecular weight *a*-PP.

The C_s -symmetric *meso* *ansa*-metallocenes have two diastereotopic sites, both being achiral, hence the lack of enantioselectivity in propene polymerization. However, from a mechanistic standpoint, these *as*-specific catalysts can be interesting and instructive as well.

Propene insertion into the Zr-CH₃ σ -bond of the catalytic system based on the *meso*- $C_2H_4(H_4\text{-}1\text{-Ind})_2ZrCl_2$ ligand was studied by Castonguay and Rappé.¹⁴⁷ Clearly, propene insertion was found to be nonenantioselective, independently of the inward or outward propene coordination position. However, they found that propene inward coordination is disfavored by roughly 5–6 kcal/mol relative to propene outward coordination, since inward-coordinated propene repulsively interacts with the six-membered rings of the ligand.

The behavior of the same *meso* catalyst when the longer and bulkier isobutyl group is used to model the growing chain was investigated by Corradini, Guerra, and co-workers.⁹² Obviously, also with a bulkier growing chain the propene insertion was calculated to be nonenantioselective. However, they also calculated that the insertion reaction proceeds smoothly only when the growing chain is outward, that is, far from the six-membered rings. In such a case, the minimum energy situations possibly close to the transition state, and sketched in Figure 27, parts A and B, show that no repulsive interactions with the ligand occur. On the contrary, when the growing chain is inward—that is, the chain sits between the two six-membered rings—the insertion reaction has not an easy path. In this case, the minimum energy situations possibly close to the transition state, and sketched in Figure 27, parts C and D, show that repulsive interactions with the ligand occur. Situations with the growing chain inward were calculated to be roughly 5 kcal/mol higher in energy relative to situations with the growing chain outward. Thus, a frequent back-skip

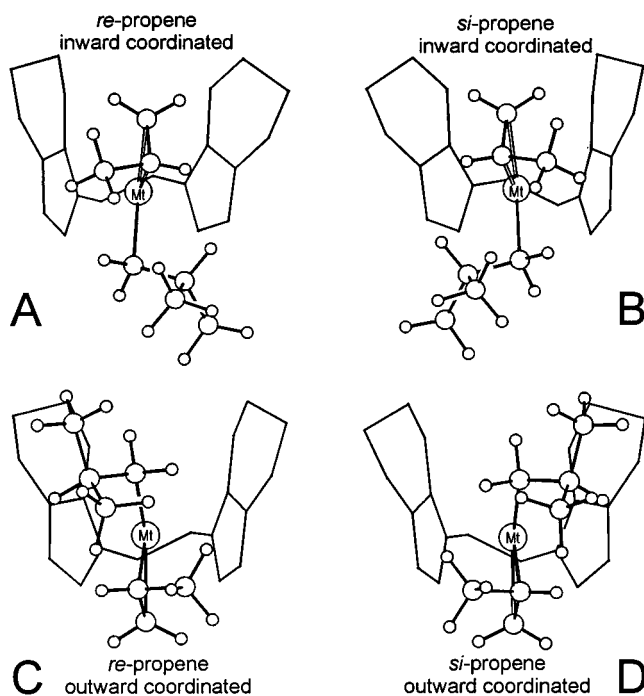


Figure 27. Molecular mechanics minimum energy geometry for *re* and *si* propene coordination on the *meso*- $C_2H_4(H_4\text{-}1\text{-Ind})_2Zr(\text{isobutyl})$ model. Inward and outward propene coordination, parts A and B, and C and D, respectively.

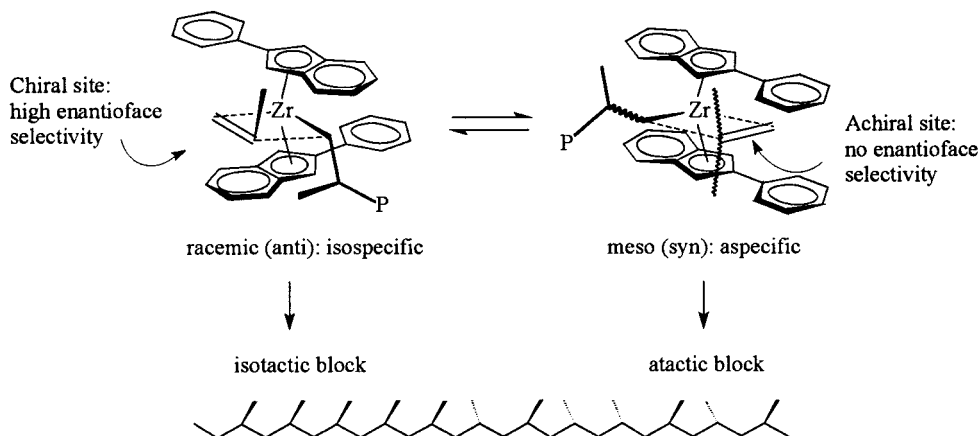
of the growing chain toward the energetically favored outward position has to be expected when the insertion reaction ends up with growing chain inward.

In conclusion, according to Rappé, propene coordination and insertion preferentially occur on the outward coordination position, whereas, according to Corradini, propene coordination and insertion preferentially occur on the inward coordination position. However, it has to be noted that the alkyl group σ -bonded to the metal considered by Rappé is the methyl group, which is smaller than the propene molecule, whereas the alkyl group σ -bonded to the metal considered by Corradini is the isobutyl group, which is bigger than the propene molecule. Therefore, both analyses concord that the bigger ligand, that is propene in Rappé's analysis and isobutyl in Corradini's analysis, is preferentially coordinated in the less encumbered outward position.^{92,147}

Waymouth and Coates combined the opposite behavior of racemic, C_2 -symmetric and *meso*, C_s -symmetric *ansa*-zirconocenes in a single catalyst design:^{343,365–373} a zirconocene catalyst that switches between two symmetries, thanks to properly substituted, unbridged indenyl ligands which rotate between two stable conformations. The prototype catalyst of this type is $(2\text{-Ph-Ind})_2ZrCl_2$, which produces a low crystallinity polypropylene with elastomeric properties. The chains of this polypropylene have a continuous distribution of block lengths, which is attributed to catalyst isomerization during chain growth: the anti-syn isomerization rate must be slower than monomer insertion, but comparable to chain growth (Scheme 26).

So far, only two modeling studies relative to unbridged metallocenes have been reported by Pietsch

Scheme 26



and Rappé³⁷⁴ and by Corradini and co-workers.³⁷⁵ Both research groups performed a molecular mechanics analysis of the bis(2-phenylindenyl)ZrCl₂ precursor. Their analysis allowed them to locate almost isoenergetic minimum energy rotational isomers close to those observed in the crystalline structure and presenting *rac*-like and *meso*-like symmetries (see Figure 28). Energy barriers in the range 5–10 kcal/mol were calculated for the conformational rearrangements between the different isomers. Pitsch and Rappé underlined the presence of stabilizing π -stacking interactions between the aromatic rings in the minimum energy geometries. Moreover, they found these stabilizing interactions also in the transition state geometry for the conformational rearrangement.³⁷⁴

A molecular mechanics analysis by Corradini and co-workers on models of the *rac*-like isomer, in which the two chlorine atoms were replaced by a σ -bonded alkyl group and a π -coordinated propene molecule, suggested that this conformer could be a potential enantioselective site. Moreover, a striking similarity between the minimum energy geometries of models with the unbridged bis(2-phenylindenyl) and bridged C₂H₄(1-Ind)₂ ligands was pointed out (Figure 29).³⁷⁵

Coming back to the realm of matter, several variations of this catalyst have been prepared (see Chart 17).

The productivity of the catalyst and the molecular weight of the resulting polymer are sensitive to the reaction conditions (see Table 7). An increase in propene pressure results in an increase in productivity and molecular weight. At a given propene pressure, a decrease in the polymerization temperature leads to an increase of the polymer molecular weight, primarily due to the increase in propene concentration in toluene with decreasing temperature.³⁶⁵

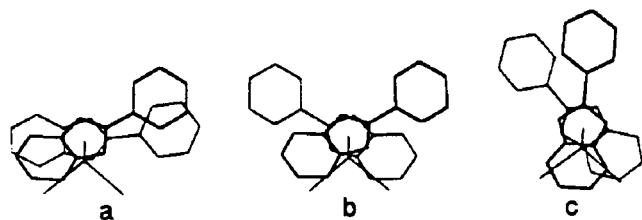


Figure 28. View of the (a) *meso*-like and (b) *rac*-like rotamers of the bis(2-phenylindenyl)ZrCl₂ complex and of the (c) transition state connecting them.³⁷⁴

The polymer microstructure is also sensitive to the reaction conditions. The *mmmm* pentad content increases with increasing propene pressure and decreasing polymerization temperature, ranging from 6.3% ($T_p = 45$ °C, $P = 1$ bar) to 28.1% ($T_p = 20$ °C, polymerization in liquid monomer). A qualitative prediction of this phenomenon is based on a polymerization rate proportional to monomer concentration and a catalyst isomerization rate independent of monomer concentration: $[mmmm] \propto k_p[M]/k_i$. The Coleman and Fox kinetic model predicts that the isotactic block length should increase with monomer concentration.^{376,377}

Broad melting transitions are observed in the DSC analyses of the more isotactic polymers, indicating a broad distribution of tacticity in the polymer. Similar melting points ($T_m = 137$ °C) but very different enthalpy of fusion ($0.2 < \Delta H < 17.4$ J/g) are observed for polymer obtained using different catalysts.³⁶⁶ The enthalpy of fusion is proportional to the *mmmm* content. The high melting points in the presence of a low *mmmm* pentad content speak for a blocky structure of the polymers. As a matter of fact, these polypropylenes contain isotactic, isotactic-*block*-atactic and atactic polypropene chains. A polypropene sample obtained with the (2-Ph-Ind)₂ZrCl₂/MAO catalyst ($T_p = 20$ °C in liquid propene) was fractionated

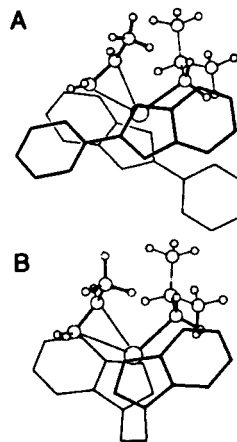


Figure 29. Models of preinsertion intermediates for the primary propene insertion including the unbridged *rac*-like bis(2-phenylindenyl) and bridged *rac*-C₂H₄(1-Ind)₂ ligands. The propene monomer is on the left, while the isobutyl group simulating the growing chain is on the right.³⁷⁵

Chart 17

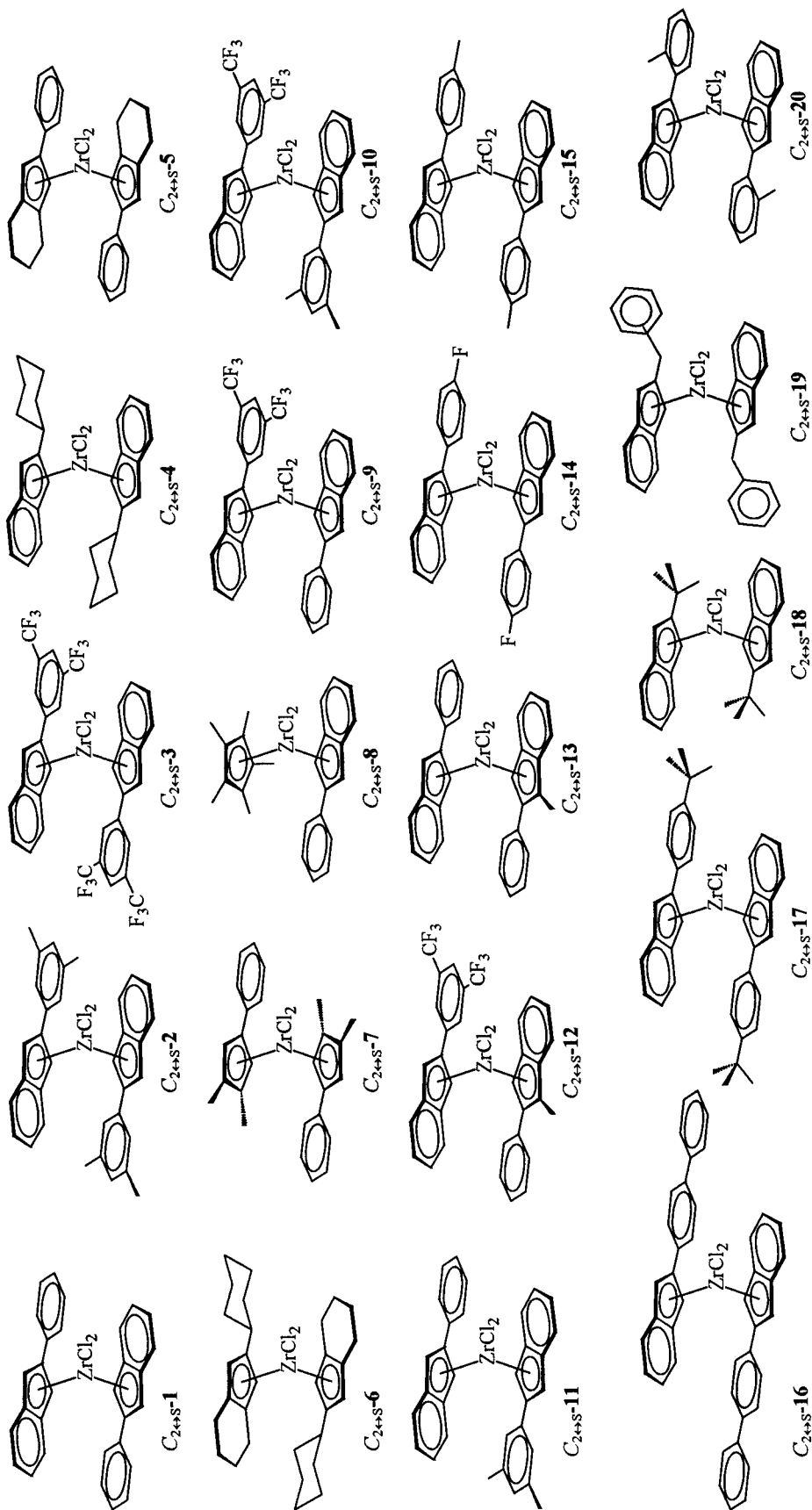


Table 7. Propene Polymerization with Representative Bis(2-aryindenyl)zirconocene/MAO Catalysts

catalyst	T_p , °C	Al _{MAO} /Zr, molar ratio	propene (solvent)	activity, kg _{PP} /(mmol _{Zr} h)	\bar{M}_w	\bar{M}_w/\bar{M}_n	T_m (ΔH), °C (J/g)	% <i>m</i> ^a	% <i>mmmm</i> ^a	ref
$C_{2\leftrightarrow S}$ - 1	50	3000	bulk	2.0	65 000 ^b	nd			24	202
	45	1033	1 bar (toluene)	0.19	24 000	2.8		52	6.3	365
	30	4800	bulk	5.6	145 000	3		70	31	396
	25	1033	1 bar (toluene)	0.31	67 000	2.7		55	9.2	365
	25	1000	1.7 bar (toluene)	0.4	179 000	3.0		62	20	366
	25	1000	3.4 bar (toluene)	0.9	241 000	3.5	137 (0.2)	66	26	366
	25	1000	6.1 bar (toluene)	2.4	369 000	3.9		73	32	366
	20	1000	3.4 bar (toluene)	1.4	310 000	3.2		69	31	367
	20	1000	5.1 bar (toluene)	1.7	369 000	3.9		70	33	371
	20	1000	bulk (toluene) ^c	2.5	542 000	3.5	30–152 (28)	70	32	367
	20	3000	bulk	10.5	123 000 ^d	nr		nr	40	372
	20	1000	bulk	1.8	572 000	3.2	82–159 (15.8)	73	39	202
	8	2230	bulk	1.5	410 000	4	141	67	29	396
	0	1033	1 bar (toluene)	0.71	183 000	2.6		57	12.3	365
	0	1033	1.3 bar (toluene)	0.27	213 000	1.5		57	11.6	365
	0	1033	2.7 bar (toluene)	0.62	395 000	1.9		57	13.2	365
	0	1033	4.4 bar (toluene)	1.04	540 000	1.7		59	15.8	365
	0	1033	6.1 bar (toluene)	1.73	604 000	1.8		61	17.4	365
	–18	1033	4.4 bar (toluene)	0.56	889 000	2.1		68	28.1	365
	–25	1033	1 bar (toluene)	1.1	330 000	2.2		60	16.1	365
$C_{2\leftrightarrow S}$ - 1-Hf	20	1000	3.4 bar (toluene)	1.5	198 000	2.0	amorphous	57	9	369
$C_{2\leftrightarrow S}$ - 2	25	1000	2.4 bar (toluene)	0.15	81 000	2.5		62	15	366
	25	1000	3.4 bar (toluene)	0.2	129 000	2.6	137 (7.3)	62	18	366
	25	1000	6.1 bar (toluene)	0.5	174 000	2.7		66	24	366
$C_{2\leftrightarrow S}$ - 3	25	1000	1.7 bar (toluene)	0.25	196 000	3.3		75	45	366
	25	1000	3.4 bar (toluene)	0.7	296 000	3.4	137 (17.4)	80	58	366
	25	1000	5.1 bar (toluene)	1.35	332 000	3.7		86	73	366
	20	3000	bulk	2.8	58 300 ^d			70		372
$C_{2\leftrightarrow S}$ - 3-Hf	25	1000	3.4 bar (toluene)	1.35	330 000	2.4		64	18	369
$C_{2\leftrightarrow S}$ - 4	20	1000	3.4 bar (toluene)	0.4	117 000	3.8	amorphous	57	11	367
	20	1000	bulk (toluene) ^c	2.3	219 000	3.3	amorphous	62	15	367
$C_{2\leftrightarrow S}$ - 5	20	1000	3.4 bar (toluene)	0.9	20 000	1.9	amorphous	46	3	367
	20	1000	bulk (toluene) ^c	2.4	40 000	1.9	amorphous	52	5	367
$C_{2\leftrightarrow S}$ - 6	20	1000	bulk	3.0	56 000 ^b		amorphous	40	9	202
$C_{2\leftrightarrow S}$ - 7	20	1000	3.4 bar (toluene)	3.7	146 000	2.0	amorphous	59	10	367
	20	1000	bulk (toluene) ^c	8.8	392 000	3.2	amorphous	59	10	367
$C_{2\leftrightarrow S}$ - 8	20	1000	5.1 bar (toluene)	0.5	100 000	6.8	34–69 (4.9)	70	30	371
	20	1000	bulk (toluene) ^e	0.8	127 000	3.5	29–87 (13.6)	74	34	371
$C_{2\leftrightarrow S}$ - 9	20	1000	bulk	1.4	348 000	3.3		35		373
$C_{2\leftrightarrow S}$ - 10	20	1000	bulk	2.2	249 000	4.4		54		373
$C_{2\leftrightarrow S}$ - 11	20	1000	bulk	1.5	313 000	2.9		21		373
$C_{2\leftrightarrow S}$ - 12	20	1000	bulk	1.8	262 000	3.7		24		373
$C_{2\leftrightarrow S}$ - 13	20	1000	bulk	2.8	293 000	3.8		14		373
$C_{2\leftrightarrow S}$ - 14	50	500	bulk	2.0	42 000 ^b			19		202
$C_{2\leftrightarrow S}$ - 2	50	3000	bulk	0.7	29 300 ^b			25		202
$C_{2\leftrightarrow S}$ - 15	50	500	bulk	1.4	52 000 ^b			28		202
$C_{2\leftrightarrow S}$ - 16	50	500	bulk	2.3	58 000 ^b			35		202
$C_{2\leftrightarrow S}$ - 17	50	500	bulk	1.0	41 000 ^b			20		202
$C_{2\leftrightarrow S}$ - 18	50	300	bulk	inactive						202
$C_{2\leftrightarrow S}$ - 19	50	3000	bulk	1.6	19 000 ^b			20		202
$C_{2\leftrightarrow S}$ - 20	50	3000	bulk	inactive						202

^a From ¹³C NMR. The values are referred to the total methyl signals. ^b \bar{M}_n from $[\eta] = KM_v^\alpha$, $\alpha = 0.74$, $K = 1.93 \times 10^{-4}$. ^c 100 mL of liquid propene + 25 mL of toluene. ^d \bar{M}_n . ^e 100 mL of liquid propene + 20 mL of toluene.

in a Kumagawa extractor using boiling solvents (sample 1 in Table 8). Fractions with rising isotacticity were obtained passing from ethyl ether to heptane, as is indicated by the increase of *mmmm* pentad content and enthalpy of fusion. The same trend is observed in the X-ray spectra of the fractions shown in Figure 30.

Similar results were reported recently by Waymouth²⁹⁴ (sample 2, shown in Table 8 for comparison).

Statistical modeling of pentad distributions of polypropenes prepared with these catalyst systems can be satisfactorily done using a two-site model^{378,379} based on a mixing of a chain-end-controlled site (to model the atactic blocks) and an enantiomorphic site (for isotactic blocks).³⁶⁵

Substituents on the phenyl ring have an unclear effect on polypropene microstructures: the 3,5-bis-

(trifluoromethyl)phenylindenyl derivative ($C_{2\leftrightarrow S}$ -**3**) produces polymers with a higher isotactic pentad content (45% < *mmmm* < 73%), while the 3,5-dimethyl one ($C_{2\leftrightarrow S}$ -**2**) is less stereoselective and generates polymers with a lower molecular weight.³⁶⁶

The influence of phenyl rings on catalytic performances of this class of metallocenes was carefully investigated by Waymouth.³⁶⁷ The replacement of the phenyl ring of the 2-phenylindenylzirconocene by a cyclohexyl group generates a catalyst ($C_{2\leftrightarrow S}$ -**4**) with a lower stereoselectivity with respect to the parent metallocene. The fully hydrogenated bis(2-cyclohexyltetrahydroindenyl) metallocene ($C_{2\leftrightarrow S}$ -**6**) is completely aspecific. Bis(2-phenyltetrahydroindenyl) zirconocene $C_{2\leftrightarrow S}$ -**5** gives low molecular weight atactic polypropene. Furthermore, hydrogenation of the π -ligands does not seem to affect catalyst activity. The metallocene containing the tetrahydroindenyl

Table 8. Fractionation of Polypropene Samples Obtained with Bis(2-phenylindenyl)zirconocene/MAO as Catalyst

fraction	% wt	\bar{M}_w	\bar{M}_w/\bar{M}_n	$T_m, ^\circ\text{C}$	$\Delta H_f, \text{J/g}$	% <i>mmmm</i> ^a	ref
Sample 1							
whole polymer ^b	100	572 000	3.2	145	15.8	39	202
ether soluble	35	380 000	3.0	amorphous		17	
hexane soluble	11	363 000	2.7	very broad		38	
heptane soluble	7	487 000	2.6	141	3.3	51	
insoluble ^c	47	860 000	3.0	145	51.3	66	
Sample 2							
whole polymer ^d	100	455 000	2.7	138.1	24	32	294
ether soluble	36	339 000	2.5	nr	nr	18	
heptane soluble	43	367 000	2.4	79.7	11	33	
insoluble	21	598 000	3.1	141.6	65	51	

^a From ¹³C NMR. The values are referred to the total methyl signals. ^b Polymerization conditions: bulk, $T_p = 20^\circ\text{C}$, $\text{Al}_{\text{MAO}}/\text{Zr} = 1000$. ^c This fraction is completely soluble in *o*-xylene. ^d Polymerization conditions: bulk, $T_p = 23^\circ\text{C}$, $\text{Al}_{\text{MAO}}/\text{Zr} = 470$.

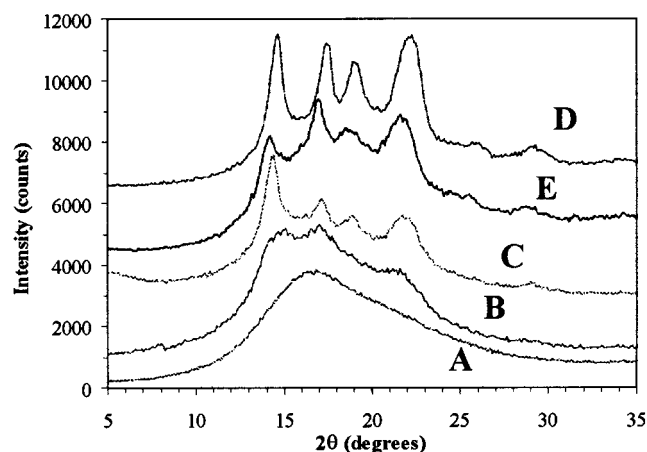


Figure 30. X-ray spectra of the fractions of a polypropene (sample 1 in Table 8) obtained with $(2\text{-Ph-Ind})_2\text{ZrCl}_2$. Fractions: A, ether soluble; B, ether insoluble, hexane soluble; C, hexane insoluble heptane soluble; D, heptane insoluble. The spectrum of the whole polymer (E) is reported for comparison.

ligand produces polymers with the lowest molecular weights. Bis(1-phenyl-3,4-dimethylcyclopentadienyl)-zirconocene ($C_{2\leftrightarrow S-7}$) is nearly 3 times more active than $C_{2\leftrightarrow S-1}$ but produces atactic polypropene.

In conclusion, the combined presence of a 2-aryl substituent and the indenyl ligand seems to be important for the formation of elastomeric polypropenes.

The introduction of a methyl group in position 1 of the 2-phenylindenyl ligand gives two catalysts (as *racemic* and *meso* isomers) with a lower activity, and both generate low molecular weight, amorphous polypropene.³⁶⁸

The influence of the transition metal atom was studied by preparing the hafnium complexes with the 2-phenylindenyl and 2-[3,5-bis(trifluoromethyl)phenyl]indenyl ligands.³⁶⁹ The precursors of this catalyst produce polypropenes with a lower *mmmm* pentad content with respect to the zirconium analogues (see Table 7). Activities and polymer molecular weight are similar for the hafnium and zirconium derivatives.

The substitution of one of the 2-phenylindenyl ligands in $C_{2\leftrightarrow S-1}$ with a pentamethylcyclopentadienyl ligand gives a less active C_1 symmetric catalyst.³⁷¹ This metallocene produces polypropenes with a *mmmm* pentad content similar to those found for polymers prepared with $(2\text{-Ph-Ind})_2\text{ZrCl}_2$ under the

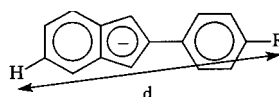


Figure 31. Definition of distance d in 2-aryl-indenyl ligands.

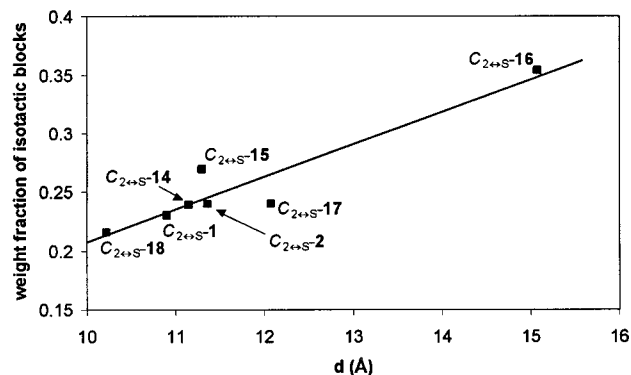


Figure 32. Correlation between ligand length d (Å) and the weight fraction of isotactic blocks.

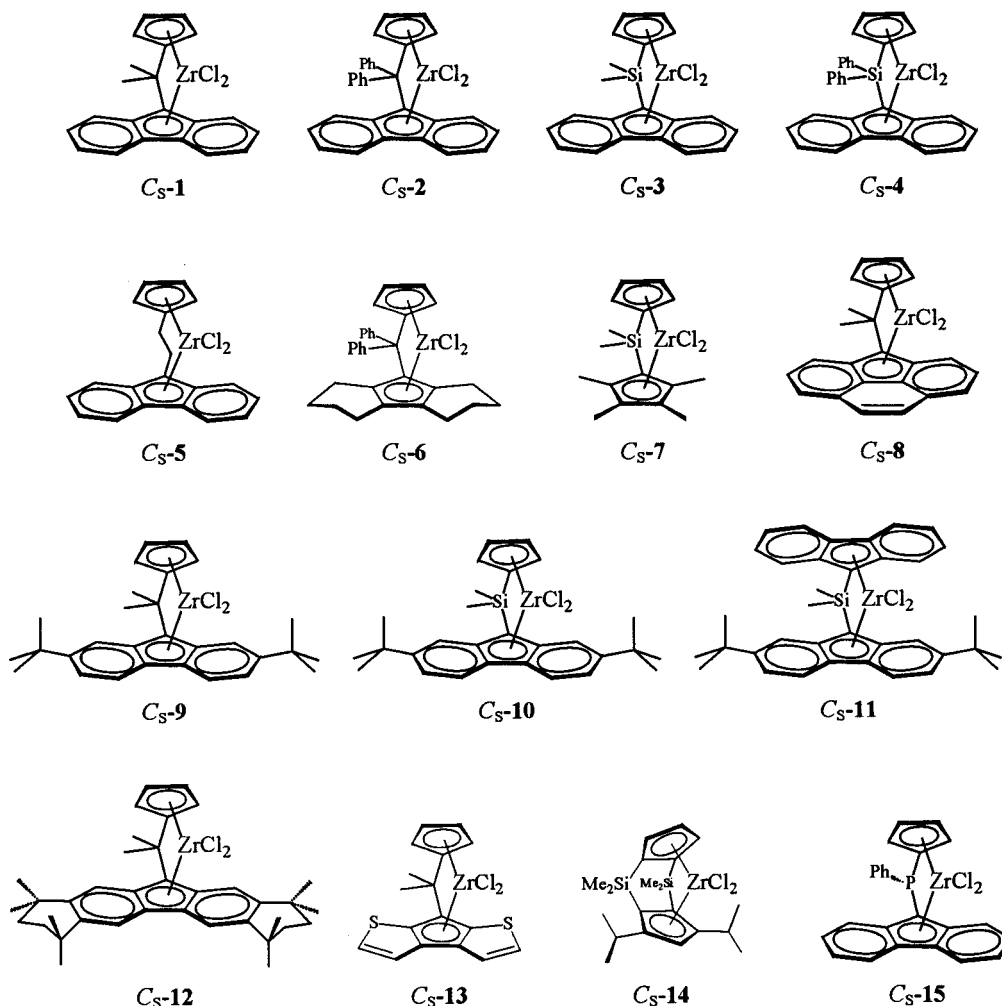
same conditions. The DSC spectra of polypropenes prepared with the (Me_5Cp) derivative show narrower melting peaks, and they are at lower temperature with respect to the $(2\text{-Ph-Ind})_2\text{ZrCl}_2$ -made polymers.

Mixed 2-arylindenyl ligand complexes possess an isospecificity intermediate to that of the corresponding bisindenyl analogues.³⁷³

Taking as a measure of the ligand bulkiness the ligand length d (the distance in Å between the two opposite sides of the molecule; see Figure 31) a correlation was found between this parameter and the weight fraction of isotactic blocks: the longer the ligand, the higher the isotacticity (see Figure 32).

Waymouth³⁷² also reported the presence of regioirregular units in some polypropenes synthesized in bulk using $C_{2\leftrightarrow S-1}$ or $C_{2\leftrightarrow S-3}$ as catalyst precursors. As they are found only in the isotactic blocks and appear in a 2,1-*erythro* configuration, they are likely formed at the *rac*-like conformation of the catalyst.

The microstructure and stereoblock distribution peculiar of polypropenes produced with this class of catalysts imparts thermoplastic elastomeric properties to the polymers. Thermoplastic elastomers or elastoplasts (TPEs) owe their elastomeric properties of resiliency and high tensile strength to physical cross-linking (formation of "hard" domains in a "soft" matrix) due to the presence of short, crystallizable

Chart 18. Examples of Syndiospecific C_s -Symmetric Metallocenes

isotactic blocks in high molecular weight, atactic chains.³⁸⁰ Thermoplastic elastomeric polypropene (TPE-PP) can be defined as a propene-*block*-homopolymer. As described above, this material is not homogeneous, as it can be fractionated by solvent extraction, and in this respect is similar to the TPE-PP produced with DuPont-type catalysts.^{381,382} TPE-PP has been previously obtained with several different heterogeneous catalysts³⁸³ and is a material of commercial interest.^{383,384} Possible applications are as a component in car bumpers, in materials for medical applications, and in general as EPR/*i*-PP compatibilizer and *a*-PP substitute. TPE-PP can also be produced by C_1 -symmetric metallocene catalysts, as described by Chien and others,^{385–395} but in this case the polymer is expected to be homogeneous with respect to composition distribution (see section IV.C).

B. Syndiotactic Polypropene: C_s -Symmetric Metallocenes

The first metallocene—and the first catalyst in general—able to produce highly syndiotactic polypropene (*s*-PP), was the C_s -symmetric $\text{Me}_2\text{C}(\text{Cp})(9\text{-Flu})\text{ZrCl}_2$ (C_S-1 in Chart 18).¹¹² The behavior of this catalyst^{46,113} and the characterization of *s*-PP^{397–407} have been extensively reviewed. A number of studies on the thermal behavior, crystal structures, and morphology of *s*-PP have appeared in the litera-

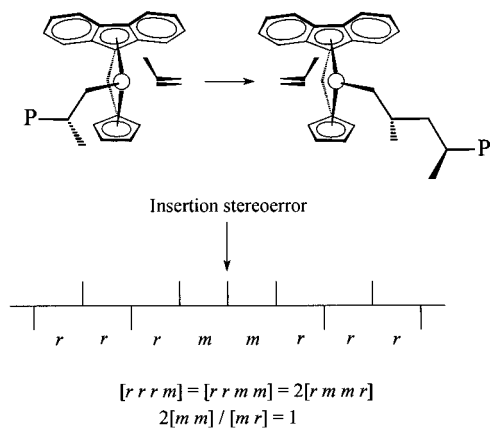
ture.^{397–406} A T_m° of 214 °C and a ΔH_u of 1.4 kJ/mol for fully syndiotactic polypropene have been extrapolated.³⁹⁷ Hence, the T_m° of *s*-PP would be notably higher than that of *i*-PP (186 °C), although in practice *s*-PP has always lower melting points than *i*-PP of comparable stereoregularity and molecular weights. More recently, a more reasonable T_m° of 182 °C has been obtained by De Rosa.⁴⁰⁵ Applications of *s*-PP are still under investigation; improvement of mechanical properties has been reported for *s*-PP/*i*-PP blends.⁴⁰⁸

The invention of syndiospecific C_s -symmetric metallocenes has marked the turning point in the understanding of the mechanism of stereocontrol with metallocene catalysts. Again, the presence of isolated insertion errors of the type *rrrrmmrrr* is consistent with site control (Scheme 27). In the case of the syndiospecific $\text{Me}_2\text{C}(\text{Cp})(9\text{-Flu})\text{ZrCl}_2$ catalyst, in which the two sites are enantiotopic, occasional “skipped” insertions produce a minor amount of insertion errors of the type *rrrrmrrrr*, which are identical to those produced by chain-end control. In the case of isospecific C_2 -symmetric metallocenes, skipped insertions would not be observable due to the presence of two homotopic sites.

The statistics of syndiospecific polymerization have been treated in detail by Farina.⁴⁰⁹

As outlined above, the syndiospecific C_s -symmetric catalysts are those for which the two available

Scheme 27. C_s -Symmetric Metallocenes: Syndiotactic Polypropene by Site Control, Showing One Isolated Stereoerror



coordination positions are enantiotopic.⁴¹⁰ In the framework of the chain migratory insertion mechanism, these catalytic systems are syndiospecific, provided that the single insertion step is enantioselective.

We first analyze the syndiospecific polymerization from a modeling standpoint. Molecular models for C_s -symmetric syndiospecific systems are substantially identical to those for C_2 -symmetric isospecific systems and have been modeled by Corradini and Guerra,⁹⁰ Rappé,¹⁴⁷ Morokuma,¹⁵⁵ Chien,²⁷⁷ and Fink⁸⁹ and their relative co-workers. As an example, the energetically favored structures for the R and S chirality at the metal atom of the model system $\text{Me}_2\text{C}(\text{Cp})(9\text{-Flu})\text{Zr}(\text{isobutyl})(\text{propene})^+$ (entry **30** in Chart 8), which can be thought to correspond to two successive insertion steps, are shown in Figure 33, parts A and B, respectively. As for the C_2 -symmetric isospecific systems previously discussed, the chirality of the catalytic system pushes the growing chain into an open sector, i.e., it imposes a *chiral orientation to the growing chain*.

Again, the favored propene enantioface is the one which places the propene methyl group anti to the growing chain, thereby minimizing repulsive interactions with the growing chain itself. In particular, the *re* and *si* propene enantiofaces are favored for the R

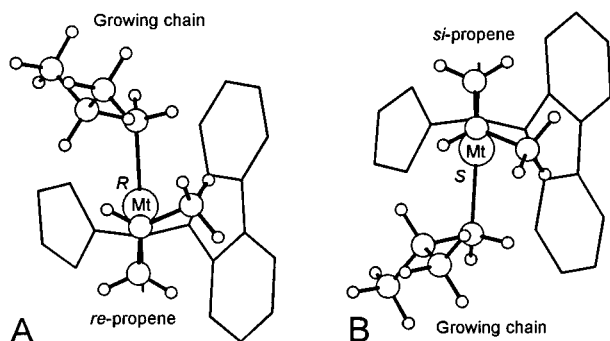


Figure 33. Molecular mechanics minimum energy geometries corresponding to two successive insertion steps with the $\text{Me}_2\text{C}(\text{Cp})(9\text{-Flu})\text{Zr}(\text{isobutyl})$ model. When the chirality at the metal atom is R (left view), coordination and insertion of the *re* propene enantioface is favored. When the chirality at the metal atom is S (right view), the *si* propene enantioface coordination and insertion is favored.

and S chirality at the metal atom, respectively. Since in two successive insertion steps opposite propene enantiofaces are inserted, the model is syndiospecific. All molecular modeling studies on C_s -catalytic systems confirm this scheme.^{89,90,147,155,277}

Morokuma and co-workers also found that the catalytic system based on the C_s -symmetric $\text{H}_2\text{Si}(2,3,4,5\text{-Me}_4\text{Cp})(\text{Cp})$ ligand should be substantially nonenantioselective, due to repulsive interactions between the methyl group of the propene and the methyl groups of the (Me_4Cp) ligand.¹⁵⁵ This is in agreement with the low syndiospecificity and activity experimentally observed for the catalyst based on this ligand.⁴⁶

Chien and co-workers predicted that a bulkier bridge, $(t\text{-Bu})(\text{H})\text{C}$ in place of Me_2C , slightly enhances the enantioselective behavior of the bridged $\text{Me}_2\text{C}(\text{Cp})(9\text{-Flu})$ ligand. Moreover, they also modeled propene insertion on a growing chain presenting different agostic interactions with the metal atom. In particular, by using geometrical constraints, they simulated the insertion of propene on growing chains showing no and α -, β -, and γ -agostic interactions. No sketches of the models are presented, making it difficult to clearly understand their results. However, according to their calculations, the presence of the α -agostic interaction slightly increases the enantioselectivity, while insertion on a β -agostic chain is substantially nonenantioselective and insertion on a γ -agostic chain is substantially enantioselective, but in favor of the opposite propene enantioface.²⁷⁷

Fink and co-workers studied the $\text{Me}_2\text{C}(\text{Cp})(9\text{-Flu})\text{Zr}(\text{R})(\text{propene})^+$ system, with R equal to CH_3 , $\text{CH}_2\text{CH}(\text{CH}_3)_2$, and the $\text{CH}_2\text{CH}(\text{CH}_3)\text{CH}_2\text{CH}(\text{CH}_3)_2$ group of both R and S chirality at the $\text{C}(2)$ atom. These groups can be considered as the alkyl group σ -bonded to the Zr atom at the first, second, and third step of polymerization, respectively. The chirality of the last group can be considered to stem from the chirality of the propene enantioface which inserted into the $\text{Zr}-\text{CH}_2\text{CH}(\text{CH}_3)_2$ bond in the second polymerization step. Again, they found a substantial enantioselectivity only with R groups bigger than methyl. Moreover, coordination of propene to systems with the $\text{CH}_2\text{CH}(\text{CH}_3)\text{CH}_2\text{CH}(\text{CH}_3)_2$ group σ -bonded to the Zr atom is scarcely dependent on the chirality of the alkyl group simulating the growing chain, i.e., the enantioselectivity is substantially independent of the chirality of the last inserted monomeric unit.⁸⁹ This conclusion, together with similar calculations performed by Corradini and co-workers on the classical heterogeneous Ziegler–Natta systems,²⁶² suggests more generally that the chirality of the tertiary C atom of the last inserted unit of the growing chain plays a negligible role in the presence of a chiral site.

Corradini and co-workers examined also a C_s -symmetric ligand presenting a further aromatic ring fused on the basic Flu ligand (entry **31** in Table 3 and $C_s\text{-8}$ in Chart 18). In agreement with the experimental results,⁴⁶ this catalytic system is calculated to be less enantioselective than the one based on the $\text{Me}_2\text{C}(\text{Cp})(9\text{-Flu})$ ligand, and this is easily rationalized in the framework of the mechanism of the *chiral orientation of the growing chain*. In fact,

Table 9. Liquid Propene Polymerization with Syndiospecific Catalysts^a

catalyst	T_p	A (kg/g _{cat} h)	\bar{M}_w	r	rr	$rrrr$	$rmmr$	$rrmr$	T_m	ref
C_S -1	0		304 000 (\bar{M}_n)			93.5	0.85	1.1	145	202
C_S -1	25	51	212 000 (\bar{M}_n)	95					145	70, 113
C_S -1	50	194	133 000	96					138	414
C_S -1	50	250	141 000 (\bar{M}_n)			87.6	1.7	1.9	139	202
C_S -1	60	188	90 000			82	1.7	2.8	137	407
C_S -1	60	370	129 000 (\bar{M}_n)						137	113
C_S -1	67	84	120 000			85			134	333
C_S -1	70	315	108 000 (\bar{M}_n)	93		78	1.8	3.6	134	113
C_S -1-Hf	50	54	777 000			74.0			118	112
C_S -1-Hf	70	32	474 000							112
C_S -2	40	37	723 000 (\bar{M}_n)			89.2			138	408
C_S -2	50	68	560 000	97.5					139	414
C_S -2	50	17	516 000			85.5	1.8	2.6	128	202
C_S -2	60	55	340 000			84			132	407
C_S -2-Hf	50	11.7	1 950 000	90.3					101	414
C_S -3	67	4	144 000 (\bar{M}_n)	80.6	67.3	51.3	3.0	12.7	—	333
C_S -4	70		46 000		74.45					419
C_S -5	40	35	284 000			82.99	1.98	4.29	125	364
C_S -5	60	50	171 000			74.31	2.48	6.91	111	364
C_S -6	60	101	65 000			58			amorph	407
C_S -7	60	180	low			14			amorph	70
C_S -8	20	2	217 000			79	2.3	3.0	130	70
C_S -8	30	10	207 000			77	2.3	3.2	127	70
C_S -8	50	23	154 000			72	2.8	4.5	119	70
C_S -8	60	32	141 000			72	3.1	6.8	116	70
C_S -8	70	23	97 000			61	2.9	9.1	amorph	70
C_S -9	40	79	34 000			94			147	407
C_S -9	60	82	79 000 (\bar{M}_n)						134	407
C_S -10	70		96 000		64.95					419
C_S -11	70		132 000		32.46					419
C_S -12	0		700 000 (\bar{M}_n)			91.7	0.6	2.7	154	202, 415
C_S -13	50	30	102 000			73.9	1.8	8.1	110	355
C_S -14	20	522	1 250 000	97.1		93.4	0.8	0.9	151	412
C_S -14	70	3150	160 000	94.1		79.5		7.3	119	412
C_S -14 ^b	24	53	101 000	97.1		90.7	<1	2.7	140	412
C_S -15	50	18	300 000	92.3	87.8	80.7	2.1	3.1	128	333
C_I -I-18	50	28	54 000			66.5	3.3	7.8	109	202
C_I -I-19	50	37	58 000			70.9	2.9	6.8	117	202

^a Diad, triad, and pentad values in percentages. ^b In toluene, $[M] = 3.4$ mol/L.

Table 10. Pentad Analysis, Bernoullian Probability of Enantioselective Insertion (b), and Probability of Back-Skip (p_{bs}) with Syndiospecific Catalysts^a

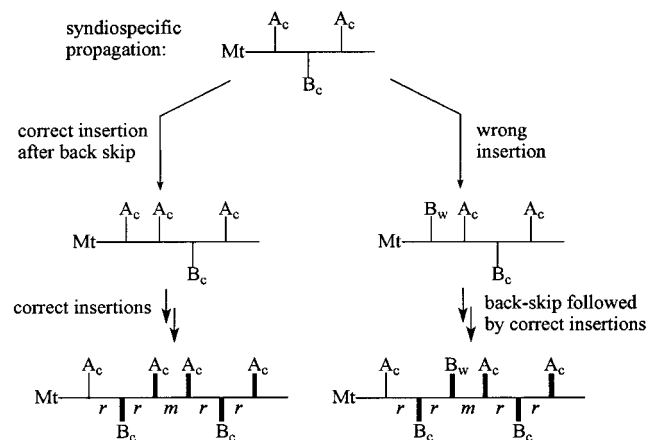
catalyst	T_p	$mmmm$	$mmmr$	$rmmr$	$mmrr$	$mmrm + rrmr$	$rrmr$	$rrrr$	$rrrm$	$mrrm$	b	p_{bs}	ref
C_S -1	0	0.0	0.0	0.9	1.7	1.1	0.0	93.6	2.7	0.0	0.991	0.055	202
C_S -1	50	0.0	0.1	1.7	3.4	1.9	0.1	87.6	5.1	0.1	0.981	0.096	202
C_S -2	50	0.0	0.2	1.8	3.7	2.6	0.2	85.5	5.9	0.1	0.979	0.013	202
C_S -3	67	1.2	1.9	3.0	7.4	0.6 + 12.7	5.9	51.3	12.0	4.0	0.942	0.089	333
C_S -5	40	0.35	0.26	1.98	3.40	4.29	0.62	82.99	5.95	0.17	0.981	0.021	364
C_S -12	0	0.0	0.0	0.6	1.2	2.7	0.1	91.7	3.8	0.0	0.994	0.014	202
C_S -13	50	0.1	0.7	2.4	5.0	9.2	0.9	68.5	12.6	0.6	0.970	0.055	202
C_S -14 ^b	24	0	0	<1	1.9	2.7	0	90.7	4.2	0	0.992	0.014	412
C_S -15	50	0.7	0.5	2.1	4.6	0 + 3.1	1.2	80.7	6.4	0.7	0.971	0.016	333
C_I -1	50	0.2	0.9	3.3	6.9	7.8	1.0	66.5	12.8	0.6	0.955	0.045	202
C_I -2	50	0.1	0.7	2.9	6.0	6.8	0.7	70.9	11.4	0.5	0.963	0.039	202

^{a,b} See Table 9.

the preferred insertion path corresponds to the growing chain chirally oriented toward the Cp ligand and to propene coordinated in a way presenting the methyl group anti to the chain, that is, closer to the bulkier π -ligand. The two additional aromatic carbon atoms of the ligand generate direct interactions with the propene coordinated with the right enantioface, thus reducing the enantioselectivity. Moreover, they also investigated ligands presenting a double bridge based on the norbornadiene skeleton²⁷¹ (entries **32** and **33** in Table 3). A substantial enantioselectivity can be achieved only when bulky *tert*-butyl substitu-

ents are considered. These predictions are qualitatively confirmed by the prevalently syndiospecific behavior experimentally exhibited by the catalyst based on the Si–Si double bridge.^{411,412}

Although less amenable to ligand variations, several modifications of Ewen's original catalyst design have been reported in the literature. The most significant examples are shown in Chart 18, while the relevant polymerization results are shown in Table 9. The improvement of Ewen's catalyst has been obtained by modifying the bridge in order to obtain higher molecular weights, by using the Ph₂C

Scheme 28. Possible Source of *rrmr* Pentads in *s*-PP from C_2 -Symmetric Zirconocenes^a


^a A and B are the two enantiotopic sites; subscripts c and w indicate correct (c) and wrong (w) insertions, according to the given enantioselectivity of each site.

rather than the Me_2C bridge,^{413,414} and the “expansion” of the fluorenyl moiety, which increased syndiotacticity.^{407,415}

The influence of the bridge is very different from what has been observed in C_2 -symmetric zirconocenes. For the series of unsubstituted *ansa*-(Cp)(9-Flu) zirconocenes, the single C bridge gives the best performance. Syndiotacticity decreases in the order $\text{Me}_2\text{C} > \text{Ph}_2\text{C} > \text{PhP} \sim \text{CH}_2\text{CH}_2 > \text{Ph}_2\text{Si} > \text{Me}_2\text{Si}$, while molecular weights decrease in the order $\text{Ph}_2\text{C} > \text{PhP} > \text{CH}_2\text{CH}_2 > \text{Me}_2\text{C} \sim \text{Me}_2\text{Si} > \text{Ph}_2\text{Si}$.

The effect of the metal is quite analogous to the case of C_2 -symmetric zirconocenes: Hf is less active and produces higher molecular weights compared to Zr, while Ti is much less active and also much less enantioselective compared to the other two metals; indeed, both $\text{Ph}_2\text{C}(\text{Cp})(9\text{-Flu})\text{TiCl}_2/\text{MAO}$ and $1,1',2,2'-(\text{Me}_2\text{Si})_2(4\text{-}i\text{-PrCp})(3,5\text{-}i\text{-Pr}_2\text{Cp})\text{TiCl}_2/\text{MAO}$ produce fully atactic PP ($[rr] = 0.23$ at -60°C).⁴¹⁶

The probability of back-skip can be calculated by the method described by Farina,⁴⁰⁹ provided the whole set of pentads is known. The available values are shown in Table 10. An ambiguity remains as to the source of *rrmr* stereoerrors, since these can arise from a skipped insertion between two stereoregular insertions or by a chain back-skip after a stereoerror (Scheme 28).¹¹³ If this were the case, then the *rrmr* pentad would not be a good indicator of the enantioface stereoerrors, since a part of these errors would be “erased” by the following back-skip and turned into a *mmrr* pentad (Scheme 28). A stereoirregular insertion could even favor back-skip. The methyl pentad region of two *s*-PP samples of different stereoregularities are compared in Figure 34.

The dependence on polymerization temperature has been studied for C_2 -**1**,^{113,417} C_2 -**5**,³⁶⁴ C_2 -**8**,⁴⁶ and C_2 -**14** (and related systems).⁴¹² For the latter system, the increase of catalyst activity and corresponding decrease in molecular weight with increasing T_p is quite remarkable.

The detrimental influence of decreasing propene concentration^{113,412} and of increasing amounts of $\text{CH}_2\text{-Cl}_2$ solvent⁴¹⁷ on syndiospecificity is in line with unimolecular chain back-skip (also called site epimer-

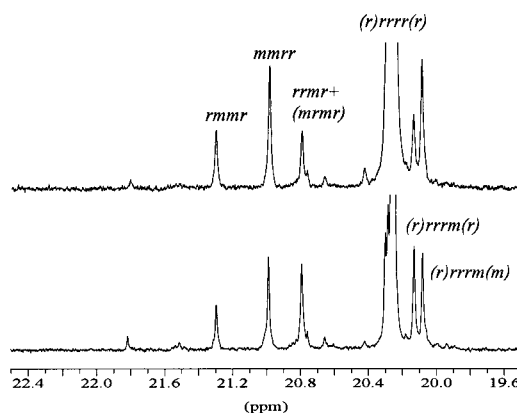


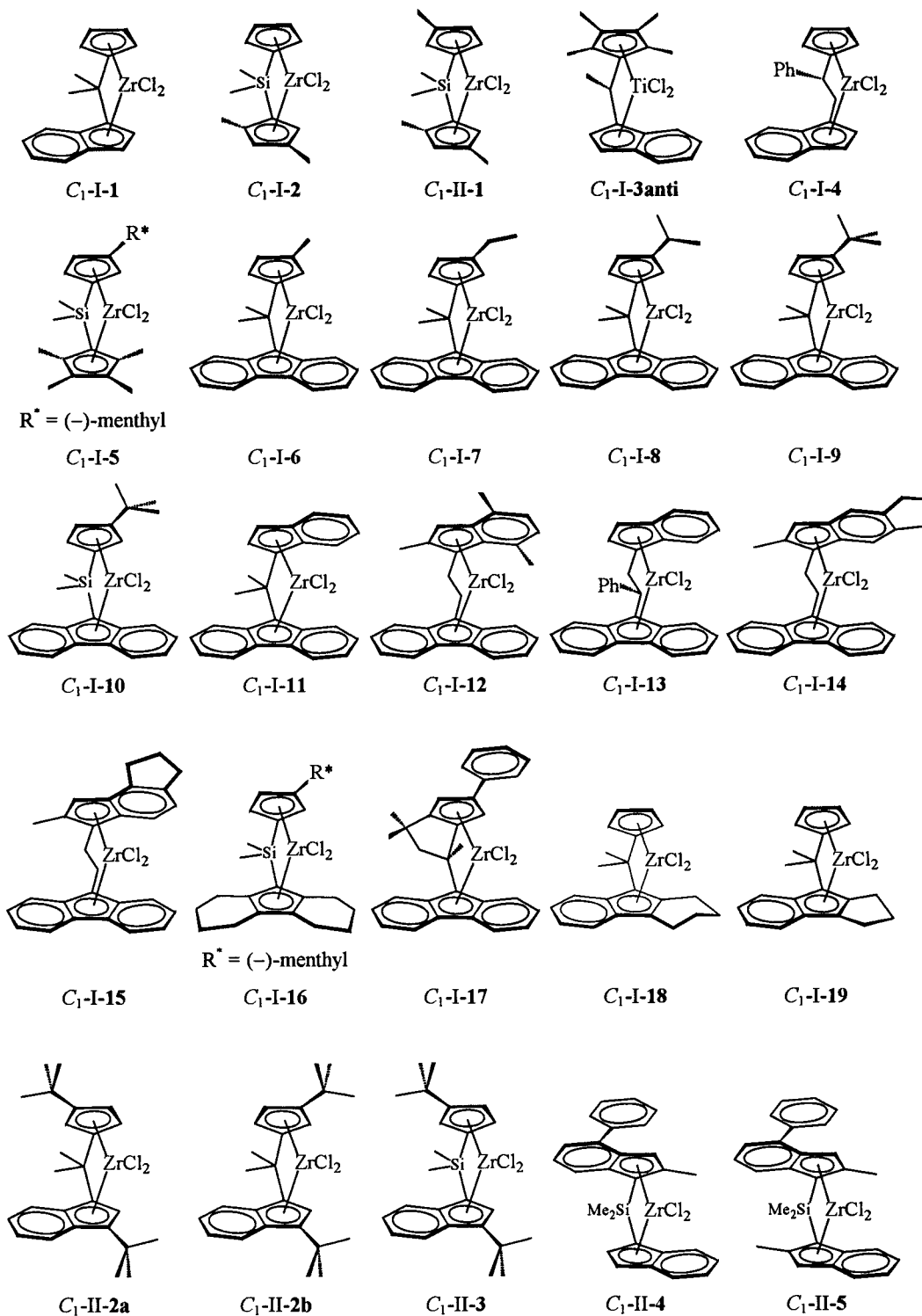
Figure 34. Methyl region of the ^{13}C NMR spectra of two *s*-PP samples showing different levels of *rrmr* (site isomerization or back-skip of the chain) and *mmrr* stereoerrors; top, prevalently enantioface errors; bottom, increased site isomerization.

ization) mechanism competing with bimolecular propagation. However, the nonlinear activity versus $[M]$ correlation for the syndiospecific C_2 -**1** catalyst¹¹³ argues against a simple bimolecular propagation scheme⁴¹⁸ (see section VIII for details). For C_2 -**5**, one can estimate a $\Delta\Delta E_{\text{enant}}^\ddagger = 2.1 \pm 0.1$ kcal/mol, in the rough estimate that the *rrmr* pentad accounts for all enantioface insertion errors.³⁶⁴ This value is similar to that found for the least isospecific C_2 -symmetric zirconocenes (see section V).

C. C_1 -Symmetric Metallocenes: from Hemiisotactic to Isotactic Polypropene

C_1 -Symmetric metallocenes are, broadly speaking, complexes lacking any symmetry element. Of course, such a broad definition includes a very large number of possible structures. For the purpose of this review, there are two types of C_1 -symmetric metallocenes which are of interest, all of them bridged, hence stereorigid: those with one (substituted or nonsubstituted) cyclopentadienyl ligand having two homotopic faces (e.g. C_1 -I-**1** in Chart 19) and those having two asymmetric cyclopentadienyls (e.g. C_1 -II-**1** in Chart 19). The first type, C_1 -I, presents a synthetic advantage with respect to the second type, and also with respect to the isospecific C_2 -symmetric complexes. In fact, a problem associated with the synthesis of *ansa*- C_2 -symmetric metallocenes is that they are almost invariably generated along with their *meso* isomers (Scheme 29), which are difficult to remove from the catalyst mixture and often produce unwanted low molecular weight atactic polypropene with nonnegligible polymerization activity. In addition, most of these modified C_2 -symmetric systems require multistep, low overall yield synthetic routes.^{320,336} On the contrary, for C_1 -symmetric systems of type I, a *meso* form does not exist (Scheme 29B). In several cases, the synthesis of the ligand is also quite simple, as in the $\text{Me}_2\text{C}(3\text{-R-Cp})(9\text{-Flu})\text{ZrCl}_2$ complexes shown in Scheme 29B.

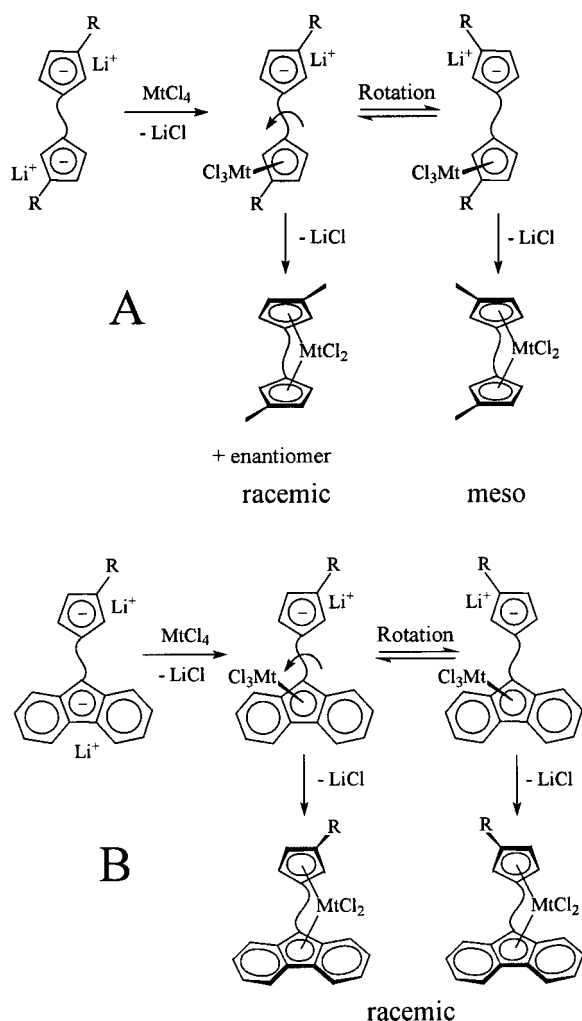
The common feature of C_1 -symmetric metallocenes is that their two coordination sites are *diastereotopic*. Because of this property, and depending on the size of the substituent on the cyclopentadienyl ligand, C_1 -

Chart 19. Representative C_1 -Symmetric Metallocenes

symmetric catalysts can vary in stereoselectivity from hemiispecific (producing *hi*-PP, which is amorphous) to partially isospecific (producing amorphous or low crystallinity PP, materials that are thermo-plastic–elastomeric in nature) to isospecific (producing crystalline *i*-PP). As in the case of C_2 -symmetric systems, all degrees of isotacticity and molecular weights can be obtained, as the possible ligand variations are even broader. Some representative metallocenes of the two types are shown in Chart 19. The simplest C_1 -symmetric complex, C_1 -I-1, its analogues with Hf or Ti, and its Me_2Si -bridged congener

have been extensively investigated, but their catalytic performances are inversely proportional to the number of studies in which they have appeared.^{390–393,395,420–423} The same low catalytic activity and low polypropene molecular weight have been observed for *erythro*/*threo*- $\text{Me}_2\text{C}(3\text{-MeCp})(1\text{-Ind})\text{-ZrCl}_2$ ⁴²⁴ and for Chisso's bicyclopentadienyl systems.³¹⁰ Going to bulkier ligands improves PP molecular weights. We start by analyzing in detail the case of the hemiispecific complexes, the prototype of which is C_1 -I-6.

Scheme 29



Hemioispecific C_1 -Symmetric Metallocenes.

The first effectively hemioispecific metallocene catalyst, $\text{Me}_2\text{C}(\text{3-MeCp})(\text{9-Flu})_2\text{ZrCl}_2$ (C_1 -I-6), and its Hf analogue, which are chiral and lacking any symmetry, and the polypropene produced therefrom have been reported by the Hoechst and Fina groups.^{46,421,425,426} Ewen correctly assigned the stereochemical distribution of the chirotopic methines in this peculiar microstructure as hemioisotactic, a microstructure previously assigned by Farina on a polymer synthesized indirectly.⁴²⁷ The catalytic synthesis of hemioisotactic polypropene, although this polymer remains a scientific curiosity, has been rather important in confirming the polymerization mechanism of metallocenes, since it could not be explained without the site-switching mechanism, as it is a case of syndiospecific polymerization. The presence on the same metal center of one isospecific and one aspecific site, together with the requirement of chain migratory insertion with site switching at (almost) every insertion, generates a unique polymer structure, in which every other methyne is in the same (isotactic) configuration, while the remaining alternating methynes are in a random configuration.^{46,427,428} Occasional back-skip of the chain accounts for the slight deviation from perfect hemioisotacticity, which requires a well-defined pentad distribution (3:2:1:4:0:0:3:2:1). Other metallocenes

with the proper ligand symmetry for hemioisotactic polymerization have been reported,^{385–395,422,429} but most of these catalysts produced low molecular weight PP. The highest molecular weights ($\bar{M}_w \sim 200\,000\text{--}300\,000$) are obtained with the hafnium analogue of C_1 -I-6, while the zirconium complex gives lower molecular weights ($\bar{M}_w \sim 50\,000$). Both catalysts have a quite low activity.⁴²⁵ No physicochemical characterization of this polymer has been reported so far, but it is expected to have some elastomeric properties. In some cases the elastomeric properties of the polypropenes have been confirmed.

As outlined above, for C_1 symmetric catalysts the two available coordination positions are nonequivalent (diastereotopic).⁴¹⁰ In this case, the stereoselectivity of models of the catalytic system depends on the energy difference between structures corresponding to propene coordination on the two nonequivalent inward and outward coordination positions, and two general cases can be considered.⁴³⁰

The Two Coordination Positions Are of Similar Energy. In the hypothesis that the chain migratory insertion mechanism is still prevailing, the model of these catalytic systems would be isospecific or syndiospecific, if the two situations originated from propene coordination on the two coordination positions are enantioselective in favor of the same or opposite propene enantiofaces, respectively. If only one situation is enantioselective, the corresponding catalytic system is hemioispecific.

The Two Coordination Positions Are of Substantially Different Energy. For models of these catalytic systems, the sequence of chain migratory insertion steps can be altered. In fact, the growing chain in successive coordination and insertion steps can often occupy the same coordination position. That is, after each migratory insertion step, in the absence of a coordinated monomer molecule, the growing chain could swing back to the previous coordination position (back-skip of the growing chain).

The driving force for the back-skip of the chain could be the energy difference between the two diastereomeric situations obtained by exchanging the relative positions of monomer and chain. Of course, the probability of occurrence of a back-skip of the chain, in the alkene-free state, is only indirectly dependent on this energy difference. In fact, it is dependent on the difference between the activation energy for the chain back-skip, $E_{\text{back-skip}}^\ddagger$, and the activation energy for the formation of the high energy alkene-bonded intermediate, $E_{\text{coord,out}}^\ddagger$ (see Scheme 30). However, since the degree to which empirical force fields can be used for prediction of transition states is not well-established and since the activation energy $E_{\text{coord,out}}^\ddagger$ is expected to increase with increasing E_{out} , for the sake of simplicity, we take $E_{\text{out}} - E_{\text{inw}}$ as a semiquantitative evaluation of the driving force for the back-skip of the chain.

The models of hemioispecific catalytic systems generally correspond to C_1 -symmetric systems for which the two coordination positions are of similar energy. The best known example is the model based on the $\text{Me}_2\text{C}(\text{3-MeCp})(\text{9-Flu})$ ligand (entry 34 in

Scheme 30

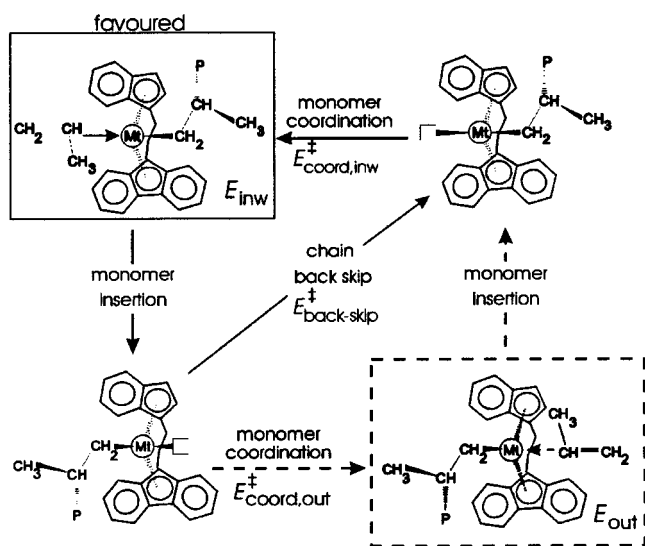


Chart 8 and Table 3), independently investigated by Corradini and Fink.^{89,90} The models of Figure 35 report the minimum energy situations corresponding to propene coordination to the catalytic system based on the aforementioned ligand.

Clearly, the model is enantioselective when the propene molecule is inward coordinated (which corresponds to a *R* chirality at the metal atom for a *R* coordination of the 3-MeCp ligand), since structure A, with a *re*-coordinated propene, is favored relative to structure B, with a *si*-coordinated propene, in the framework of the mechanism of the chiral orientation of the growing chain. In fact, structure B is disfavored by repulsive interactions between the growing chain and the fluorenyl ligand. On the contrary, the model is nonenantioselective when the growing chain is σ -bonded in the inward coordination position (which correspond to a *S* chirality at the metal atom for a *R* coordination of the 3-MeCp ligand) since structures C and D are equally hampered by repulsive interactions of the growing chain either with the 9-Flu ligand (structure C) or with the methyl group of the 3-MeCp ligand (structure D). Moreover, it can be reasonably assumed that the polymerization prevalently occurs according to a regular chain migratory insertion mechanism, since the situation corresponding to inward propene coordination is only slightly favored with respect to situations with outward propene coordination.^{89,90} Hence, every each other insertion is enantioselective, while the other is nonenantioselective. Consequently, the model is hemiispecific. This analysis is in qualitative agreement with the experimentally observed production of hemiisotactic polymer, with catalytic systems based on the bridged (3-MeCp)(9-Flu) ligand.^{46,118,421} Furthermore, Fink systematically investigated the effect of the alkyl group R in position 3, by considering also systems with R = ethyl and isopropyl. Both systems have been calculated to have one poorly enantioselective geometry (when the growing chain is inward coordinated) and one nicely enantioselective geometry (when the growing chain is outward coordinated). Since enantioselective geometries are slightly lower in energy than nonenantioselective

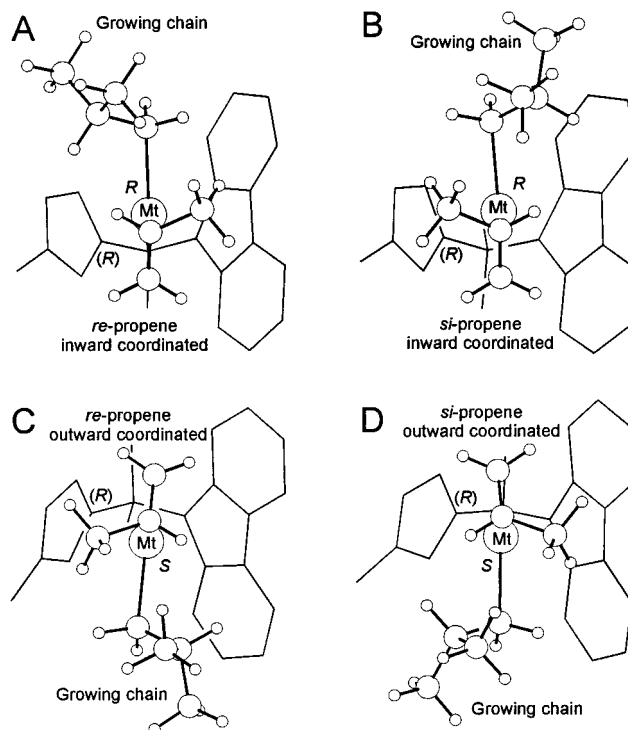


Figure 35. Molecular mechanics minimum energy geometry for *re* and *si* propene coordination on the $\text{Me}_2\text{Si}(3\text{-Me-Cp})(9\text{-Flu})\text{Zr}(\text{isobutyl})$ model with a *R* and *S* chirality at the metal atom, parts A and B, and C and D, respectively. (*R*) is the chirality of coordination of the 3-Me-Cp ligand.

geometries (less than 1.5 kcal/mol), the corresponding catalytic systems should be hemiispecific. This prediction⁸⁹ has been confirmed experimentally only in general terms, by polymerizations catalyzed with $C_1\text{-I-7}$ and $C_1\text{-I-8}$ ⁴³¹ (see below).

For the C_1 symmetric ligand $\text{Me}_2\text{C}(\text{Cp})(1\text{-Ind})$, similar calculations have shown that the geometry with a propene molecule inward coordinated is nonenantioselective, while a weak enantioselectivity is calculated when the propene molecule is outward coordinated.^{89,390,423} This is in qualitative agreement with the experimentally observed production of prevalently atactic polymer and of hemiisotactic polymer at low temperatures, with catalytic systems based on $C_1\text{-I-1}$ and related systems, although the low PP molecular weights hamper a precise methyl pentad analysis, because of extensive overlapping with resonances due to end groups.^{390–393,395,420–423}

Isospecific C_1 -Symmetric Metallocenes. Perfect hemiisotacticity requires that $mmmm = 18.75\%$. Deviating from the structure of $C_1\text{-I-6}$ in general makes the complexes more isospecific. Fink studied the series $C_1\text{-I-6} - C_1\text{-I-9}$ where the R substituent on Cp increases from methyl to *tert*-butyl. While the ethyl derivative produces a polypropylene very similar to that (prevalently hemiisotactic) made with the methyl derivative $C_1\text{-I-6}$, the 3-*i*-PrCp derivative $C_1\text{-I-8}$ ⁴³¹ and its Me_2Si -bridged analogue³⁴¹ produce PP with $mmmm$ of 44% ($T_p = 70^\circ\text{C}$) and 64.4% ($T_p = 60^\circ\text{C}$) respectively, compared to 14–27% with $C_1\text{-I-6}$.⁴³¹ While $C_1\text{-I-11}$ produces a hemiisotactic PP ($mmmm = 9.9\text{--}12.0\%$ on going from $T_p = 10$ to $T_p = 70^\circ\text{C}$ at 2 bar propene),⁴³¹ $\text{Me}_2\text{Si}(1\text{-Ind})(9\text{-Flu})\text{ZrCl}_2$ produces (at $T_p = 50^\circ\text{C}$) PP with $mmmm \sim 57\%$.⁴³² On going

to the 3-*t*-BuCp, the catalyst isospecificity (within this class) is maximized.⁴³³ C_1 -I-9 produces *i*-PP with relatively high *mmmm* pentad contents from 77.5% ($T_p = 60^\circ\text{C}$ in liquid monomer³⁶⁴) to 87.8%. ($T_p = 50^\circ\text{C}$ in toluene at 2 bar propene⁴³¹). Its Me₂Si-bridged congener is even more isospecific, producing *i*-PP with higher melting points (e.g. $T_m = 161^\circ\text{C}$ vs 130°C with C_1 -I-9, for $T_p = 30^\circ\text{C}$).⁴³³

Similar results have been reported by Marks with C_1 -I-5 (*mmmm* = 35% at $T_p = 25^\circ\text{C}$) and its Hf analogue (*mmmm* = 60–83% at $T_p = 25^\circ\text{C}$ —quite remarkable is the higher isospecificity of Hf vs Zr)⁴³⁴ and C_1 -I-16 (*mmmm* = 83% at $T_p = 25^\circ\text{C}$).⁴³⁵

Compared to the best C_2 -symmetric catalysts, C_1 -I-5 and related systems have lower stereoselectivity and produce *i*-PP with modest molecular weights. Possibly because of the presence of one highly hindered polymerization site, their polymerization activities and molecular weights seem in general lower than those of the more isospecific C_2 -symmetric systems.

Along the same line, Miyake and co-workers have developed a class of C_1 -symmetric systems which are highly isospecific (e.g. *threo*-Me₂C(3-*t*-Bu-Cp)(3-*t*-Bu-1-Ind)ZrCl₂, C_1 -II-2a) but again produce low molecular weight *i*-PP. In this case, the *meso*-like (*erythro*) isomer (C_1 -II-2b, less active than the racemic one) is partially isospecific.³²³ C_1 -II-2a is remarkably insensitive to the polymerization temperature in terms of isospecificity,^{323,339} while molecular weights drop from 100 000 to 9 000 on going from 1 to 60 °C.³²³ The Ti analogue of C_1 -II-2a offers a rare example of a titanocene being more active than the corresponding zirconocene, while the same very high isospecificity is maintained. The Hf analogue obeys the general rule, showing a 20-fold decrease in polymerization activity compared to C_1 -II-2a. The silicon-bridged C_1 -II-3 is less active and less stereoselective, and produces lower molecular weights than C_1 -II-2a. Both C_1 -II-2a and C_1 -I-9^{323,364} produce *i*-PP containing minor amounts of regioirregularities, being more regioselective than most C_2 -symmetric catalysts. The influence of [M] (propene concentration) on the isospecificity of C_1 -II-2a is low compared to the C_2 -symmetric systems (see section V). Interestingly, the isospecificity of C_1 -I-9 also seems to be independent of T_p .³⁶⁴ However, Fink has reported an increase of isotacticity from 83.5 to 87.8% *mmmm* on going from $T_p = 10$ to 50 °C, operating at constant propene pressure of 2 bar, rather than at constant [M].⁴³¹ Hence this effect can be ascribed to a lower propene concentration at the higher temperature, which increases the chance of unimolecular chain back-skip over insertion.

The best performance of a C_1 -symmetric system so far has been attained by Spaleck and co-workers with the zirconocenes C_1 -II-4 and C_1 -II-5,⁴³⁶ which combine the indenyl substitution of two different C_2 -symmetric zirconocenes previously described by the Hoechst group, thus providing both high stereoregularity and high molecular weights (for example, C_1 -II-5 gives *i*-PP with *mm* = 96%, 2,1 = 0.4%, $T_m = 155^\circ\text{C}$ and $\bar{M}_w = 530\,000$, at the relatively high polymerization temperature of 70 °C).

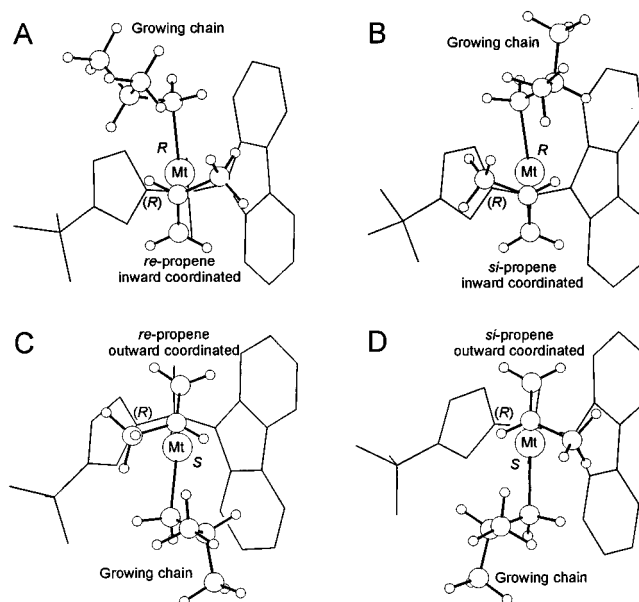


Figure 36. Molecular mechanics minimum energy geometry for *re* and *si* propene coordination on the Me₂Si(3-*t*-Bu-Cp)(9-Flu)Zr(isobutyl) model with a *R* and *S* chirality at the metal atom, parts A and B, and C and D, respectively. (*R*) is the chirality of coordination of the 3-*t*-Bu-Cp ligand.

All these aspects can be fully rationalized by molecular modeling, by the usual nonbonded interaction analysis. From a molecular modeling standpoint, Morokuma,²⁷⁵ Fink,⁸⁹ and Corradini²⁷³ have confirmed that the size of the substituent in position 3 has a remarkable relevance also for these C_1 symmetric catalysts based on the H₂Si(Cp)(9-Flu)²⁷⁵ and Me₂C(Cp)(9-Flu)^{89,273} ligands, the latter corresponding to entry 30 in Chart 8. All authors agree that replacing hydrogen with a *tert*-butyl group in position 3 of the Cp ring (see Figure 36) turns the catalyst from syndiospecific to isospecific. However, some subtle differences do exist between the different calculations. According to Morokuma, the presence of the *tert*-butyl group forbids the growing chain to be located in the inward position (i.e. close to the *tert*-butyl group). In particular, in the absence of the monomer molecule, as probably occurs at the end of each insertion step, the steric pressure of the ligand skeleton could force the growing chain to skip back to the less crowded outward position. Hence, insertion always occurs with the same relative disposition of the monomer and of the growing chain (inward and outward, respectively), and the model is consequently isospecific. On the contrary, Fink and Corradini have found that insertion can occur with the growing chain in the crowded inward position as well, since the growing outward chain is favored relative to the growing inward chain by roughly 1–4 kcal/mol.^{89,273} However, both geometries (corresponding to inward and outward growing chain coordination) favor the same propene enantioface (in the models of Figure 36, insertion of the *re* enantioface is favored for both inward and outward propene coordinations). Hence, also the models of Fink⁸⁹ and Corradini²⁷³ are able to rationalize the experimental isospecific behavior of this catalyst.⁴³³ Probably, the frequency of back-skip of the growing chain in the less crowded outward

position is considerably high for this catalyst, although consequences on stereoselectivity are scarce, since whatever the coordination position of the growing chain, enantioselectivity is reasonably high and in the favor of the same propene enantioface.

It is clear that the most important aspect of C_1 -symmetric zirconocenes is the wide variability of their isospecificity, which has allowed the preparation of novel PP materials. This avenue has been opened by Chien and Rausch, who reported the preparation of thermoplastic–elastomeric polypropene (TPE-PP) with C_1 -I-**3-anti** and its more active isomer C_1 -I-**3-syn**.^{385–388,437} The Zr analogue of C_1 -I-**3** is practically inactive.³⁸⁹ It is worth noting here that the TPE-PP produced with the Chien/Rausch catalysts is markedly different from the TPE-PP made with Waymouth's catalysts. In fact, the former (*mmmm* ~ 40%) has a very low crystallinity (T_m ~ 50–65 °C, ΔH_f ~ 3 cal/g after annealing) and is an elastomeric polymer fully soluble in Et₂O,⁴³⁷ while TPE-PP from (2-Ar-Ind)₂ZrCl₂ catalysts can be separated in fractions of widely different crystallinity, although the average methyl pentad content is quite similar in the two cases (see section IV.A.3).

Following this path, several examples of C_1 -symmetric zirconocenes which produce elastomeric polypropenes of different tacticity have been produced.

Rieger prepared the C_1 -symmetric zirconocenes *rac*-C₂H₄(9-Flu)(1-Ind)ZrCl₂ and the two diastereoisomers of *rac*-C₂H₃-1-(*R,S*)Ph-1-(9-Flu)-2-((*R,S*)-1-Ind)ZrCl₂ (C_1 -I-**13**) and of *rac*-C₂H₃-1-(*R,S*)Ph-(Cp)-((*R,S*)-1-Ind)ZrCl₂ (C_1 -I-**4**).⁴³⁸ In particular, *rac*-C₂H₃-1-(*R*)Ph-1-(9-Flu)-2-((*R*)-1-Ind)ZrCl₂ is the most isospecific. Interestingly, this catalyst produces a low melting PP (T_m = 98–121 °C), although molecular weights are too low for any practical use. The latter have a low enantioselectivity.

Me₂Si(Cp)(2-*p*-tolyl-1-Ind)ZrCl₂ produces (in toluene at 1.2 atm propene and 25 °C) an atactic polypropene (*mm* = 31%) of remarkably high molecular weight (M_v = 377 000).⁴³⁹

Low-pressure propene polymerization with *anti*-Me₂Si(1-Ind)(3-Me-1-Ind)ZrCl₂ produces elastomeric PP with *mmmm* contents of 30–50% depending on propene concentration and polymerization temperature.³⁹⁴ C_1 -I-**12** and related systems produce PP with *mmmm* pentad contents ranging from 7 to 80% but of very low molecular weights.⁴⁴⁰ C_1 -I-**14** and C_1 -I-**15** again produce PP with *mmmm* ranging from 54 to 80% but with higher molecular weights.²⁹⁵ The large difference in molecular weights between C_1 -I-**12** and the sterically very similar C_1 -I-**15** is quite surprising. High molecular weights have also been reported with C_1 -I-**17** which produces (30 °C, toluene, [M] = 1.29 mol/L) PP with *mmmm* = 57.5%.⁴⁴¹

Corradini and co-workers modeled the catalysts based on the C₂H₃[1-(9-Flu)-1-Ph-2-(1-Ind)] and on the C₂H₃[1-Cp-1-Ph-2-(1-Ind)] ligands presenting *R* and *S* chirality, at the C(1) atom of the ethylene bridge (entries **36** and **38** and entries **37** and **39** in Chart 8).⁹² The *R* and *S* configurations at the C(1) atom of the bridge favor the δ - and λ -bridge conformations, respectively.^{438,442,443} For the complex containing the C₂H₃[1-(9-Flu)-1-Ph-2-(1-Ind)] ligand with

δ -bridge conformation (entry **36** in Table 3), the situations corresponding to outward and inward propene coordination are partially and strongly enantioselective, respectively, in favor of the *same* enantioface, while for the same ligand but with λ -bridge conformation (entry **37** in Table 3), the situations corresponding to outward and inward propene coordination are partially and strongly enantioselective in favor of *opposite* enantiofaces. Hence, the model with δ -bridge conformation tends to be isospecific, whereas the model with λ -bridge conformation is substantially hemiispecific. Analogously, for the complex containing the C₂H₃[1-Cp-1-Ph-2-(1-Ind)] ligand, the model with δ -bridge conformation has a slight tendency to be isospecific with respect to the model with λ -bridge conformation (entries **37** and **39** in Table 3, respectively). Moreover, for the complex containing the C₂H₃[1-(9-Flu)-1-Ph-2-(1-Ind)] ligand, the more enantioselective geometry is favored by more than 2 kcal/mol over the poorly enantioselective geometry, independently of the bridge conformation. Hence, at low monomer concentration a more frequent back-skip of the chain toward the energetically favored and more enantioselective geometry is reasonable. This could explain the experimentally observed increase of stereospecificity at low monomer concentration.⁴³⁸ Differently, for the complex containing the C₂H₃[1-Cp-1-Ph-2-(1-Ind)] ligand, the more enantioselective geometry is only slightly favored (roughly 0.5 kcal/mol) over the poorly enantioselective geometry, independently of the bridge conformation. Hence, a driving force for a frequent back-skip of the chain toward the more enantioselective geometry is absent. This could explain the substantial independence of the stereospecificity from monomer concentration experimentally observed.⁴³⁸

The energy differences between minima corresponding to diastereomeric preinsertion intermediates with different chiralities at the central metal atom ($E_{out} - E_{inw}$) for several catalytic models with C_1 -symmetric metallocenes are listed in the last column of Table 3. It is worth noting that, when substantial energy differences between minimum energy diastereomeric intermediates are present, lower energies correspond to the monomer coordination in the (more crowded) inward coordination position. In particular, it is reasonable to expect that, for models with large $E_{out} - E_{inw}$ values (**34–37**), the growing chain in successive coordination steps can occupy frequently the (less crowded) outward coordination position, leaving the inward position free for the monomer coordination. For all these models, the lower energy diastereomer with inward monomer coordination is more enantioselective than the higher energy diastereomer with outward monomer coordination.

As a concluding remark, C_1 -symmetric metallocenes have been quite valuable in at least three aspects: (i) increasing the range of achievable microstructures and indeed giving access to a range of thermoplastic–elastomeric, homogeneous polypropenes; (ii) increasing the complexity of the polymerization mechanism, hence providing new stimuli which in turn gave a deeper understanding of the

correlation between ligand structure and polymerization conditions on one side, and kinetics of insertion/site isomerization on the other; and (iii) providing models for the $\text{MgCl}_2/\text{TiCl}_4$ heterogeneous catalysts which proved better than those based on C_2 -symmetric active centers.⁴⁴⁴

V. Stereocontrol: Influence of Polymerization Conditions

The catalytic performance of metallocene catalysts depends strongly on the polymerization conditions, much more so than, for example, in the case of MgCl_2 -supported TiCl_4 catalysts. The crucial importance of this behavior has been overlooked for many years. In fact, until recently, low-pressure propene polymerizations in toluene were the typical way metallocene catalysts were investigated. In these experiments, propene concentrations vary dramatically, especially when different polymerization temperatures are compared or high productivities are involved (because of diffusion-limited monomer concentrations). As a consequence, literature data on polymerization activity and degree of regio- and stereoselectivity of the prototypical isospecific metallocene catalysts varied in a wide range and made comparisons difficult. Although differences in catalyst activities could be readily explained in terms of the different experimental conditions such as handling procedures, source of the MAO cocatalyst, and purity of the metallocene precatalyst, the scatter of polymer regioregularity, stereoregularity, molecular weight, solubility, and melting point data could not be explained by the usual differences among different laboratories.

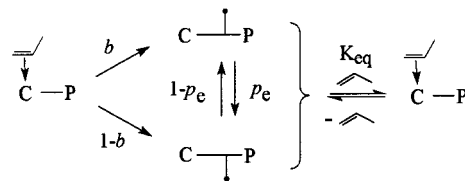
The first studies on the dependence of catalyst performance on propene concentration with zirconocene catalysts have been reported by Ewen, for the syndiospecific catalyst C_5 -1,¹¹³ and by Rieger, for a series of C_1 -symmetric zirconocenes.⁴³⁸ The influence of monomer concentration on the behavior of *isospecific* C_2 -symmetric metallocenes has been neglected for a long time, with the exception of an early work,³⁰⁵ which, however, was limited in its scope to propagation rate and molecular weight aspects with the system C_2 -I-1/MAO in a relatively narrow monomer concentration range, until at the STEPOL meeting in 1994, two groups independently reported on the dramatic influence of propene concentration, $[M]$, on the stereoselectivity of C_2 -symmetric zirconocene catalysts.^{445,446} While providing a much needed explanation for the observed inconsistency of experimental data, this finding has washed away a lot of previous experimental work. In the following two sections, we discuss the influence of monomer concentration first, and then the influence of polymerization temperature on those investigations only that have taken into account the influence of $[M]$.

A. Influence of Monomer Concentration

1. C_2 -Symmetric Catalysts

Several C_2 -symmetric *ansa*-zirconocenes have been studied to determine the extent of the influence of monomer concentration on catalyst activity, *i*-PP stereoregularity, and molecular weight. Brintzinger

Scheme 31. Kinetic Scheme for Epimerization. $K_{\text{eq}} = [\text{C}\cdot\text{M}]/([\text{C}][\text{M}])$ (Modified from ref 232)



showed that the molecular weight dependence on monomer concentration can be explained by the competition between monomolecular (β -hydrogen transfer to the metal) and bimolecular (β -hydrogen transfer to the monomer) chain release reactions and that the ratio between the two reaction rates strongly depends on the type of cyclopentadienyl ligand.³³⁶ The increase of *i*-PP molecular weight with propene concentration had been reported by Kaminsky, who explored the range 0.6–5 mol/L at 35 °C with C_2 -I-1/MAO³⁰⁵ and then obtained propene oligomers with a related catalyst at 50 °C and very low monomer concentration.¹²⁷ While the effect of $[M]$ on molecular weight and type of regioerrors was to be expected (and actually prompted our original study of this variable), the detrimental influence of $[M]$ on isotacticity was totally unexpected.

For both benchmark catalysts C_2 -I-1 and C_2 -I-1H₄, isotacticity (% *mmmm*) decreases substantially, e.g. from 87 to 54.7% by decreasing the monomer concentration from 11 to 0.4 mol/L in the case of C_2 -I-1. Under “catalyst starvation” conditions, that is $[M] \rightarrow 0$, the resulting oligomers were *fully atactic*.²³²

On the basis of what we have discussed above, as far as enantioface selectivity is concerned, C_2 -symmetric chiral metallocenes should not sense on what side, and how often, a monomer approaches the metal center. Indeed, the site control mechanism of these catalysts requires that the stereochemistry of insertion is independent from the previous insertion. The loss of stereospecificity with the decrease in monomer concentration has been accounted for, from a kinetic standpoint, with an equilibrium between active sites having a coordinated monomer ($\text{C}\cdot\text{M}$) and sites without coordinated monomer (C) (Scheme 31).

It is apparent from Scheme 31 that C , not having a coordinated monomer molecule, cannot generate *m*, *r* diads by monomer insertion. As a consequence, C must be able to racemize the chiral carbon of the last inserted unit, that is, as also pointed out by Busico and Cipullo and experimentally proven by Brintzinger and Leclerc by polymerizing *Z*- and *E*-propene-1-*d*,^{194,196} C is an epimerization catalyst. In other words, the loss of isospecificity with decreasing $[M]$ must be caused by a unimolecular process. The mechanisms proposed for this epimerization reaction are discussed in section V.C.

In Scheme 31, p_c is the probability of epimerization (racemization) of the last stereogenic methine, b is the probability of a correct enantioface insertion (*re* at a (*R,R*) center and *si* at a (*S,S*) center in the case of C_2 -I-1 and related catalysts), and the sites C and $\text{C}\cdot\text{M}$ are related by

$$[\text{C}\cdot\text{M}] = [\text{C}]K_{\text{eq}}[\text{M}]$$

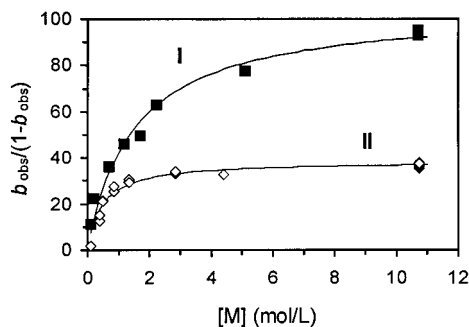


Figure 37. Experimental $b_{\text{obs}}/(1 - b_{\text{obs}})$ values: (■) $C_2\text{-I-35/MAO}$ (50 °C, propene/pentane); (◇) $C_2\text{-I-1/MAO}$ (50 °C, propene/toluene); solid line: fitting to eq 1. From ref 230.

Hence, assuming $p_e = 1 - p_e = 0.5$ (i.e. assuming C to lose any enantioface selectivity in the absence of coordinated monomer, as experimentally observed in the case of $[M] \rightarrow 0$), eq 1 is obtained:

$$\frac{b_{\text{obs}}}{1 - b_{\text{obs}}} = \frac{0.5 + bK_{\text{eq}}[M]}{0.5 + (1 - b)K_{\text{eq}}[M]} \quad (1)$$

where b_{obs} and $(1 - b_{\text{obs}})$ (obtained through a least-squares method from the methyl pentad distribution of i -PP) represent the *observed* concentration of correct and wrong primary insertions, respectively, at a given $[M]$ and T_p , and the Bernoullian probability parameter b is the inherent enantioface selectivity which depends on the catalyst structure and T_p , but is independent from $[M]$. For $C_2\text{-I-1/MAO}$ and related catalysts, in liquid monomer at T_p below 70 °C, $b_{\text{obs}} \rightarrow b$, while the plateau regime is not reached for higher temperatures or for the bulkier 3-*t*Bu-indenyl system $C_2\text{-I-35}$. The consequence of the above results is that the active center needs a coordinated monomer molecule in order to retain its stereoselectivity. Also the stereoselectivity of both C_1 -symmetric (see sections IV.C and V.A.2 below) and unbridged catalysts appears to have a relevant dependence on monomer concentration, but for different reasons.^{386,431}

The experimental $b_{\text{obs}}/(1 - b_{\text{obs}})$ values, fitted to eq 1, for $C_2\text{-I-1/MAO}$ and $C_2\text{-I-35/MAO}$ are shown in Figure 37.

2. C_1 -Symmetric Catalysts

C_1 -symmetric zirconocenes behave rather differently. Rieger found an *inverse* dependence of isotacticity on monomer concentration for the C_1 -symmetric zirconocenes $rac\text{-}C_2H_4(9\text{-Flu})(1\text{-Ind})ZrCl_2$ and the two diastereoisomers of $rac\text{-}1\text{-}(R,S)\text{Ph-C}_2H_3\text{-}1\text{-}(9\text{-Flu})\text{-}2\text{-}((R,S)\text{-}1\text{-Ind})ZrCl_2$, while the related $rac\text{-}1\text{-}(R,S)\text{Ph-C}_2H_3(\text{Cp})((R,S)\text{-}1\text{-Ind})ZrCl_2$ has a low enantioselectivity, independent of monomer concentration.⁴³⁸ In particular, $rac\text{-}C_2H_3\text{-}1\text{-}(R)\text{Ph-}1\text{-}(9\text{-Flu})\text{-}2\text{-}1(R)\text{-Ind-}ZrCl_2$ is the most isospecific, and $mmmm$ increases from 46 to 80% on lowering $[M]$ from 3.38 to 0.45 mol/L. The most likely explanation of this behavior is the back-skip of the chain (see section IV.C).

The highly isospecific C_1 -symmetric $threo\text{-Me}_2\text{C}(3\text{-}t\text{-Bu-Cp})(3\text{-}t\text{-Bu-}1\text{-Ind})ZrCl_2/MAO$ suffers only a minor decrease of isospecificity at 40 °C in toluene by lowering $[M]$, producing i -PP with $mmmm$ from

> 99.5% at $[M] \geq 2$ mol/L down to 95.6% at $[M] = 0.2$ mol/L.⁴⁴⁷

B. Influence of Polymerization Temperature

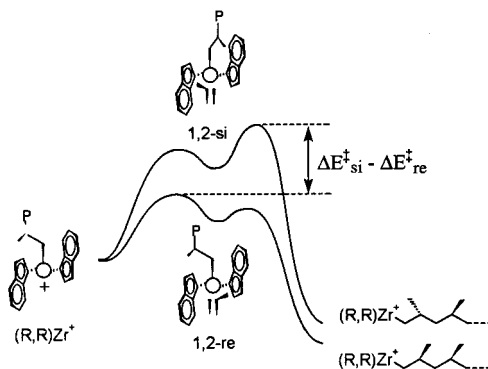
Another most important source of variability in the molecular architecture of polypropylenes obtained from *ansa*-zirconocenes, besides the biscyclopentadienyl ligand structure and monomer concentration, is the polymerization temperature, T_p . Unfortunately, most of the earlier catalytic studies on the performance of metallocene catalysts have been carried out in solution at largely different propene concentrations, so changes in the latter due to lower propene concentrations at the higher T_p become the primary cause for changes on both polymer properties and polymerization kinetics, rather than T_p itself (see previous section). It is therefore of the utmost importance, when comparing the polymerization performance of different zirconocene catalysts, to perform the experiments under high and identical monomer concentrations, and preferably in liquid propene, to minimize the extent of chain-end epimerization.

Several $C_2\text{-I}$ -type zirconocenes have been investigated. Both isotacticity and molecular weight of i -PP decrease by increasing T_p , while the amount of secondary insertions, when present, increases slightly.

For example, upon increasing T_p from 20 to 70 °C, $C_2\text{-I-1/MAO}$ yields polypropylenes with decreasing \bar{M}_v values from 56 000 to 19 600, percent $mmmm$ pentads from 92 to 83%, and corresponding melting temperatures from 142 to 125 °C. Furthermore, the overall fraction of regioirregularities (2,1 and 3,1 insertions) increases from 0.4 to 0.7%. $C_2\text{-I-9}$, which is slightly less isospecific than $C_2\text{-I-1/MAO}$ due to a wider "bite angle" β (see Table 1), produces i -PP with percent $mmmm$ pentads decreasing from 88 to 77% by increasing T_p from 20 to 70 °C. The regioselectivity of $C_2\text{-I-9}$ is slightly higher (percent 2,1 insertions from 0.14 at 0 °C to 0.60% at 70 °C) than that of $C_2\text{-I-1}$. It is worth noting here that there is no detectable 2,1 \rightarrow 3,1 isomerization with $C_2\text{-I-9/MAO}$, as only 2,1-*erythro* and 2,1-*threo* units were observed (see section VII.A for details). As the 2,1 \rightarrow 3,1 isomerization reaction would be faster (relative to the following primary insertion) than epimerization, its absence (or very low extent, as in $C_2\text{-I-1/MAO}$) is an indication of the absence of epimerization in liquid monomer.

Molecular weights of i -PP from $C_2\text{-I-9/MAO}$ are lower than those obtained from $C_2\text{-I-1/MAO}$ at any temperature in the range investigated, ranging (assuming $\bar{M}_v/\bar{M}_n \approx 2$) from $\bar{M}_v \approx 20$ 000 ($\bar{M}_n = 11$ 000 at $T_p = 0$ °C) to $\bar{M}_v \approx 12$ 000 ($\bar{M}_n = 6000$ at $T_p = 70$ °C). It is also interesting that the temperature dependence of molecular weights of i -PP from $C_2\text{-I-9/MAO}$ is lower than that shown by $C_2\text{-I-1/MAO}$ (see below).

Ewen has reported that $rac\text{-}C_2H_4(3\text{-Me-}1\text{-Ind})_2\text{-}ZrCl_2/MAO$ catalyst ($C_2\text{-I-31/MAO}$) is nearly aspecific despite its C_2 -symmetry.¹¹⁶ We have reinvestigated the behavior of $C_2\text{-I-31/MAO}$ in liquid monomer and confirmed that it is far less isospecific than $C_2\text{-I-1/MAO}$: percent $mmmm$ pentads decrease from 36 to 14% ($b_{50} \text{ °C} = 0.723_3$) by increasing T_p from 0 to 70 °C.⁵⁰

Scheme 32. Schematic Representation of the Origin of $\Delta\Delta E^\ddagger$ in (R,R) - C_2 -I-1


The polymerization mechanism is not immediately obvious by looking at the pentad region of the ^{13}C NMR, due to the presence of all 10 pentads. Application of the statistical triad tests allows one to identify the source of the weak enantioface selectivity in C_2 -I-31/MAO as being enantiomorphic site control, as it is the case of all other C_2 -symmetric systems. This is possible by looking at the T_p dependence of the E and B triad tests (see section II.G): only the correct mechanism shows invariance with T_p of the corresponding triad test.

The isospecific and highly regioselective C_2 -I-35/MAO catalyst also shows a strong dependence toward T_p , producing *i*-PP with *mmmm* ranging from 97% at 20 °C to 91% at 70 °C and average viscosity molecular weights from 410 000 at 20 °C to 25 000 at 70 °C.⁵⁰

The isospecificity of a catalyst is defined by the statistical parameter *b*, which represents the probability of a "correct" monomer insertion in the enantiomorphic site, at a given polymerization temperature. Assuming epimerization to be negligible in liquid monomer ($b_{\text{obs}} = b$), the Arrhenius plot of $\ln[b/(1-b)]$ versus $1/T_p$ yields straight lines of slope $\Delta\Delta E^\ddagger/R$, from which the values of enantioface selectivity $\Delta\Delta E^\ddagger_{\text{enant}} = |\Delta E^\ddagger_{\text{si}} - \Delta E^\ddagger_{\text{re}}|$ is estimated (Scheme 32).

A series of selected experimental $\Delta\Delta E^\ddagger_{\text{enant}}$ values are compared in Table 11, while some of the $\ln[b/(1-b)]$ versus $1/T_p$ plots for these systems are shown in Figure 38.

The $\Delta\Delta E^\ddagger$ values for C_2 -I-1 and C_2 -I-9 are intermediate between that of enantiomorphic site control of highly isospecific Ti catalysts (4.8 kcal/mol)¹¹⁴ and

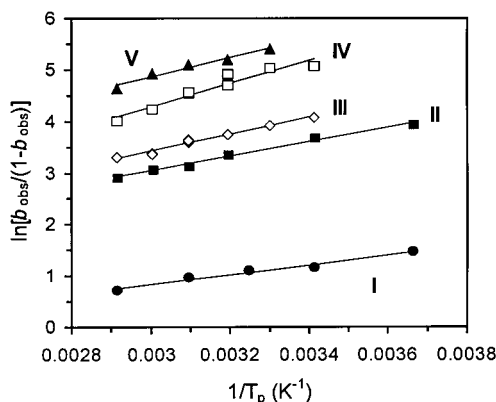


Figure 38. Arrhenius plots of $\ln[b/(1-b)]$ versus $1/T_p$ for selected C_2 -symmetric, bisindenyl zirconocenes. I: C_2 -I-31/MAO; II: C_2 -I-9/MAO; III: C_2 -I-1/MAO; IV: C_2 -I-35/MAO; V: C_2 -I-36/MAO. All polymerization in liquid propene.

that of chain-end control (ca. 2 kcal/mol).^{115,284} The lower isospecificity of C_2 -I-31 can be accounted for by the lesser steric difference between the facing methyl and benzene rings in the 3-methylindenyl moiety. The higher isospecificities of C_2 -I-35 and C_2 -I-36 compared to C_2 -I-1 are remarkable, but $\Delta\Delta E^\ddagger$ in the case of C_2 -I-35 is overestimated due to residual epimerization even in liquid monomer.²²⁹

C. Epimerization of the Primary Growing Chain

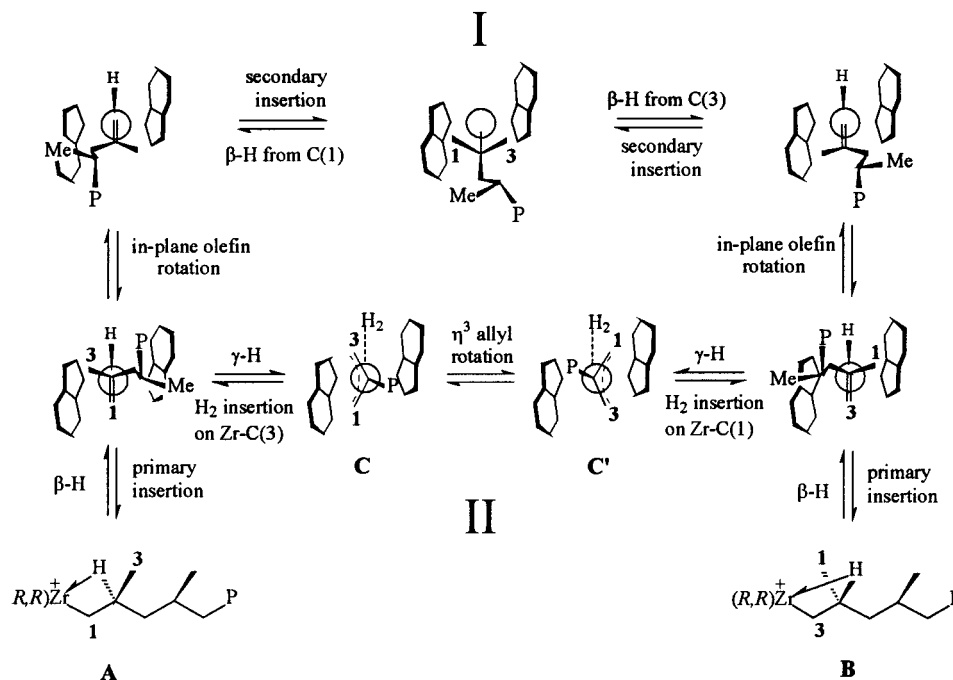
As discussed in section V.A, in the case of propene polymerization with C_2 -symmetric zirconocenes, the isotacticity of PP decreases at lower propene concentrations, due to unimolecular primary-growing-chain-end epimerization, which scrambles the chirality of the last chirotopic methine of the growing chain. The extent of epimerization at a given [M] depends strongly on the nature of the *ansa*- π -ligand^{252,446,448–450} and on the polymerization temperature.⁴⁴⁶ Epimerization has been explained by two mechanisms, both requiring formation of a Zr–H(CH₂=CMeP) olefin complex via unimolecular β -H transfer. Busico's mechanism (I in Scheme 33)⁴⁴⁸ involves a sequence of β -H transfers, double bond reorientations, and insertions. On the basis of literature precedents,^{144,225,253,255,451–457} Resconi has proposed that the reversible formation of a zirconocene allyl dihydrogen complex (II in Scheme 33) could be used to explain growing-chain epimerization.^{231,458} Formation of an allyl intermediate also accounts for the presence of

Table 11. Experimental and Calculated $\Delta\Delta E^\ddagger_{\text{enant}}$ for Various C_2 -Symmetric Zirconocenes

<i>rac</i> -zirconocene	$\Delta\Delta E^\ddagger_{\text{enant}}$, kcal/mol, obsd	$\Delta\Delta E^\ddagger_{\text{enant}}$, ^a kcal/mol, calcd	$\Delta\Delta E^\ddagger_{\text{enant}}$, ^b kcal/mol, calcd	ref ^c
$C_2H_4(1\text{-Ind})_2ZrCl_2$ (C_2 -I-1)	3.3 ± 0.2	4.3	3.5	50
$C_2H_4(3\text{-Me-1-Ind})_2ZrCl_2$ (C_2 -I-31)	1.9 ± 0.2	1.4	1.3	50
$C_2H_4(4,7\text{-Me}_2\text{-1-Ind})_2ZrCl_2$ (C_2 -I-18)	3.1 ± 0.2	5.7	3.2	202
$Me_2C(1\text{-Ind})_2ZrCl_2$ (C_2 -I-9)	2.8 ± 0.2	3.8	2.3	50
$Me_2C(3\text{-Me}_3\text{Si-1-Ind})_2ZrCl_2$ (C_2 -I-33)	2.6 ± 0.2	3.5	2.9	50
$Me_2C(3\text{-}t\text{-Bu-1-Ind})_2ZrCl_2$ (C_2 -I-35)	4.5 ± 0.5	4.3	4.3	50
$H_2C(3\text{-}t\text{-Bu-1-Ind})_2ZrCl_2$ (C_2 -I-36)	3.7 ± 0.4			324

^a $\Delta\Delta E^\ddagger_{\text{enant}}$ is the energy difference between the olefin complexes corresponding to the two propene enantiofaces, calculated by Corradini, Guerra, Cavallo, and co-workers according to the method described in refs 91 and 272. ^b $\Delta\Delta E^\ddagger_{\text{enant}}$ is the energy difference between the approximated transition state geometries corresponding to the two propene enantiofaces, calculated by Corradini, Guerra, Cavallo, and co-workers according to the method described in refs 91 and 272. ^c The references reported in this column refer to the experimental $\Delta\Delta E^\ddagger_{\text{enant}}$ values.

Scheme 33. Epimerization via Double Bond Reorientation (I) or Reversible Formation of a (R,R)Zr(allyl)(H₂) Cation (II)^a



^a The ligand bridge is omitted for clarity.

internal unsaturations^{131,229} and provides a model for reversible catalyst deactivation.^{225,453,454} Allyl rotation has been shown experimentally to be feasible in related systems.^{181,254} Both mechanisms take into account the analysis of Leclerc and Brintzinger,^{194,196} who have shown that primary-growing-chain-end epimerization occurs with exchange of the methylene and methyl carbons of the stereoinverted unit (**A** → **B** in Scheme 33). Further investigation is obviously required to assess if, and which one of these two mechanisms produces the epimerization of a growing chain end.

VI. Statistics of Polymerization

A. General Remarks

The polymerization reaction is a sequence of different events, such as monomer insertions, site isomerizations, and chain release reactions. The polymer chain can be seen as a permanent picture of the sequence of these events, and it is possible to use a statistical approach to study their distribution along the chain to increase our knowledge on polymerization mechanisms. As a consequence, a mathematical model of the polymerization can be built by assigning a probability at each event in our system. In the case of propene homopolymerization, this approach is (largely) used to study the mechanisms governing the stereoselectivity of the catalyst from the ¹³C NMR spectrum of the polymer. In fact, the type and the relative amount of the stereosequences present in the chain are obtained from the methyl region of the spectrum and are usually determined at the pentad level (see section II.G). This distribution can be studied using insertion probabilities for propene enantiofaces, which depend on the type of stereocontrol mechanism active for the catalytic

system. Due to the large variety of achievable structures, metallocene-based catalysts have been used to develop and to test these statistical models. A rationalization was made by Farina⁴⁵⁹ that divided metallocenes in different classes according to their symmetry and indicated possible statistical models to describe the polymerization behavior of each class. In the following sections this classification is also taken into account.

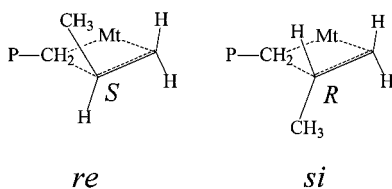
Metallocene are characterized by the presence of two catalytic sites (see section II) for monomer insertion (Scheme 10 and related discussion), and the polymer chain migrates from one site to the other at each monomer insertion. The statistical parameters for enantioface selection for the two sites could be equal or different, depending on the symmetry elements present in the complex.⁴⁵⁹

In some cases, a "site isomerization" (i.e. a chain migration from a site to the other without monomer insertion) can occur. When this mechanism influences the stereosequence distribution (as is the case in syndiotactic polymerizations), the statistical model should contain a probability parameter to describe this event.

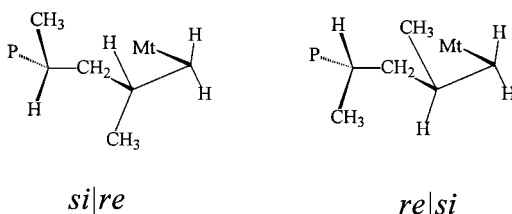
B. Mechanisms of Stereocontrol and Statistical Models

As reported in section II.E, the two main mechanisms of stereocontrol in 1-olefin polymerization arise from the chirality of the catalytic site (*enantiomorphic site control*) and from the chirality of the last methine in the polymer chain (*chain-end control*). Two statistical models, based on these basic mechanisms, have been developed and used by different authors and are known as the *enantiomorphic site model*²⁹⁶ and the *Bernoullian model*.⁴⁶⁰

Scheme 34



Scheme 35



1. Chain-End Control (Bernoullian Model)

As indicated by Tulleken,⁴⁶¹ there is a “nomenclature” problem with the term *Bernoullian* to indicate the chain-end model. As it is the last inserted monomer unit that controls the insertion of the following olefin, it would be better to use the term “*symmetric*” Markovian model.

For achiral metallocene-based catalysts (C_{2v} and achiral C_s metallocenes in Chart 2) the chain-end control is present as the only stereocontrol mechanism. It derives from the presence of an asymmetric carbon atom on the last inserted monomer. The chirality (R or S) of this atom is related to the enantiotopic face of the olefin where the insertion took place (Scheme 34). In the ^{13}C NMR spectrum of the polymer we lose this kind of information, as two successive insertions of the *re* olefin face and two successive insertions of the *si* face produce the same *m* diad (see section II.G). As a consequence, we can observe only the relative chirality between consecutive inserted monomer units (S,S or R,R as *m* diads and S,R or R,S as *r* diads) disregarding the absolute configuration of tertiary atoms. We prefer to use the *re* and *si* nomenclature indicating the stereochemistry of the methines in the polymer chain (Scheme 35), bearing in mind that the insertion of the *re* propene enantioface will produce an S configuration on the methine.

The approaching monomer experiences the chirality of the last inserted monomer and therefore four options are possible:

	last inserted monomer	approaching monomer	resulting diad
1	<i>re</i>	<i>si</i>	<i>r</i>
2	<i>si</i>	<i>re</i>	<i>r</i>
3	<i>re</i>	<i>re</i>	<i>m</i>
4	<i>si</i>	<i>si</i>	<i>m</i>

As the catalyst does not possess any chirality (and neglecting any penultimate effect), the two first alternatives are “mirror images” (see Scheme 35) and they must be equiprobable.

The same is true for *re-re* and *si-si* options. The statistical modeling of experimental pentad distribution can be performed by considering a first-order Markovian model. The insertion probability for a *si*

Table 12. Pentad Fractions for the Symmetric First-Order Markov Model

pentad	probability expressions	pentad	probability expressions
<i>mmmm</i>	$[1 - p(r)]^4$	<i>rmrm</i>	$2[p(r)]^2[1 - p(r)]^2$
<i>mmmr</i>	$2[p(r)][1 - p(r)]^3$	<i>rrrr</i>	$[p(r)]^4$
<i>rmmr</i>	$[p(r)]^2[1 - p(r)]^2$	<i>rrrm</i>	$2[p(r)]^3[1 - p(r)]$
<i>mmrr</i>	$2[p(r)]^2[1 - p(r)]^2$	<i>mrrm</i>	$[p(r)]^2[1 - p(r)]^2$
<i>rmrr</i>	$2[p(r)]^3[1 - p(r)]$		

monomer after a *re* inserted monomer is indicated as $p(\text{si}|re)$. The other probabilities will be $p(re|si)$, and $p(\text{si}|si)$, $p(re|re)$. Neglecting the presence of chain termination (high molecular weight polymers), we have the following relations between the probabilities:

$$p(re|si) + p(\text{si}|si) = 1 \quad p(\text{si}|re) + p(re|re) = 1$$

The aforementioned equiprobabilities between some of the possible insertions can be expressed using the symmetric first-order Markovian model where the following relations are applied:

$$p(re|si) = p(\text{si}|re) = p(r) \quad p(\text{si}|si) = p(re|re) = p(m)$$

where $p(r)$ is the probability of formation of *r* diads and $p(m)$ is the probability of formation of *m* diads. Only one probability is independent ($p(r)$, for example) while the other is given by

$$p(m) = 1 - p(r)$$

As no effect of the penultimate inserted unit is taken into account, the formation of *r* or *m* diads is a random process that follows the Bernoullian statistic. Therefore, the symmetric first-order Markovian model becomes Bernoullian when diad formation is considered. This fact explains why this model is usually called *Bernoullian*.

The resulting probability expressions for pentad distribution are collected in Table 12.

This model was employed by Ewen²² to describe the low-temperature polymerization with $\text{Cp}_2\text{TiPh}_2/\text{MAO}$ catalyst.

2. Enantiomorphic Site Control

Catalysts based on metallocenes belonging to the C_2 , prochiral C_s , and C_1 classes (see Chart 2) are, in principle, able to direct 1-olefin insertion.

Isotactic Control. Olefin insertion in C_2 -symmetric metallocenes occurs preferentially with the same face at both sites leading to an isotactic polymer. The isotacticity of the polymer chain depends on the metallocene structure. The chain-end control can be active, but for highly isotactic polymers it is difficult to check its presence as the pentads representing two consecutive wrong insertions have too low an intensity for a correct evaluation.

When the chain-end control can be neglected, we can define the probability of insertion of the preferred olefin face using one probability parameter, b . As in the ^{13}C NMR spectrum, we can observe only the stereochemical relation between contiguous units in terms of *m* and *r* diads, we can arbitrarily express b

Table 13. Pentad Fractions for an Isotactic Bernoullian Model

pentad	probability expressions	pentad	probability expressions
<i>mmmm</i>	$b^5 + (1 - b)^5$	<i>rmrm</i>	$2[b^3(1 - b)^2 + b^2(1 - b)^3]$
<i>mmmr</i>	$2[b^4(1 - b) + b(1 - b)^4]$	<i>rrrr</i>	$b^3(1 - b)^2 + b^2(1 - b)^3$
<i>rmrr</i>	$b^3(1 - b)^2 + b^2(1 - b)^3$	<i>rrrm</i>	$2[b^3(1 - b)^2 + b^2(1 - b)^3]$
<i>mmrr</i>	$2[b^4(1 - b) + b(1 - b)^4]$	<i>mrrm</i>	$b^4(1 - b) + b(1 - b)^4$
<i>mrrr</i>	$2[b^3(1 - b)^2 + b^2(1 - b)^3]$		

as the probability of an olefin insertion with the *re* enantioface (the insertion probability of a *si* olefin face will be $1 - b$).

The resulting isotactic Bernoullian model (this is a true Bernoullian model, as the chain end effect is neglected) gives the calculated pentad distribution reported in Table 13. Each pentad contains two symmetric contributions; for example, the *mmmm* pentad derives from the two possibilities

$$\begin{aligned}
 \text{all insertions are correct} & \quad \begin{array}{c} re-re-re-re-re \\ \text{all insertions are correct} \end{array} \\
 \text{all insertions are wrong} & \quad \begin{array}{c} si-si-si-si-si \\ \text{all insertions are wrong} \end{array} \\
 mmmm = & \quad b^5 + (1 - b)^5
 \end{aligned}$$

The pentad fraction distribution is symmetric with respect to $b = 0.5$, as we obtain the same values using $b = p$ or $b = 1 - p$ ($0 \leq p \leq 1$); therefore, we could add the restriction $0.5 \leq b \leq 1$.

It would be easy to show that this model satisfies the ratio $[mmmr]:[mmrr]:[mrrm] = 2:2:1$ as experimentally found for isotactic polymers.

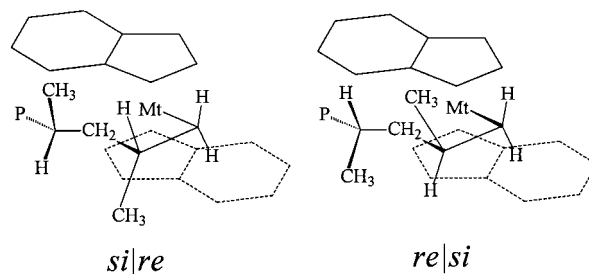
This model can be applied to evaluate the pentad distribution from ^{13}C NMR spectra of metallocene-based isotactic polypropenes in which overlapping with peaks from end group or regioirregular units (2,1 and 3,1) occurs.²³² In this case only the peaks of *mmmm*, *mmmr*, *mmrr*, and *mrrm* pentads can be obtained from direct spectrum integration. Furthermore, the *mmmr* peak overlaps with the *mmmm* base, and the *mmrr* has to be correct by subtracting the contribution from the 2,1-*erythro* unit. The total pentad distribution is calculated under the hypothesis that the polymerization statistic follows a pure enantiomorphic site control, using the expressions reported in Table 13 as follows:

$$\begin{aligned}
 mmmm + mmmr &= b^5 + (1 - b)^5 + 2[b^4(1 - b) + b(1 - b)^4] \\
 mmrr &= 2[b^4(1 - b) + b(1 - b)^4] \\
 mrrm &= b^4(1 - b) + b(1 - b)^4
 \end{aligned}$$

The best fit between experimental and calculated areas is searched through a least-squares method, minimizing the function:

$$f(b) = \sum_i (A_i^{\text{exp}} - kA_i^{\text{calc}})^2$$

where the sum is extended over the three groups of pentads, A_i^{exp} are the experimental areas, A_i^{calc} are

Scheme 36

the calculated ones, and k is a normalization constant calculated at each minimization step as:

$$k(b) = \frac{A_{mmmm+mmmr}^{\text{exp}} + A_{mmrr}^{\text{exp}} + A_{mrrm}^{\text{exp}}}{A_{mmmm+mmmr}^{\text{calc}} + A_{mmrr}^{\text{calc}} + A_{mrrm}^{\text{calc}}}$$

Enantiomorphic Site with Chain-End Control. In the case of less stereoselective C_2 -symmetric metallocene catalysts, the magnitude of chain-end control can be comparable to that of site control. In this case, obviously, the former has to be added to the model using Markovian statistics. The probability parameters are the same found for pure chain-end control: $p(si|re)$, i.e., the probability of insertion of a *si* monomer enantioface after a monomer inserted with the *re* face, $p(re|si)$, $p(si|si)$, and $p(re|re)$. In this case, the metallocene chirality prevents the equiprobability of the *si* olefin insertion after a *re* inserted monomer (see structure on the left in Scheme 36) and *re* olefin insertion after a *si* inserted monomer (see structure on the right in Scheme 36).

Furthermore, one of the two enantiofaces of the monomer is preferred for insertion (right picture in Scheme 36) with respect to the other. Only two probability parameters are independent as the other two are linked by the following relations:

$$p(si|re) + p(re|re) = 1 \quad p(re|si) + p(si|si) = 1$$

The parameter $p(re|re)$ represents the isospecific propagation at this site (two successive *re* insertions), while $p(re|si)$ is the probability of "error correction" after a stereoerror. This model is called the *asymmetric* Markovian model and the mathematical expressions for pentad distribution are collected in Table 14.

Syndiotactic Control. In prochiral C_s -symmetric metallocenes (Chart 2), one site favors the insertion of an olefin enantioface and the other preferably inserts the opposite one and a syndiotactic polymer is obtained.

If we neglect the effect of the chain end, we can use a statistical model analogous to that shown for isotactic polymers with a different definition of the probability parameter.

In this case the probability of insertion of a monomer with a given enantioface at site 1 is equal to the probability of insertion of a monomer with the opposite enantioface at site 2. This probability is indicated with the parameter a . The resulting expressions for pentad distribution for the syndiotactic Bernoullian model are reported in Table 15.

Table 14. Pentad Fractions with the Asymmetric Markovian Model

pentad	probability expressions
<i>mmmm</i>	$\{p(re si)p(re re)^4 + [1 - p(re si)][1 - p(re si)]^4\}/[1 - p(re re) + p(re si)]$
<i>mmmr</i>	$2\{p(re re)^3p(re si)[1 - p(re re)] + [1 - p(re si)]^3[1 - p(re re)]p(re si)\}/[1 - p(re re) + p(re si)]$
<i>rmrr</i>	$\{p(re si)p(re re)^2[1 - p(re re)]^2 + [1 - p(re si)]^2[1 - p(re re)]p(re si)^2\}/[1 - p(re re) + p(re si)]$
<i>mmrr</i>	$2\{p(re si)^2p(re re)^2[1 - p(re re)] + [1 - p(re si)]^2[1 - p(re re)]^2p(re si)\}/[1 - p(re re) + p(re si)]$
<i>mmrm</i> + <i>rmrr</i>	$2\{[1 - p(re si)]p(re re)^2[1 - p(re re)]p(re si) + [1 - p(re si)]^2p(re re)[1 - p(re re)]p(re si) + p(re re)p(re si)^2[1 - p(re re)]^2 + [1 - p(re si)][1 - p(re re)]^2p(re si)^2\}/[1 - p(re re) + p(re si)]$
<i>rmrm</i>	$2\{p(re re)[1 - p(re si)][1 - p(re re)]p(re si)^2 + p(re re)[1 - p(re si)][1 - p(re re)]^2p(re si)\}/[1 - p(re re) + p(re si)]$
<i>rrrr</i>	$\{p(re si)^3[1 - p(re re)]^2 + p(re si)^2[1 - p(re re)]^3\}/[1 - p(re re) + p(re si)]$
<i>rrrm</i>	$2\{p(re si)^2p(re re)[1 - p(re re)]^2 + [1 - p(re si)]^2[1 - p(re re)]p(re si)\}/[1 - p(re re) + p(re si)]$
<i>mrrm</i>	$\{p(re si)^2p(re re)^2[1 - p(re re)] + [1 - p(re si)]^2[1 - p(re re)]^2p(re si)\}/[1 - p(re re) + p(re si)]$

Table 15. Calculated Pentad Distribution with the Syndiotactic Bernoullian Model

pentad	probability expressions	pentad	probability expressions
<i>mmmm</i>	$a^3(1 - a)^2 + a^2(1 - a)^3$	<i>rmrr</i>	$2a^3(1 - a)^2 + 2a^2(1 - a)^3$
<i>mmmr</i>	$2a^2(1 - a)^3 + 2a^3(1 - a)^2$	<i>rmrm</i>	$2a^3(1 - a)^2 + 2a^2(1 - a)^3$
<i>rmrr</i>	$a^4(1 - a) + a(1 - a)^4$	<i>rrrr</i>	$a^5 + (1 - a)^5$
<i>mmrr</i>	$2a^4(1 - a) + 2a(1 - a)^4$	<i>rrrm</i>	$2a(1 - a)^4 + 2a^4(1 - a)$
<i>mmrm</i>	$2a^3(1 - a)^2 + 2a^2(1 - a)^3$	<i>mrrm</i>	$a^2(1 - a)^3 + a^3(1 - a)^2$

The pentad fraction distribution is symmetric with respect to $a = 0.5$, as we obtain the same values using $a = p$ or $a = 1 - p$ ($0 \leq p \leq 1$). It would be easy to show that this model satisfies the ratio $[mmmr]:[mmrr]:[rrrm] = 1:2:2$, as experimentally observed for syndiotactic polymers obtained with "sitecontrolled" catalysts.

The presence of isolated *m* diads in ^{13}C NMR spectra (*rmrm* pentad) of these polymers is attributable to an isomerization of the site due to a "skipped" monomer insertion during chain growth (see section IV.B).

This fact can be included in the model considering the probability of site isomerization p_{bs} , in the expressions for pentad distribution. The final result is shown in Table 16.

Elastomeric Polypropene. To model the propene polymerization to elastomeric polypropene catalyzed by bis(2-aryllindenyl)zirconocenes³⁷⁰ or C_1 -symmetric $\text{Me}_2\text{X}(\text{Cp})(1\text{-Ind})$ metallocenes,³⁹³ the consecutive two-state model originally described by Coleman and Fox^{376,377} was used.

Due to the complexity of the model and the limited number of experimental points (only the nine pentad areas) used in the fitting procedure, it was not possible to unambiguously determine the overall propagation mechanism that leads to the microstructure of these polymers.

Information on the relative abundance of isotactic and atactic blocks can be obtained using a statistical modeling of pentad distributions based on a competitive two-site model^{378,379} based on a mixing of a chain-end-controlled site (to model the atactic blocks) and an enantiomorphic site (for isotactic blocks).³⁶⁵

C. Use of Matrix Multiplication Methods in Statistical Models

All the models described above imply the obtainment of a series of equations to express the pentad fractions as a function of the probability parameters. This could be a problem if models with a relatively high number of independent parameters are used or

if we need to fit longer stereosequences. To overcome these problems, an interesting method was reported by Busico and Vacatello.⁴⁶² This is based on the Markov chain matrix mathematics, and we report it here as an interesting and powerful system to easily solve complicated problems.

First, we have to found the "stochastic" matrix, that is, the matrix containing all the probability parameters of our model. The matrix for the syndiospecific polymerization with site isomerization is chosen as an example:

$$\mathbf{A} = \begin{array}{c} \begin{array}{cccc} & re(1) & si(1) & re(2) & si(2) \\ \begin{array}{l} re(1) \\ si(1) \\ re(2) \\ si(2) \end{array} & \left| \begin{array}{cccc} ap_{bs} & (1-a)p_{bs} & (1-a)(1-p_{bs}) & a(1-p_{bs}) \\ ap_{bs} & (1-a)p_{bs} & (1-a)(1-p_{bs}) & a(1-p_{bs}) \\ a(1-p_{bs}) & (1-a)(1-p_{bs}) & (1-a)p_{bs} & ap_{bs} \\ a(1-p_{bs}) & (1-a)(1-p_{bs}) & (1-a)p_{bs} & ap_{bs} \end{array} \right. \end{array} \end{array}$$

The rows are indexed to the last-inserted monomer enantioface (*re* or *si*) and to the site where insertion took place (1 or 2). The columns are indexed to the enantioface of the inserting unit and to the site. The probability parameters have the same meaning as in the aforementioned syndiotactic model.

When the preferred enantioface for site 1 is *re*, then for site 2 it is *si*, and vice versa. If $p_{bs} = 0$, no site isomerization is present and the model collapses to the normal syndiospecific one.

The sum of the elements in a row must be equal to one, i.e., monomer insertion has to occur!

To evaluate the sequence (pentad) distribution we obtain the two matrixes \mathbf{A}_m and \mathbf{A}_r defined as

$$\mathbf{A}_m = \begin{array}{c} \begin{array}{cccc} & re(1) & si(1) & re(2) & si(2) \\ \begin{array}{l} re(1) \\ si(1) \\ re(2) \\ si(2) \end{array} & \left| \begin{array}{cccc} ap_{bs} & 0 & (1-a)(1-p_{bs}) & 0 \\ 0 & (1-a)p_{bs} & 0 & a(1-p_{bs}) \\ a(1-p_{bs}) & 0 & (1-a)p_{bs} & 0 \\ 0 & (1-a)(1-p_{bs}) & 0 & ap_{bs} \end{array} \right. \end{array} \end{array}$$

$$\mathbf{A}_r = \begin{array}{c} \begin{array}{cccc} & re(1) & si(1) & re(2) & si(2) \\ \begin{array}{l} re(1) \\ si(1) \\ re(2) \\ si(2) \end{array} & \left| \begin{array}{cccc} 0 & (1-a)p_{bs} & 0 & a(1-p_{bs}) \\ ap_{bs} & 0 & (1-a)(1-p_{bs}) & 0 \\ 0 & (1-a)(1-p_{bs}) & 0 & ap_{bs} \\ a(1-p_{bs}) & 0 & (1-a)p_{bs} & 0 \end{array} \right. \end{array} \end{array}$$

They represent the probability of having, respectively, *m* or *r* diads along the polymer chain.

The probability of a given stereosequence $d_1d_2d_3\dots d_n$ ($d_i = m$ for *meso* diads and $d_i = r$ for *racemic* diads)

Table 16. Pentad Fractions for a Syndiospecific Bernoullian Model in Presence of Site Isomerization^a

pentad	E_0	E_1	E_2	E_3	E_4	total ^b
<i>mmmm</i>	p_3	$4p_3$	$3p_4 + 3p_3$	$2p_4 + 2p_3$	p_5	$E_0(1 - p_{bs})^4 + E_1(1 - p_{bs})^3 p_{bs} +$
<i>mmmr</i>	$2p_3$	$2(2p_4 + 2p_3)$	$2(p_4 + 5p_3)$	$2(p_5 + p_4 + 2p_3)$	$2p_4$	$E_2(1 - p_{bs})^2 p_{bs}^2 +$
<i>rmmr</i>	p_4	$4p_3$	$p_5 + 2p_4 + 3p_3$	$2(p_4 + p_3)$	p_3	$E_3(1 - p_{bs}) p_{bs}^3 + E_4 p_{bs}^4$
<i>mmrr</i>	$2p_4$	$2(p_4 + 3p_3)$	$2(p_5 + p_4 + 4p_3)$	$2(p_4 + 3p_3)$	$2p_4$	
<i>xmrxc</i>	$4p_3$	$2(p_5 + 3p_4 + 4p_3)$	$2(4p_4 + 8p_3)$	$2(p_5 + 3p_4 + 4p_3)$	$4p_3$	
<i>rmrm</i>	$2p_3$	$2(p_4 + 3p_3)$	$2(p_5 + 3p_4 + 2p_3)$	$2(p_4 + 3p_3)$	$2p_3$	
<i>rrrr</i>	p_5	$2(p_4 + p_3)$	$3p_4 + 3p_3$	$4p_3$	p_3	
<i>rrrm</i>	$2p_4$	$2(p_5 + p_4 + 2p_3)$	$2(p_4 + 5p_3)$	$2(2p_4 + 2p_3)$	$2p_3$	
<i>mrrm</i>	p_3	$2(p_4 + p_3)$	$p_5 + 2p_4 + 3p_3$	$4p_3$	p_4	

^a $p_5 = a^5 + (1 - a)^5$, $p_4 = a^4(1 - a) + a(1 - a)^4$, and $p_3 = a^3(1 - a)^2 + a^2(1 - a)^3$. ^b p_{bs} is the probability of site isomerization (see text); only the first expression is reported as the others are identical. ^c $xmrxc = mrrm + rmrr$.

is given by the matricial multiplication

$$\mathbf{f}(d_1 d_2 d_3 \dots d_n) = \mathbf{f}_0 \mathbf{T} \mathbf{A}_1 \mathbf{A}_2 \mathbf{A}_3 \dots \mathbf{A}_n \mathbf{J}$$

where the matrix $\mathbf{A}_i = \mathbf{A}_m$ when $d_i = m$ and $\mathbf{A}_i = \mathbf{A}_r$ when $d_i = r$, $\mathbf{J} = |\mathbf{1111}|^T$, and $\mathbf{f}_0 \mathbf{T}$ is a row vector and represents the vector of “stationary probabilities” of the four states and is evaluated by numerically solving the system of equations

$$\mathbf{f}_0 \mathbf{T} \mathbf{A} = \mathbf{f}_0 \mathbf{T}$$

Or from the relation

$$\lim_{N \rightarrow \infty} \mathbf{A}^N = \mathbf{F}$$

where each row of the \mathbf{F} matrix is the vector $\mathbf{f}_0 \mathbf{T}$ (in some models, the elements of $\mathbf{f}_0 \mathbf{T}$ can be obtained also as a function of the probability parameters).

The probability of the *rrmmrrr* heptad can be obtained easily as

$$\mathbf{f}(rrmmrrr) = 2\mathbf{f}_0 \mathbf{T} \mathbf{A}_r \mathbf{A}_r \mathbf{A}_m \mathbf{A}_m \mathbf{A}_r \mathbf{A}_r \mathbf{A}_r \mathbf{J}$$

VII. Regiocontrol

One of the features of most isospecific metallocene catalysts is their generally lower regioselectivity compared to heterogeneous Ziegler–Natta catalysts: indeed, despite the fact that primary propene insertion is clearly favored by electronic factors (see section III.E), isolated secondary propene units are often detectable in *i*-PP samples and their presence is the signature of a metallocene catalyst. These regiodefects have a strong effect in the lowering crystallinity and melting point of *i*-PP. At the same time, there is also a close correlation between catalyst regioselectivity on one side and catalyst activity and polymer molecular weight on the other, due to the lower monomer insertion rate at a secondary growing chain end and the competing β -H transfer to the monomer after a secondary insertion. Because of these two aspects, understanding the factors controlling the regioselectivity of a metallocene catalyst is important for catalyst design. The characterization of the different regiodefects by ¹³C NMR and the molecular modeling studies performed on the subject are discussed in section VII.A. The relative amounts of these regiodefects are highly dependent on the metallocene ligand structure and the polymerization conditions employed (polymerization temperature

and monomer concentration). Unfortunately, possibly due to the often low concentration of regioerrors and the requirement of a high-field NMR instrument and long acquisition times, few detailed studies have been carried out on the regioselectivity of metallocene catalysts and the dependence of the type and amounts of regioerrors on ligand structure and polymerization conditions. The available data are discussed in sections VII.C–E. The lower reactivity of a secondary growing chain with respect to a primary growing chain has been confirmed in three ways: by studying the activating effect of hydrogen (see section IX), by copolymerization with ethene,^{126–129} and by end group analysis.^{130,131} The latter two aspects are discussed in section VII.B. In section VII.F we discuss the proposed mechanisms of isomerization of a secondary growing chain into a 3,1 unit.

A. Stereochemistry of Regioirregular Insertion

1. ¹³C NMR Analysis

As briefly seen in section II.F, secondary propene insertions, currently referred to as 2,1 insertions, occur in *i*-PP from isospecific metallocene catalysts with high but opposite (with respect to primary insertions) enantioface selectivity (Scheme 14).

¹³C NMR analysis has shown that these 2,1 units are always isolated between two isotactic blocks and, depending on the enantioselectivity of the following primary insertion on the secondary growing-chain end, give rise to 2,1 *erythro* (*e*) and 2,1 *threo* (*t*) sequences and to the formation of tetramethylene sequences (3,1 units), arising from the unimolecular isomerization of the secondary unit (Scheme 37). The stereochemical environment of the secondary 2,1 units and of the 3,1 unit have been assigned by ¹³C NMR analysis of *i*-PP made with *rac*-C₂H₄(1-Ind)₂-ZrCl₂ and *rac*-C₂H₄(H₄-1-Ind)₂ZrCl₂.^{117,126,198,199,463} A previous misassignment of the structure of the 2,1 *threo* unit^{117,198} has been corrected by Mizuno.^{199,304} A sequence of two secondary insertions has never been detected. Thus, in terms of regiochemistry, three propagation reactions occur, i.e., primary on primary chain end, secondary on primary chain end, and primary on secondary chain end. Because of the absence of sequences of two secondary insertions, the last two values must be equal, that is the probability of primary insertions on primary chain ends (p_p) obeys the relationship $p_p = 1 - 2p_s$, where p_s is the number of primary insertions on secondary chain ends, estimated from the intensity of the ¹³C NMR

Scheme 37

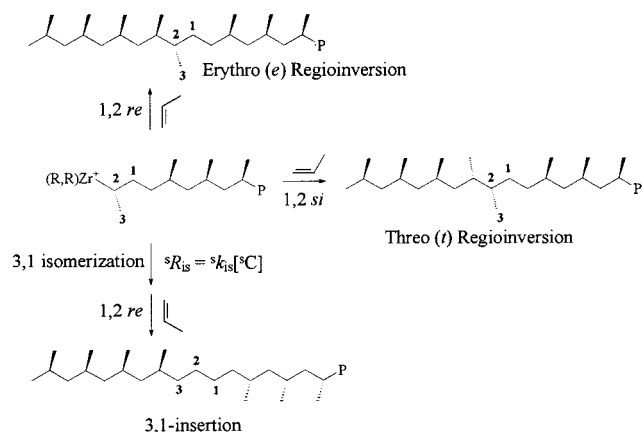
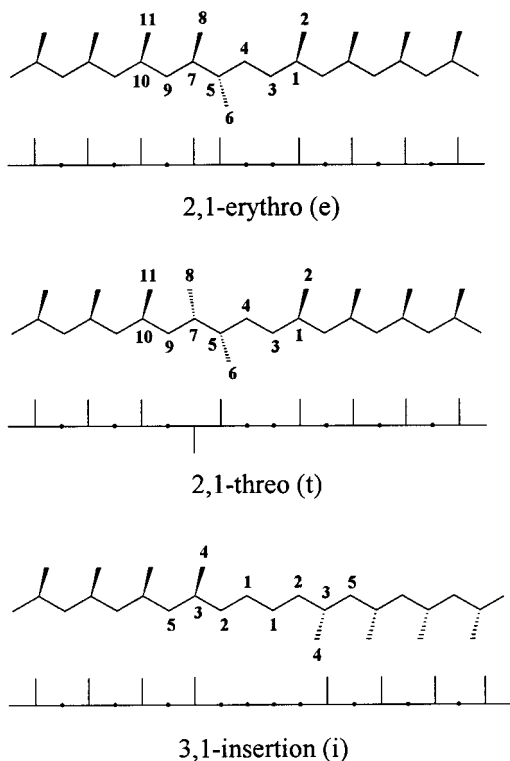


Chart 20. Chain Microstructure Defects Generated by Isolated Secondary (2,1) Insertion: erythro (meso), threo (racemic) Secondary Units and 3,1 Unit^a



^a The saturated end group due to chain start lays on the right of the chain segment, the unsaturated one generated by chain release on the left.

methylene peaks t_9 and e_9 (see carbon labeling in Chart 20).

The ^{13}C NMR spectra of three *i*-PP containing regioirregularities of the three types are shown in Figure 39, while the relevant chain segments are reported in Chart 20. *rac*- $\text{C}_2\text{H}_4(\text{H}_4\text{-1-Ind})_2\text{ZrCl}_2/\text{MAO}$ (Figure 39 (top)) produces *i*-PP with almost only 3,1 units (~1%), while *rac*- $\text{C}_2\text{H}_4(4,7\text{-Me}_2\text{-1-Ind})_2\text{ZrCl}_2$ (Figure 39 (middle)) produces a lower molecular weight *i*-PP with a higher amount (~2%) of both *e* and *t* 2,1 units. The Targor catalyst *rac*- $\text{Me}_2\text{Si}(2\text{-Me-4-Ph-1-Ind})_2\text{ZrCl}_2$ (Figure 39 (bottom)) represents a limit situation in which secondary insertions (~1%, only *e* type, indicating a highly enantioselective

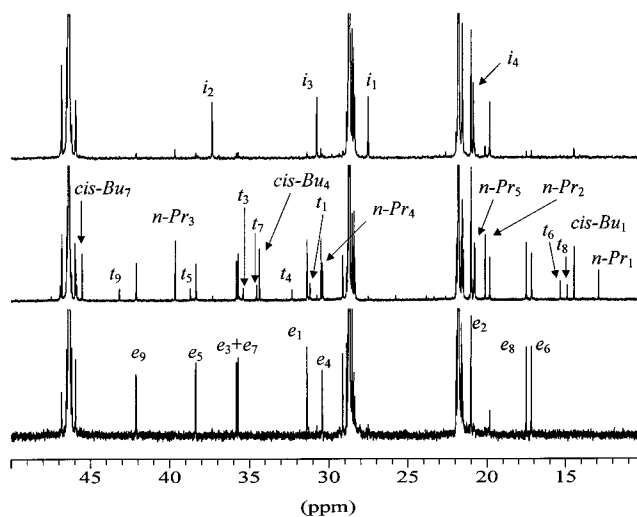


Figure 39. ^{13}C NMR spectra (100 MHz, $\text{C}_2\text{D}_2\text{Cl}_4$, 120 °C, ref *mmmm* at 21.8 ppm) of three *i*-PP containing regioirregularities: from *rac*- $\text{C}_2\text{H}_4(\text{H}_4\text{-1-Ind})_2\text{ZrCl}_2/\text{MAO}$ (top); from *rac*- $\text{C}_2\text{H}_4(4,7\text{-Me}_2\text{-1-Ind})_2\text{ZrCl}_2$ (middle); from *rac*- $\text{Me}_2\text{Si}(2\text{-Me-4-Ph-1-Ind})_2\text{ZrCl}_2$ (bottom). For carbon numbering, see Chart 20 and Table 2. For polymerization conditions, see Table 17. *cis*-Bu = *cis*-2-butenyl, *n*-Pr = *n*-propyl.

primary insertion following the regioerror) are far more frequent (in liquid propene polymerization) than primary *stere*errors. The regioselectivity of propene insertion into a Zr–H bond (initiation) is discussed in section IX.

2. Molecular Modeling

Before discussing the correlation between the regioselectivity of a given metallocene and its symmetry, we start to discuss the enantioselectivity of regioirregular insertions in isospecific polymerization. As seen above, ^{13}C NMR analysis of the stereochemical environment of a secondary unit shows that the regioirregular (secondary) propene insertion is highly enantioselective.

The modeling tools used to investigate the enantioselectivity of primary insertions can be used also to investigate the enantioselectivity of secondary insertions. Nonetheless, this kind of analysis was somewhat overlooked in the first studies on the enantioselectivity of primary propene insertions. Corradini,²⁶³ Rappé,¹⁴⁷ and Morokuma¹⁵⁵ and their co-workers could have sentenced (but they did not) that for a C_2 -symmetric catalyst secondary insertions are enantioselective. However, the authors focused most on the enantioselectivity of primary insertions²⁶³ or on the steric effects favoring primary over secondary insertion^{147,155} and did not discuss the enantioselectivity of secondary insertion.

The first detailed analysis on the enantioselectivity of secondary propene insertion on isospecific C_2 -symmetric catalysts was performed by Corradini and co-workers.²⁰⁰ The models reported in Figure 40 represent energy minima corresponding to coordination of propene suitable for secondary insertion into the model complex based on the (*R,R*)- $\text{Me}_2\text{Si}(1\text{-Ind})_2$ ligand. Structure A, with a *re*-coordinated propene, is higher by nearly 5 kcal/mol with respect to structure B, with a *si*-coordinated propene. The

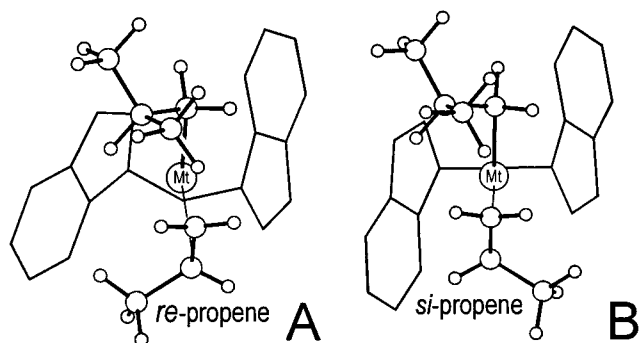


Figure 40. Models for secondary propene insertion into a primary polypropylene growing chain, when the aromatic ligand is $\text{Me}_2\text{Si}(1\text{-Ind})_2$. A and B correspond to *re* and *si* propene coordinations, respectively. Model B, with a *si* coordinated propene, is the only one suitable for monomer insertion.²⁰⁰

higher energy of the model with the *re*-coordinated propene is due to the repulsive interactions of the methyl group of propene with the six-membered rings of one of the indenyl ligands. Similar conclusions have been obtained with model complexes containing the $(R,R)\text{-C}_2\text{H}_4(\text{H}_4\text{-1-Ind})_2$ and $(R,R)\text{-Me}_2\text{C}(1\text{-Ind})_2$ ligand.^{91,200}

It is worth noting that the enantioselectivity in the secondary insertion is due to direct interaction of the monomer with the ligand, while the growing chain plays no role, whereas the enantioselectivity in the primary insertion is due to the chiral orientation of the growing chain (forced by the ligand) and that direct interaction of the monomer with the ligand is, in general, negligible. Moreover, for a (R,R) coordination of the aromatic ligand, the *re* propene enantioface is favored for primary insertion, on models of the type described above. In short, the C_2 -symmetric isospecific models above-mentioned are substantially enantioselective for the lower energy (and experimentally observed) primary monomer insertion as well as for the higher energy (experimentally detected) secondary monomer insertion. Anyhow, it is worth noting that the *enantioselectivity of the isospecific model site is in favor of opposite monomer prochiral faces, for primary and secondary insertions.*²⁰⁰ This result is in perfect agreement with the observed microstructure of polypropylene chains obtained by isospecific catalytic systems including the aforementioned ligands, as discussed in section VII.1, and it is consistent with the *in nuce* results of Corradini,²⁶³ Rappé,¹⁴⁷ and Morokuma¹⁵⁵ mentioned above.

Furthermore, for models of catalyst based on the $(R,R)\text{-C}_2\text{H}_4(1\text{-Ind})_2$ and $(R,R)\text{-C}_2\text{H}_4(\text{H}_4\text{-1-Ind})_2$ ligands, a detailed molecular mechanics analysis has been conducted also for the case of primary or secondary propene insertions on secondary polypropylene chains (for which the last propene insertion has been secondary) by Corradini, Guerra, and co-workers²⁰⁰ and by Yu and Chien.²⁷⁶ According to this analysis, the enantioselectivities observed after an occasional secondary monomer insertion are easily accounted for in the framework of the mechanism of the "chiral orientation of the growing chain". In fact, substituting the usual primary growing chain with a secondary

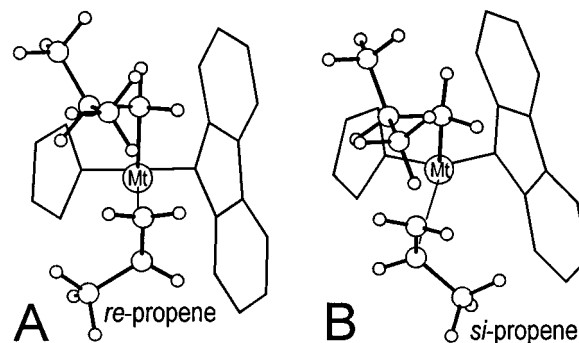
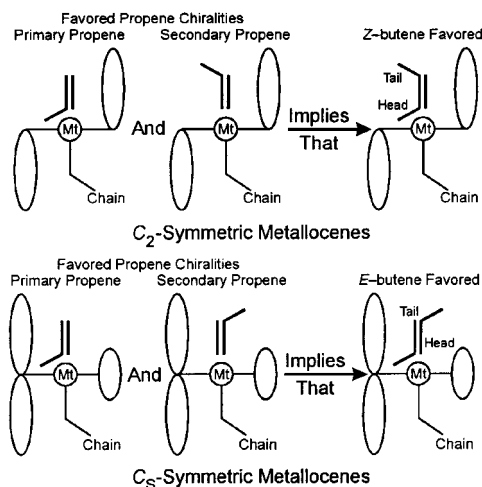


Figure 41. Models for the secondary propene insertion into a primary polypropylene growing chain, when the aromatic ligand is $\text{Me}_2\text{C}(\text{Cp})(9\text{-Flu})$. A and B correspond to *re* and *si* propene coordinations, respectively. Model A, with a *re* coordinated propene, is the only one suitable for monomer insertion.⁹¹

growing chain reduces the preference for one particular chiral orientation of the growing chain, since the first C atom of a secondary chain bears two C atoms (the C_β of the chain and the CH_3 of the secondary inserted monomer) that can repulsively interact with the ligand's framework. Moreover, a secondary growing chain corresponds to a reduced bulkiness of the substituents of the second carbon atom of the chain (which is secondary carbon for the secondary chain, but is tertiary carbon for the primary chain). Wherefore, the energy differences between models with the different propene enantiofaces is reduced, leading to a less pronounced enantioselectivity.^{200,276} These results are able to rationalize the probability distributions of stereochemical configurations of regioirregular units in isotactic polymer samples prepared in the presence of the corresponding catalytic systems.^{198,199} Finally, Yu and Chien also found that propene insertion on the secondary chain is of considerably higher energy, roughly 10 kcal/mol, relative to propene insertion on a primary chain, supporting the broadly accepted idea that after secondary propene insertion the polymerization is essentially stalled.

The same modeling used to investigate the enantioselectivity of secondary insertion with C_2 -symmetric metallocenes was applied to the enantioselectivity of secondary insertion with C_5 -symmetric metallocenes.^{91,277} Yu and Chien found that the same propene enantioface is favored for both primary and secondary propene insertions, on models based on the $\text{Me}_2\text{C}(\text{Cp})(9\text{-Flu})$ ligand, by roughly 2–3 kcal/mol.²⁷⁷ Corradini, Guerra and co-workers rationalized these findings using the models reported in Figure 41, which represent energy minima corresponding to coordination of propene suitable for secondary insertion into the model complex based on the $\text{Me}_2\text{C}(\text{Cp})(9\text{-Flu})$ ligand, with *R* chirality at the metal atom.⁹¹ As for the models of C_2 -symmetric metallocenes, the higher energy, about 5 kcal/mol,⁹¹ of the model with the unfavored secondary propene coordination (*si* in this case) is due to the repulsive interactions of the methyl group of propene with the bulkier moiety (the fluorenyl group in this case) of the ligand. In summary, also models for syndiospecific C_5 -symmetric metallocenes are substantially enantioselective for the lower energy primary monomer insertion as well

Scheme 38¹⁴⁵

as for the higher energy secondary monomer insertion. Anyhow, it is worth noting that differently from the isospecific C_2 -symmetric models, the *enantioselectivity of the syndiospecific model site is in favor of the same monomer prochiral face, for primary and secondary insertions*.^{91,277}

Syndiospecific catalytic systems based on C_s -symmetric metallocenes are more regioselective than the C_2 -symmetric metallocenes of class II. As a consequence, the enantioselectivity in regioirregular insertions have been experimentally investigated for propene-based copolymers only.^{464,465} In particular, ^{13}C NMR characterization of ethene-1- ^{13}C /propene copolymers suggests that the very low amount (0.03–0.07%) of regioirregular 2,1 units are substantially stereoirregular.⁴⁶⁴ On the contrary, NMR characterization of propene/styrene/ethene terpolymers has shown that insertions of propene (primary) and of styrene (secondary) occur with the same enantioface.⁴⁶⁵

The main conclusion of the previously reported experimental and theoretical studies is that *opposite enantiofaces* are favored for primary and secondary propene insertion on C_2 -symmetric metallocenes, whereas *the same enantioface* is favored for primary and secondary insertion on C_s -symmetric metallocenes. A further proof of this mechanistic picture has been obtained by Corradini and co-workers through a combination of primary and secondary propene insertions into one single insertion step, by using 2-butene as monomer.¹⁴⁵ They argued that, within the above framework, insertion of Z-butene should be favored with C_2 -symmetric metallocenes, whereas insertion of E-butene should be favored with C_s -symmetric metallocenes, as sketched in Scheme 38, provided that *the same steric interactions which rule the enantioselectivity of primary and secondary propene insertions hold for 2-butene*.

The QM/MM transition states for Z- and E-butene insertion into the Zr–C(*n*-propyl) σ -bond of the C_2 - and C_s -symmetric $\text{Me}_2\text{Si}(\text{1-Ind})_2$ and $\text{Me}_2\text{Si}(\text{Cp})(9\text{-Flu})$ metallocenes are reported in Figure 42, parts A–B, and C–D, respectively. According to the mechanism of the chiral orientation of the growing chain, the *n*-propyl group used to simulate a polyethylenic growing chain assumes a conformation which mini-

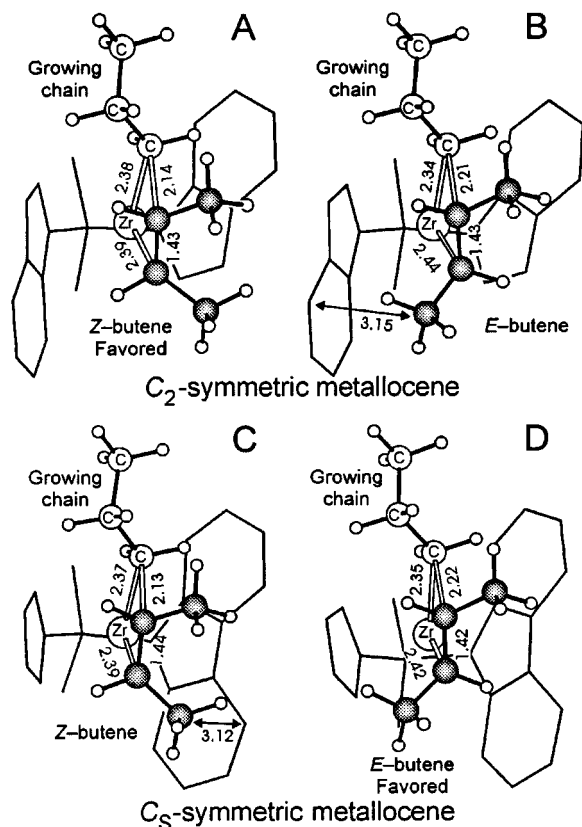


Figure 42. QM/MM transition states of 2-butene insertion reaction into the Zr–C σ -bond with the C_2 - and C_s -symmetric metallocenes. Parts A and B correspond to Z- and E-butene insertion with the C_2 -symmetric $\text{Me}_2\text{Si}(\text{1-Ind})_2\text{Zr}(\textit{n}$ -propyl)⁺ metallocene, respectively. Parts C and D correspond to Z- and E-butene insertion with the C_s -symmetric $\text{Me}_2\text{Si}(\text{Cp})(9\text{-Flu})\text{Zr}(\textit{n}$ -propyl)⁺ metallocene, respectively. For clarity, the 2-butene C atoms are shaded.¹⁴⁵

mize repulsive interactions with the metallocene ligand, and the head-methyl group is pushed to the opposite side relative to the growing chain to minimize steric interactions between the methyl group itself and the growing chain. This orientation of the head-methyl group implies that, for C_2 -symmetric metallocene, Z-butene insertion is favored relative to E-butene insertion, since for Z-butene the tail-methyl group is located far from the six-membered aromatic rings of the metallocene ligand. On the contrary, for C_s -symmetric metallocene, E-butene insertion is favored relative to Z-butene insertion, since for E-butene the tail-methyl group is located far from the six-membered aromatic rings of the metallocene ligand.¹⁴⁵

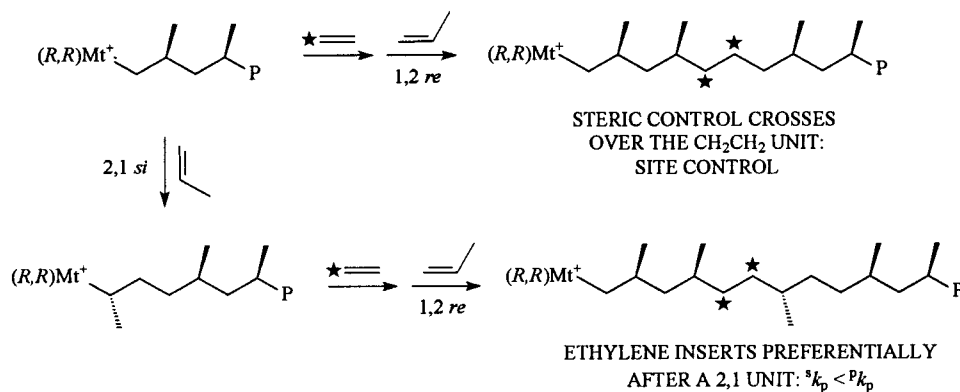
These predictions were confirmed by ethene/2-butene copolymerizations. In fact, C_2 -symmetric metallocenes scarcely insert, less than 2%, E-butene, while they insert relevant fractions, 25%, of Z-butene; analogously, C_s -symmetric metallocenes insert less than 2% of Z-butene, while inserting 14% of E-butene.¹⁴⁵

B. Reactivity of a Secondary Growing Chain

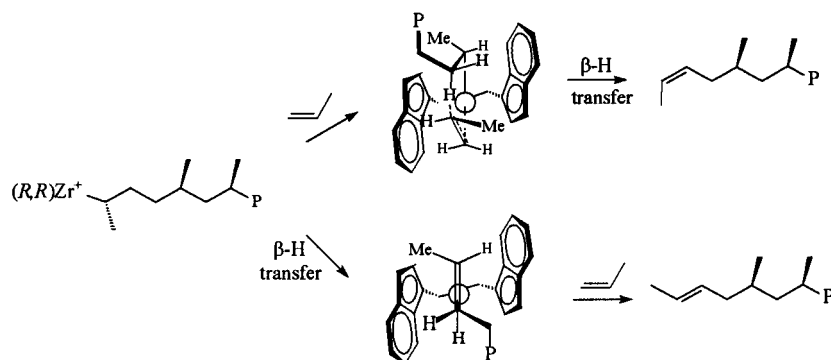
1. Copolymerization with Ethene

When low amounts of ethene are added to a propene polymerization with a non-fully-regioelec-

Scheme 39



Scheme 40



tive catalyst, a series of mechanistic information can be obtained. The use of ^{13}C -labeled ethene allows the detection of very low amounts of regioerrors.^{126,464,466} In addition, to provide further proof for site versus chain-end control, ^{13}C NMR analysis of isotactic propene/ethene copolymers made with $\text{rac-C}_2\text{H}_4(1\text{-Ind})_2\text{ZrCl}_2/\text{MAO}$ and $\text{rac-C}_2\text{H}_4(\text{H}_4\text{-1-Ind})_2\text{ZrCl}_2/\text{MAO}$ has given the following results (Scheme 39): (i) Ethene inserts preferentially after a secondary propene insertion. This means that primary propene insertion on a secondary growing chain is slower than on a primary growing chain: $^s k_p < ^p k_p$. Indeed, small amounts of ethene added to a $\text{rac-C}_2\text{H}_4(1\text{-Ind})_2\text{ZrCl}_2/\text{MAO}$ -catalyzed propene polymerization increase catalyst activity.³⁰⁴ For the same reason, ethene generates an increase in molecular weight, by reducing chain release after a secondary insertion.¹²⁹ (ii) The enantioselectivity of the secondary insertion is confirmed to be high and opposite to that of primary insertion. (iii) The fact that the $-(\text{CH}_2)_4-$ chain segment is produced by a 3,1 propene insertion is confirmed. (iv) The $2,1 \rightarrow 3,1$ isomerization is faster than ethene insertion, at least with the $\text{rac-C}_2\text{H}_4(1\text{-Ind})_2\text{ZrCl}_2/\text{MAO}$ catalyst, arguing in favor of a unimolecular isomerization mechanism.¹²⁶

2. Chain Release

Chain release after a 2,1 insertion has been already described in section III.F. Recent studies on chain release mechanisms have shown that, when even low amounts of secondary insertions occur, 2-butenyl end groups become relevant, and often more frequent than the vinylidene end group. This has been observed, for example, in C_2 -symmetric *ansa*-zirconocenes such as $\text{rac-C}_2\text{H}_4(1\text{-Ind})_2\text{ZrCl}_2$, $\text{rac-C}_2\text{H}_4$ -

$(4,7\text{-Me}_2\text{-1-Ind})_2\text{ZrCl}_2$,¹³⁰ $\text{rac-C}_2\text{H}_4(\text{H}_4\text{-1-Ind})_2\text{ZrCl}_2$, and $\text{rac-Me}_2\text{Si}(\text{Benz}[e]\text{ind})_2\text{ZrCl}_2$.⁴⁶⁷ Almost always the stereochemistry of the terminal double bond is *cis*, and formation of the *cis*-2-butenyl end group has been attributed to β -H transfer to the monomer after a secondary insertion. Unimolecular chain release would be expected to produce a *trans*-butenyl end group (Scheme 40).¹³⁰ This end group has been detected in a PP sample produced in liquid monomer by the low activity $\text{rac-C}_2\text{H}_4(4,7\text{-Me}_2\text{-H}_4\text{-1-Ind})_2\text{ZrCl}_2$ catalyst.¹³¹ The exceptions are *ansa*-zirconocenes with 2-methylindenyl ligands, for which chain release after a secondary unit is effectively suppressed.^{154,467}

C. Regioselectivity: Influence of the Catalyst Structure

1. Influence of the Metal

The influence of the metal can be gathered by comparing the results reported in ref 466 with those of refs 304 and 468: $\text{rac-C}_2\text{H}_4(1\text{-Ind})_2\text{TiCl}_2/\text{MAO}$ is both less stereoselective and less regioselective than its Zr analogue. $\text{rac-C}_2\text{H}_4(1\text{-Ind})_2\text{HfCl}_2/\text{MAO}$ gives *i*-PP which is very similar to that obtained with Zr. Other ligands seem to give the opposite effect: $\text{rac-Me}_2\text{Si}(2\text{-Me-4-Ph-1-Ind})_2\text{TiCl}_2/\text{MAO}$ has been reported to be more regioselective than its Zr and Hf analogues.⁴⁶⁹ There are however too few examples of stereoselective Ti and Hf complexes to allow a good comparison, mainly due to the generally lower activity of the Hf and Ti complexes.

2. Influence of the Cocatalyst

There is some controversy about the influence of the type of cocatalyst on either the stereo- or regio-

Table 17. Propene Polymerization with Zirconocene/MAO Catalysts: Synthesis and Microstructure^a

zirconocene	Al/Zr, molar ratio	A, kg/(mmol _{Zr} h)	tacticity ^b		regioinversions (%) ^c			end groups	total	ref
			<i>b</i> _{obs} ^d	% <i>mmmm</i>	2,1 <i>e</i>	2,1 <i>t</i>	3,1			
C₂ (racemic)										
CH ₂ (1-Ind) ₂ ZrCl ₂	4 000	62	0.9349	71.4 ₀	0.2 ₆	0.2 ₁	0.0		0.4 ₇	51
Me ₂ C(1-Ind) ₂ ZrCl ₂	3 000	66	0.9580	80.6 ₉	0.2 ₀	0.1 ₈	0.0		0.3 ₈	50
Me ₂ C(H ₄ -1-Ind) ₂ ZrCl ₂	3 000	37	0.9916	95.8 ₈	0.3 ₁	0.0 ₉	0.1 ₈		0.5 ₈	131
C ₂ H ₄ (1-Ind) ₂ ZrCl ₂ ^e	8 000	140	0.9736	87.4 ₇	0.3 ₅	0.1 ₉	0.0 ₁		0.5 ₅	50
C ₂ H ₄ (H ₄ -1-Ind) ₂ ZrCl ₂	20 000	37	0.9824	91.5 ₀	0.1 ₁	0.0 ₆	0.8 ₀		0.9 ₇	131
C ₂ H ₄ (4,7-Me ₂ -1-Ind) ₂ ZrCl ₂ ^e	2 000	72	0.9831	91.8 ₄	1.2 ₉	0.4 ₅	0.0 ₅	1	2.8 ₀ ^f	50
C ₂ H ₄ (4,7-Me ₂ -H ₄ -1-Ind) ₂ ZrCl ₂	2 000	5	nd	nd	0.0	0.0	18.9		18.9	131
CH ₂ (2-Me-1-Ind) ₂ ZrCl ₂	2 000	56	0.9145	63.9 ₆	0.2 ₄	0.1 ₁	0.0		0.3 ₅	202
Me ₂ Si(1-Ind) ₂ ZrCl ₂	3 000	17	0.9798	90.3 ₀	0.2 ₇	0.2 ₁	0		0.4 ₈	50
Me ₂ Si(H ₄ -1-Ind) ₂ ZrCl ₂	8 000	54	0.9896	94.9 ₁	0.1 ₄	0.0 ₀	0.3 ₉		0.5 ₃	131
Me ₂ Si(2-Me-1-Ind) ₂ ZrCl ₂	4 000	33	0.9882	94.2 ₅	0.3 ₃	0	0		0.3 ₃	50
Me ₂ Si(4-Ph-2-Me-1-Ind) ₂ ZrCl ₂ ^g	10 000	1300	0.9991	99.5 ₅	0.4 ₆	0	0		0.4 ₆	324
C ₂ H ₄ (3-Me-1-Ind) ₂ ZrCl ₂	8 000	28	0.7233	19.9 ₆	0	0	0	0	0	50
Me ₂ C(3- <i>t</i> -Bu-1-Ind) ₂ ZrCl ₂	8 000	125	0.9894	94.8 ₀	0	0	0	0	0	50
C₁ (isospecific)										
Me ₂ C(3- <i>t</i> -Bu-Cp)(9-Flu)ZrCl ₂ ^h	nr	23	—	77.4 ₇	nd	nd	0.44		0.44	470
Me ₂ C(3- <i>t</i> -Bu-Cp)(9-Flu)HfCl ₂	nr	nr	—	72.3 ₉	nd	nd	0.55		0.55	470

^a Polymerization conditions: 1-L stainless steel autoclave, 0.4 L of propene, 50 °C, 1 h, zirconocene/MAO aged 10 min.

^b Determined assuming the enantiomorphic site model, on primary insertions only; see ref 232. ^c Determined as described in ref 232; end groups not included. ^d In liquid monomer, *b*_{obs} → *b*. ^e Average values. ^f End groups included. ^g *T*_p = 70 °C. ^h *T*_p = 60 °C.

selectivity of insertion.^{46,70,71–77} We observed that by changing the cocatalyst from MAO to isobutyl alumoxane in *rac*-C₂H₄(1-Ind)₂ZrCl₂ catalyzed polymerization of liquid propene, the resulting *i*-PP have virtually identical microstructures even in the type and amount of regioerrors, although catalyst activity varies considerably. Since the role of MAO is discussed in detail by Chen and Marks in this issue of *Chemical Reviews*, this aspect is not further analyzed here.

3. Influence of the π -Ligands: Experimental Data

The microstructure of low molecular weight *a*-PP from Cp₂ZrCl₂ has been studied in detail: no internal 2,1 units were detected by ¹³C NMR,²¹⁴ while less than 1% of end groups are *cis*-2-butenyl, the rest being vinylidene.²⁰² This suggests that Cp₂ZrCl₂ is highly regioselective and chain propagation cannot proceed after an occasional secondary insertion. Similarly, the more active (MeCp)₂ZrCl₂ produces *a*-PP oligomers without detectable internal 2,1 units and 3.6% 2-butenyl end groups.¹³¹ The propene oligomerization catalysts (Me₅Cp)₂ZrCl₂ and its Hf analogue are even more regioselective, since secondary units could not be detected even as chain ends. The Me₂Si(9-Flu)₂ZrCl₂ catalyst for high molecular weight atactic polypropene is of similar high regioselectivity. (Ind)₂ZrCl₂ and (H₄Ind)₂ZrCl₂/MAO catalysts, on the contrary, produce low molecular weight *a*-PP with about 1% of 3,1 units and about 10% 2-butenyl end groups. Both the C₅-symmetric syndiospecific zirconocenes Me₂C(Cp)(9-Flu)ZrCl₂ and Ph₂C(Cp)(9-Flu)₂ZrCl₂ show, in liquid propene polymerization, no detectable 2,1 units. However, by using 1-[¹³C]-ethene in propene polymerization with a similar catalyst system, Busico was able to detect ≤0.08% 2,1 units.⁴⁶⁴

C₂-symmetric zirconocenes show the greatest variability in terms of both stereo- and regioselectivities, with total regioerrors ranging from almost 20% in

PP (practically a 1,2-propene-*co*-3,1-propene alternating copolymer) made with *rac*-C₂H₄(4,7-Me₂-H₄-1-Ind)₂ZrCl₂³⁴¹ down to virtually zero in the newest generation of highly isospecific zirconocenes developed by Montell.^{50,230,324} Due to the presence of growing-chain-end isomerization reactions and to the fact that regioselectivity can be monomer concentration dependent (see section VII.D), as it is the case of isospecificity, also the regioselectivity of *ansa*-zirconocenes has to be evaluated at the same propene concentration and polymerization temperature and, if possible, in *liquid monomer*. Such a comparison is shown in Table 17 for a series of *i*-PP samples prepared with a wide range of bridged C₂-symmetric zirconocene/MAO catalysts in liquid propene. Inspection of the data in Table 17 shows that hydrogenated ligands generate more stereoselective but less regioselective catalysts. The same effect occurs by methyl substitution on the frontal (4) position of indene: noteworthy, with respect to Brintzinger's benchmark catalyst *rac*-C₂H₄(1-Ind)₂ZrCl₂/MAO, is the higher stereoselectivity but much lower regioselectivity of the *rac*-C₂H₄(4,7-Me₂-1-Ind)₂ZrCl₂/MAO catalyst. Clearly the more open sites are less isospecific and more regioselective compared with sites bearing bulkier ligands. As seen in section V.A.1, C₂-I-9, having a wider "bite angle" β (see Table 1), is slightly less isospecific but more regioselective than C₂-I-1/MAO: these findings are in agreement with, and explained by, the mechanistic model proposed by Guerra, which connects regioselectivity to stereoselectivity in propene polymerization (see section VI-I.C.5).⁹¹ Spaleck and co-workers have shown that combining hydrogenation and 4-methyl substitution, as in the *rac*-C₂H₄(4,7-Me₂-H₄-1-Ind)₂ZrCl₂/MAO catalyst with the 4- and 7-methyl groups *endo* oriented, results in a dramatic loss of regioselectivity.³⁴¹ Another relevant effect of tetrahydroindenyl-based *ansa*-ligands is that the fraction of secondary units undergoing 2,1 → 3,1 isomerization is always much

higher compared to their indenyl-based analogues: in the case of *rac*-C₂H₄(4,7-Me₂-H₄-1-Ind)₂ZrCl₂, regioinversions are observed as 3,1 units *only*, indicating that, for this system, the site bearing a secondary growing chain end (secondary active site) cannot insert further monomer without previous isomerization to the linear chain (secondary growing-chain-end isomerization). An interesting case is that of the highly active, highly stereoselective *rac*-Me₂Si(2-Me-4-Ph-1-Ind)₂ZrCl₂ catalyst, which produces, in liquid monomer, very high molecular weight *i*-PP with pentad content over 99% and about 0.5% 2,1 *erythro* units. In this case, secondary growing chains do not seem to influence catalyst activity, since in polymerizations carried out in the presence of ethene these 2,1 units are maintained in the polymer. The last, most recent class of C₂-symmetric *ansa*-zirconocenes to be developed, of general formula *rac*-R₂C(3-R-1-Ind)₂ZrX₂, show a very high regioselectivity. For example, careful inspection of 100 MHz ¹³C NMR spectra of *i*-PP made with *rac*-Me₂C(3-*t*-Bu-1-Ind)₂ZrCl₂ revealed no trace of 2,1 units (that is, given the signal-to-noise ratio in these spectra, a concentration lower than 0.02%) in the chain and none (2-butenyl end groups < 1/200 000 units) in the chain end groups.^{50,230}

Concerning C₂-symmetric systems, the data shown in Table 17 are easily summarized by the following observations: (i) only the dimethyl-substituted bis-indenyl derivatives (such as *rac*-C₂H₄(4,7-Me₂-1-Ind)₂ZrCl₂ and *rac*-C₂H₄(4,7-Me₂-H₄-1-Ind)₂ZrCl₂) allow a significant degree of secondary insertions; (ii) hydrogenation of the indenyl moiety promotes a higher amount of 2,1 → 3,1 isomerization, (iii) substitution in C(2) increases regioselectivity as well as stereoselectivity; and (iv) substitution in C(3) produces highly regioselective catalysts, among the most regioselective of all metallocenes.

Very few data are available concerning the regioselectivity of the aspecific, C_s-symmetric *meso* isomers of C₂-symmetric *racemic* metallocenes: both *meso*-C₂H₄(1-Ind)₂ZrCl₂/MAO⁹¹ and *meso*-Me₂Si(2-Ph-1-Ind)₂ZrCl₂/MAO were shown to produce *a*-PP free of regioerrors.³⁴³ Also *meso*-Me₂Si(2-Me-4-Ph-1-Ind)₂ZrCl₂/MAO is much more regioselective (no regioerrors could be detected in the 100 MHz ¹³C NMR spectra of an *a*-PP sample prepared in liquid monomer at 70 °C) than *rac*-Me₂Si(2-Me-4-Ph-1-Ind)₂ZrCl₂/MAO.²⁰²

Waymouth's catalyst, (2-Ph-Ind)₂ZrCl₂, is more regioselective than both (Ind)₂ZrCl₂ and *rac*-C₂H₄(1-Ind)₂ZrCl₂; the same holds true for the analogue [2-(3,5-CF₃)₂C₆H₃-Ind]₂ZrCl₂.³⁷² For these systems, regioerrors are found only within the isotactic stereoblocks; thus, a secondary insertion can occur only when the catalyst is in an enantioselective conformation.

C₁-symmetric catalysts are slightly more regioselective compared to benchmark class II zirconocenes: Me₂C(3-*t*-Bu-Cp)(9-Flu)ZrCl₂ and Me₂C(3-*t*-Bu-Cp)(9-Flu)HfCl₂ show 0.44 and 0.55% 3,1 units respectively, at T_p = 60 °C.⁴⁷⁰

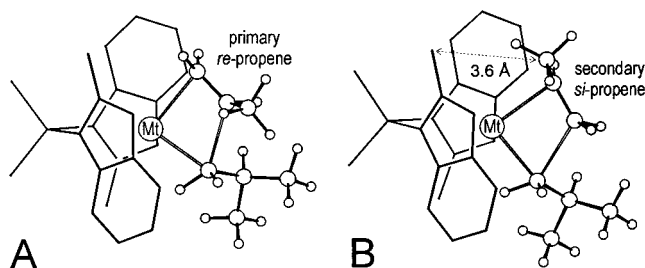


Figure 43. Pseudotransition states for monomer orientations suitable for the favored primary (part A) and secondary (part B) propene insertions into a primary polypropylene growing chain, for the case of the (*R,R*) coordinated C₂-symmetric *rac*-Me₂Si(2-Me-1-Ind)₂ ligand. Short nonbonded distances between the methyl group of propene and a methyl group of the ligand are indicated.²⁷²

4. Influence of the π -Ligands: Molecular Modeling Analysis

Before relating about the conclusions obtained by different research groups, it has to be noted that the energy difference between the secondary and primary propene insertion, ΔE_{regio} , can be considered composed by two main contributions, electronic and steric. The electronic contribution has been treated previously, while here we focus on the steric contribution to ΔE_{regio} , due to steric interaction among the monomer, the growing chain, and the ligand skeleton.

The substantial influence of methyl groups in position 2 of the ligand on the regioselectivity of the catalyst has been rationalized by Morokuma^{155,275} and Corradini²⁷² and their co-workers. Their molecular mechanics calculations clearly show that the energy difference between secondary and primary propene insertion into the Zr–C(chain) σ -bond increases by roughly 1–5 kcal/mol with respect to the analogous energy difference of the corresponding unsubstituted parent ligand, when a methyl group is added on the C(2) position of the ligands, as in the H₂Si(2,4-Me₂-Cp)₂,¹⁵⁵ H₂Si(2-Me-1-Ind)₂,²⁷⁵ Me₂Si(2-Me-1-Ind)₂,²⁷² and Me₂Si(2-Me-4-*t*-Bu-Cp)₂.²⁷²

The increased regioselectivity of 2-methyl-substituted catalysts is due to direct repulsive interaction of the methyl group of the monomer in a geometry suitable for secondary insertion, with the methyl group on C(2). The geometries of approximated transition states for primary and secondary propene insertion on the zirconocene based on the Me₂Si(2-Me-1-Ind)₂ ligand are sketched in Figure 43. Clearly, model B, suitable for secondary insertion, presents one of the methyl groups in position 2 of the ligand at a short distance from the methyl group of the propene. On the contrary, the distances between the methyl substituents in position 2 of the ligand and the methyl group of propene are larger than 5 Å in model A, suitable for primary insertion. This accounts for the increased steric contribution to ΔE_{regio} calculated for catalysts based on ligands bearing methyl substituents in position 2.^{155,272,275}

Moreover, Morokuma^{155,275} and Corradini²⁷² and their co-workers also rationalized the reduced steric contribution to ΔE_{regio} when an alkyl group is present in position 4. Morokuma and co-workers calculations on the H₂Si(4-*i*-Pr-1-Ind)₂ ligand and on the H₂Si(2-Me-4-alkyl-1-Ind)₂ ligands, with the alkyl group in

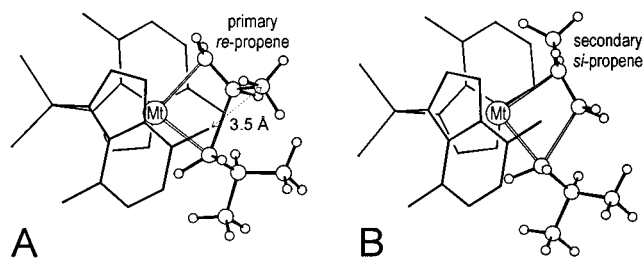


Figure 44. Pseudotransition states for monomer orientations suitable for the favored primary (part A) and secondary (part B) propene insertions into a primary polypropene growing chain, for the case of the (R,R) coordinated C_2 -symmetric rac - $Me_2Si(4,7-Me_2-1-Ind)_2$ ligand. Short non-bonded distances between the methyl group of propene and a methyl group of the ligand are indicated.²⁷²

position 4 in the series methyl, ethyl, *tert*-butyl,²⁷⁵ predicted that the energy difference between secondary and primary insertions is reduced by 2–8 kcal/mol, relative to the same energy difference with the parent 4-unsubstituted ligand. This holds also for the $H_2Si(2-Me-Benz[e]ind)_2$ ligand. In fact, the steric contribution to ΔE_{regio} for the catalyst based on this ligand has been calculated to be 3.5 kcal/mol lower than the steric contribution to ΔE_{regio} for the catalyst based on the $H_2Si(2-Me-1-Ind)_2$ ligand.²⁷⁵

The diminished regioselectivity of catalysts based on ligands containing methyl groups in position 4 (and 7) is due to direct repulsive interaction of the methyl group of the monomer in a geometry suitable for primary insertion, with the methyl group in position 4. The geometries of approximated transition states for primary and secondary propene insertion on the zirconocene based on the $Me_2Si(4,7-Me_2-1-Ind)_2$ ligand are sketched in Figure 44. Clearly, model A, suitable for primary insertion, presents one of the methyl groups in position 4 of the ligand at short distance from the methyl group of the propene. On the contrary, the distances between the methyl substituents in positions 4 and 4' of the ligand and the methyl group of propene are larger than 5 Å in model B, suitable for secondary insertion. This accounts for the reduced steric contribution to ΔE_{regio} calculated for catalysts based on ligands bearing methyl substituents in position 4 (and 7).²⁷² This feature is particularly enhanced when the methyl groups point toward the equatorial belt of the metallocene, as for the catalyst based on the (R,R) coordinated $C_2H_4(4,7-Me_2-H_4-1-Ind)_2$ ligand with *R* chirality at the 4,4' and *S* chirality at the 7,7' C atoms. In this case, the steric contribution to ΔE_{regio} is lower by almost 2 kcal/mol relative to the steric contribution to ΔE_{regio} calculated for the catalyst based on the unsubstituted coordinated $C_2H_4(H_4-1-Ind)_2$ ligand.

As for the effect of an alkyl group substituted in position 3, Morokuma and co-workers²⁷⁵ predicted that a methyl substituent in position 3 of the $Me_2Si(1-Ind)_2$ ligand should increase the steric contribution to ΔE_{regio} , whereas Corradini and co-workers found that the same methyl group should slightly decrease this steric contribution.⁴⁷¹ Finally, when the alkyl group substituted in position 3 is the bulky *tert*-butyl group, a higher steric contribution to ΔE_{regio} , roughly 2 kcal/mol, is predicted instead.²⁷²

5. Relationship between Regioselectivity and Type of Stereoselectivity

Finally, we turn our attention to the relationship between regioselectivity and type of stereoselectivity, that is, between the regioselectivity of a catalyst and its symmetry. In fact, as discussed above, syndiospecific and aspecific zirconocene catalytic systems are in general more regioselective than class II isospecific systems, most of which produce *i*-PP containing substantial amounts of regioirregular monomeric units, independently of the nature of the π -ligands and of the bridge between them (with the notable exception of 3-substituted bisindenyl systems). This dependence of the degree of regioselectivity on the symmetry rather than on the nature of the π -ligands and of the bridge between them (unless suitable substitutions of the ligands are involved) is not easy to rationalize by invoking differences in the electronic contributions to regioselectivity.

On the other hand, the results discussed in the previous sections indicate that the steric contribution to the energy differences between secondary and primary propene insertion, for zirconocene-based catalytic models, is not greatly dependent on the symmetry of the π -ligands and hence on their stereoselectivity. However, the calculated energy difference between secondary and primary propene insertion for a given enantioface of the monomer is strongly dependent on the symmetry, and hence stereoselectivity, of the catalysts. In particular, for the syndiospecific C_s -symmetric catalysts a large steric contribution to regioselectivity is calculated for the enantioface which is *wrong* (subscript w in the following) for the primary insertion, whereas for the C_2 -symmetric isospecific catalysts a large steric contribution to regioselectivity is calculated for the enantioface which is *right* (subscript r in the following) for primary insertion. In short, the very same propene enantioface is favored for primary and secondary propene insertion with the C_s -symmetric syndiospecific catalysts,^{90,91,155,277} whereas opposite propene enantiofaces are favored for primary and secondary propene insertion with the C_2 -symmetric isospecific catalysts.^{91,147,155,200,276}

On the basis of this modeling background, Corradini and co-workers developed a model able to relate regioselectivity on the type of stereoselectivity.⁹¹ For generic aspecific, syndiospecific, and isospecific model complexes, schematic plots of the internal energy versus the reaction coordinate, both for primary and secondary insertions, are sketched in Figure 45, parts A, B, and C, respectively. The minima at the center and at the ends of the energy curves correspond to propene-free intermediates including a growing chain with n and $n + 1$ monomeric units, respectively (just as an example, a possible geometry for these intermediate could correspond to the β -agostic geometry hypothesized as the resting state by several authors). Movements from the central minimum toward the left and the right correspond to possible reaction pathways leading to primary and secondary propene insertions, respectively. For the enantioselective complexes, the reaction pathways for monomer enantiofaces which are right and wrong for primary

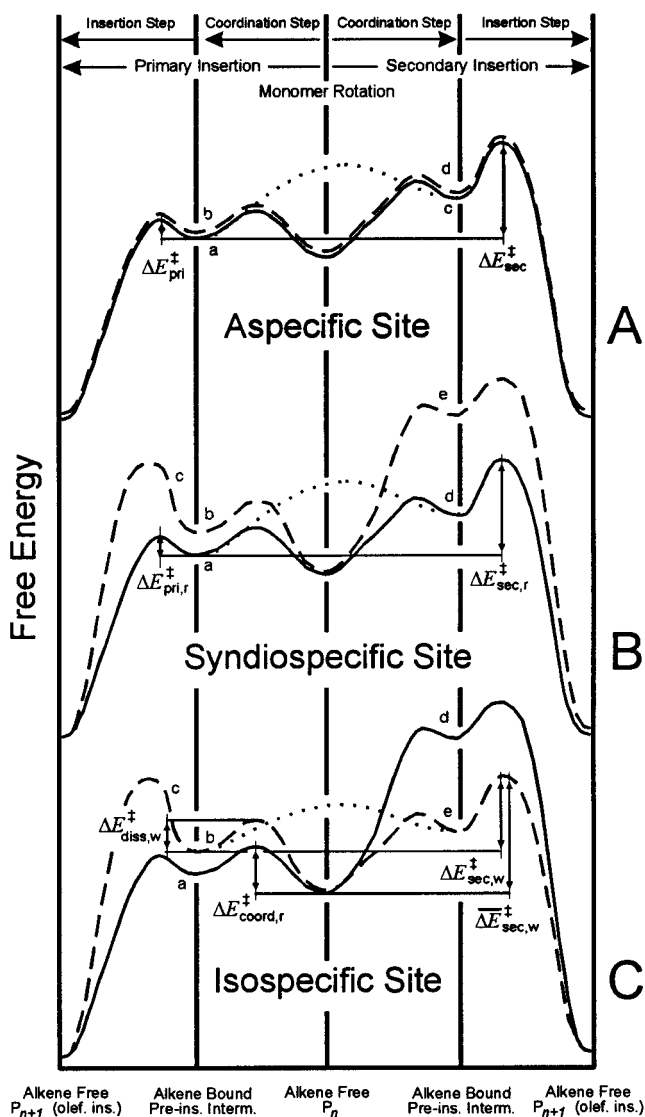


Figure 45. Schematic plots of the internal energy versus the reaction coordinate, for both primary and secondary insertions, for generic aspecific (A), syndiospecific (B), and isospecific (C) model complexes. The minima at the centers and at the ends of the energy curves correspond to alkene-free catalytic intermediates including a growing chain with n and $n + 1$ monomeric units, respectively. Movements from the central minima toward the left and the right correspond to possible reaction pathways leading to primary and secondary insertions, respectively. For the enantioselective complexes (B,C), the reaction pathways for monomer enantiofaces being right (r) and wrong (w) for primary insertion are different and are indicated by full and dashed lines, respectively. The two energy barriers encountered for each pathway correspond to the coordination and insertion steps. The energy minima between the energy barriers for the monomer coordination and insertion correspond to alkene-bonded catalytic intermediates.⁹¹

insertion are different, and are indicated by full and dashed lines, respectively. For each pathway, the two energy barriers correspond to the coordination and insertion steps.

The energy minima between the energy barriers for the monomer coordination and insertion, labeled as preinsertion intermediates in Figure 45, correspond to propene-bonded (π -complex) intermediates of the type used by several authors to discuss the enantioselectivity of propene insertion.^{89,90,147,200,274,276,277}

The possible dissociation of the monomer coordinated with the wrong enantioface can lead back to the propene-free intermediate or, directly, to the propene-bonded intermediate with the right enantioface (through a ligand substitution reaction).

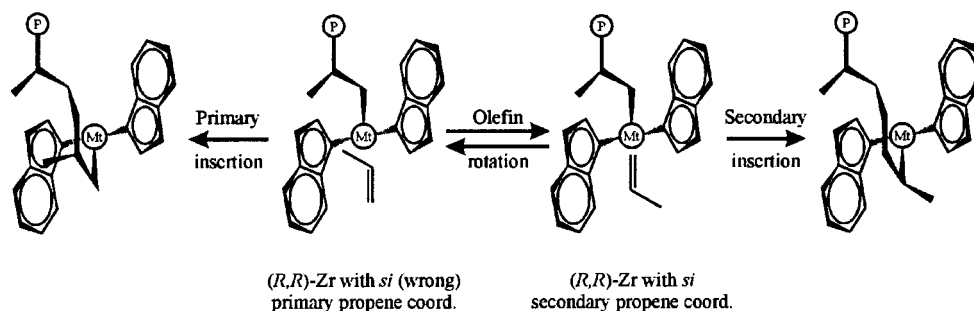
For the sake of simplicity, minimum energy pathways that according to the calculations are expected to be similar, have been assumed to be identical, independently of the symmetry (stereoselectivity) of the catalyst. However, the plots for the syndiospecific (Figure 45B) and isospecific (Figure 45C) models are different since, as previously discussed, the enantioselectivities for primary and secondary insertions are in favor of the same or opposite monomer enantiofaces, respectively.

In this framework, the lower regioselectivity of class II C_2 -symmetric isospecific metallocenes can be rationalized by assuming that the activation energy for rotation of propene coordinated with the "wrong" enantioface, between the orientations suitable for primary and secondary insertions (schematically shown by dotted lines in Figure 45), is in general lower than (or comparable to) the activation energy for a primary insertion leading to a stereoerror^{91,155} (see Scheme 41).

On the other side, highly substituted C_2 -symmetric *ansa*-metallocenes, such as *rac*- $C_2H_4(4,7-Me_2-1-Ind)_2-ZrCl_2$, *rac*- $C_2H_4(4,7-Me_2-H_4-1-Ind)_2ZrCl_2$, and *rac*- $Me_2-Si(2-Me-4-Ph-1-Ind)_2ZrCl_2$, show relevant amounts of secondary insertions that molecular modeling indicates are due to a direct interaction between a correct primary coordinated propene and the substituent on C(4) of indene, the same substituent that is the key to high isospecificity in these systems. Hence stereoselectivity and regioselectivity are strictly related. As a rule-of-thumb, for zirconocenes of the general formula shown in Chart 7, the more stereoselective the catalyst, the less regioselective it is.

For syndiospecific model complexes, since their enantioselectivity is in favor of the same monomer enantioface both for primary and secondary insertions, when coordination of the monomer occurs with the wrong enantioface for primary insertion, the most probable event is the dissociation of the monomer. With lower probability, primary insertion of the wrong enantioface is also possible, thus introducing a stereoirregularity in the polymer chain. Secondary insertions are expected to be essentially absent (see the high energy of situations d and e in Figure 45B). With the assumption of a low-energy barrier for rotation of the propene molecule between the orientations suitable for primary and secondary insertions, regioselectivity would be simply determined by the differences between the activation energies for secondary and primary insertions of the more suitable enantioface ($\Delta E_{sec,r}^\ddagger - \Delta E_{pri,r}^\ddagger$) (and independent of the energy barrier for the monomer coordination). Moreover, regioselectivity is expected to be high and similar to that of the corresponding aspecific catalytic complex.⁹¹

For isospecific model complexes, since their enantioselectivity is in favor of opposite monomer enantiofaces for primary and secondary insertions, when the coordination of the monomer with the enantioface

Scheme 41. Influence of Nonbonded Interactions on Regiochemistry

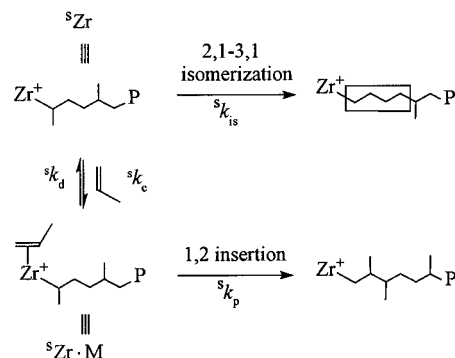
unsuitable for the primary insertion occurs, besides the dissociation of the coordinated monomer and besides a low probability primary insertion (generating the stereoirregularities), also a low probability secondary insertion (generating the regioirregularities) would be possible. This is due to the fact that the barrier for the dissociation of the coordinated monomer is not expected to be negligible with respect to the activation energy for the secondary insertion. Hence, for these isospecific model complexes, the amount of regioirregularities in the polymer chains would be not determined (as for the cases of aspecific and syndiospecific model complexes) by the differences between the activation energies for the secondary and primary insertions. Instead, it would be related to the difference between the activation energies for the dissociation of the monomer (coordinated with the wrong enantioface) and the activation energy for its secondary insertion ($\Delta E_{\text{sec.w}}^{\ddagger} - \Delta E_{\text{diss.w}}^{\ddagger}$).

D. Influence of Monomer Concentration

The important influence of propene concentration and polymerization temperature on the regioregularity and end group structure of metallocene *i*-PP have been realized only recently, thanks to detailed ^1H and ^{13}C NMR analysis of the polymers made with some prototypical zirconocenes. No data are available on the corresponding hafnocenes or titanocenes. With the moderately isospecific *rac*- $\text{C}_2\text{H}_4(1\text{-Ind})_2\text{ZrCl}_2/\text{MAO}$ catalyst, the total amount of secondary insertions does not depend on monomer concentration, while it shows a dependence on polymerization temperature. On the other hand, the chemical structure of the chain fragment generated by an isolated secondary unit does depend on both polymerization temperature and monomer concentration.

Busico²⁵² and Resconi²³² have shown that 2,1 \rightarrow 3,1 isomerization is a unimolecular process, as the ratio of [2,1]/[3,1] follows a simple first-order dependence on monomer concentration (see Scheme 42): the 2,1 units are more likely to isomerize into 3,1 propene units when the monomer concentration is lowered (or the polymerization temperature increased).

The kinetics of isomerization have been described by eq 2, where sR_p and $^s k_p$ are the rate and constant of insertion of a primary unit onto an active site with a secondary chain end, $^sR_{\text{is}}$ and $^s k_{\text{is}}$ are the rate and constant of secondary chain end isomerization, and sC and $^sC\cdot M$ are the active centers having a secondary chain end and none or one coordinated monomer

Scheme 42

molecules, respectively, and are correlated by the equilibrium constant for monomer coordination, $^sK = [^sC\cdot M]/[^sC][M]$:

$$\frac{[2,1]}{[3,1]} = \frac{^sR_p}{^sR_{\text{is}}} = \frac{^s k_p [^sC\cdot M]}{^s k_{\text{is}} [^sC]} = \frac{^s k_p {}^sK [M]}{^s k_{\text{is}}} \quad (2)$$

The monomer concentration dependence of the 2,1 \rightarrow 3,1 isomerization in the case of the less regioselective *rac*- $\text{C}_2\text{H}_4(4,7\text{-Me}_2\text{-1-Ind})_2\text{ZrCl}_2/\text{MAO}$ catalyst has been investigated by Resconi and co-workers.³⁴² While for *rac*- $\text{C}_2\text{H}_4(1\text{-Ind})_2\text{ZrCl}_2/\text{MAO}$ at 50 °C in the system toluene/propene, both the 2,1/2,1 t ratio ($e/t \approx 2$) and the overall percentage ($\approx 0.6\%$) of regio-inverted units including 3,1 remains approximately constant with $[M]$,²³² however, in the case of *rac*- $\text{C}_2\text{H}_4(4,7\text{-Me}_2\text{-1-Ind})_2\text{ZrCl}_2/\text{MAO}$ the total amount of secondary units decreases distinctly with decreasing monomer concentration, from ca. 3% in liquid monomer to almost 1% at $[M] \rightarrow 0$ (Figure 46). In this case,

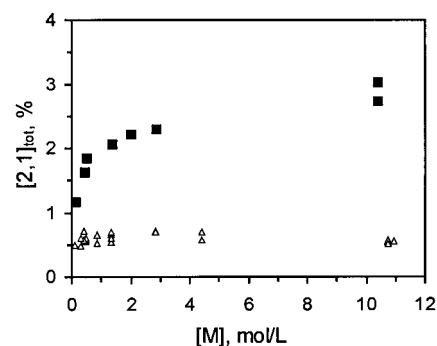


Figure 46. Total secondary insertions, including end groups, versus propene concentration in *i*-PP samples from *rac*- $\text{C}_2\text{H}_4(1\text{-Ind})_2\text{ZrCl}_2/\text{MAO}$ (Δ) and *rac*- $\text{C}_2\text{H}_4(4,7\text{-Me}_2\text{-1-Ind})_2\text{ZrCl}_2/\text{MAO}$ (\blacksquare) (50 °C, toluene).³⁴²

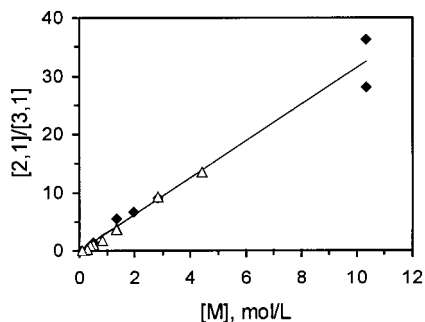


Figure 47. [2,1]/[3,1] ratio (determined by ^{13}C NMR) versus propene concentration in *i*-PP samples from $\text{rac-C}_2\text{H}_4(1\text{-Ind})_2\text{ZrCl}_2/\text{MAO}$ (Δ) and $\text{rac-C}_2\text{H}_4(4,7\text{-Me}_2\text{-1-Ind})_2\text{ZrCl}_2/\text{MAO}$ (\blacklozenge) (50 °C, toluene). For both ($^s\text{K}^s k_p / ^s k_{is}$) $_{50^\circ\text{C}} = 3$.³⁴²

we can no longer assume that regioselectivity is independent from monomer concentration.

However, the experimental [2,1]/[3,1] ratios for samples from $\text{rac-C}_2\text{H}_4(1\text{-Ind})_2\text{ZrCl}_2/\text{MAO}$ and $\text{rac-C}_2\text{H}_4(4,7\text{-Me}_2\text{-1-Ind})_2\text{ZrCl}_2/\text{MAO}$ show the same linear dependence on propene concentration with a correlation parameter $R = 0.989$, from which we obtain the same $^s\text{K}^s k_p / ^s k_{is} = 3$ (Figure 47). Hence, despite their different regioselectivities and activities, the rate of isomerization for these two zirconocenes is the same. These results confirm that (i) both the fraction of 2,1 insertions and the rate of isomerization, relative to primary insertion, *increase* by increasing the bulkiness of the ligand, (ii) isomerization is a unimolecular process, with a zero-order dependence on monomer concentration, and (iii) differences in the ligands have no influence on the isomerization mechanism.

E. Influence of Polymerization Temperature

As already discussed in the section dedicated to stereoregularity, besides the biscyclopentadienyl ligand structure and the concentration of propene, the polymerization temperature is another important source of variability in the microstructure of polypropenes obtained from *ansa*-zirconocenes. In *liquid monomer*, both the amount of secondary insertions and the rate of 2,1 \rightarrow 3,1 isomerization increase with increasing T_p . For example, for $\text{rac-C}_2\text{H}_4(1\text{-Ind})_2\text{ZrCl}_2/\text{MAO}$ and $\text{rac-C}_2\text{H}_4(4,7\text{-Me}_2\text{-1-Ind})_2\text{ZrCl}_2/\text{MAO}$, total 2,1 units (including end groups) increase, between 20 and 70 °C, from 0.4 to 0.7% and from 2.5 to 4.3%, respectively.³⁴² The C_1 -symmetric $\text{Me}_2\text{C}(3\text{-}t\text{-Bu-Cp})(9\text{-Flu})\text{ZrCl}_2$ interestingly shows a near constancy of the 3,1 units ($\sim 0.4\%$) with T_p .⁴⁷⁰

F. 2,1 \rightarrow 3,1 Isomerization Mechanism

As discussed above, based on kinetic evidence, the 2,1 \rightarrow 3,1 isomerization reaction must be unimolecular. Possible mechanisms of 2,1 \rightarrow 3,1 isomerization have been discussed by Soga,⁴⁶³ Chien,⁴⁷³ and Kaminsky⁴⁷⁴ and more recently by Proscenc and Brintzinger,²¹⁵ but no conclusive evidence has been presented. Chien suggested that isomerization occurs by a two-step mechanism (that is, first β -H transfer from the methyl group of the last (secondary) inserted unit, rotation of the coordinated α -olefin end group from

secondary to primary, and then reinsertion into the metal–hydrogen bond. This mechanism is shown in detail in Scheme 43.

The modeling work of Proscenc and Brintzinger on the Cp_2ZrR^+ site ($R = n$ -propyl, isobutyl) led them to conclude that a mechanism occurring through β -H transfer, olefin rotation about the Zr–H bond, and reinsertion would be the lowest in energy, and hence the most likely one.²¹⁵ Their modeling investigated the isomerization of an *n*-propyl or an isobutyl alkyl group to isopropyl or *tert*-butyl groups. The first step, β -hydrogen transfer to the metal, is the one with the higher activation barrier, about 10 kcal/mol for both alkyl groups. The second step, rotation of the olefin, was calculated to be of very low energy, about 1 kcal/mol, in agreement with similar conclusions of other authors.^{56,146,176} The last step to complete the isomerization reaction requires insertion of the rotated olefin into the Zr–H bond, a step of usually negligible barrier.^{152–154,215,475} Very similar conclusions have been obtained by Rytter, Ystenes, and co-workers, who studied the same isomerization reaction of the longer *n*-butyl group in the $\text{Cp}_2\text{ZrC}_4\text{H}_9^+$ and $(\text{Me}_5\text{-Cp})_2\text{ZrC}_4\text{H}_9^+$ systems.⁴⁷⁵ Moreover, they found that the olefin rotation step was not hampered by steric pressure also with the bulkier Me_5Cp ligands.

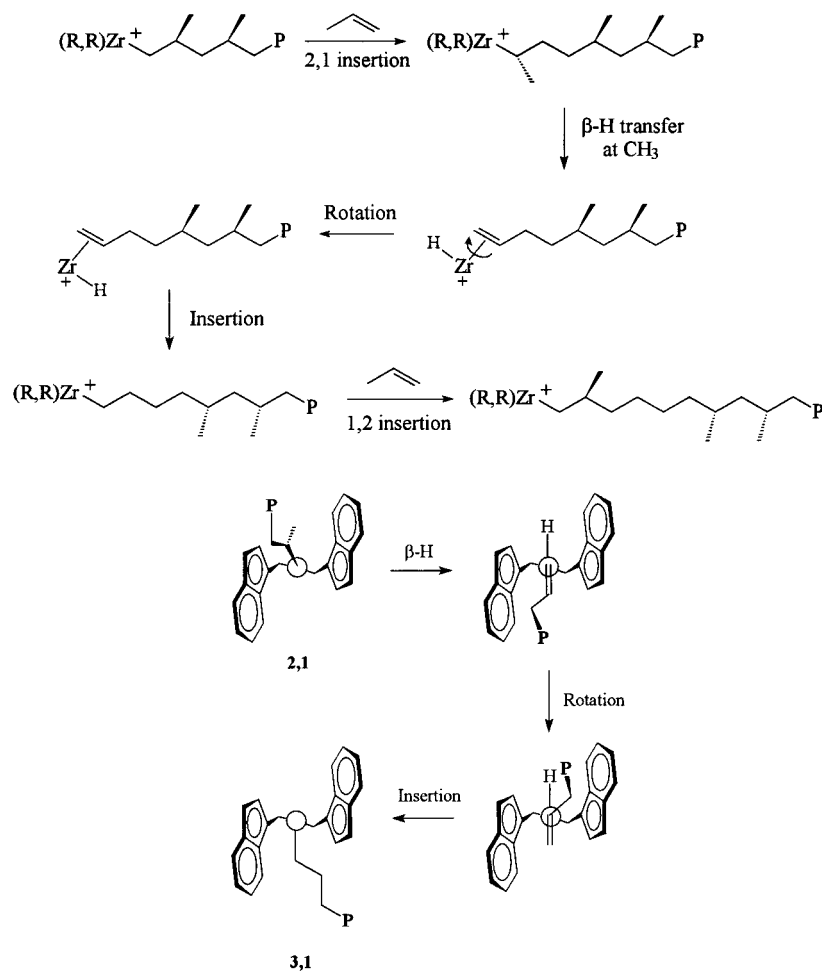
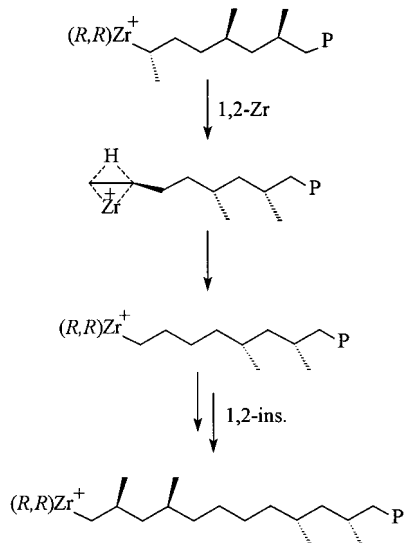
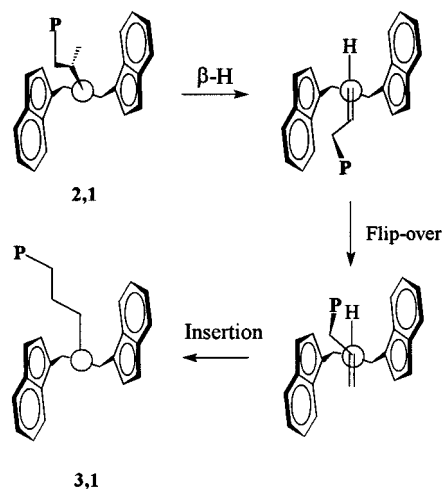
Proscenc and Brintzinger also discussed two other possible mechanisms, that is, a concerted 1,2-H/2,1-Zr shift (mechanism II, shown in Scheme 44), in which the Zr center at the C_α and one of the H atoms at the C_β exchange their positions simultaneously, and a third one involving a flip-over of the coordinated olefin, after the usual β -H transfer step, via a transition state in which the flipping olefin is edge-on coordinated to the metal center through a double σ -CH coordination (mechanism III, shown in Scheme 45).²¹⁵

They calculated a high activation barrier for a direct 1,2-hydrogen shift, roughly 40 kcal/mol, which rules out the direct 1,2-H shift as a viable mechanism, while the olefin flip costs about 7 kcal/mol from the ordinary π -coordination geometry.²¹⁵

VIII. Kinetics

Although Ziegler–Natta polymerization catalysts are extremely important and have been the subject of intense investigation for over 45 years, there is still a lot of controversy about the intimate nature of the active species and the mechanisms involved in this highly stereospecific chain growth process.⁴⁴⁴ At their appearance, stereoselective metallocenes were heralded as the first well-defined working model for heterogeneous Ziegler–Natta catalysts, and kinetic analysis was hence applied to this new class of catalysts aiming at a better understanding of the polymerization pathways. The more extensively metallocenes polymerizations were studied, the more evident the profound difference between the two catalyst families became and how much more complicated the polymerization pathways of the homogeneous catalysts could be.

Kinetics describes reaction rates and their dependence from the reaction parameters. As we have extensively discussed in the previous sections, in

Scheme 43. Mechanism I, Showing Stereochemistry of Olefin Coordination**Scheme 44. Mechanism II****Scheme 45. Mechanism III, Showing Stereochemistry of Olefin Coordination**

catalytic olefin polymerization several different reactions can occur at the active center. The relative values of the rate constants of these different possible reactions determine the microstructure of the obtained polymer under certain polymerization conditions. Kinetic analysis, hence, is one of the most powerful tools for the comprehension of reaction mechanisms.

Concerning activity, the propagation elementary step obeys the simple relationship: $R_p = k_p[C][M]$. Under usual polymerization conditions, chain release and deactivation affect the number of active centers, hampering the correct evaluation of the propagation constant. To eliminate or reduce the effect of these *side reactions* two methods are used for kinetic investigation of the propagation step: living polymerization or stopped flow measurements. Living po-

lymerization conditions can be achieved by decreasing the polymerization temperature until chain termination and deactivation are so slow that propagation is the only mechanism taking place during the observation time, i.e., the duration of the experiment. This implies that the range of temperature in which is possible to have living polymerization is far from the typical range of polymerization temperatures. Propene living polymerization with the [*t*-BuNSiMe₂-Flu]TiMe₂/B(C₆F₅)₃ catalytic system at -50 °C was recently investigated to provide direct evidence of a second-order dependence of propagation rate on monomer concentration.⁴⁷⁶ In the case of stopped-flow technique, the reduction of the deactivation is achieved by shortening the time of the experiment, typically on the order of a fraction of a second. The stopped-flow approach was widely used in studying propene polymerization promoted by heterogeneous Ziegler–Natta catalysts. Shiono et al.⁴⁷⁷ and Busico et al.⁴⁷⁸ applied this technique to the kinetic investigation of ethene and propene polymerization with homogeneous catalytic systems. Busico investigated ethene and propene polymerization in the temperature range 20–60 °C with the homogeneous system *rac*-Me₂Si-(2-Me-Benz[*e*]ind)₂ZrCl₂/MAO; he obtained turnover frequencies of monomer insertion of 6.5×10^4 and 1.6×10^3 s⁻¹ at 40 °C, respectively, for ethene and propene polymerization. In the case of polyethylene, the propagation rate measured under these short time of polymerization are 2 orders of magnitude higher than those reported for polymerization runs at higher reaction time. This can suggest that diffusion limitations occur at longer time. For polypropene, diffusion limitations seem to be less important, perhaps because of the lower rate of propagation or the higher solubility of the polymer in the reaction medium.

Apart these specialistic approaches, in the following paragraphs the reported kinetic investigations are referred to experiments under more *conventional* polymerization conditions.

A. Activity versus Metal

Several transition metals have been found to give active metallocene catalysts, all among groups 3 and 4 and the lanthanides and actinides. Almost always, Zr is the most active, although there are important exceptions to this rule. For example, the titanocenes *C*₁-I-3-**anti/syn** are much more active than the corresponding zirconocenes.³⁸⁹ In most instances, both Hf and Ti give much less active catalysts, and often these are inactive. Sc and Y also have very low activities. The generally low activity of Ti can be attributed to its tendency to reduction, while the low activity of Hf complexes has been attributed to the higher strength of the Hf–C bond compared to the Zr–C bond.

B. Activity versus Catalyst/Cocatalyst Ratio

Since the discovery of methylalumoxane as effective cocatalyst for the activation of metallocenes, many studies have been devoted to a better understanding of the nature of the active species and of

the role of MAO as cocatalyst. It is now generally accepted that MAO first alkylates metallocenes dichloride and then generates cationic species by abstracting and complexing the counterion.^{417,479} The cationic nature of the active species was clearly demonstrated by the results obtained by Jordan et al.,⁴⁸⁰ who showed that the zirconium complex [Cp₂ZrCH₃-(THF)]⁺[BPh₄]⁻ polymerizes ethene in a polar solvent, such as methylene chloride, without any activator. Subsequently, many MAO-free cationic metallocene systems, able to polymerize ethene, propene, and higher α -olefins, even in nonpolar solvent, were developed.^{224,225,481,482} Several ¹H and ¹³C NMR investigations^{483–485} as well as spectroscopic (UV/visible)^{21,486–488} and conductometric studies^{487,488} were performed to obtain insight into the mechanism of active species formation. Depending on the Al/Zr molar ratio, the formation of monomeric or dimeric structures (in which the vacant site is stabilized by a μ -CH₃ coordination) has been postulated, each with different activity, leading to different activity at different Al/Zr. Despite these extensive efforts in the study of the interactions between MAO and metallocenes, it is still unclear why a large excess of MAO is required to achieve the maximum activity. It is generally reported in the literature^{417,489,490} that activity increases by increasing the Al/Zr molar ratio up to an optimal value, after which a decrease of the polymerization rate is observed or, as reported in other papers,^{479,487,488,491} up to a plateau value. This behavior is common to many different catalytic systems either syndio- or iso- or aspecific and also to MAO-free catalysts.^{74,485} Fink et al.⁴⁸⁹ investigated ethene and propene homopolymerization by means of the *C*_s- (Me₂C(Cp)(9-Flu)ZrCl₂/MAO) and *C*₂-symmetric (Me₂Si(1-Ind)₂ZrCl₂/MAO) catalytic systems in toluene at different catalyst concentration and different Al/Zr molar ratios. They found a first-order dependence of the polymerization rate from [Zr] at constant monomer concentration and Al/Zr. By varying the Al/Zr molar ratio at constant [Zr] and [M], the activity of the Me₂Si(1-Ind)₂ZrCl₂/MAO catalytic system shows a maximum at Al/Zr \approx 27 000 for ethene and Al/Zr \approx 11 000 for propene polymerization. In the case of the Me₂C(Cp)(9-Flu)ZrCl₂/MAO system, a similar behavior was observed with the maximum at Al/Zr \approx 5100 for ethene and Al/Zr \approx 1300 for propene polymerization. Furthermore, with the *C*_s-symmetric catalyst, the fraction of *rmrr* pentads and the molecular weights decrease with increasing Al/Zr ratio. On the contrary, PP stereoregularity and molecular weights remain constant in the case of the *C*₂-symmetric catalyst. The increase of the *rmrr* pentad indicates a dependence of the rate of chain back-skip on the counterion, that is, complex reaction mechanisms which might be composed of several single steps and equilibria. At low Al/Zr molar ratio, MAO may not be sufficient to convert all the metallocene into active cationic catalyst. At optimum Al/Zr ratio the metallocene is converted to cationic complexes with weakly coordinating MAO-complexed counterions. At higher Al/Zr, the excess of MAO and olefin can compete for vacant coordination sites. The different effect of the MAO concentration on the

microstructure of the obtained polymer for the two catalysts is due, according to Fink, to the different ligand geometry. The $\text{Me}_2\text{C}(\text{Cp})(9\text{-Flu})$ ligand has a shorter bridge and therefore a larger angle between the planes of the π -ligands system than the $\text{Me}_2\text{Si}(1\text{-Ind})_2$ ligand. Hence, in $\text{Me}_2\text{C}(\text{Cp})(9\text{-Flu})$ the Zr atom is less shielded by the ligand and the interaction between Zr and MAO component is more efficient. As a consequence of the tight contact ion pair, the maximum activity appears at much lower Al/Zr molar ratios both for ethene and propene than for $\text{Me}_2\text{Si}(1\text{-Ind})_2\text{ZrCl}_2$. In a further investigation⁴²³ using the $\text{Me}_2\text{C}(3\text{-MeCp})(9\text{-Flu})\text{ZrCl}_2/\text{MAO}$ catalytic system for propene polymerization, the maximum activity vs Al/Zr was observed at a still lower ratio, Al/Zr \approx 500, suggesting that the shielding effect in this case is still lower due to the higher hindrance of the methyl group on the Cp ligand.

Mülhaupt⁴⁷⁹ investigated propene polymerization with the $\text{rac-Me}_2\text{Si}(2\text{-Me-Benz}[e]\text{ind})_2\text{ZrCl}_2/\text{MAO}$ system in toluene and found a similar bell-shaped profile for activity vs cocatalyst concentration. In the same direction, a decrease of the molecular weight but no effect on stereospecificity was found. According to Mülhaupt, at high [MAO], coordination of MAO instead of the olefin can lead to polymerization-inactive species that can undergo chain termination via β -H elimination, generating a different R_p/R_t ratio and hence affecting the molecular weight. He concluded that it is the overall MAO concentration that plays a crucial role in the activation of the metallocene and not the Al/Zr molar ratio. Considering that MAO is a gel rather than a true solution, the dilution of this component can affect the actual efficiency of the cocatalyst. Further evidence that the close contact of the cocatalyst to the catalyst is a key point comes from the supportation results: supported catalyst systems reach high activities at much lower MAO/metallocene ratios compared to the homogeneous systems.

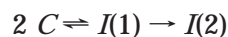
Fink extended his investigation on the effect of the cocatalyst/catalyst ratio to the system $\text{Me}_2\text{Si}(1\text{-Ind})_2\text{ZrCl}_2/[\text{Bu}_3\text{NH}][\text{B}(\text{C}_6\text{F}_5)_4]$ ⁷⁴ for ethene and propene polymerization in comparison with the same MAO-activated catalyst. The plot of the activity vs [metallocene]/[ammonium borate] is a sigmoidal curve, indicating the existence of two or more successive equilibrium reactions. The plot of activity vs [ammonium borate]/[metallocene] in the range 0–3 presents a maximum as in the case of the MAO-activated system, but now the maximum corresponds to cocatalyst/catalyst = 1.

The polymers obtained with $\text{Me}_2\text{Si}(1\text{-Ind})_2\text{ZrCl}_2$ activated by either $[\text{Bu}_3\text{NH}][\text{B}(\text{C}_6\text{F}_5)_4]$ or MAO show the same microstructure, indicating that the stereoselectivity of the metallocene catalysts does not depend on the nature of the cocatalyst and that the active species are similar in the two cases. This is a key observation, in accordance with the report of Ewen⁴⁶ and our own experience. Nevertheless, the two catalyst systems differ considerably in the mechanism of formation of these active species. Similarly, Mülhaupt et al. found for propene polymerization with $\text{rac-Me}_2\text{Si}(2\text{-Me-Benz}[e]\text{ind})_2\text{ZrX}_2$ (X = Cl, Me)

that polypropene melting temperature and isotacticities are independent of the catalyst source (metallocenedichloride or dimethyl) and of the cocatalyst nature (MAO or cationic activators).⁴⁹²

C. Activity versus Time

Most of the studies on olefin polymerization with metallocenes were performed under polymerization conditions in which deactivation occurs, which makes it difficult to determine the precise number of active centers and hampers a correct kinetic analysis. There are a few studies in the literature reporting the deactivation behavior of metallocene catalysts as a function of temperature. Both for ethene and propene homopolymerization typically the polymerization rate reaches its maximum immediately after the reaction is initiated. Sometimes an induction period is observed,⁴⁹³ and then the rate gradually decreases with time to a lower steady-state value.^{438,494–496} The decay profile depends mainly on the polymerization temperature. The time to reach the steady-state activity ranges between minutes (for temperature of 40–60 °C) to hours (for temperature of 0–20 °C). Mülhaupt and Fischer have studied propene polymerization kinetics using the achiral, nonstereoselective (aspecific) $\text{Cp}_2\text{ZrCl}_2/\text{MAO}$ catalyst in the temperature range 0–60 °C, in toluene at the same propene partial pressure (2 bar).⁴⁹⁶ The total catalyst productivity increases by increasing the polymerization temperature (taking into account the higher propene concentration at lower temperature). At all the temperatures the authors observe that the maximum catalyst activity is reached within few seconds; hence, they conclude that there is no induction period and that the activation of the catalytic complex is very fast. For temperatures below 40 °C they observe a slow decrease of activity over a period of several hours, and at higher temperature there is a very rapid initial decay followed by a second deactivation process. They propose a two-step deactivation process in which the active centers C are deactivated through a reversible intermediate $I(1)$, followed by an irreversible process to form the inactive species $I(2)$:

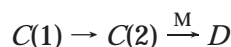


The irreversible process is introduced at the higher temperatures to account for the second slow decay. On the basis of this model, both processes are second-order with respect to the active sites.

Rempel investigated the kinetics of propene polymerization with the stereoselective system $\text{rac-C}_2\text{H}_4(1\text{-Ind})_2\text{ZrCl}_2/\text{MAO}$ in a gas-phase reactor aiming at studying the effect of [Zr], [Al]/[Zr], and temperature on the catalyst activity.⁴⁹⁵ The authors report that, also in this case, the polymerization rate reaches its maximum in a short time and then gradually decreases with reaction time. They conclude that there is no induction period at the beginning of the polymerization. The conclusion of their study is that polymerization temperature is the most important factor influencing polymerization kinetics, because the catalyst is less stable at higher temperature and deactivates faster. Higher level of [Al]/[Zr]

enhances the catalyst activity but shows no effect on catalyst deactivation. To explain their experimental results, the authors propose the existence of two types of active centers, species A(1) and A(2). Species A(1) is highly active but unstable at elevated temperature, while species A(2) is very stable but has low activity. Species A(1) can be irreversibly transformed into species A(2).

Vela Estrada and Hamielec⁴⁹⁷ as well as Chien and Wang⁴⁹⁸ investigated ethene polymerization again with the $\text{Cp}_2\text{ZrCl}_2/\text{MAO}$ catalytic system. Although ethene polymerization is out of the scope of this review, Hamielec's work is cited because he proposes a kinetic model for the deactivation that has been verified later also in the case of propene polymerization. The experimental data show that a higher deactivation takes place at a polymerization temperature of 50 °C with respect to 70 °C; moreover, always at 50 °C, GPC analysis shows a bimodal molecular weight distribution that the authors interpretate as the evidence of the existence of two catalyst site types. To justify these experimental findings they postulate a rapid initial formation of the active center type C(1) that in part are converted to a second type of active site C(2), which can deactivate through a bimolecular mechanism:



More recently, Rytter et al. investigated the polymerization of propene and the deactivation rates of $\text{Me}_2\text{Si}(1\text{-Ind})_2\text{ZrCl}_2/\text{MAO}$ and $\text{Me}_2\text{Si}(2\text{-Me-1-Ind})_2\text{ZrCl}_2/\text{MAO}$ as a function of [Zr], temperature (in the T_p range from 40 to 130 °C), and pressure (in the range 1–2.5 bar).⁴⁹³ The authors attempt to describe the polymerization profiles of both catalysts using different models described in the literature and discuss also their validity. Differently from most previous investigations, Rytter states the existence of an activation period, i.e., a period of increasing polymerization rate before maximum activity is reached, followed by a period of deactivation. About the activation period, on the basis of their experimental findings, they are able to discard possible causes such as the slow alkylation of the metallocene by MAO (reported in ref 499). In fact, the catalyst is allowed to react with MAO before being injected into the reactor; moreover, increasing the aging time of the catalyst/MAO solution or the activation temperature of the same solution does not shorten or remove the activation period observed during the polymerization. The explanation proposed is a slow rate of insertion of the first monomer unit in the Zr–methyl bond of the alkylated metallocene. Concerning deactivation, the authors took into account the hypothesis developed in the literature of the formation of latent and permanently deactivated sites. They combine in a very complete kinetic model the activation step, the polymerization, the deactivation, and the dependence of the different rate constants upon the temperature. The experimental and calculated polymerization rate profiles of $\text{Me}_2\text{Si}(1\text{-Ind})_2\text{ZrCl}_2/\text{MAO}$ are well in agreement over the entire temperature range (40–130 °C), whereas the polymerization rate of $\text{Me}_2\text{Si}(2\text{-Me-1-}$

$\text{Ind})_2\text{ZrCl}_2/\text{MAO}$ is adequately described only over a limited temperature range. A possible deactivation mechanism is proposed: a reversible formation of latent deactivated sites, which is first-order with respect to propagating sites, and an irreversible formation of permanently deactivated sites, which is second-order with respect to propagating sites. A first-order formation of the permanently deactivated sites, rather than a second-order one, gives a better fit of the rate profiles of $\text{Me}_2\text{Si}(1\text{-Ind})_2\text{ZrCl}_2/\text{MAO}$ at higher temperature. A different hypothesis on the nature of the latent or dormant sites can be found in the literature. Busico et al.²⁵² estimated that more than 90% of the active sites are “trapped” in a dormant state by 2,1-propene insertion: this assumption requires that the deactivation rate should be monomer dependent. To verify this hypothesis Rytter et al. performed some experiments with interrupted monomer flow, and under these conditions the catalyst continues to deactivate, even when no polymerization occurs. That means that, at least for the catalysts and under the experimental conditions described by Rytter, monomer misinsertion cannot be the cause of rate decay, that is, the deactivation mechanism is monomer independent. Rytter observed that the rate of decay highly depends on the Zr concentration: at low Zr level the polymerization rate is quite constant versus polymerization time, and at high Zr level there is a fast decrease in polymerization rate during the first hour. Other studies show that the maximum activity increases by increasing catalyst concentration, but at the same time a more quick deactivation occurs.⁴⁹⁹ NMR studies^{484,485} have shown the existence of monomeric and dimeric metallocene/cocatalyst ion pairs in equilibrium, depending upon the catalyst concentration, the catalyst/cocatalyst ratio, the nature of the cocatalyst, and the temperature. MAO too is observed to affect activity.⁵⁰⁰ Rytter observed that at high MAO concentration the maximum activity is lower but the polymerization rate is more stable than at low MAO concentration. It is possible that if deactivation is caused by two metallocene molecules reacting to form a nonactive species, MAO can compete in this reaction and prevent the formation of deactivated sites.

After the kinetic study of propene polymerization with the aspecific $\text{Cp}_2\text{ZrCl}_2/\text{MAO}$ system, Mülhaupt widens the investigation to two *ansa*-zirconocenes (*rac*- $\text{C}_2\text{H}_4(1\text{-Ind})_2\text{ZrCl}_2$ and *rac*- $\text{C}_2\text{H}_4(\text{H}_4\text{-1-Ind})_2\text{ZrCl}_2$) aiming at investigating the effect of the addition of Lewis acids and bases on the activity of the catalytic system.⁵⁰⁰ The kinetic profiles found in the case of the two stereoselective catalysts are similar to those reported for the $\text{Cp}_2\text{ZrCl}_2/\text{MAO}$ system. In this paper he suggests that the reversible second-order deactivation may result from zirconocene dimerization or disproportionation and that “MAO may be involved in the dynamic equilibrium between neutral dormant sites and cationic active sites”.⁵⁰⁰ The addition of Lewis acids or bases can influence these equilibria, affecting catalyst productivity but not the steric control.

D. Kinetic Models: Activity versus Monomer Concentration

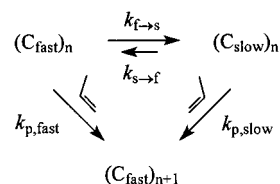
According to the Cossee mechanism, the two key steps in Ziegler–Natta polymerizations are monomer coordination and migratory insertion into the metal–polymer chain bond (Scheme 10). In analogy to heterogeneous Ziegler–Natta catalysis, a first-order reaction rate with respect to monomer concentration is generally *assumed* also for metallocene-based catalysts, that is,

$$R_p = k_p[C][M] \quad (3)$$

Equation 3, however, requires that monomer coordination is the rate-determining step. However, there are many observations which are very difficult to explain by a simple *single-site* Cossee mechanism, such as a reaction rate order higher than one reported for propene,^{113,230,232,417,428,441,467,501} ethene,⁵⁰¹ styrene,⁵⁰² and diene^{503,504} polymerizations.

To fit these observations, some authors^{113,501} have proposed that the active center can coordinate two monomer molecules. Ystenes, following a different approach, proposed a different model able to explain a reaction rate order higher than 1.^{203,505} This mechanism (dubbed the “trigger mechanism”) involves a transition state in which the insertion of a coordinated monomer is triggered by a second monomer. The main assumptions of this model are (i) the active site is never vacant, as a new monomer will coordinate to the site at the same time the previously coordinated monomer is inserted; (ii) the insertion will not proceed or will proceed more slowly in the absence of the new monomer unit; (iii) in the transition state two monomer units interact with each other and with the metal atom. On the basis of these assumptions, the propagation step must be first-order with respect to monomer concentration, but the number of active centers may be dependent on the monomer concentration, as a monomer unit is needed for the formation of an active center. Hence the overall polymerization rate can be anything between first- and second-order with respect to monomer concentration. This effect may disappear in the case of saturation (all the active centers are propagating) or of monomer diffusion control. The existence of physical limitations was one of the most typical explanations invoked for the deviation from a linear dependence of the activity on monomer concentration. This kind of indirect reason, such as mass transfer or heat transfer, for propene polymerizations has been ruled out by careful experiments by Mülhaupt and co-workers,⁴⁶⁷ who pointed out that “equilibria involving the active species are responsible for this effect” and that “propene might be involved in an equilibrium between dormant and active sites”. Busico and co-workers,^{250,252} investigating the isospecific *rac*-C₂H₄(1-Ind)₂ZrCl₂/MAO system for propene polymerization, reported an effect of monomer concentration not only on the activity but also on the regioselectivity of the catalytic system. It is stated that it is the occurrence of regioirregular 2,1 insertions that slows down chain propagation. The active centers bearing a secondary growing chain would be

Scheme 46



trapped in a dormant state, because of higher steric hindrance to following primary insertion, that is, $^s k_p \ll ^p k_p$. It is difficult to consider this hypothesis as a general one, because a reaction order > 1 is observed also for the much more regioselective Me₂C(Cp)(Flu)-ZrCl₂ catalyst^{112,113,417,428} and for the *rac*-C₂H₄(1-Ind)₂-ZrCl₂/MAO catalyst, for which the total amount of secondary units appears to be constant with propene concentration. Resconi et al.^{232,418} proposed a model in which at the steady state the active center can be in two active states that differ for their monomer insertion or coordination rates. The main assumptions of this model are (i) the two states differ for their propagation rate constants (a faster propagating state C_{fast} and a slower one C_{slow}), (ii) the two states are interconverting and their interconversion does not involve the monomer, and (iii) monomer insertion transforms a slow center into a fast one (see Scheme 46).

According to this kinetic scheme, the propagation rate law results:

$$\frac{R_p}{[C]} = \frac{\left(k_{f \rightarrow s} + \frac{k_{p,fast} k_{s \rightarrow f}}{k_{p,slow}}\right)[M] + k_{p,fast}[M]^2}{\left(\frac{k_{f \rightarrow s} + k_{s \rightarrow f}}{k_{p,slow}} + [M]\right)} \quad (4)$$

A reaction rate order higher than 1 is due to the decrease of the concentration of the slower state as the monomer increases. The ability of this equation to reproduce the trends of the experimental activity depends on the relative value of the kinetic rate constants. It is worth noting that eq 4 converts to the first reaction order for $k_{s \rightarrow f} \geq k_{f \rightarrow s}$, or $k_{p,slow}[M] \gg k_{f \rightarrow s}$, $k_{s \rightarrow f}$, for which $R_p \approx k_{p,fast}[C][M]$.

On the other hand, eq 4 approaches the second reaction order, $R_p \approx k_{p,fast}[C][M]^2$, when $k_{p,fast}[M] \gg k_{f \rightarrow s} \gg k_{p,slow}[M] \gg k_{s \rightarrow f}$.

Hence, eq 4 corresponds to a reaction order higher than 1 on monomer concentration for $k_{p,fast}[M] > k_{f \rightarrow s} > k_{p,slow}[M] > k_{s \rightarrow f}$, that is, when the slower state of the catalytic center is of lower energy with respect to the faster one, and the interconversion rate between the fast and the slow state is intermediate between the fast and the slow chain propagation rates. Figure 48 shows three series of experimental activity data for propene polymerization, obtained with zirconocenes of three different symmetries, and their best fit to eq 4.

A possible set of kinetic constants relative to propene polymerization with the two catalytic systems Me₂Si(2-Me-Benz[e]ind)₂ZrCl₂/MAO and Me₂C(Cp)(9-Flu)ZrCl₂/MAO were derived on the basis of the suggested model. The kinetic scheme proposed requires two different alkene-free states of the cata-

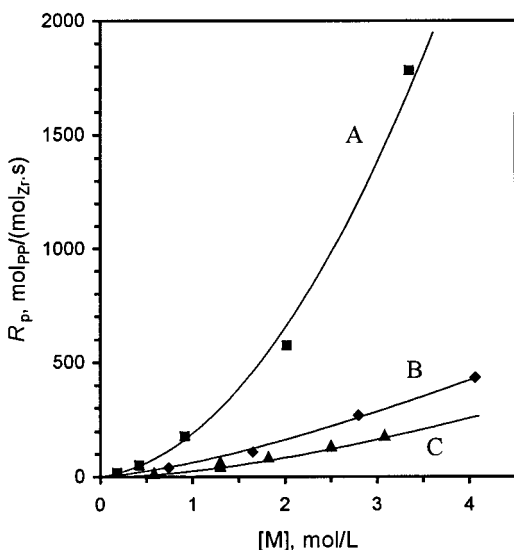


Figure 48. Experimental activity versus $[M]$ data for three stereoselective zirconocene/MAO catalysts, and their best fit to eq 4: A, $\text{Me}_2\text{Si}(2\text{-Me-Benz}[e]\text{ind})_2\text{ZrCl}_2/\text{MAO}$;⁴⁶⁷ B, $\text{Me}_2\text{C}(\text{Cp})(\text{Flu})\text{ZrCl}_2/\text{MAO}$;⁴¹⁷ C, $\text{Me}_2\text{C}(3\text{-PhCp})(\text{Flu})\text{ZrCl}_2/\text{MAO}$.⁴⁴¹

lyst active center: a higher energy state faster in monomer insertion and a lower energy state slower in monomer insertion. The authors give a possible interpretation of the nature of the two states, suggesting that they can differ in the conformation of the growing polymer chain. Several theoretical calculations have in fact indicated that the kinetic product of monomer insertion is a γ -hydrogen agostic intermediate, while the resting state has the β -hydrogen agostic interaction.

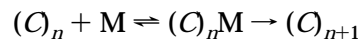
Other possibilities can be proposed to explain the nature of the slow state of an active polymerization center, which can be different for different catalytic systems, monomers, and experimental conditions. For instance, Richardson assumes an ion-pairing equilibrium between a metal–methyl cationic species and the counterion, which is in competition with initiation, but of course not with propagation.⁴⁵⁷ This assumption seems questionable especially for the common case of prevailing chain termination by β -hydrogen transfer to the monomer. In fact, in the latter case, an alkyl group with at least two carbon atoms (hence a steric requirement similar to that of the growing chain) is already coordinated to the metal center at the initiation step.

The same effect could be generated by a coordinated AlR_3 or neutral zirconocene species.^{506–508}

It is worth noting that, when β -transfer events are not negligible with respect to propagation, the slower state could correspond to initiation centers deriving from some kind of chain release that does not involve the monomer (e.g., a β -hydrogen transfer to the metal rather than to a coordinated monomer molecule). The occurrence of a nonlinear propagation rate law is discussed in ref 509.

Marques and co-workers considered the two limiting situations, a single monomer coordination and a double monomer coordination, and their combination.^{501,510,511} In the first case a two-step kinetic scheme is reported: the coordination of the monomer

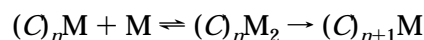
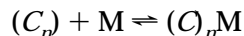
to the active species C (as an equilibrium with the free monomer) and the insertion step,



for which the overall reaction rate law is

$$R_p = A[M]/(1 + B[M]) \quad (5)$$

In the case of a double monomer coordination, the model requires three steps:



In this case the rate law is

$$R_p = A[M]^2/(1 + B[M] + C[M]^2) \quad (6)$$

They consider also a more general situation in which both singly and doubly coordinated complexes can exist, and both of them can be active in polymerization. The more complex rate law is

$$R_p = (A[M] + B[M]^2)/(1 + C[M] + D[M]^2) \quad (7)$$

The last equation was used to fit the experimental trend of activity versus monomer concentration with three different catalytic systems: the $[2\text{-}(N,N\text{-dimethyl)aminoethyl]cyclopentadienyl-TiCl}_3/\text{MAO}$ complex for ethene and propene polymerization, the $\text{rac-C}_2\text{H}_4(1\text{-Ind})_2\text{ZrCl}_2/\text{MAO}$ system, and the two analogues, $\text{Me}_2\text{Si}(\text{Benz}[e]\text{ind})_2\text{ZrCl}_2/\text{MAO}$ and $\text{Me}_2\text{Si}(2\text{-Me-Benz}[e]\text{ind})_2\text{ZrCl}_2/\text{MAO}$, for propene polymerization. In all three equations A , B , C , and D are apparent constants which are a combination of the real kinetic constants. The number of parameters that can be changed to fit the experimental curves is so high that almost every possible kind of curve can easily be reproduced. In the absence of a straight correlation between the value of the parameters and their physical meaning, the fitting of experimental results cannot prove the mechanism.

Recently Brintzinger et al.⁵¹² reconsidered the consistency of the trigger mechanism. Although molecular model considerations would suggest that for steric reasons is impossible to have two monomer units simultaneously coordinated to the metal, they evaluate the influence of a second propene molecule on the energy reaction path for the insertion of the propene ligand into the Zr-C bond. The calculations were made under certain assumptions: the $[(\text{C}_5\text{H}_5)_2\text{-Zr-Ethyl(propene)}]^+$ cation was chosen as a good compromise between computational time and a reasonable reliability as a model for the Zr-polymeryl active species. Moreover, the calculations are based on the assumption of a cationic species in vacuo rather than in a condensed medium and that the olefin insertion is the rate-determining step of the overall kinetics of polymerization. Two possible transition states are proposed, which differ for the presence in the second one of a propene unit approaching the reaction complex. The proximity of a second monomer unit decreases the activation energy for the insertion for the latter transition state. An interest-

ing feature of the proposed reaction sequence is the circumstance that the final insertion product has its next olefin already in place for the following insertion. The reaction rate law based on the mechanism proposed is

$$R_p = [C]_{\text{tot}}(A[M]^2 + B[M])/([M]^2 + C[M] + D) \quad (8)$$

Equation 8 predicts a reaction rate order between 1 and 2. The fitting of the turnover frequencies data for the system $\text{Me}_2\text{Si}(2\text{-Me-Benz}[e]\text{ind})_2\text{ZrCl}_2/\text{MAO}$ with eq 8 is adequate only for certain reciprocal values of the parameters, which turned out to be inconsistent with the kinetic scheme; hence, additional hypothesis and calculations will have to be worked out.

Recently Kaminsky et al. reported the results of the investigation of propene polymerization with C_1 -symmetric zirconocenes.⁴⁴¹ The three catalytic systems investigated, $\text{Me}_2\text{C}(3\text{-PhCp})(\text{Flu})\text{ZrCl}_2$, $\text{Me}_2\text{C}(3\text{-CyHexCp})(\text{Flu})\text{ZrCl}_2$, and $(\text{PhMe}_3\text{PenFlu})\text{ZrCl}_2$ (C_1 -I-17), all show a nonlinear dependence of activity on $[M]$, with reaction order between 1.4 and 1.5. This finding confirms the report of Fink on the hemiispecific zirconocene C_1 -I-6.⁴¹⁷

Hence, a reaction order on monomer concentration higher than 1 is a common feature for all stereoselective metallocenes. The exception to this rule is offered by the aspecific C_2 -symmetric catalysts, like Cp_2ZrCl_2 ⁴⁹⁶ and $\text{Me}_2\text{Si}(9\text{-Flu})_2\text{ZrCl}_2$,¹²³ that have activities that are first order in monomer concentration. At present, no definite explanation for this difference has been provided.

In light of the results discussed above, it appears that literature reports on the effect of polymerization conditions (such as temperature, Al/Zr ratio, cocatalyst, and solvent type) on chiral metallocene performance (not only activity but also stereo- and regio-regularity, propagation/transfer rates), unless obtained in liquid propene, should be taken with some precautions.

E. Activity versus Temperature

Studies of temperature effects on propene polymerization of a number of metallocene catalyst systems show that the stereoregularity, stereospecificity, and molecular weight of polypropene decrease with increasing polymerization temperature, whereas the polymerization activity increases.^{50,252,438,467,472,493,499} As discussed in the previous paragraphs, using experimental data of polymerization rate obtained at different temperature and different monomer concentration to calculate the activation energy of the propagation can alter the value of the true ΔE^\ddagger by neglecting the influence of monomer concentration on activity. Moreover, deactivation has different rates at different temperature. For these reasons data of activation energy for the same catalytic system obtained from polymerization runs performed under different conditions can be very different. Again, it must be stressed that, when comparing the polymerization performance of different zirconocene catalysts, the experiments must be performed under high and identical monomer concentrations, and prefer-

ably in liquid propene, to minimize the extent of chain-end epimerization and other parasitic reactions (see sections V and VII).

One of the earliest papers on kinetic investigation³⁰⁵ reported the study of propene polymerization with C_2 -I-1/MAO in a bubble reactor in the temperature range 15–65 °C. Kaminsky found that the activity has a linear dependence on monomer concentration at 35 °C in the propene concentration range 2–5 mol/L. Below 2 mol/L, the observed deviation from linearity is explained as due to mass-transfer control. In the same range the molecular weight also increases linearly by increasing monomer concentration. A first-order propagation rate was assumed and the authors calculate the activation energy for the polymerization process by plotting the logarithm of the propagation kinetic constant versus $1/T$. The diagram shows an abrupt deviation from linearity for temperature above 45 °C. Only the linear part of the diagram was used to determine the activation energy that resulted, 7.6 kcal/mol. Later Mülhaupt et al.⁴⁶⁷ investigated the influence of polymerization temperature on activity for propene polymerization with the two isospecific catalysts, $rac\text{-Me}_2\text{Si}(\text{Benz}[e]\text{ind})_2\text{ZrCl}_2$ (C_2 -I-24) and $rac\text{-Me}_2\text{Si}(2\text{-Me-Benz}[e]\text{ind})_2\text{ZrCl}_2$ (C_2 -I-25). Both catalysts show a dependence of activity on propene concentration of the same rate order of 1.7 and the same activity/time profile. Polymerization runs at 20, 40, and 60 °C at a total pressure of 2 bar were performed for both catalysts. $rac\text{-Me}_2\text{Si}(2\text{-Me-Benz}[e]\text{ind})_2\text{ZrCl}_2$ shows a very strong increase of activity with temperature, becoming faster than $rac\text{-Me}_2\text{Si}(\text{Benz}[e]\text{ind})_2\text{ZrCl}_2$ at 60 °C. This behavior agrees with Spaleck's observation that catalyst activity for the 2-methyl derivative is higher than that of the nonsubstituted catalyst at 70 °C in liquid propene.^{320,335} The maximum activity observed was used for the Arrhenius plot, giving a $\Delta E^\ddagger = 6.7$ kcal/mol for C_2 -I-24 and $\Delta E^\ddagger = 12.9$ kcal/mol for the 2-methyl derivative. The activation energy for C_2 -I-25 is surprisingly higher in comparison with the values for the C_2 -I-24 catalyst and $\text{Cp}_2\text{-ZrCl}_2$. Rytter investigated the same two catalytic systems,⁴⁹³ but to evaluate the activation energy, he used the averaged activity, determined by the amount of polymer produced during 1 h of polymerization. The experimental polymerization temperature range is wider (40–130 °C) with respect to that reported by Mülhaupt. Under this scenario the overall as well the maximum activity of C_2 -I-25 is always higher than that of C_2 -I-24. The activation energies for propagation calculated by Rytter are $\Delta E^\ddagger = 7.6$ kcal/mol for C_2 -I-24 and $\Delta E^\ddagger = 8.8$ kcal/mol for C_2 -I-25.

Recently Resconi et al.^{50,472} investigated the polymerization of propene with several C_2 -symmetric zirconocene/MAO catalysts in liquid monomer and in the temperature range 20–70 °C. The catalytic systems investigated are C_2 -I-1, C_2 -I-9, C_2 -I-31, C_2 -I-34, C_2 -I-35, and C_2 -I-36. The plot of $\ln(A/[M])$ versus $1/T_p$ gives the apparent activation energy values of the polymerization process, which are 11.4, 13.9, and 15 kcal/mol for the catalysts C_2 -I-1, C_2 -I-9, C_2 -I-31, respectively. For C_2 -I-34–36, a linear correlation in all the T_p range could not be obtained, due to reactor

fouling and, possibly, partial catalyst deactivation at the higher temperature. The same has been observed, for two C_1 -symmetric catalysts, by Kaminsky.⁴⁴¹ The value of activation energy = 11.4 kcal/mol found for C_2 -I-1/MAO is similar to the reported activation energy for propene polymerization with heterogeneous catalysts,²⁴⁵ which is in the range 10–13 kcal/mol and significantly higher than the value of 7.6 kcal/mol reported by Kaminsky under nonconstant monomer concentration conditions.³⁰⁵

F. Activity versus Solvent

As previously described and generally accepted, the active species in the polymerization of olefins with metallocene systems is an ion pair. It is clear that, depending on the polarity of the solvent, the strength of association of the ion pair can change, and hence, an effect on the activity of the catalytic system can be expected. There are several papers dealing with the solvent effect on the polymerization activity in polar solvent. In 1989 Oliva et al.⁵⁰² reported that, by polymerizing propene with the $Cp_2TiCl_2/Al(CH_3)_3/Al(CH_3)_2F$ system in CH_2Cl_2 , a conversion 100 times larger than in toluene was found. Several polymerization runs were performed at different compositions of the polymerization medium. Despite the strong effect on the activity, the stereochemical structure of the polymers obtained is quite the same in every case. The larger conversion observed in CH_2Cl_2 may be due to a larger amount of dissociated cationic species in a polymerization medium with a higher dielectric constant. The investigation was extended to an isospecific catalytic system (*rac*- $C_2H_4(H_4-1-Ind)_2-ZrCl_2/Al(CH_3)_3/Al(CH_3)_2F$ for propene polymerization. Changing the solvent from toluene to methylene chloride yielded a 10-fold increase of the polymerization rate. Both the titanocene and the zirconocene systems showed the same behavior in the different polymerization media.

Later Fink et al.^{74,489,513,514} studied propene polymerization with the syndiospecific $Me_2C(Cp)(9-Flu)-ZrCl_2/MAO$ and the isospecific $Me_2Si(1-Ind)_2ZrCl_2/MAO$ systems in toluene/methylene chloride solvent mixtures. In the case of the C_s -symmetric $Me_2C(Cp)(9-Flu)ZrCl_2$, increasing the dielectric constant of the solvent mixture increases the polymerization rate linearly, and in nearly pure CH_2Cl_2 a polymerization rate higher by a factor 6 than in pure toluene is observed. In the same range of toluene/methylene chloride composition, the *rrrr* pentads almost linearly decrease from 89% in pure toluene to 42% in pure CH_2Cl_2 , and consequently, the melting point of the polymer shifts from 143.7 to 47.4 °C. In the case of the isotactic $Me_2Si(1-Ind)_2ZrCl_2/MAO$, a similar enhancement of activity by increasing the polarity of the solvent is observed, but the stereoselectivity remains constant over the entire range of compositions. Hence, the stereospecificity of these catalysts is connected with the existence of a polarized Zr–Cl–Al complex (in toluene) or of a tight ion pair with a stereoregulating role of the counterion. The loss of stereoselectivity in polar solvents is caused by an isomerization of the solvent-separated zirconocene species via migration of the growing chain before the

next monomer insertion. But in the case of the C_2 -symmetric $Me_2Si(1-Ind)_2ZrCl_2/MAO$ system, the migration of the growing polymer chain causes no isomerization because the sites are identical by virtue of the C_2 symmetry. More recently Deffieux et al.⁴⁹¹ studied the polymerization of 1-hexene with C_2 -I-1/MAO system in solvents of different polarity (toluene, methylene chloride, and heptane). Polymerization kinetics was monitored by dilatometry. Also in this case a strong enhancement of the polymerization rate is observed in pure CH_2Cl_2 compared to that measured in pure toluene. The use of methylene chloride allows one to reduce the amount of MAO by a factor of 20 to reach the plateau of maximum activity. No effect on the stereoselectivity of the catalyst is observed. Again the increase of the activity is explained by an easier ionic dissociation of the Zr–X bond (X = Cl or CH_3), which increases the population of the cationic active species and to the low-coordinating power of the CH_2Cl_2 molecule. In this study it is reported that a preactivation of the catalyst in methylene chloride allows retention of the high activity also if the following step of polymerization is performed in toluene or heptane. Since the amount of CH_2Cl_2 used in the preactivation step is only about 5% of the total volume of polymerization, the activation effect cannot be interpreted as due to an increase of the polarity of the polymerization medium. The polymerization rate observed in toluene, after catalyst preformation in CH_2Cl_2 , is very close to the one found in pure methylene chloride. A strong improvement is found also for the polymerization in heptane by using the preactivation in polar solvents. This suggests that the active species are long-lived and, once formed, their concentration is quite insensitive to the nature of the polymerization medium. A possible explanation is that during the formation of the ionized metallocenium species assisted by MAO the chloride anion can be trapped by the cocatalyst and hence would be no more able to regenerate the starting inactive covalent species. A similar behavior was found by comparing ethene polymerization rate with the same catalytic system with and without preactivation in CH_2Cl_2 .

G. Molecular Weight

The molecular weight and molecular weight distribution are among the most important properties of a polymer, and this is true also for polymers that can have stereoregularity like polypropene, since a practical application can be found or foreseen for any polypropene tacticity, provided it has the *right molecular weight*.

This means that molecular weights must fit both performance and processability requirements, and for the most part this means viscosity average molecular weights in the range 40 000–300 000. The molecular weight of a polyolefin (here defined as the average degree of polymerization, \bar{P}_n) made with *single-center* metallocene catalysts (which operate by coordination polyinsertion mechanism) is given by

$$\bar{P}_n = \frac{\sum R_p}{\sum R_r}$$

That is, in terms of reaction rates, the molecular weight of polyolefins is given by the ratio between the overall rate of propagation (R_p) and the sum of all rates of chain release (R_r) reactions: this means that the molecular weight is dependent on the type of catalyst *and* the kinetics of the process, that is, the polymerization conditions (polymerization temperature, monomer concentration, catalyst/cocatalyst ratio). Hence, understanding the details of the mechanisms of chain release reactions is the key to molecular weight control in metallocene-catalyzed olefin polymerization. Here, chain release reactions (usually referred to as termination or transfer reactions) are all those steps that cause release of the polymer chain from the active catalyst, with the formation of a new initiating species (see section III.F).

Molecular weight measurements are far less sensitive to variables which are by their nature most affected by experimental error, such as catalyst amount or catalyst/monomer purity, and, more important, on the number of active centers, but are highly sensitive to the catalyst structure, monomer concentration, and polymerization temperature. Hence, reliable molecular weights can give much information on the nature of the active sites. Studies of this kind have been reported by Mülhaupt and Brintzinger⁴⁶⁷ on catalysts C_2 -I-**24** and **25**, by Kaminsky and Werner⁴⁴¹ on three C_1 -symmetric zirconocenes, and by Resconi and co-workers,^{50,229,230,232,472} who investigated the dependence of molecular weight on the type of ligand, the polymerization temperature, and the concentration of propene for the C_2 -symmetric zirconocenes C_2 -I-**1**, C_2 -I-**9**, C_2 -**18**, C_2 -**33**, C_2 -**35**, and C_2 -**36**.

The molecular masses of polypropenes obtained with metallocenes are clearly dependent on several factors. Among the most important substitution patterns are 2-alkyl and 3-alkyl substitutions. Methyl substituents on position 2 of the C_2 -symmetric skeleton have been shown to increase the molecular weights of the produced polymers considerably. A molecular modeling rationalization of this behavior has been proposed by Cavallo and Guerra.¹⁵⁴ Approximated transition state geometries for the β -hydrogen transfer to monomer with the $\text{Me}_2\text{Si}(\text{Benz}[e]\text{ind})_2$ ligand without and with a methyl group in position 2, are reported in Figure 49, parts A and B, respectively.

The short distances between the CH_2 groups of the growing chain and of the monomer with the methyl groups of the substituted $\text{Me}_2\text{Si}(\text{Benz}[e]\text{ind})_2$ ligand suggest that a repulsive interaction between the substituted ligand with the growing chain and monomer are present. This destabilizing interaction is clearly absent when the unsubstituted $\text{Me}_2\text{Si}(\text{Benz}[e]\text{ind})_2$ ligand is considered. In agreement with the results discussed in section IV.A, similar calculations performed on coordination intermediates for the propagation reaction indicated that the methyl groups in position 2 do not destabilize the insertion reaction.

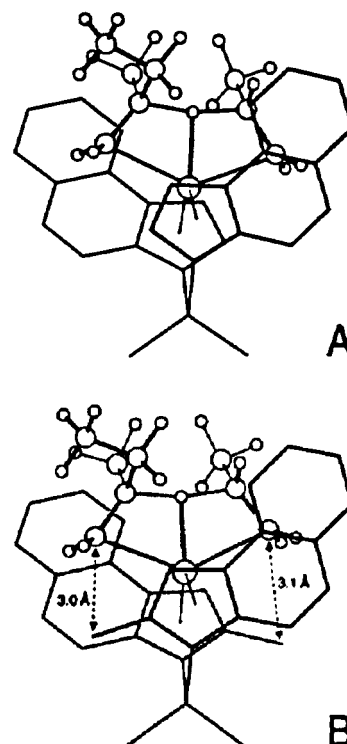


Figure 49. Approximated transition state geometries for the β -hydrogen transfer to the monomer reaction on the systems based on the $\text{Me}_2\text{Si}(\text{Benz}[e]\text{ind})_2\text{Zr}$ ligand (part A) and its 2-methyl-substituted derivative (part B). The growing-chain is on the left, while the propene monomer is on the right. Short distances in Å. Adapted from ref 154.

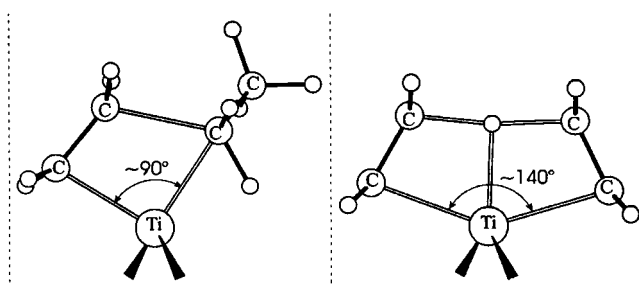


Figure 50. Transition state geometries for the insertion reaction of ethene into the Ti-ethyl σ -bond, on the left, and for the β -hydrogen transfer to the monomer reaction, on the right. The metal ligands, not shown for clarity, are Cp rings.¹⁷⁵

Hence, the only net effect is that methyl groups selectively destabilize the β -hydrogen transfer to monomer reaction, resulting in polymers with higher molecular weights.

This behavior is due to the very different geometries assumed by the transition states of the propagation reaction and of the β -hydrogen transfer to monomer. The first transition state assumes a compact four-center geometry, and the angle spanned by the reacting atoms is roughly 90° . On the contrary, the latter transition state corresponds to a bulkier six-center geometry, and the angle spanned by the reacting atoms is roughly 140° (Figure 50). Due to these geometrical differences, the β -hydrogen transfer to monomer reaction is much more space demanding and is easily destabilized by the steric pressure of substituents on the ligand, whereas the propagation reaction can smoothly occur also in smaller

Table 18. Summary of Kinetic Data for Selected Isospecific, *ansa*-Bisindenyl Zirconocenes

<i>rac</i> -zirconocene	$\Delta\Delta E^\ddagger$, (kcal/mol)	ref
Me ₂ C(1-Ind) ₂ ZrCl ₂	1.9 ± 0.1	50
C ₂ H ₄ (1-Ind) ₂ ZrCl ₂	3.9 ± 0.4	50
C ₂ H ₄ (4,7-Me ₂ -1-Ind) ₂ ZrCl ₂	1.6 ± 0.2	50
C ₂ H ₄ (3-Me-1-Ind) ₂ ZrCl ₂	4.1 ± 0.8	50
Me ₂ C(3-Me ₃ Si-1-Ind) ₂ ZrCl ₂	4.1 ± 0.3	50
Me ₂ C(3- <i>t</i> -Bu-1-Ind) ₂ ZrCl ₂	10.7 ± 0.4	50
H ₂ C(3- <i>t</i> -Bu-1-Ind) ₂ ZrCl ₂	11.2 ± 0.5	324

reactive pockets. This feature is relevant not only for the C₂-symmetric group 4 metallocenes but has been shown to be extremely effective also with ethene polymerization catalysts based on Ni^{141,515,516} and probably is also very relevant for the heterogeneous catalysts as well, due to the different coordination (octahedral) around the Ti atom, which clearly reduces the space available for the bulkier β-hydrogen transfer to monomer reaction.²¹³

On the other side, 3-alkyl substitution on bisindenyl systems has a strong influence on increasing the energy of β-H transfers, but for this class of metallocenes then β-methyl transfer becomes competitive. The net result is that these catalysts produce high molecular weight PP at the highest monomer concentrations but low molecular weights similar to the unsubstituted systems at the lower [M].

The ln(\bar{P}_n) versus 1/*T_p* plots give the overall activation energy barrier for chain release. The $\Delta\Delta E^\ddagger$ values for a series of C₂-symmetric zirconocenes are reported in Table 18. The higher energy barrier to transfer measured for C₂-I-35/MAO and C₂-I-36/MAO (10.7 and 11.2 kcal/mol, respectively) and the lower ones obtained from catalysts C₂-I-1, C₂-I-9, C₂-I-31, and C₂-I-33 have been attributed to the higher conformational freedom of the growing chain or the longer, more flexible C(3)–Si bond in C₂-I-33.

The analysis of the influence of monomer concentration on molecular weight is complicated by the competition between so many different chain release reactions, by the presence of two interconverting catalyst states, and by the onset of growing chain end isomerization reactions. Such an analysis is best done from end group structure analysis by ¹H NMR, but it requires of course relatively low molecular weight polymers, to be able to quantify the end groups. Such an analysis has been carried out so far on only a few systems (see Figure 51).^{131,230,231}

IX. Influence of Hydrogen

Molecular hydrogen is used to regulate the molecular weight of polyolefins in both heterogeneous^{247,517} and metallocene catalysts.^{83,248,249,252,467,518,519}

Hydrogen response in metallocene-catalyzed propene polymerization seems to be wide-ranging and reflects the strong dependence of the performance of metallocene catalysts on both their π-ligands structure and on the polymerization conditions. Addition of molecular hydrogen produces much different levels of molecular weight depression depending on the hydrogen level, the concentration of the monomer, the type of catalyst, and the polymerization temperature. In addition, hydrogen often shows an activat-

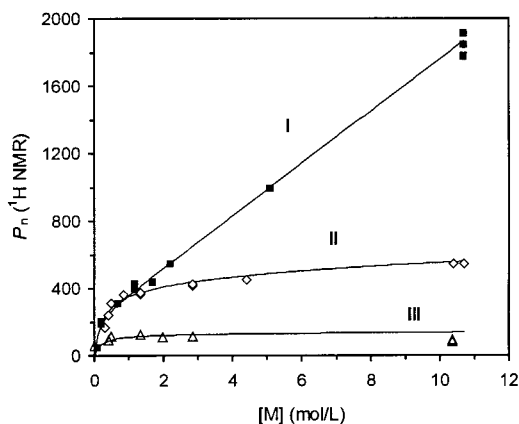
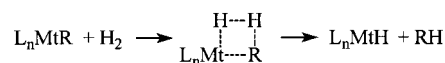


Figure 51. Average degree of polymerization (by ¹H NMR) as a function of [M]: I, *i*-PP from C₂-I-35/MAO; II, *i*-PP from C₂-I-1/MAO; III, *i*-PP from C₂-I-18/MAO. *T_p* = 50 °C.

Scheme 47



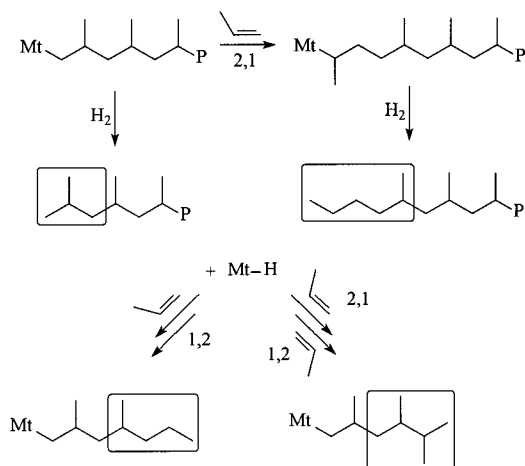
ing effect for both families of catalysts. Because of these two features, hydrogen has been often used for mechanistic studies. For example, high hydrogen pressures have been used to produce propene oligomers (in the so-called hydrooligomerization reaction^{83–86,250,251,520}) in order to determine the regiochemistry and stereochemistry of initiation and propagation. Pino applied the hydrooligomerization and deuteriooligomerization reactions, catalyzed by (–)-(R,R)-C₂H₄(H₄-1-Ind)₂ZrMe₂/MAO, to propene and other 1-olefins. By analyzing the structures of the propene oligomers and measuring their optical rotations, he was able to show that monomer insertion is largely predominantly primary, that after an occasional 2,1 insertion chain growth is terminated by hydrogen with formation of the *n*-butyl end group, and that the (R,R) catalyst enantiomer preferentially selects the *re* monomer enantioface.⁸³ This experimental observation enabled him to confirm the validity of Corradini's model, that is, to conclude that enantioface discrimination in chiral *ansa*-metallocenes arises from the steric interaction of the monomer with the growing chain in its chiral orientation, which in turn is determined by the chirality of the catalytic complex (see section III).

Activation can be moderate or quite substantial (up to 10-fold increase in catalyst productivity). The most likely mechanism of hydrogenolysis is the direct insertion of H₂ into the metal–carbon bond (Scheme 47).^{103,521–526}

However, since in a few instances H₂ (especially at the highest concentrations) has been shown to decrease catalyst activity,^{124,125} other mechanisms could be possible, for example hydrogenolysis of one Mt–Cp bond.^{523,525,527} The structures of saturated PP end groups that can be produced in the presence of hydrogen are shown in Scheme 48.

Two hypothesis have been described to explain the activating effect of hydrogen in propene polymerization with Ziegler–Natta catalysts: hydrogenation of a “dormant” secondary growing chain,^{248–252,518} or reactivation of a “torpid” allyl zirconocene.^{144,225,230,453,454,458}

Scheme 48



Tsutsui and Kashiwa described the influence of hydrogen on the catalytic efficiency of *rac*-C₂H₄(1-Ind)₂ZrCl₂/MAO in toluene at 30 °C and low propene concentration.^{248,249} On the basis of the strong activating effect of hydrogen on this catalyst, the presence of *n*-butyl end groups, and the disappearance of regioerrors, they concluded that the activation is due to hydrogenolysis of a secondary growing chain, which must then have a lower *k_p* compared to a primary growing chain, that is, *s**k_p* < *p**k_p*.

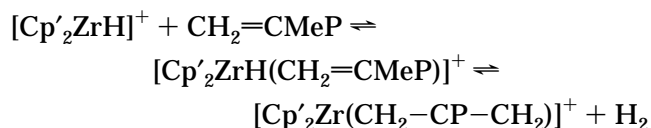
The same effect has been observed in 1-butene polymerization.⁵¹⁸

Analysis of the hydrogen effect on the more stereoselective zirconocenes *rac*-Me₂Si(Benz[*e*]ind)₂ZrCl₂ and *rac*-Me₂Si(2-Me-Benz[*e*]ind)₂ZrCl₂⁴⁶⁷ showed a limited catalyst activation (38 and 17% respectively, 0.35 bar H₂, 40 °C in toluene with 1.9 bar propene), a reduction of internal secondary units with formation of *n*-Bu end groups (in the expected 1:1 ratio to the *n*-Pr end group), and a quite strong hydrogen response in terms of molecular weight reduction, with *i*-PP from the most regioselective system (*rac*-Me₂-Si(2-Me-Benz[*e*]ind)₂ZrCl₂) having the strongest decrease (6-fold) of *P_n*. This strong molecular weight reduction, together with the reduction in regioerrors, is consistent with chain release to hydrogen at secondary growing chains being much faster than at primary chains for these two zirconocenes, since no isobutyl end groups were detectable. An appreciable amount of internal regioerrors can still be observed in the *i*-PP samples prepared in the presence of H₂ with both systems, showing that, at the low amount of hydrogen used, propene insertion into a secondary growing chain is still competitive with hydrogenolysis. The authors realized that catalyst activation is too low to account for the increase in *n*-butyl end groups and postulated two possibilities, that is, either the inequality of the rate constants of hydrogenolysis for secondary and primary growing chains or a reinitiation slower than propagation. A scenario considering a reaction similar to the latter hypothesis has been modeled and is discussed further on.

Carvill and co-workers⁵¹⁹ carried out a similar study on a broader set of zirconocenes, confirming the results of Mitsui and Kashiwa, and Jüngling and co-workers, and reached the same conclusion that the

extent of catalyst activation is not fully consistent with the amount of *n*-butyl end groups. Also the results of Lin and Waymouth (Table 19)³⁷² hint at the inadequacy of the secondary chain activation mechanism.

The second mechanism requires the formation of a zirconocene allyl complex, which is in turn formed from the Cp'₂ZrH(CH₂=CMeP), the product of β-H transfer after a primary insertion (see section V.C). This mechanism is more general, since it can work with any polymerization catalysts. Here, hydrogen activates the catalyst by converting the Mt(allyl) species, which have been shown to be effectively deactivated with respect to propene insertion,^{144,225,229} into Mt-H, that is, by shifting to the left the equilibria



Since in all cases H₂ generates Mt-H as the initiating species, the issue of propene insertion into the Mt-H bond deserves consideration. Some research groups have detected, under specific polymerization conditions and with zirconocenes of quite different regioselectivities, the presence of the 2,3-dimethylbutyl end group,⁵²⁸⁻⁵³¹ which must arise from a secondary propene insertion into the Zr-H bond (Scheme 48).

Moscardi has modeled the insertion of propene into the Zr-H bond and found that secondary propene insertion into the Zr-H bond with formation of the Zr(*i*-Pr) initiating species is indeed competitive with primary insertion, even on highly regioselective catalysts.⁵²⁹ This molecular modeling study has also shown that the Zr(*i*-Pr) initiating species is slower compared to Zr(*n*-Pr) with respect to the following propene insertion and that isomerization of Zr(*i*-Pr) to Zr(*n*-Pr) can follow a relatively low energy pathway by associative displacement with the monomer after β-H transfer on the Zr(*i*-Pr) species (Scheme 49).

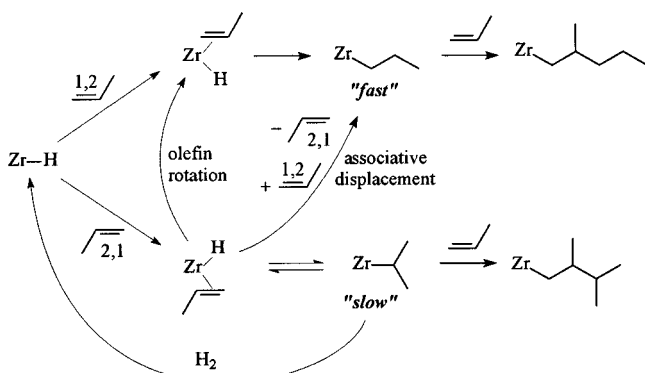
This scenario can explain, at least in part, the lower than expected catalyst activation by low hydrogen levels observed by some authors: hydrogenolysis reactivates both Zr-secondary growing chain and Zr(allyl) species with formation of Zr-H initiating species, but at the same time the activation is limited by the formation of secondary, slower Zr(*i*-Pr) initiating species, which require either isomerization to *n*-propyl or a new hydrogenolysis to be converted in the faster centers.

This mechanism explains why, for example, the 2,3-dimethylbutyl group is not observed at low propene concentrations (isomerization is faster than primary insertion into the Zr(*i*-Pr) species)^{252,519} or high hydrogen concentrations (hydrogenolysis is faster than primary insertion into the Zr(*i*-Pr) species),⁵²⁹ and also explains the lower than expected activating effect of hydrogen on systems which are not fully regioselective⁴⁶⁷ and the activation of highly regioselective systems such as the aspecific (Me₃Cp)₂ZrMe⁺²²⁵

Table 19. Influence of Hydrogen in Propene Polymerization with Bis(2-aryindenyl)zirconocene/MAO Catalysts³⁷²

catalyst ^a	hydrogen, mmol	activity, kg _{PP} /(mmol _{Zr} h)	relative activity	\bar{M}_n	% <i>mmmm</i> ^b	% 2,1 ^c
(2-Ph-Ind) ₂ ZrCl ₂	0	18	1	130 000	51	trace
(2-Ph-Ind) ₂ ZrCl ₂	2.6	39	2.2	12 000	28	0.1 (0.1)
(2-Ph-Ind) ₂ ZrCl ₂	3.9	111	6.1	12 000	25	nd (0.1)
[2-(3,5-(CF ₃) ₂ -Ph)-Ind] ₂ ZrCl ₂	0	3.7	1	68 000	70	0.2 (0.2)
[2-(3,5-(CF ₃) ₂ -Ph)-Ind] ₂ ZrCl ₂	2.6	13.0	3.5	8 000	64	nd (0.2)
[2-(3,5-(CF ₃) ₂ -Ph)-Ind] ₂ ZrCl ₂	3.9	42	11	6 000	56	nd (0.3)

^a Polymerization conditions: bulk, $T_p = 20\text{ }^\circ\text{C}$, $\text{Al}_{\text{MAO}}/\text{Zr} = 3000$, From ¹³C NMR. ^b The values are referred to the total methyl signals. ^c Total of internal regioerrors (total including end groups). nd = not detected (see section VII).

Scheme 49^a

^a Reprinted from ref 529. Copyright 1999 American Chemical Society.

and the isospecific *rac*-Me₂C(3-*t*-Bu-1-Ind)₂ZrCl₂/MAO.^{230,529}

However, the possibility that hydrogen reactivates other types of reversibly deactivated metal species (such as Mt–Mt dimers, Mt–Al complexes), should be always kept in mind. One might consider that all these mechanisms will operate to different extents, depending on the type of catalyst and the polymerization conditions.

Analysis of the unsaturated region of the ¹H NMR spectra of *i*-PP prepared with different chiral zirconocenes in the presence of hydrogen shows that H₂ addition suppresses the formation of internal vinylidenes,^{458,519} lending further support to the hypothesis of the allyl intermediate. We have also observed that the highly isospecific, but poorly regioselective, *rac*-Me₂Si(2-Me-4-Ph-1-Ind)₂ZrCl₂/MAO produces *i*-PP with roughly the same amount of 2,1 units with or without hydrogen, despite the fact that catalyst activity is increased by H₂ addition, and that ethene is inserted after a primary or a secondary unit without preference, showing that, for this catalyst system, a secondary growing chain is not a dormant site.

Apparently, also isotacticity is affected by hydrogen, and opposite results have been reported for different systems. Tsutsui and Kashiwa³⁰⁵ reported a slight decrease in stereoregularity, from 91.7 to 89.0% *mm* triads. A stronger, negative effect was found by Lin and Waymouth (Table 19).³⁷² No effect of hydrogen on isotacticity has been found in liquid propene at 50 °C with the *rac*-Me₂C(3-*t*-Bu-1-Ind)₂ZrCl₂/MAO catalyst system.⁵²⁹ Also Carvill reported that low hydrogen levels do not influence tacticity.⁵¹⁹ Opposite results have been reported for *rac*-C₂H₄(1-Ind)₂ZrCl₂/MAO and *rac*-Me₂Si(1-Ind)₂ZrCl₂/MAO un-

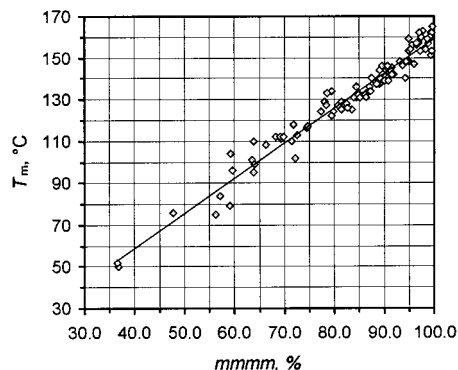


Figure 52. PP melting point as a function of isotactic pentad content. Data from our laboratories and from ref 295.

der very similar conditions (benzene, $[M] \sim 1.2\text{ mol/L}$, $T_p = 30, 60, 80\text{ }^\circ\text{C}$) to those employed by Kashiwa, but with a higher H₂ concentration.²⁵² This aspect of the influence of hydrogen clearly requires further investigation.

X. Outlook

Metallocene catalysts are emerging as a successful catalyst technology and, to our view, represent the future of polyolefins not only in the realm of specialty polymers but, in the long run, for improved performance commodities as well. However, in the case of highly crystalline *i*-PP, despite a general belief to the contrary, metallocene catalysts are far less active and efficient than the newest supported Ti/MgCl₂ catalysts and are unlikely to replace them in any foreseeable future. So, why use metallocenes to make *i*-PP? In one sentence, *because i-PP properties can be tailored!* For example, *i*-PP can be made from fully amorphous to highly crystalline and *anything* in between. This full control over the degree of isotacticity means control over crystallinity and melting point (Figure 52), which recently allowed the preparation of thermoplastic elastomers of varying degrees of crystallinity. Soon, some of these new PP grades will target applications typical of polystyrene and plasticized PVC.

In general, it seems likely that the success of metallocene catalysts for propene-based polymers, if any, will come from the production of materials that *cannot* be made with heterogeneous catalysts.

In terms of catalysis, there are several issues that still require investigation. One is, obviously, improving ligand design and synthesis to lower manufacturing costs, on one side, and improve molecular weight

control, on the other. Still, some mechanistic points need to be clarified, such as growing-chain-end isomerization reactions and their dependence on catalyst structure and polymerization conditions. Understanding the details of the mechanisms of regio- and stereoselectivity is the key to rational catalyst design. To achieve this goal, a full understanding of the mechanisms driving enantioface selectivity and chain growth/chain release processes is required. The details of catalyst–cocatalyst interactions, although well studied in model systems, are far from understood on the real catalysts, for example, on supported systems. Last but not least, catalyst activity will have to be improved: apparently, we have not yet reached the point of monomer diffusion limitations, even with the most active systems. To close on a positive note, we expect several more years of productive research in metallocene–PP.

XI. Acknowledgments

The development of metallocenes is the story of the successful collaboration between organic, organometallic, inorganic, theoretical, polymer, and material chemists (and patent attorneys and research managers, too!), and as for many other technological revolutions, has been based on teamwork, stimulating competition, and free scientific exchanges. It has been both the scientific challenge and getting to know the human being behind the scientists that have made these 15 years of research so exciting for us. We are deeply indebted to all our colleagues at the Montell Research Centers in Ferrara and Elkton, at the Shell Research Center in Amsterdam, and at the University of Naples and Salerno, and to John Bercaw, Hans-Herbert Brintzinger, Vincenzo Busico, Paolo Corradini, John Ewen, Umberto Giannini, Robert Grubbs, Gaetano Guerra, Richard Jordan, Ilya Nifant'ev, Robert Waymouth, Adolfo Zambelli, Tom Ziegler, and many other scientists, who, through both their published work and many personal discussions, provided us with the present state of understanding of these highly sophisticated catalyst systems. We also thank Isabella Camurati for the NMR analysis of the polypropenes discussed in this review, Pasquale Longo for the sample of chain-end-controlled *i*-PP, and Steve Miller and John Bercaw for a sample of *s*-PP. L.C. thanks the MURST of Italy for financial support (Grant PRIN98, "Polimerizzazione stereoselettiva: nuovi catalizzatori e nuovi materiali polimerici").

XII. References

- Herrmann, W. A.; Cornils, B. *Angew. Chem., Int. Ed. Engl.* **1997**, *36*, 1048.
- Thomas, J. M. *Angew. Chem., Int. Ed. Engl.* **1994**, *33*, 913.
- Metallocene-Catalyzed Polymers: Materials, Properties, Processing and Markets*; Benedikt, G. M., Goodall, B. L., Eds.; Plastics Design Library: New York, 1998.
- Wilkinson, G.; Birmingham, J. M. *J. Am. Chem. Soc.* **1954**, *76*, 4281.
- Natta, G.; Pino, P.; Mazzanti, G.; Giannini, U.; Mantica, E.; Peraldo, M. *J. Polym. Sci.* **1957**, *26*, 120.
- Breslow, D. S.; Newburg, N. R. *J. Am. Chem. Soc.* **1957**, *79*, 5072.
- Breslow, D. S.; Newburg, N. R. *J. Am. Chem. Soc.* **1959**, *81*, 81.
- Long, W. P. *J. Am. Chem. Soc.* **1959**, *81*, 5312.
- Long, W. P.; Breslow, D. S. *J. Am. Chem. Soc.* **1960**, *82*, 1953.
- Natta, G.; Mazzanti, G. *Tetrahedron* **1960**, *8*, 86.
- Breslow, D. S. U.S. Patent 2,924,593 to Hercules, 1960.
- Long, W. P.; Breslow, D. S. *Liebigs Ann. Chem.* **1975**, 463.
- Andresen, A.; Cordes, H. G.; Herwig, J.; Kaminsky, W.; Merck, A.; Mottweiler, R.; Pein, J.; Sinn, H.; Vollmer, H. *J. Angew. Chem., Int. Ed. Engl.* **1976**, *15*, 630.
- Sinn, H.; Kaminsky, W. *Adv. Organomet. Chem.* **1980**, *18*, 99.
- This is chemistry that must be treated with the greatest attention and always in the rigorous exclusion of air and moisture: aluminum alkyl compounds are pyrophoric, and AlMe₃ in particular is extremely flammable and cannot be handled without the proper precautions and protections.
- Kaminsky, W.; Arndt, M. *Adv. Polym. Sci.* **1997**, *127*, 143.
- Schnutenhaus, H.; Brintzinger, H.-H. *Angew. Chem., Int. Ed. Engl.* **1979**, *18*, 777.
- Wild, F.; Zsolnai, L.; Huttner, G.; Brintzinger, H.-H. *J. Organomet. Chem.* **1982**, *232*, 233.
- Wild, F.; Wasiucione, M.; Huttner, G.; Brintzinger, H.-H. *J. Organomet. Chem.* **1985**, *288*, 63.
- Ewen, J. A. In *Catalytic Polymerization of Olefins, Studies in Surface Science and Catalysis*; Keii, T., Soga, K., Eds.; Elsevier: New York, 1986; p 271.
- Giannetti, E.; Nicoletti, G.; Mazzocchi, R. *J. Polym. Sci. Polym. Chem.* **1985**, *23*, 2117.
- Ewen, J. A. *J. Am. Chem. Soc.* **1984**, *106*, 6355.
- Kaminsky, W.; Külper, K.; Brintzinger, H.; Wild, F. *Angew. Chem., Int. Ed. Engl.* **1985**, *24*, 507.
- Chirik, P. J.; Bercaw, J. E. In *Metallocenes: synthesis reactivity applications*; Togni, A., Halterman, R. L., Eds.; Wiley-VCH: Weinheim, 1998; p 111.
- Cardin, D. J.; Lappert, M. F.; Raston, C. L. *Chemistry of Organozirconium and -Hafnium Compounds*; Wiley: New York, 1986.
- Halterman, R. L. *Chem. Rev.* **1992**, *92*, 965.
- Halterman, R. L. In *Metallocenes: synthesis reactivity applications*; Togni, A., Halterman, R. L., Eds.; Wiley-VCH: Weinheim, 1998; p 455.
- McKnight, A. L.; Waymouth, R. M. *Chem. Rev.* **1998**, *98*, 2587.
- Okuda, J.; Eberle, T. In *Metallocenes: synthesis reactivity applications*; Togni, A., Halterman, R. L., Eds.; Wiley-VCH: Weinheim, 1998; p 415.
- Britovsek, G. J. P.; Gibson, V. C.; Wass, D. F. *Angew. Chem., Int. Ed.* **1999**, *38*, 428.
- We adopt the definition of *stereospecific polymerization* to refer to the process leading to a tactic (*stereoregular*) polymer produced with a *stereoselective* catalyst.³² The terms *stereoselective* (or *enantioselective*) and *regioselective* will also be used to refer to the single insertion event.³³ Given their widespread use, we will also use the terms *aspecific*, *isospecific*, and *syndiospecific*, referring to the type of enantioselectivity of a catalyst.
- Jenkins, A. D. *Pure Appl. Chem.* **1981**, *53*, 733.
- Muller, P. *Pure Appl. Chem.* **1994**, *66*, 1077.
- Gupta, V. K.; Satish, S.; Bhardwaj, I. S. *J. Macromol. Sci. Rev. Macromol. Chem. Phys.* **1994**, *439*, 439.
- Möhring, P. C.; Coville, N. J. *J. Organomet. Chem.* **1994**, *479*, 1.
- Brintzinger, H.-H.; Fischer, D.; Mülhaupt, R.; Rieger, B.; Waymouth, R. M. *Angew. Chem., Int. Ed. Engl.* **1995**, *34*, 1143.
- Reddy, S. S.; Sivaram, S. *Prog. Polym. Sci.* **1995**, *20*, 309.
- Huang, J.; Rempel, G. L. *Prog. Polym. Sci.* **1995**, *20*, 459.
- Coates, G. W.; Waymouth, R. M. In *Comprehensive Organometallic Chemistry II*; Wilkinson, G., Stone, F. G. A., Abel, W., Eds.; Pergamon Press: Oxford, 1995; Vol. 12, p 1193.
- Hlatky, G. G. in *Enc. Inorg. Chem.*; King, R. B., Ed.; Wiley: Chichester, 1994; Vol. 5, p 2728.
- Bochmann, M. *J. Chem. Soc., Dalton Trans* **1996**, 255.
- Kaminsky, W. *Macromol. Chem. Phys.* **1996**, *197*, 3907.
- Hamielec, A. E.; Soares, J. B. P. *Prog. Polym. Sci.* **1996**, *21*, 651.
- Mashima, K.; Nakayama, Y.; Nakamura, A. *Adv. Polym. Sci.* **1997**, *133*, 1.
- Metallocene-Based Polyolefins. Preparation, Properties and Technology*; Scheirs, J.; Kaminsky, W., Eds.; Wiley: New York, 1999.
- Ewen, J. A.; Elder, M. J.; Jones, R. L.; Haspeslagh, L.; Atwood, J. L.; Bott, S. G.; Robinson, K. *Makromol. Chem., Macromol. Symp.* **1991**, *48/49*, 253.
- van der Ven, S. *Study in Polymer Science, Polypropylene and other Polyolefins, Polymerization and Characterization*; Elsevier: Amsterdam, 1990; Vol. 7.
- Polypropylene Handbook*; Moore, E. P., Ed.; Hanser: Munich, 1996.
- Tattum, L. *Chem. Week* **1999**, S1–S21.
- Resconi, L.; Piemontesi, F.; Camurati, I.; Sudmeijer, O.; Nifant'ev, I. E.; Ivchenko, P. V.; Kuz'mina, L. G. *J. Am. Chem. Soc.* **1998**, *120*, 2308.
- Dang, V. A.; Yu, L.-C.; Balboni, D.; Dall'Occo, T.; Resconi, L.; Mercandelli, P.; Moret, M.; Sironi, A. *Organometallics* **1999**, *18*, 3781.
- Brintzinger, H.-H.; Bartell, L. J. *J. Am. Chem. Soc.* **1970**, *92*, 1105.
- Alcock, N. W. *J. Chem. Soc. A* **1967**, 2001.
- Petersen, J. L.; Dahl, L. F. *J. Am. Chem. Soc.* **1974**, *96*, 2248.

- (55) Green, M. L. H. *Pure Appl. Chem.* **1972**, *30*, 373.
- (56) Lauher, J. W.; Hoffmann, R. *J. Am. Chem. Soc.* **1976**, *98*, 1729.
- (57) Jordan, R. F. *Adv. Organomet. Chem.* **1991**, *32*, 325.
- (58) Lasserre, S.; Derouault, J. *Nouv. J. Chim.* **1983**, *7*, 659.
- (59) Sinn, H.; Bliemeister, J.; Clausnitzer, D.; Tikwe, L.; Winter, H.; Zarncke, O. In *Transition Metals and Organometallics as Catalysts for Olefin Polymerization*; Kaminsky, W., Sinn, H., Eds.; Springer-Verlag: Berlin, 1988.
- (60) Sinn, H. *Macromol. Symp.* **1995**, *97*, 27.
- (61) Cam, D.; Albizzati, E.; Giannini, U. *Makromol. Chem.* **1990**, *191*, 1641.
- (62) Sugano, T.; Matsubara, K.; Fujita, T.; Takahashi, T. *J. Mol. Catal.* **1993**, *82*, 93.
- (63) Mason, M. R.; Smith, J. M.; Bott, S. G.; Barron, A. R. *J. Am. Chem. Soc.* **1993**, *115*, 4971.
- (64) Harlan, C. J.; Mason, M. R.; Barron, A. R. *Organometallics* **1994**, *13*, 3, 2957.
- (65) Zakharov, I. I.; Zakharov, V. A.; Potapov, A. G.; Zhidomirov, G. M. *Macromol. Theory Simul.* **1999**, *8*, 272.
- (66) Tsutsui, T.; Yoshitsugu, K.; Ueda, T. Eur. Pat. Appl. 452,920 to Mitsui PC, 1991.
- (67) Resconi, L.; Galimberti, M.; Piemontesi, F.; Guglielmi, F.; Albizzati, E. U.S. Pat. 5,910,464 to Montell Technology Co., 1999.
- (68) Resconi, L.; Giannini, U.; Dall'Occo, T. In *Metalocene-Based Polyolefins*; Scheirs, J., Kaminsky, W., Eds.; Wiley: 1999; Vol. 1, p 69.
- (69) Dall'Occo, T.; Galimberti, M.; Resconi, L.; Albizzati, E.; Pennini, G. U.S. Pat. 5,849,653 to Montell Technology Co., 1998.
- (70) Chien, J. C. W.; Song, W.; Rausch, M. D. *Macromolecules* **1993**, *26*, 3239.
- (71) Ewen, J. A.; Elder, M. J. *Makromol. Chem., Macromol. Symp.* **1993**, *66*, 179.
- (72) Bochmann, M.; Lancaster, S. J.; Hursthouse, M. B.; Malik, K. M. A. *Organometallics* **1994**, *13*, 2235.
- (73) Chien, J.; Tsai, W.-M.; Rausch, M. *J. Am. Chem. Soc.* **1991**, *113*, 8570.
- (74) Herfert, N.; Fink, G. *Makromol. Chem. Rapid Commun.* **1993**, *14*, 91.
- (75) Yang, X.; Stern, C. L.; Marks, T. J. *J. Am. Chem. Soc.* **1991**, *113*, 3623.
- (76) Yang, X.; Stern, C. L.; Marks, T. J. *J. Am. Chem. Soc.* **1994**, *116*, 10015.
- (77) Tsai, W.-M.; Rausch, M. D.; Chien, J. C. W. *Appl. Organomet. Chem.* **1993**, *7*, 71.
- (78) Matsumoto, J.; Okamoto, T.; Watanabe, M.; Ishihara, N. Eur. Pat. Appl. 513,380 to Idemitsu, 1992.
- (79) Hanson, K. R. *J. Am. Chem. Soc.* **1966**, *88*, 2731.
- (80) Corradini, P.; Paiaro, G.; Panunzi, A. *J. Polym. Sci. Part C* **1967**, *16*, 2906.
- (81) Cahn, R. S.; Ingold, C.; Prelog, V. *Angew. Chem., Int. Ed. Engl.* **1966**, *5*, 385.
- (82) Prelog, V.; Helmchem, G. *Angew. Chem., Int. Ed. Engl.* **1982**, *21*, 567.
- (83) Pino, P.; Cioni, P.; Wei, J. *J. Am. Chem. Soc.* **1987**, *109*, 6189.
- (84) Pino, P.; Cioni, P.; Galimberti, M.; Wei, J.; Piccolrovazzi, N. In *Transition Metals and Organometallics as Catalysts for Olefin Polymerization*; Kaminsky, W., Sinn, H., Eds.; Springer-Verlag: Berlin, 1988; p 269.
- (85) Pino, P.; Galimberti, M. *J. Organomet. Chem.* **1989**, *370*, 1.
- (86) Pino, P.; Galimberti, M.; Prada, P.; Consiglio, G. *Makromol. Chem.* **1990**, *191*, 1677.
- (87) Schlögl, K. *Top. Stereochem.* **1966**, *1*, 39.
- (88) Stanley, K.; Baird, M. C. *J. Am. Chem. Soc.* **1975**, *97*, 6598.
- (89) van der Leek, Y.; Angermund, K.; Reffke, M.; Kleinschmidt, R.; Goretzki, R.; Fink, G. *Chem. Eur. J.* **1997**, *3*, 585.
- (90) Cavallo, L.; Guerra, G.; Vacatello, M.; Corradini, P. *Macromolecules* **1991**, *24*, 1784.
- (91) Guerra, G.; Longo, P.; Cavallo, L.; Corradini, P.; Resconi, L. *J. Am. Chem. Soc.* **1997**, *119*, 4394.
- (92) Guerra, G.; Cavallo, L.; Moscardi, G.; Vacatello, M.; Corradini, P. *Macromolecules* **1996**, *29*, 4834.
- (93) Cossee, P. *Tetrahedron Lett.* **1960**, *17*, 12.
- (94) Cossee, P. *Tetrahedron Lett.* **1960**, *17*, 17.
- (95) Arlman, E. J.; Cossee, P. *J. Catal.* **1964**, *3*, 99.
- (96) Cossee, P. *J. Catal.* **1964**, *3*, 80. Cossee, P. In *The Stereochemistry of Macromolecules*; Ketley, A. D., Ed.; Marcel Dekker: New York, 1967; Vol. 1.
- (97) Allegra, G. *Makromol. Chem.* **1971**, *145*, 235.
- (98) Ivin, K. J.; Rooney, J. J.; Stewart, C. D.; Green, M. L. H.; Mahtab, R. *J. Chem. Soc., Chem. Commun.* **1978**, 604.
- (99) Dawoodi, Z.; Green, M. L. H.; Mtetwa, V. S. B.; Prout, K. *J. Chem. Soc., Chem. Commun.* **1982**, 1410.
- (100) Brookhart, M.; Green, M. L. H. *J. Organomet. Chem.* **1983**, *250*, 395.
- (101) Laverty, D. T.; Rooney, J. J. *J. Chem. Soc., Faraday Trans. 1* **1983**, *79*, 869.
- (102) Grubbs, R. H.; Coates, G. W. *Acc. Chem. Res.* **1996**, *29*, 85.
- (103) Nolan, S. P.; Marks, T. J. *J. Am. Chem. Soc.* **1989**, *111*, 8538.
- (104) Spencer, M. D.; Morse, P. M.; Wilson, S. R.; Girolami, G. S. *J. Am. Chem. Soc.* **1993**, *115*, 2057.
- (105) Wu, Z.; Jordan, R. F. *J. Am. Chem. Soc.* **1995**, *117*, 5867.
- (106) Casey, C. P.; Hallenbeck, S. L.; Pollock, D. W.; Landis, C. R. *J. Am. Chem. Soc.* **1995**, *117*, 9770.
- (107) Casey, C. P.; Hallenbeck, S. L.; Wright, J. M.; Landis, C. R. *J. Am. Chem. Soc.* **1997**, *119*, 9680.
- (108) Casey, C. P.; Fagan, M. A.; Hallenbeck, S. L. *Organometallics* **1998**, *17*, 287.
- (109) Witte, P. T.; Meetsma, A.; Hessen, B. *J. Am. Chem. Soc.* **1997**, *119*, 10561.
- (110) Lee, H.; Hascall, T.; Desrosiers, P. J.; Parkin, G. *J. Am. Chem. Soc.* **1998**, *120*, 5830.
- (111) Galakhov, M. V.; Heinz, G.; Royo, P. *Chem. Commun.* **1998**, 17.
- (112) Ewen, J. A.; Jones, R. L.; Razavi, A.; Ferrara, J. *J. Am. Chem. Soc.* **1988**, *110*, 6255.
- (113) Ewen, J. A.; Elder, M. J.; Jones, R. L.; Curtis, S.; Cheng, H. N. In *Catalytic Olefin Polymerization, Studies in Surface Science and Catalysis*; Keii, T., Soga, K., Eds.; Elsevier: New York, 1990; p 439.
- (114) Zambelli, A.; Locatelli, P.; Zannoni, G.; Bovey, F. A. *Macromolecules* **1978**, *11*, 923.
- (115) Resconi, L.; Abis, L.; Francisocono, G. *Macromolecules* **1992**, *25*, 6814.
- (116) Ewen, J. A.; Haspelslagh, L.; Elder, M. J.; Atwood, J. L.; Zhang, H.; Cheng, H. N. In *Transition Metals and Organometallics as Catalysts for Olefin Polymerization*; Kaminsky, W., Sinn, H., Eds.; Springer-Verlag: Berlin, 1988; p 281.
- (117) Cheng, H. N.; Ewen, J. A. *Makromol. Chem.* **1989**, *190*, 1931.
- (118) Ewen, J. A.; Elder, M. J.; Jones, R. L.; Curtis, S.; Cheng, H. N. *Stud. Surf. Sci. Catal.* **1990**, *56*, 439.
- (119) Resconi, L.; Piemontesi, F.; Francisocono, G.; Abis, L.; Fiorani, T. *J. Am. Chem. Soc.* **1992**, *114*, 1025.
- (120) Collins, S.; Gauthier, W. J.; Holden, D. A.; Kuntz, B. A.; Taylor, N. J.; Ward, D. G. *Organometallics* **1991**, *10*, 2061.
- (121) Winter, A.; Antberg, M.; Bachmann, B.; Dolle, V.; Küber, F.; Rohrmann, J.; Spaleck, W. Eur. Pat. Appl. 584,609 to Hoechst, 1994.
- (122) Chen, Y.-X.; Rausch, M. D.; Chien, J. C. W. *Macromolecules* **1995**, *28*, 5399.
- (123) Resconi, L.; Jones, R. L.; Rheingold, A. L.; Yap, G. P. A. *Organometallics* **1996**, *15*, 998.
- (124) Resconi, L.; Piemontesi, F.; Jones, R. L. In *Metalocene-catalyzed polymers. Properties, processing & markets*; Benedikt, G. M., Goodall, B. L., Eds.; Plastics Design Library: New York, 1998; p 43.
- (125) Resconi, L. In *Metalocene-Based Polyolefins. Preparation, Properties and Technology*; Kaminsky, W., Scheirs, J., Eds.; Wiley: 1999; Vol. 1, p 467.
- (126) Grassi, A.; Ammendola, P.; Longo, P.; Albizzati, E.; Resconi, L.; Mazzocchi, R. *Gazz. Chim. Ital.* **1988**, *118*, 539.
- (127) Kaminsky, W.; Ahlers, A.; Möller-Lindenhof, N. *Angew. Chem., Int. Ed. Engl.* **1989**, *28*, 1216.
- (128) Kaminsky, W. *Angew. Makromol. Chem.* **1986**, *145*, 149.
- (129) Zeigler, R.; Rychlicki, H.; Resconi, L.; Piemontesi, F.; Baruzzi, G. *Polym. Prepr. Am. Chem. Soc., Div. Polym. Chem.* **1997**, *38*, 847.
- (130) Resconi, L.; Piemontesi, F.; Camurati, I.; Balboni, D.; Sironi, A.; Moret, M.; Rychlicki, H.; Zeigler, R. *Organometallics* **1996**, *15*, 5046.
- (131) Resconi, L.; Camurati, I.; Sudmeijer, O. *Top. Catal.* **1999**, *7*, 145.
- (132) Randall, J. C. *Polymer Sequence Determination*; Academic Press: New York, 1977.
- (133) Bovey, F. A.; Mirau, P. A. *NMR of Polymers*; Academic Press: New York, 1996.
- (134) Farina, M. *Top. Stereochem.* **1987**, *17*, 1.
- (135) Tonelli, A. E. *NMR Spectroscopy and Polymer Microstructure: The Conformational Connection. Methods in Stereochemical Analysis*; Marchand, A. P., Ed.; VCH: New York, 1989.
- (136) Heatley, F.; Zambelli, A. *Macromolecules* **1969**, *2*, 618.
- (137) Singh, U. C.; Kollmann, P. A. *J. Comput. Chem.* **1986**, *7*, 718.
- (138) Field, M. J.; Bash, P. A.; Karplus, M. *J. Comput. Chem.* **1990**, *11*, 700.
- (139) Maseras, F.; Morokuma, K. *J. Comput. Chem.* **1995**, *16*, 1170.
- (140) Froese, R. D. J.; Musaev, D. G.; Morokuma, K. *J. Am. Chem. Soc.* **1998**, *120*, 1581.
- (141) Deng, L.; Woo, T. K.; Cavallo, L.; Margl, P.; Ziegler, T. *J. Am. Chem. Soc.* **1997**, *119*, 6177.
- (142) Woo, T. K.; Cavallo, L.; Ziegler, T. *Theor. Chem. Acc.* **1998**, *100*, 307.
- (143) Cavallo, L.; Woo, T. K.; Ziegler, T. *Can. J. Chem.* **1998**, *76*, 1457.
- (144) Margl, P. M.; Woo, T. K.; Ziegler, T. *Organometallics* **1998**, *17*, 4997.
- (145) Guerra, G.; Longo, P.; Corradini, P.; Cavallo, L. *J. Am. Chem. Soc.* **1999**, *121*, 8651.
- (146) Kawamura-Kuribayashi, H.; Koga, N.; Morokuma, K. *J. Am. Chem. Soc.* **1992**, *114*, 2359.
- (147) Castonguay, L. A.; Rappé, A. K. *J. Am. Chem. Soc.* **1992**, *114*, 5832.

- (148) Axe, F. U.; Coffin, J. M. *J. Phys. Chem.* **1994**, *98*, 2567.
- (149) Weiss, H.; Ehrig, M.; Ahlrichs, R. *J. Am. Chem. Soc.* **1994**, *116*, 4919.
- (150) Jensen, V. D.; Børve, K. J. *J. Comput. Chem.* **1998**, *19*, 947.
- (151) Bierwagen, E. P.; Bercaw, J. E.; Goddard, W. A., III *J. Am. Chem. Soc.* **1994**, *116*, 1481.
- (152) Woo, T. K.; Fan, L.; Ziegler, T. *Organometallics* **1994**, *13*, 2252.
- (153) Yoshida, T.; Koga, N.; Morokuma, K. *Organometallics* **1995**, *14*, 746.
- (154) Cavallo, L.; Guerra, G. *Macromolecules* **1996**, *29*, 2729.
- (155) Kawamura-Kuribayashi, H.; Koga, N.; Morokuma, K. *J. Am. Chem. Soc.* **1992**, *114*, 8687.
- (156) Meier, R. J.; van Doremaele, G. H. J.; Iarlori, S.; Buda, F. *J. Am. Chem. Soc.* **1994**, *116*, 7274.
- (157) Margl, P.; Deng, L.; Ziegler, T. *Organometallics* **1998**, *17*, 933.
- (158) Ziegler, T.; Tschinke, V.; Versluis, L.; Baerends, E. J. *Polyhedron* **1988**, *7*, 1625.
- (159) Brookhart, M.; Green, M. L. H.; Wong, L. *Prog. Inorg. Chem.* **1988**, *36*, 1.
- (160) Crabtree, R. *Angew. Chem., Int. Ed. Engl.* **1993**, *32*, 789.
- (161) Crabtree, R. H.; Hamilton, D. G. *Adv. Organomet. Chem.* **1988**, *28*, 299.
- (162) Jordan, R. F.; LaPointe, R. E.; Bradley, P. K.; Baezinger, N. *Organometallics* **1989**, *8*, 2892.
- (163) Jordan, R. F.; Bradley, P. K.; Baenziger, N. C.; LaPointe, R. J. *J. Am. Chem. Soc.* **1990**, *112*, 1289.
- (164) Hlatky, G. G.; Turner, H. W.; Eckman, R. R. *J. Am. Chem. Soc.* **1989**, *111*, 2728.
- (165) Erker, G.; Fromberg, W.; Angermund, K.; Schlund, R.; Kruger, C. *J. Chem. Soc., Chem. Commun.* **1986**, 372.
- (166) Cayais, J. Z.; Babiain, E. A.; Hrcir, D. C.; Bott, S. G.; Atwood, J. L. *J. Chem. Soc., Dalton Trans.* **1986**, 2743.
- (167) Obara, S.; Koga, N.; Morokuma, K. *J. Am. Chem. Soc.* **1984**, *106*, 4625.
- (168) Obara, S.; Koga, N.; Morokuma, K. *J. Organomet. Chem.* **1984**, *270*, C33.
- (169) Lohrenz, J. C. W.; Woo, T. K.; Ziegler, T. *J. Am. Chem. Soc.* **1995**, *117*, 2793.
- (170) Jolly, C. A.; Marynick, D. S. *J. Am. Chem. Soc.* **1989**, *111*, 7968.
- (171) Thorshaug, K.; Støvneng, J. A.; Rytter, E.; Ystenes, M. *Macromolecules* **1998**, *31*, 7149.
- (172) Fusco, R.; Longo, L.; Masi, F.; Garbassi, F. *Macromolecules* **1997**, *30*, 7673.
- (173) Fusco, R.; Longo, L.; Proto, A.; Masi, F.; Garbassi, F. *Macromol. Rapid Commun.* **1998**, *19*, 257.
- (174) Woo, T. K.; Fan, L.; Ziegler, T. *Organometallics* **1994**, *13*, 432.
- (175) Cavallo, L.; Moscardi, G. Unpublished results.
- (176) Margl, P.; Lohrenz, J. C. W.; Ziegler, T.; Blöchl, P. E. *J. Am. Chem. Soc.* **1996**, *118*, 4434.
- (177) Fan, L.; Harrison, D.; Woo, T. K.; Ziegler, T. *Organometallics* **1995**, *14*, 2018.
- (178) Rix, F. C.; Brookhart, M.; White, P. S. *J. Am. Chem. Soc.* **1996**, *118*, 4746.
- (179) Musaev, D. G.; Froese, R. D. J.; Svensson, M.; Morokuma, K. *J. Am. Chem. Soc.* **1997**, *119*, 367.
- (180) Casey, C. P.; Carpenetti II, D. W.; Sakurai, H. *J. Am. Chem. Soc.* **1999**, *121*, 9483.
- (181) Abrams, M. B.; Yoder, J. C.; Loeber, C.; Day, M. W.; Bercaw, J. E. *Organometallics* **1999**, *18*, 1389.
- (182) Karl, J.; Dahlmann, M.; Erker, G.; Bergander, K. *J. Am. Chem. Soc.* **1998**, *120*, 5643.
- (183) Blomberg, M. R.; Siegbahn, P. E.; Svensson, M. *J. Phys. Chem.* **1992**, *96*, 9794.
- (184) Sodupe, M.; Bauschlicher, C. W., Jr.; Langhoff, S. R.; Partridge, H. *J. Phys. Chem.* **1992**, *96*, 2118.
- (185) Fujimoto, H.; Yamasaki, T.; Mizutani, H.; Koga, N. *J. Am. Chem. Soc.* **1985**, *107*, 6157.
- (186) Shiga, A.; Kawamura, H.; Ebara, T.; Sasaki, T.; Kikuzono, Y. *J. Organomet. Chem.* **1989**, *366*, 95.
- (187) Proscen, M.-H.; Janiak, C.; Brintzinger, H.-H. *Organometallics* **1992**, *11*, 4036.
- (188) Janiak, C. *J. Organomet. Chem.* **1993**, *452*, 63.
- (189) Støvneng, J. A.; Rytter, E. *J. Organomet. Chem.* **1996**, *519*, 277.
- (190) Cruz, V. L.; A., M.-E.; Martinez-Salazar, J. *Polymer* **1996**, *37*, 1663.
- (191) Margl, P.; Deng, L.; Ziegler, T. *J. Am. Chem. Soc.* **1998**, *120*, 5517.
- (192) Fujimoto, H.; Koga, N.; Fukui, K. *J. Am. Chem. Soc.* **1981**, *103*, 7452.
- (193) Krauledat, H.; Brintzinger, H.-H. *Angew. Chem., Int. Ed. Engl.* **1990**, *29*, 1412.
- (194) Leclerc, M. K.; Brintzinger, H.-H. *J. Am. Chem. Soc.* **1995**, *117*, 1651.
- (195) Clawson, L.; Soto, J.; Buchwald, S. L.; Steigerwald, M. L.; Grubbs, R. H. *J. Am. Chem. Soc.* **1985**, *107*, 3377.
- (196) Leclerc, M. K.; Brintzinger, H.-H. *J. Am. Chem. Soc.* **1996**, *118*, 9024.
- (197) Piers, W. E.; Bercaw, J. E. *J. Am. Chem. Soc.* **1990**, *112*, 9406.
- (198) Grassi, A.; Zambelli, A.; Resconi, L.; Albizzati, E.; Mazzocchi, R. *Macromolecules* **1988**, *21*, 617.
- (199) Mizuno, A.; Tsutsui, T.; Kashiwa, N. *Polymer* **1992**, *33*, 254.
- (200) Guerra, G.; Cavallo, L.; Moscardi, G.; Vacatello, M.; Corradini, P. *J. Am. Chem. Soc.* **1994**, *116*, 2988.
- (201) Ziegler, T.; Folga, E.; Berces, A. *J. Am. Chem. Soc.* **1993**, *115*, 636.
- (202) Unpublished data from our laboratories.
- (203) Ystenes, M. *J. Catal.* **1991**, *129*, 383.
- (204) Blomberg, M. R.; Siegbahn, P. E.; Svensson, M. *J. Am. Chem. Soc.* **1992**, *114*, 6095.
- (205) Siegbahn, P. E. *J. Am. Chem. Soc.* **1993**, *115*, 5803.
- (206) Burger, B. J.; Thompson, M. E.; Cotter, W. D.; Bercaw, J. E. *J. Am. Chem. Soc.* **1990**, *112*, 1566.
- (207) Hajela, S.; Bercaw, J. E. *Organometallics* **1994**, *13*, 1147.
- (208) Alelyunas, Y. W.; Guo, Z.; LaPointe, R. E.; Jordan, R. F. *Organometallics* **1993**, *12*, 544.
- (209) Guo, Z.; Swenson, D.; Jordan, R. *Organometallics* **1994**, *13*, 1424.
- (210) Zakharov, V. A.; Bukatov, G. D.; Yermakov, Y. I. *Adv. Polym. Sci.* **1983**, *51*, 61.
- (211) Kashiwa, N.; Yoshitake, J. *Polym. Bull.* **1984**, *11*, 479.
- (212) Pino, P.; Rotzinger, B.; von Achenbach, E. *Makromol. Chem.* **1985**, *25*, 461.
- (213) Cavallo, L.; Guerra, G.; Corradini, P. *J. Am. Chem. Soc.* **1998**, *120*, 2428.
- (214) Tsutsui, T.; Mizuno, A.; Kashiwa, N. *Polymer* **1989**, *30*, 428.
- (215) Proscen, M.-H.; Brintzinger, H.-H. *Organometallics* **1997**, *16*, 3889.
- (216) Ayland, G. H.; Findley, T. J. V. *SI Chemical Data*, 2nd ed., Wiley: Australia, 1974.
- (217) Margl, P.; Deng, L.; Ziegler, T. *J. Am. Chem. Soc.* **1999**, *121*, 154.
- (218) Jeske, G.; Schock, L. E.; Swepston, P. N.; Schumann, H.; Marks, T. J. *J. Am. Chem. Soc.* **1985**, *107*, 8103.
- (219) Yang, X.; Jia, L.; Marks, T. J. *J. Am. Chem. Soc.* **1993**, *115*, 3392.
- (220) Yang, X.; Seyam, A. M.; Fu, P.-F.; Marks, T. J. *Macromolecules* **1994**, *27*, 4625.
- (221) Jia, L.; Yang, X.; Yang, S.; Marks, T. J. *J. Am. Chem. Soc.* **1996**, *118*, 1547.
- (222) Bunel, E.; Burger, B. J.; Bercaw, J. E. *J. Am. Chem. Soc.* **1988**, *110*, 976.
- (223) Watson, P. L.; Roe, D. C. *J. Am. Chem. Soc.* **1982**, *104*, 6471.
- (224) Eshuis, J. J. W.; Tan, Y. Y.; Teuben, J. H.; Renkema, J. *J. Mol. Catal.* **1990**, *62*, 277.
- (225) Eshuis, J. J. W.; Tan, Y. Y.; Meetsma, A.; Teuben, J. H.; Renkema, J.; Evens, G. G. *Organometallics* **1992**, *11*, 362.
- (226) Yang, X.; Stern, C. L.; Marks, T. J. *Angew. Chem., Int. Ed. Engl.* **1992**, *31*, 1375.
- (227) Mise, T.; Kageyama, A.; Miya, S.; Yamazaki, H. *Chem. Lett.* **1991**, 1525.
- (228) Sini, G.; Macgregor, S. A.; Eisenstein, O.; Teuben, J. H. *Organometallics* **1994**, *13*, 1049.
- (229) Resconi, L.; Fait, A.; Piemontesi, F.; Camurati, I.; Moscardi, G. Submitted for publication.
- (230) Camurati, I.; Fait, A.; Piemontesi, F.; Resconi, L.; Tartarini, S. *Transition Metal Catalysis in Macromolecular Design*; Boffa, L. S., Novak, B. M., Eds.; ACS Symposium Series 760; American Chemical Society: Washington, DC, in press.
- (231) Resconi, L. *Polym. Mater. Sci. Eng.* **1999**, *80*, 421.
- (232) Resconi, L.; Fait, A.; Piemontesi, F.; Colonna, M.; Rychlicki, H.; Zeigler, R. *Macromolecules* **1995**, *28*, 6667.
- (233) Jüngling, S.; Mülhaupt, R.; Stehling, U.; Brintzinger, H.-H.; Fischer, D.; Langhauser, F. *J. Polym. Sci.: Part A: Polym. Chem.* **1995**, *33*, 1305.
- (234) Schneider, M. J.; Mülhaupt, R. *Macromol. Chem. Phys.* **1997**, *198*, 1121.
- (235) Zambelli, A.; Sacchi, M. C.; Locatelli, P.; Zannoni, G. *Macromolecules* **1982**, *15*, 211.
- (236) Zambelli, A.; Locatelli, P.; Sacchi, M. C.; Tritto, I. *Macromolecules* **1982**, *15*, 831.
- (237) Sacchi, M. C.; Shan, C.; Locatelli, P.; Tritto, I. *Macromolecules* **1990**, *23*, 383.
- (238) Sacchi, M. C.; Barsties, E.; Tritto, I.; Locatelli, P.; Brintzinger, H.-H.; Stehling, U. *Macromolecules* **1997**, *30*, 3955.
- (239) Chien, J. C. W.; Kuo, C.-I. *J. Polym. Sci.: Part A: Polym. Chem.* **1986**, *24*, 1779.
- (240) Chien, J. C. W.; Wang, B. P. *J. Polym. Sci., A: Polym. Chem.* **1988**, *26*, 3089.
- (241) Chien, J. C. W.; Razavi, A. *J. Polym. Sci., A: Polym. Chem.* **1988**, *26*, 3269.
- (242) Chien, J. C. W.; Wang, B. P. *J. Polym. Sci., A: Polym. Chem.* **1990**, *28*, 15.
- (243) Resconi, L.; Bossi, S.; Abis, L. *Macromolecules* **1990**, *23*, 4489.
- (244) Naga, N.; Mizunuma, K. *Polymer* **1998**, *39*, 5059.
- (245) Kissin, Y. V. *Isospecific Polymerization of Olefins*; Springer-Verlag: New York, 1985.
- (246) Hayashi, T.; Inoue, Y.; Chūjō, R.; Asakura, T. *Macromolecules* **1988**, *21*, 2675.

- (247) Chadwick, J. C.; Morini, G.; Albizzati, E.; Balbontin, G.; Mingozzi, I.; Cristofori, A.; Sudmeijer, O.; van Kessel, G. M. M. *Macromol. Chem. Phys.* **1996**, *197*, 2501.
- (248) Tsutsui, T.; Kashiwa, N.; Mizuno, A. *Makromol. Chem., Rapid Commun.* **1990**, *11*, 565.
- (249) Kashiwa, N.; Kioka, M. *Polym. Mater. Sci. Eng.* **1991**, *64*, 43.
- (250) Busico, V.; Cipullo, R.; Corradini, P. *Makromol. Chem., Rapid Commun.* **1993**, *14*, 97.
- (251) Busico, V.; Cipullo, R.; Corradini, P. *Makromol. Chem.* **1993**, *194*, 1079.
- (252) Busico, V.; Cipullo, R.; Chadwick, J. C.; Modder, J. F.; Sudmeijer, O. *Macromolecules* **1994**, *27*, 7538.
- (253) Margl, P. M.; Woo, T. K.; Blöchl, P. E.; Ziegler, T. *J. Am. Chem. Soc.* **1998**, *120*, 2174.
- (254) Lieber, S.; Proscenc, M.-H.; Brintzinger, H.-H. *Organometallics* **2000**, *19*, 377.
- (255) Teske, G.; Lauke, H.; Mauermann, H.; Schumann, H.; Marks, T. J. *J. Am. Chem. Soc.* **1985**, *107*, 8111.
- (256) Horton, A. D. *Organometallics* **1996**, *15*, 2675.
- (257) van der Heijden, H.; Hessen, B.; Orpen, A. G. *J. Am. Chem. Soc.* **1998**, *120*, 1112.
- (258) Corradini, P.; Barone, V.; Fusco, R.; Guerra, G. *Eur. Polym. J.* **1979**, *15*, 133.
- (259) Corradini, P.; Barone, V.; Fusco, R.; Guerra, G. *J. Catal.* **1982**, *77*, 32.
- (260) Corradini, P.; Barone, V.; Guerra, G. *Macromolecules* **1982**, *15*, 1242.
- (261) Corradini, P.; Barone, V.; Fusco, R.; Guerra, G. *Gazz. Chim. Ital.* **1983**, *113*, 601.
- (262) Corradini, P.; Guerra, G.; Barone, V. *Eur. Polym. J.* **1984**, *20*, 1177.
- (263) Corradini, P.; Guerra, G.; Vacatello, M.; Villani, V. *Gazz. Chim. It.* **1988**, *118*, 173.
- (264) Cavallo, L.; Guerra, G.; Oliva, L.; Vacatello, M.; Corradini, P. *Polym. Commun.* **1989**, *30*, 16.
- (265) Corradini, P.; Busico, V.; Guerra, G. In *Transition Metals and Organometallics as Catalysts for Olefin Polymerization*; Kaminsky, W., Sinn, H., Eds.; Springer-Verlag: Berlin, 1988; p 337.
- (266) Corradini, P.; Guerra, G. *Prog. Polym. Sci.* **1991**, *16*, 239.
- (267) Cavallo, L.; Corradini, P.; Guerra, G.; Vacatello, M. *Polymer* **1991**, *32*, 1329.
- (268) Cavallo, L.; Guerra, G.; Vacatello, M.; Corradini, P. *Chirality* **1991**, *3*, 299.
- (269) Corradini, P.; Guerra, G.; Cavallo, L.; Moscardi, G.; Vacatello, M. In *Ziegler Catalysts*; Fink, G., Müllhaupt, R., Brintzinger, H.-H., Eds.; Springer-Verlag: Berlin, 1995; p 237.
- (270) Guerra, G.; Corradini, P.; Cavallo, L.; Vacatello, M. *Makromol. Chem., Macromol. Symp.* **1995**, *89*, 307.
- (271) Cavallo, L.; Corradini, P.; Guerra, G.; Resconi, L. *Organometallics* **1996**, *15*, 2254.
- (272) Toto, M.; Cavallo, L.; Corradini, P.; Moscardi, G.; Resconi, L.; Guerra, G. *Macromolecules* **1998**, *31*, 3431.
- (273) Corradini, P.; Cavallo, L.; Guerra, G. In *Metallocene Catalysts*; Kaminsky, W., Scheirs, J., Eds.; Wiley: New York, 1999; Vol 2, p 3.
- (274) Hart, J. A.; Rappé, A. K. *J. Am. Chem. Soc.* **1993**, *115*, 6159.
- (275) Yoshida, T.; Koga, N.; Morokuma, K. *Organometallics* **1996**, *15*, 766.
- (276) Yu, Z. T.; Chien, J. C. W. *J. Polym. Sci.: Part A: Polym. Chem.* **1995**, *33*, 125.
- (277) Yu, Z. T.; Chien, J. C. W. *J. Polym. Sci.: Part A: Polym. Chem.* **1995**, *33*, 1085.
- (278) Longo, P.; Grassi, A.; Pellicchia, C.; Zambelli, A. *Macromolecules* **1987**, *20*, 1015.
- (279) Dahlmann, M.; Erker, G.; Nissinen, M.; Fröhlich, R. *J. Am. Chem. Soc.* **1999**, *121*, 2820.
- (280) Longo, P.; Proto, A.; Grassi, A.; Ammendola, P. *Macromolecules* **1991**, *24*, 4624.
- (281) Erker, G.; Nolte, R.; Aul, R.; Wilker, S.; Krüger, C.; Noe, R. *J. Am. Chem. Soc.* **1991**, *113*, 7594.
- (282) Gilchrist, J. H.; Bercaw, J. E. *J. Am. Chem. Soc.* **1996**, *118*, 12021.
- (283) Erker, G.; Korek, U.; Petrenz, R.; Rheingold, A. L. *J. Organomet. Chem.* **1991**, *421*, 215.
- (284) Erker, G.; Fritze, C. *Angew. Chem., Int. Ed. Engl.* **1992**, *31*, 199.
- (285) Hagihara, H.; Shiono, T.; Ikeda, T. *Macromol. Chem. Phys.* **1999**, *199*, 243.
- (286) Naga, N.; Mizunuma, K. *Polymer* **1998**, *39*, 2703.
- (287) De Candia, F.; Russo, R.; Vittoria, V. *Makromol. Chem.* **1988**, *189*, 815.
- (288) De Candia, F.; Russo, R. *Therm. Acta* **1991**, *177*, 221.
- (289) Venditto, V.; Guerra, G.; Corradini, P.; Fusco, R. *Polymer* **1990**, *31*, 530.
- (290) Hine, J. *J. Org. Chem.* **1966**, *31*, 1236.
- (291) Hine, J. *Adv. Phys. Org. Chem.* **1977**, *15*, 1977.
- (292) Grasmeyer, J. R. *Proceedings of New Plastics '98*; London; 1998.
- (293) Mehta, A. K.; Chen, M. C.; McAlpin, J. J. In *Metallocene-catalyzed polymers. Properties, processing & markets*; Benedikt, G. M., Goodall, B. L., Eds.; Plastics Design Library: New York, 1998.
- (294) Hu, Y.; Krejchi, M. T.; Shah, C. D.; Myers, C. L.; Waymouth, R. M. *Macromolecules* **1998**, *31*, 6908.
- (295) Dietrich, U.; Hackmann, M.; Rieger, B.; Klinga, M.; Leskelä, M. *J. Am. Chem. Soc.* **1999**, *121*, 4348.
- (296) Shelden, R. A.; Fueno, T.; Tsunetsugu, T.; Furukawa, J. *J. Polym. Sci., Polym. Lett. Ed.* **1965**, *3*, 23.
- (297) Lee, J.; Gauthier, W. J.; Ball, J.; Iyengar, B.; Collins, S. *Organometallics* **1992**, *11*, 2115.
- (298) Grossman, R.; Doyle, R. A.; Buchwald, S. *Organometallics* **1991**, *10*, 1501.
- (299) Diamond, G. M.; Jordan, R. F.; Petersen, J. L. *J. Am. Chem. Soc.* **1996**, *118*, 8024.
- (300) Piemontesi, F.; Camurati, I.; Resconi, L.; Balboni, D.; Sironi, A.; Moret, M.; Zeigler, R.; Piccolrovazzi, M. *Organometallics* **1995**, *14*, 1256.
- (301) Nifant'ev, I. E.; Ivchenko, P. V. *Organometallics* **1997**, *16*, 713.
- (302) Yang, Q.; Jensen, M. D. *Synlett* **1996**, *2*, 147.
- (303) Lisowsky, R. Eur. Pat. Appl. 669,340 to Witco, 1995.
- (304) Tsutsui, T.; Ishimaru, N.; Mizuno, A.; Toyota, A.; Kashiwa, N. *Polymer* **1989**, *30*, 1350.
- (305) Drögemüller, H.; Niedoba, S.; Kaminsky, W. *Polym. React. Eng.* **1986**, 299.
- (306) Doman, T. N.; Landis, C. R.; Bosnich, B. *J. Am. Chem. Soc.* **1992**, *114*, 7264.
- (307) Hollis, T. K.; Burdett, J. K.; Bosnich, B. *Organometallics* **1993**, *12*, 3385.
- (308) Doman, T. N.; Hollis, T. K.; Bosnich, B. *J. Am. Chem. Soc.* **1995**, *117*, 1352.
- (309) Höweler, U.; Mohr, R.; Knickmeier, M.; Erker, G. *Organometallics* **1994**, *13*, 2380.
- (310) Mise, T.; Miya, S.; Yamazaki, H. *Chem. Lett.* **1989**, 1853.
- (311) Mise, T.; Miya, S.; Yamazaki, H. In *Catalytic Olefin Polymerization, Studies in Surface Science and Catalysis*; Keii, T., Soga, K., Eds.; Kodansha-Elsevier: Tokyo, 1990; p 531.
- (312) Ushioda, T.; Fujita, H.; Saito, J. In *Proceeding of the Seventh International Business Forum on Specialty Polyolefins (SPO '97)*, Houston, TX, 1997; p 103 (available from Scotland Business Res., Skillman, NJ 08558).
- (313) Resconi, L.; Piemontesi, F.; Nifant'ev, I.; Ivchenko, P. PCT Int. Appl. WO 96/22995 to Montell, 1995.
- (314) Fischer, D.; Langhauser, F.; Schweire, G.; Brintzinger, H.-H.; Leyser, N. Int. Pat. Appl. WO 96/26211 to BASF, 1996.
- (315) Mengele, W.; Diebold, J.; Troll, C.; Röhl, W.; Brintzinger, H.-H. *Organometallics* **1993**, *12*, 1931.
- (316) Mansel, S.; Rief, U.; Proscenc, M.-H.; Kirsten, R.; Brintzinger, H.-H. *J. Organomet. Chem.* **1996**, *512*, 225.
- (317) Huttenloch, M. E.; Diebold, J.; Rief, U.; Brintzinger, H.-H.; Gilbert, A. M.; Katz, T. J. *Organometallics* **1992**, *11*, 3600.
- (318) Coughlin, E. B.; Bercaw, J. E. *J. Am. Chem. Soc.* **1992**, *114*, 7606.
- (319) Ihara, E.; Nodono, M.; Katsura, K.; Adachi, Y.; Yasuda, H.; Yamagashira, M.; Hashimoto, H.; Kanehisa, N.; Kai, Y. *Organometallics* **1998**, *17*, 3945.
- (320) Spaleck, W.; Küber, F.; Winter, A.; Rohrmann, J.; Bachmann, B.; Antberg, M.; Dolle, V.; Paulus, E. *Organometallics* **1994**, *13*, 954.
- (321) Rieger, B.; Reinmuth, A.; Röhl, W.; Brintzinger, H.-H. *J. Mol. Catal.* **1993**, *82*, 67.
- (322) Ewen, J. A. *Macromol. Symp.* **1995**, *89*, 181.
- (323) Miyake, S.; Okumura, Y.; Inazawa, S. *Macromolecules* **1995**, *28*, 3074.
- (324) Resconi, L.; Balboni, D.; Baruzzi, G.; Fiori, C.; Guidotti, S. *Organometallics* **2000**, *19*, 420.
- (325) Antberg, M.; Spaleck, W.; Rohrmann, J.; Luker, H.; Winter, A. U.S. Pat. 5,086,134 to Hoechst, 1992.
- (326) Cohen, S. A.; Cartwright, C. E. Poster P-44 presented at the ISHC 8, Amsterdam; 1992.
- (327) Han, T. K.; Woo, B. W.; Park, J. T.; Do, Y.; Ko, Y. S.; Woo, S. I. *Macromolecules* **1995**, *28*, 4801.
- (328) Herrmann, W. A.; Rohrmann, J.; Herdtweck, E.; Spaleck, W.; Winter, A. *Angew. Chem., Int. Ed. Engl.* **1989**, *28*, 1511.
- (329) Liang, B.; Li, Y.; Xie, G. *Macromol. Rapid Commun.* **1996**, *17*, 193.
- (330) Lofthuis, O. W.; Sledobnick, C.; Deck, P. A. *Organometallics* **1999**, *18*, 3702.
- (331) Ashe, A. J., III; Fang, X.; Kampf, J. W. *Organometallics* **1999**, *18*, 2288.
- (332) Reetz, M. T.; Willuhn, M.; Psiorz, C.; Goddard, R. *Chem. Commun.* **1999**, 1105.
- (333) Schaverien, C. J.; Ernst, R.; Terlouw, W.; Schut, P.; Sudmeijer, O.; Budzelaar, P. H. M. *J. Mol. Catal. A: Chem.* **1998**, *128*, 245.
- (334) Alt, H. G.; Jung, M. **1998**, *568*, 127.
- (335) Spaleck, W.; Antberg, M.; Rohrmann, J.; Winter, A.; Bachmann, B.; Kiprof, P.; Behm, J.; Herrmann, W. *Angew. Chem., Int. Ed. Engl.* **1992**, *31*, 1347.

- (336) Stehling, U.; Diebold, J.; Kirsten, R.; Röhl, W.; Brintzinger, H.-H.; Jüngling, S.; Mülhaupt, R.; Langhauser, F. *Organometallics* **1994**, *13*, 964.
- (337) Kashiwa, N.; Kojoh, S.; Imuta, J.; Tsutsui, T. In *Metalorganic Catalysts for Synthesis and Polymerization*; Kaminsky, W., Ed.; Springer-Verlag: Berlin, 1999; p 30.
- (338) Fukuoka, D.; Tashiro, T.; Kawaai, K.; Saito, J.; Ueda, T.; Kiso, Y.; Mizuno, A.; Kawasaki, M.; Itoh, M.; Imuta, J.; Fujita, T.; Nitabaru, M.; Yoshida, M.; Hashimoto, M. Eur. Pat. Appl. 629,632 to Mitsui Petrochemical, 1994.
- (339) Deng, H.; Winkelbach, H.; Taeji, K.; Kaminsky, W.; Soga, K. *Macromolecules* **1996**, *29*, 6371.
- (340) Winter, A.; Antberg, M.; Dolle, V.; Rohrmann, J.; Spaleck, W. Eur. Pat. Appl. to Hoechst, 1992.
- (341) Spaleck, W.; Antberg, M.; Aulbach, M.; Bachmann, B.; Dolle, V.; Haftka, S.; Küber, F.; Rohrmann, J.; Winter, A. In *Ziegler Catalysts*; Fink, G., Mülhaupt, R., Brintzinger, H.-H., Eds.; Springer-Verlag: Berlin, 1995; p 83.
- (342) Resconi, L.; Colonnesi, M.; Rychlicki, H.; Piemontesi, F.; Camurati, I. ISHC, 11th international symposium on homogeneous catalysis; p P 128, St Andrews, Scotland; 1998.
- (343) Maciejewski Petoff, J. L.; Agoston, T.; Lal, T. K.; Waymouth, R. M. *J. Am. Chem. Soc.* **1998**, *120*, 11316.
- (344) Ellis, W. W.; Hollis, T. K.; Odenkirk, W.; Whelan, J.; Ostrander, R.; Rheingold, A. L.; Bosnich, B. *Organometallics* **1993**, *12*, 4391.
- (345) Halterman, R. L.; Ramsey, T. M. *Organometallics* **1993**, *12*, 2879.
- (346) Schaverien, C.; Ernst, R.; Schut, P.; Skiff, W.; Resconi, L.; Barbassa, E.; Balboni, D.; Dubitsky, Y.; Orpen, A. G.; Mercandelli, P.; Moret, M.; Sironi, A. *J. Am. Chem. Soc.* **1998**, *120*, 9945.
- (347) Kato, T.; Uchino, H.; Iwama, N.; Imaeda, K.; Kashimoto, M.; Osano, Y.; Sugano, T. In *Metalorganic Catalysts for Synthesis and Polymerization*; Kaminsky, W., Ed.; Springer-Verlag: Berlin, 1999; p 192.
- (348) Halterman, R. L.; Tretyakov, A.; Combs, D.; Chang, J.; Khan, M. *Organometallics* **1997**, *16*, 3333.
- (349) Hitchcock, S. R.; Situ, J. J.; Covell, J. A.; Olmstead, M. M.; Nantz, M. H. *Organometallics* **1995**, *14*, 3732.
- (350) Schaverien, C. J.; Ernst, R.; van Loon, J.-D.; Dall'Occo, T. Eur. Pat. Appl. 941,997 to Montell, 1999.
- (351) Winter, A.; Rohrmann, J.; Antberg, M.; Spaleck, M.; Herrmann, W. A.; Riepl, H. Eur. Pat. Appl. 582,195 to Hoechst, 1993.
- (352) Barsties, E.; Schaible, S.; Prose, M.-H.; Rief, U.; Röhl, W.; Weyand, O.; Dorer, B.; Brintzinger, H.-H. *J. Organomet. Chem.* **1996**, *520*, 63.
- (353) Leino, R.; Luttikhedde, H. J. G.; Lehmus, P.; Wilén, C.-E.; Sjöholm, R.; Lehtonen, A.; Seppala, J.; Nasman, J. H. *Macromolecules* **1997**, *30*, 3477.
- (354) Leino, R.; Luttikhedde, H.; Wilén, C.-E.; Sillanpaa, R.; Nasman, J. H. *Organometallics* **1996**, *15*, 2450.
- (355) Ewen, J. A.; Jones, R. L.; Elder, M. J.; Rheingold, A. L.; Liable-Sands, L. M. *J. Am. Chem. Soc.* **1998**, *120*, 10786.
- (356) Ostoja Starzewski, K. A.; Kelly, W. M.; Stumpf, A.; Freitag, D. *Angew. Chem., Int. Ed. Engl.* **1999**, *38*, 2439.
- (357) Rieger, B. *Polym. Bull.* **1994**, *32*, 41.
- (358) Alt, H. G.; Zenk, R. *J. Organomet. Chem.* **1996**, *512*, 51.
- (359) Alt, H. G.; Milius, W.; Palackal, S. J. *Organomet. Chem.* **1994**, *472*, 113.
- (360) Erker, G.; Nolte, R.; Tsay, Y.-H.; Krüger, C. *Angew. Chem., Int. Ed. Engl.* **1989**, *28*, 628.
- (361) Erker, G.; Temme, B. *J. Am. Chem. Soc.* **1992**, *114*, 4004.
- (362) Erker, G.; Aulbach, M.; Knickmeier, M.; Wingbermuehle, D.; Krüger, C.; Nolte, M.; Werner, S. *J. Am. Chem. Soc.* **1993**, *115*, 4590.
- (363) Razavi, A.; Atwood, J. L. *J. Am. Chem. Soc.* **1993**, *115*, 7529.
- (364) Razavi, A.; Vereecke, D.; Peters, L.; Den Dauw, K.; Nafpliotis, L.; Atwood, J. L. In *Ziegler Catalysts*; Fink, G., Mülhaupt, R., Brintzinger, H.-H., Eds.; Springer-Verlag: Berlin, 1995; p 111.
- (365) Coates, G. W.; Waymouth, R. M. *Science* **1995**, *267*, 217.
- (366) Hauptman, E.; Waymouth, R. M.; Ziller, J. W. *J. Am. Chem. Soc.* **1995**, *117*, 11586.
- (367) Maciejewski Petoff, J. L.; Bruce, M. D.; Waymouth, R. M.; Masood, A.; Lal, T. K.; Quan, R. W.; Behrend, S. J. *Organometallics* **1997**, *16*, 5909.
- (368) Kravchenko, R.; Masood, A.; Waymouth, R. M. *Organometallics* **1997**, *16*, 3635.
- (369) Bruce, M. D.; Coates, G. W.; Hauptman, E.; Waymouth, R. M.; Ziller, J. W. *J. Am. Chem. Soc.* **1997**, *119*, 11174.
- (370) Bruce, M. D.; Waymouth, R. M. *Macromolecules* **1998**, *31*, 2707.
- (371) Kravchenko, R. L.; Masood, A.; Waymouth, R. M.; Myers, C. L. *J. Am. Chem. Soc.* **1998**, *120*, 2039.
- (372) Lin, S.; Waymouth, R. M. *Macromolecules* **1999**, *32*, 8283.
- (373) Tagge, C. D.; Kravchenko, R. L.; Lal, T. K.; Waymouth, R. M. *Organometallics* **1999**, *18*, 380.
- (374) Pietsch, M. A.; Rappé, A. K. *J. Am. Chem. Soc.* **1996**, *118*, 10908.
- (375) Cavallo, L.; Guerra, G.; Corradini, P. *Gazz. Chim. Ital.* **1996**, *126*, 463.
- (376) Coleman, B. D.; Fox, T. G. *J. Polym. Sci., Part A* **1963**, *1*, 3183.
- (377) Coleman, B. D.; Fox, T. G. *J. Chem. Phys.* **1963**, *38*, 1065.
- (378) Zambelli, A.; Locatelli, P.; Provasoli, A.; Ferro, D. R. *Macromolecules* **1980**, *13*, 267.
- (379) Inoue, Y.; Itabashi, Y.; Chūjō, R.; Doi, Y. *Polymer* **1984**, *25*, 1640.
- (380) *Thermoplastic Elastomers. A Comprehensive Review*; Legge, N. R.; Holden, G.; Schroeder, H. E., Eds.; Hanser: Munich, 1987.
- (381) Collette, J. W.; Tullock, C. W.; MacDonald, R. N.; Buck, W. H.; Su, A. C. L.; Harrell, J. R.; Mülhaupt, R.; Anderson, B. C. *Macromolecules* **1989**, *22*, 3851.
- (382) Tullock, C. W.; Tebbe, F. N.; Mülhaupt, R.; Ovenall, D. W.; Setterquist, R. A.; Ittel, S. D. *J. Polym. Sci. Part A: Polym. Chem.* **1989**, *27*, 3063.
- (383) Smith, C. Eur. Pat. Appl. 423,786 to Himont, 1991.
- (384) Ittel, S. *Am. Chem. Soc. Polym. Prepr.* **1994**, *35*, 665.
- (385) Chien, J. C. W.; Llinas, G. H.; Rausch, M. D.; Lin, Y.-G.; Winter, H. H. *J. Am. Chem. Soc.* **1991**, *113*, 8569.
- (386) Llinas, G. H.; Chien, J. C. W. *Polym. Bull.* **1992**, *28*, 41.
- (387) Chien, J. C. W.; Llinas, G. H.; Rausch, M. D.; Lin, Y.-G.; Winter, H. H.; Atwood, J. L.; Bott, S. G. *J. Polym. Sci.: Part A: Polym. Chem.* **1992**, *30*, 2601.
- (388) Babu, G. N.; Newmark, R. A.; Cheng, H. N.; Llinas, G. H.; Chien, J. C. W. *Macromolecules* **1992**, *25*, 7400.
- (389) Llinas, G. H.; Day, R. O.; Rausch, M. D.; Chien, J. C. W. *Organometallics* **1993**, *12*, 1283.
- (390) Fierro, R.; Chien, J. C. W.; Rausch, M. D. *J. Polym. Sci.: Part A: Polym. Chem.* **1994**, *32*, 2817.
- (391) Gauthier, W. J.; Collins, S. *Macromol. Symp.* **1995**, *98*, 223.
- (392) Gauthier, W. J.; Corrigan, J. F.; Taylor, N. J.; Collins, S. *Macromolecules* **1995**, *28*, 3771.
- (393) Gauthier, W. J.; Collins, S. *Macromolecules* **1995**, *28*, 3779.
- (394) Bravakis, A. M.; Bailey, L. E.; Pigeon, M.; Collins, S. *Macromolecules* **1998**, *31*, 1000.
- (395) Xin, S.; Mohammed, M.; Collins, S. *Polym. Mater. Sci. Eng.* **1999**, *80*, 441.
- (396) Tsvetkova, V. I.; Nedorezova, P. M.; Bravaya, N. M.; Savinov, D. V.; Dubnikova, I. L.; Optov, V. A. *Polym. Sci., Ser. A* **1997**, *39*, 235.
- (397) Balbontin, G.; Dainelli, D.; Galimberti, M.; Paganetto, G. *Makromol. Chem.* **1992**, *193*, 693.
- (398) Galambos, A.; Wolkowicz, M.; Zeigler, R. In *Catalysis in Polymer Synthesis*; ACS Symp. Ser. Vol. 496; Vandenberg, E. J., Salamone, J. C., Eds.; American Chemical Society: Washington, DC, 1992; p 104.
- (399) Lovinger, A. J.; Lotz, B.; Davis, D. D.; Padden, F. J. *Macromolecules* **1993**, *26*, 3494.
- (400) Sozzani, P.; Simonutti, R.; Galimberti, M. *Macromolecules* **1993**, *26*, 5782.
- (401) De Rosa, C.; Corradini, P. *Macromolecules* **1993**, *26*, 5711.
- (402) Rodriguez-Arnold, J.; Zhang, A.; Cheng, S. D. Z.; Lovinger, A.; Hsieh, E. T.; Chu, P.; Johnson, T. W.; Honnell, K. G.; Geerts, R. G.; Palackal, S. J.; Hawley, G. R.; Welch, M. B. *Polymer* **1994**, *35*, 1884.
- (403) Rodriguez-Arnold, J.; Bu, Z.; Cheng, S. Z. D.; Hsieh, E. T.; Johnson, T. W.; Geerts, R. G.; Palackal, S. J.; Hawley, G. R.; Welch, M. B. *Polymer* **1994**, *35*, 5194.
- (404) Lovinger, A. J.; Lotz, B.; Davis, D. D.; Schumacher, M. *Macromolecules* **1994**, *27*, 6603.
- (405) De Rosa, C.; Auriemma, F.; Vinti, V.; Galimberti, M. *Macromolecules* **1998**, *31*, 6206.
- (406) Rodriguez-Arnold, J.; Bu, Z.; Cheng, S. Z. D. *J. Macromol. Sci. Rev. Macromol. Chem. Phys.* **1995**, *C35*, 117.
- (407) Shiomura, T.; Kohno, M.; Inoue, N.; Asanuma, T.; Sugimoto, R.; Iwatani, T.; Uchida, O.; Kimura, S.; Harima, S.; Zenkoh, H.; Tanaka, E. *Macromol. Symp.* **1996**, *101*, 289.
- (408) Shiomura, T.; Kohno, M.; Inoue, N.; Yokote, Y.; Akiyama, M.; Asanuma, T.; Sugimoto, R.; Kimura, S.; Abe, M. In *Catalyst Design for Tailor-Made Polyolefins, Studies in Surface Science Catalysis Vol. 89*; Soga, K., Terano, M., Eds.; Elsevier: Amsterdam, 1994; p 327.
- (409) Farina, M.; Terragni, A. *Makromol. Chem., Rapid Commun.* **1993**, *14*, 791.
- (410) Mislow, K.; Raban, M. *Top. Stereochem.* **1967**, *2*, 1.
- (411) Herzog, T. A.; Zubris, D. L.; Bercaw, J. E. *J. Am. Chem. Soc.* **1996**, *118*, 11988.
- (412) Veghini, D.; Henling, L. M.; Burkhardt, T. J.; Bercaw, J. E. *J. Am. Chem. Soc.* **1999**, *121*, 564.
- (413) Herrmann, W. A.; Rohrmann, J.; Herdtweck, E.; Spaleck, W.; Winter, A. *Angew. Chem., Int. Ed. Engl.* **1989**, *28*, 1511.
- (414) Razavi, A.; Atwood, J. L. *J. Organomet. Chem.* **1993**, *459*, 117.
- (415) Miller, S. A.; Bercaw, J. E. *217th American Chemical Society National Meeting Poster INOR 151*; Anaheim, CA; 1999.
- (416) Grisi, F.; Longo, P.; Zambelli, A.; Ewen, J. A. *J. Mol. Catal. A: Chem.* **1999**, *140*, 225.
- (417) Fink, G.; Herfert, N.; Montag, P. In *Ziegler Catalysts*; Fink, G., Mülhaupt, R., Brintzinger, H.-H., Eds.; Springer-Verlag: Berlin, 1995; p 159.
- (418) Fait, A.; Resconi, L.; Guerra, G.; Corradini, P. *Macromolecules* **1999**, *32*, 2104.
- (419) Patsidis, K.; Alt, H. G.; Milius, W.; Palackal, S. J. *Organomet. Chem.* **1996**, *509*, 63.

- (420) Spaleck, W.; Antberg, M.; Dolle, V.; Klein, R.; Rohrmann, J.; Winter, A. *New J. Chem.* **1990**, *14*, 499.
- (421) Antberg, M.; Dolle, V.; Klein, R.; Rohrmann, J.; Spaleck, W.; Winter, A. In *Catalytic Olefin Polymerization, Studies in Surface Science and Catalysis*; Keii, T., Soga, K., Eds.; Kodansha-Elsevier: Tokyo, 1990; p 501.
- (422) Green, M. L. H.; Ishihara, N. *J. Chem. Soc., Dalton Trans.* **1994**, 657.
- (423) Montag, P.; van der Leek, Y.; Angermund, K.; Fink, G. *J. Organomet. Chem.* **1995**, *497*, 201.
- (424) Kaminsky, W.; Engehausen, R.; Zoumis, K.; Spaleck, W.; Rohrmann, J. *Makromol. Chem.* **1992**, *193*, 1643.
- (425) Dolle, V.; Rohrmann, J.; Winter, A.; Antberg, M.; Klein, R. Eur. Pat. Appl. 399,347 to Hoechst, 1990.
- (426) Ewen, J. A.; Elder, M. J.; Harlan, C. J.; Jones, R. L.; Alwood, J. L.; Bott, S. G.; Robinson, K. *Am. Chem. Soc. Polym. Prepr.* **1991**, *32*, 469.
- (427) Farina, M.; Di Silvestro, G.; Sozzani, P. *Macromolecules* **1993**, *26*, 946.
- (428) Herfert, N.; Fink, G. *Makromol. Chem., Macromol. Symp.* **1993**, *66*, 157.
- (429) Rohrmann, J. Eur. Pat. Appl. 528,287 to Hoechst, 1993.
- (430) Although the *R, S* nomenclature used to characterize the chirality at the metal atom for the C_3 symmetric ligands can be used also for the C_1 symmetric ligands of this section, in this case we preferred the more mnemonic and explanatory notation according to which, the relative disposition of the ligands that presents the coordinated monomer in the more (less) crowded region, is referred to as "inward (outward) propene coordination".⁹²
- (431) Kleinschmidt, R.; Reffke, M.; Fink, G. *Macromol. Rapid Commun.* **1999**, *20*, 284.
- (432) Chen, Y.-X.; Rausch, M. D.; Chien, J. C. W. *J. Organomet. Chem.* **1995**, *497*, 1.
- (433) Ewen, J. A.; Elder, M. J. In *Ziegler Catalysts*; Fink, G., Mülhaupt, R., Brintzinger, H.-H., Eds.; Springer-Verlag: Berlin, 1995; p 99.
- (434) Giardello, M.; Eisen, M.; Stern, C. L.; Marks, T. J. *J. Am. Chem. Soc.* **1995**, *117*, 12114.
- (435) Obora, Y.; Stern, C. L.; Marks, T. J.; Nickias, P. N. *Organometallics* **1997**, *16*, 2503.
- (436) Spaleck, W.; Kuber, F.; Bachmann, B.; Fritze, C.; Winter, A. *J. Mol. Catal. A: Chem.* **1998**, *128*, 279.
- (437) Mallin, D. T.; Rausch, M. D.; Lin, Y.-G.; Dong, S.; Chien, J. C. W. *J. Am. Chem. Soc.* **1990**, *112*, 2030.
- (438) Rieger, B.; Jany, G.; Fawzi, R.; Steimann, M. *Organometallics* **1994**, *13*, 647.
- (439) Yoon, S. C.; Han, T. K.; Woo, B. W.; Song, H.; Woo, S. I.; Park, J. T. *J. Organomet. Chem.* **1997**, *534*, 81.
- (440) Thomas, E. J.; Chien, J. C. W.; Rausch, M. D. *Organometallics* **1999**, *18*, 1439.
- (441) Kaminsky, W.; Werner, R. In *Metalorganic Catalysts for Synthesis and Polymerization*; Kaminsky, W., Ed.; Springer-Verlag: Berlin, 1999; p 170.
- (442) Corey, E. J.; Bailar, J. C., Jr. *J. Am. Chem. Soc.* **1959**, *81*, 2620.
- (443) Schäfer, A.; Karl, E.; Zsolnai, L.; Huttner, G.; Brintzinger, H.-H. *J. Organomet. Chem.* **1987**, *328*, 87.
- (444) Busico, V.; Cipullo, R.; Talarico, G.; Segre, A. L.; Chadwick, J. C. *Macromolecules* **1997**, *30*, 4786.
- (445) Balbontin, G.; Fait, A.; Piemontesi, F.; Resconi, L.; Rychlicki, H. Poster 40 presented at STEPOL; Book of Abstracts p 205, Milano, Italy; June 1994.
- (446) Busico, V.; Cipullo, R. *Macromol. Symp.* **1995**, *89*, 277.
- (447) Schneider, M. J.; Kaji, E.; Uozumi, T.; Soga, K. *Macromol. Chem. Phys.* **1997**, *198*, 2899.
- (448) Busico, V.; Cipullo, R. *J. Am. Chem. Soc.* **1994**, *116*, 9329.
- (449) Busico, V.; Cipullo, R. *J. Organomet. Chem.* **1995**, *497*, 113.
- (450) Busico, V.; Brita, D.; Caporaso, L.; Cipullo, R.; Vacatello, M. *Macromolecules* **1997**, *30*, 3971.
- (451) Karol, F. J.; Kao, S.; Wasserman, E. P.; Brady, R. C. *New J. Chem.* **1997**, *21*, 797.
- (452) Wasserman, E. P.; Hsi, E.; Young, W.-T. *Am. Chem. Soc. Polym. Prepr.* **1998**, *39*, 425.
- (453) Guyot, A.; Spitz, R.; Journaud, C. *Am. Chem. Soc. Polym. Prepr.* **1994**, *35*, 671.
- (454) Guyot, A.; Spitz, R.; Journaud, C. In *Catalyst Design for Tailor-Made Polyolefins, Studies in Surface Catalysis Vol. 89*; Soga, K., Terano, M., Eds.; Elsevier: Amsterdam, 1994; p 43.
- (455) Horton, A. D. *Organometallics* **1992**, *11*, 3271.
- (456) Feichtinger, D.; Plattner, D. A.; Chen, P. *J. Am. Chem. Soc.* **1998**, *120*, 7125.
- (457) Richardson, D. E.; Alameddini, N. G.; Ryan, M. F.; Hayes, T.; Eyler, J. R.; Siedle, A. R. *J. Am. Chem. Soc.* **1996**, *118*, 11244.
- (458) Resconi, L. *J. Mol. Catal.* **1999**, *146*, 177.
- (459) Farina, M.; Di Silvestro, G.; Terragni, A. *Macromol. Chem. Phys.* **1995**, *196*, 353.
- (460) Bovey, F. A.; Tiers, G. V. D. *J. Polym. Sci.* **1960**, *44*, 173.
- (461) van der Burg, M.; Chadwick, J.; Sudmeijer, O.; Tulleken, H. *Makromol. Chem., Theory Simul.* **1993**, *2*, 399.
- (462) Busico, V.; Cipullo, R.; Monaco, G.; Vacatello, M.; Segre, A. L. *Macromolecules* **1997**, *30*, 6251.
- (463) Soga, K.; Shiono, T.; Takemura, S.; Kaminsky, W. *Makromol. Chem., Rapid Commun.* **1987**, *8*, 305.
- (464) Busico, V.; Cipullo, R.; Talarico, G.; Segre, A. L.; Caporaso, L. *Macromolecules* **1998**, *31*, 8720.
- (465) Caporaso, L.; Zappile, S.; Izzo, L.; Oliva, L. *XIV convegno italiano di macromolecole*; Salerno, Italy; September, 13–16, 1999.
- (466) Zambelli, A.; Longo, P.; Ammendola, P.; Grassi, A. *Gazz. Chim. Ital.* **1986**, *116*, 731.
- (467) Jüngling, S.; Mülhaupt, R.; Stehling, U.; Brintzinger, H.-H.; Fischer, D.; Langhauser, F. *J. Polym. Sci. A: Polym. Chem.* **1995**, *33*, 1305.
- (468) Kioka, M.; Tsutsui, T.; Ueda, T.; Kashiwa, N. In *Catalytic Olefin Polymerization, Studies in Surface Science and Catalysis*; Keii, T., Soga, K., Eds.; Elsevier: New York, 1990; p 483.
- (469) Ewen, J. A.; Zambelli, A.; Longo, P.; Sullivan, J. M. *Macromol. Rapid Commun.* **1998**, *19*, 71.
- (470) Razavi, A. J. *Macromol. Symp.* **1995**, *89*, 345.
- (471) The origin of this different result is difficult to rationalize. In fact, experimentally the 3-methyl-substituted catalyst is substantially aspecific (nonenantioselective) and highly regioselective,⁴⁷² and the high regioselectivity could suggest a high ΔE_{Regio} . However, all the aspecific catalysts are generally highly regioselective, as are those based on the bare biscyclopentadienyl ligand, for which a low steric contribution to ΔE_{Regio} has been calculated.^{91,155}
- (472) Resconi, L.; Piemontesi, F.; Camurati, I.; Rychlicki, H.; Colonnesi, M.; Balboni, D. *Polym. Mater. Sci. Eng.* **1995**, *73*, 516.
- (473) Rieger, B.; Mu, X.; Mallin, D. T.; Rausch, M. D.; Chien, J. C. W. *Macromolecules* **1990**, *23*, 3559.
- (474) Schupfner, G.; Kaminsky, W. *J. Mol. Catal. A: Chem.* **1995**, *102*, 59.
- (475) Jensen, V. R.; Børve, K. J.; Ystenes, M. *J. Am. Chem. Soc.* **1995**, *117*, 4109.
- (476) Hagihara, H.; Shiono, T.; Ikeda, T. *Macromol. Rapid Commun.* **1999**, *20*, 200.
- (477) Shiono, T.; Ohgizawa, M.; Soga, K. *Polymer* **1994**, *35*, 187.
- (478) Busico, V.; Cipullo, R.; Esposito, V. *Macromol. Rapid Commun.* **1999**, *20*, 116.
- (479) Jüngling, S.; Mülhaupt, R. *J. Organomet. Chem.* **1995**, *497*, 27.
- (480) Jordan, R.; Bajgur, C.; Willet, R.; Scott, B. *J. Am. Chem. Soc.* **1986**, *108*, 7410.
- (481) Bochmann, M.; Lancaster, S. J. *Organometallics* **1993**, *12*, 633.
- (482) Bochmann, M.; Lancaster, S. J. *J. Organomet. Chem.* **1992**, *434*, C1.
- (483) Cam, D.; Giannini, U. *Makromol. Chem.* **1992**, *193*, 1049.
- (484) Tritto, I.; Donetti, R.; Sacchi, M. C.; Locatelli, P.; Zannoni, G. *Macromolecules* **1997**, *30*, 1247.
- (485) Beck, S.; Proscenc, M.-H.; Brintzinger, H.-H.; Goretzki, R.; Herfert, N.; Fink, G. *J. Mol. Catal. A: Chem.* **1996**, *111*, 67.
- (486) Kaminsky, W. *Macromol. Symp.* **1995**, *89*, 203.
- (487) Coevoet, D.; Cramail, H.; Deffieux, A. *Macromol. Chem. Phys.* **1998**, *199*, 1451.
- (488) Coevoet, D.; Cramail, H.; Deffieux, A. *Macromol. Chem. Phys.* **1998**, *199*, 1459.
- (489) Herfert, N.; Fink, G. *Makromol. Chem.* **1992**, *193*, 1359.
- (490) Coevoet, D.; Cramail, H.; Deffieux, A. *Macromol. Chem. Phys.* **1999**, *200*, 1208.
- (491) Coevoet, D.; Cramail, H.; Deffieux, A. *Macromol. Chem. Phys.* **1996**, *197*, 855.
- (492) Beck, S.; Brintzinger, H.-H.; Suhm, J.; Mülhaupt, R. *Macromol. Rapid Commun.* **1998**, *19*, 235.
- (493) Wester, T. S.; Johnsen, H.; Kittilsen, P.; Rytter, E. *Macromol. Chem. Phys.* **1998**, *199*, 1989.
- (494) Herwig, J.; Kaminsky, W. *Polym. Bull.* **1983**, *9*, 464.
- (495) Huang, J.; Rempel, G. *Stud. Surf. Sci. Catal.* **1992**, *73*, 169.
- (496) Fischer, D.; Mülhaupt, R. *J. Organomet. Chem.* **1991**, *417*, C7.
- (497) Vela Estrada, J. M.; Hamielec, E. A. *Polymer* **1994**, *35*, 808.
- (498) Chien, J. C. W.; Wang, B. P. *J. Polym. Sci. A: Chem. Ed.* **1990**, *28*, 15.
- (499) Huang, J.; Rempel, G. C. *Ind. Eng. Chem. Res.* **1997**, *36*, 1151.
- (500) Fischer, D.; Jüngling, S.; Mülhaupt, R. *Makromol. Chem., Macromol. Symp.* **1993**, *66*, 191.
- (501) Chien, J. C. W.; Yu, Z.; Marques, M. M.; Flores, J. C.; Rausch, M. D. *J. Polym. Sci.: Part A: Polym. Chem.* **1998**, *36*, 319.
- (502) Longo, P.; Oliva, L.; Grassi, A.; Pellicchia, C. *Makromol. Chem.* **1989**, *190*, 2357.
- (503) Dolgoplosk, B. A. *Vysokomol. Soedin., Ser. A* **1971**, *13*, 325.
- (504) Novikova, E. S.; Parenago, O. P.; Frolov, V. M.; Dolgoplosk, B. A. *Kinet. Katal.* **1976**, *17*, 928.
- (505) Ystenes, M. *Makromol. Chem., Macromol. Symp.* **1993**, *66*, 71.
- (506) Bochmann, M.; Lancaster, S. J. *Angew. Chem., Int. Ed. Engl.* **1994**, *33*, 1634.
- (507) Haselwander, T.; Beck, S.; Brintzinger, H.-H. In *Ziegler Catalysts*; Fink, G., Mülhaupt, R., Brintzinger, H.-H., Eds.; Springer-Verlag: Berlin, 1995; p 181.
- (508) Erker, G.; Albrecht, M.; Werner, S.; Kruger, C. *Z. Naturforsch. B* **1990**, *45*, 1205.

- (509) Tait, P. J. T.; Watkins, N. D. In: Allen, G., Bevington, J. C., Eastmond, G. C., Ledwith, A., Russo, S., Sigwalt, P., Eds., 1989; Vol. 4, p 533.
- (510) Marques, M. M.; Costa, C.; Lemos, F.; Ramôa Ribeiro, F.; Dias, A. R. *React. Kinet. Catal. Lett.* **1997**, *62*, 9.
- (511) Marques, M. M.; Dias, A. R.; Costa, C.; Lemos, F.; Ramôa Ribeiro, F. *Polym. Int.* **1997**, *43*, 77.
- (512) Prosenc, M.-H.; Schaper, F.; Brintzinger, H.-H. In *Metalorganic Catalysts for Synthesis and Polymerization*; Kaminsky, W., Ed.; Springer-Verlag: Berlin, 1999; p 223.
- (513) Herfert, N.; Fink, G. *Makromol. Chem.* **1992**, *193*, 773.
- (514) Herfert, N.; Montag, P.; Fink, G. *Makromol. Chem.* **1993**, *194*, 3167.
- (515) Killian, C. M.; Tempel, D. J.; Johnson, L. K.; Brookhart, M. *J. Am. Chem. Soc.* **1996**, *118*, 11664.
- (516) Johnson, L. K.; Mecking, S.; Brookhart, M. *J. Am. Chem. Soc.* **1996**, *118*, 267.
- (517) Chadwick, J. C.; van Kessel, G. M. M.; Sudmeijer, O. *Macromol. Chem. Phys.* **1995**, *196*, 1431.
- (518) Kioka, M.; Mizuno, A.; Tsutsui, T.; Kashiwa, N. In *Catalysis in Polymer Synthesis*; ACS Symp. Ser. Vol. 496; Vandenberg, E. J., Salamone, J. C., Eds.; American Chemical Society: Washington, DC, 1992; p 72.
- (519) Carvill, A.; Tritto, I.; Locatelli, P.; Sacchi, M. C. *Macromolecules* **1997**, *30*, 7056.
- (520) Corradini, P.; Busico, V.; Cipullo, R. *Makromol. Chem., Rapid Commun.* **1992**, *13*, 21.
- (521) Gell, K. I.; Schwartz, J. *J. Am. Chem. Soc.* **1978**, *100*, 3246.
- (522) Gell, K. I.; Posin, B.; Schwartz, J.; Williams, G. M. *J. Am. Chem. Soc.* **1982**, *104*, 1846.
- (523) McAlister, D. R.; Erwin, D. K.; Bercaw, J. E. *J. Am. Chem. Soc.* **1978**, *100*, 5966.
- (524) Brintzinger, H.-H. *J. Organomet. Chem.* **1979**, *171*, 337.
- (525) Wochner, F.; Brintzinger, H.-H. *J. Organomet. Chem.* **1986**, *309*, 65.
- (526) Sperry, C. K.; Bazan, G. C.; Cotter, W. D. *J. Am. Chem. Soc.* **1999**, *121*, 1513.
- (527) Guo, Z.; Bradley, P. K.; Jordan, R. F. *Organometallics* **1992**, *11*, 2690.
- (528) Randall, J. C.; Ruff, C. J.; Vizzini, J. C.; Speca, A. N.; Burkhardt, T. J. In *Metalorganic Catalysts for Synthesis and Polymerisation*; Kaminsky, W., Ed.; Springer-Verlag: Berlin, 1999; p 601.
- (529) Moscardi, G.; Piemontesi, F.; Resconi, L. *Organometallics* **1999**, *18*, 5264.
- (530) Busico, V. Personal communication.
- (531) Chadwick, J. C. Personal communication.

CR9804691

